University of Rome

*"La Sapienza"*

Faculty of Engineering

# Aeroelastic modeling and MDO analysis of aircraft wings

A dissertation submitted for the degree of

Doctor of Philosophy in Aerospace Engineering

Advisor

Prof. Franco Mastroddi

PhD Candidate

Paola Conti Puorger

Co-advisor

Dr. Daniele Dessi

XX Ciclo Dottorato di Ricerca in Ingegneria aerospaziale

a.a. 2008-2009

# Contents

# Acknowledgements

A profound thanks to my advisor Prof. Franco Mastroddi and to my co-advisor Dr. Daniele Dessi for the teachings and the support they have shown to me during my PhD path. Their devotion to work and interest in any research field have deeply inspired me and helped in times when the end of this work was seeming very far.

Furthermore, a sincere and deep thanks goes to all my family for the love and support they have always provided to me overall during the most stressing stages of my PhD.

# Introduction and summary

The thesis deals with the *Aeroelastic modeling and MDO analysis of aircraft wings*. Both the concepts of aeroelastic modeling and MDO (*Multidisciplinary Design Optimization*) analysis convey general contents that can have several implications. Thus, the first purpose is to properly define the study performed in the present work.

The *aeroelastic modeling* considered herein has to be intended as the effort and the research work carried out in order to contribute in an innovative way to an extension of the Theodorsen theory, well known in aeroelasticity and valid for unsteady aerodynamics in unbounded domain, for the ground effect case, that is a bounded domain case. Indeed, the ground effect flying condition, thanks to the remarkable increase of the aerodynamic efficiency, is a flying condition that has notable and interesting application still in development in the industry field. An example could be the concept of *wing in ground effect (WIG)* craft that perform their cruise on the sea surface and that can be adopted not only for passengers but also for improving the transportation of merchandise by sea hence lightening the ground shipping. Other relevant applications are the fire extinguisher craft that have to perform their mission in the ground proximity. Thus, for such vehicles, it seems evident how important can be the evaluation of the unsteady aerodynamic loads in the peculiar condition of ground proximity. Accordingly, the aim of the present work is to fulfill the intention of attempting a possible solution for the evaluation of the lift coefficient in unsteady aerodynamics for craft operating in the ground effect flying condition.

The theoretical roots for the aeroelastic methodology suggested in this work rely on two main theories: the Theodorsen theory for unsteady two-dimensional potential flows in unbounded domain and the Keldysh-Lavrentiev methodology for the evaluation of the steady lift coefficient in bounded domain. Furthermore, it is worth to remark that the mentioned Keldysh-Lavrentiev methodology allows the evaluation of the steady aerodynamic coefficient in any bounded domain, that is it is applicable not only in the airfoil in ground effect case but also in the symmetric problem of submerged hydrofoils. This consideration adds value to the effort of finding an expression for unsteady aerodynamic coefficients in bounded domain since it is possible to use the same theory for hydroelastic problems. Thus, matching the two mentioned theories, the focus of the methodology suggested in the present work consists in the

use of a series expansion, respect to the ground interface clearance, of the kernel function obtained by the image method and that belong to the Theodorsen integral equation of the vorticity problem.

The second major concept explored in the thesis concerns the *MDO analysis*. Indeed, the *Multidisciplinary Design Optimization (MDO)* research field has been quickly developing and assuming its own features, in the few past decades, thanks to its relevance in many engineering applications. It has to be underlined that the achievement of an optimum design of an advanced aerospace vehicle relies not only on obtaining maximum performances, but on matching several targets like performances, manufacturability, serviceability and overall life-cycle cost effectiveness. Furthermore, all the listed capabilities have to be implemented in a systematic and mathematically based procedure. Thus, the MDO approach is a tool that enables engineers to make design decision on a rational basis integrating several disciplines and giving the worth consideration to their interaction or influence on the complex system analysis.

Several aspects make the MDO research field a challenging one like the choice of the appropriate algorithmic formulation of the problem, the needing of integrating the different disciplines while trying to optimize them concurrently and in a modular way that allows the designers to interfere at any step with the optimization procedure, the management of the disciplines interaction as an industrial setting could require in order to allow different specialist engineers subgroups to work in relative isolation but still optimizing the overall project, the entity of the computational costs and so on.

Another aspect to do not underestimate concerns the lack in literature of textbooks effective on the MDO topics, indeed, there are several valid ones, but they typically cover only a subset of topics. This aspect makes the MDO field even more challenging since the broad number of issues related to the concept of MDO.

With the mentioned considerations, in the present work has been explored the availability of the MDO code MAGIC (Multidisciplinary Aircraft desiGn of Innovative Configurations) for the optimization of aircraft wings focusing on its relevance in the MDO worldwide formulation scenario and underlining its potentiality. Due to the code modularity and versatility has been also explored the possibility of introducing the Keldysh-Lavrentiev methodology allowing the code to optimize the wing of an aircraft performing special missions accounting the peculiar flying condition of ground effect.

Summarizing, in the first chapter a concise but detailed overview of the most adopted MDO formulations will be presented. Their relevance and implications in literature will also be widely explored. Thus, the chapter consists in a survey on the state-of-art in the MDO field in order to state some general concepts that are fundamental in the MDO topics comprehension.

In the second chapter the MAGIC code structure as well as its features and potentiality will be addressed. Furthermore, having in mind the formulations presented in the first chapter, the code will

be placed in the MDO worldwide algorithmic formulations scenario. An applicative part will follow presenting some results for the optimization of a wing-box structure first, and then for the optimization of the wing of a civil large aircraft. In the finite wing case the optimization process will be considered increasing the number of the disciplines accounted in the code and allowing the code to interface the MSC NASTRAN commercial code for the finite element analysis. Furthermore, the optimization of the wing performed adopting a penalty function method, core of the optimization algorithm of MAGIC, will be also compared with the optimization of the same wing obtained interfacing MAGIC with the commercial optimizer SNOPT 6.0.

The third chapter focuses on the aeroelastic modeling previously mentioned. Indeed, after presenting the main problems related to a foil operating in ground effect, the Keldysh-Lavrentiev approach for the evaluation of the aerodynamic coefficient of a lifting surface in ground effect for the steady aerodynamic case will be addressed. The extension of the Keldysh-Lavrentiev approach matched with the Theodorsen theory in order to account unsteady aerodynamics in the ground effect flying condition will be then widely discussed exploring the problems related to such an extension while presenting and assessing the innovative obtained results. An extension in ground effect of the Wagner problem will be considered as well in order to validate the presented methodology.

In the fourth chapter will be considered the insertion of the ground effect flying condition in the optimization code MAGIC. Thus, a complete different aircraft will be implemented in the code. The Keldysh-Lavrentiev methodology for the evaluation of the aerodynamic coefficients will be adopted and the pertinent evaluations due to the adoption of a two-dimensional theory for a finite wing optimization will be discussed. Furthermore the results of the optimization process will be presented and treated considering a multi-objective optimization and adopting two different functional relationships for the multi-objective function considered. The comparison of the results obtained using the two different functional relationships will be discussed as well.

Some concluding remarks will concern the possible theoretical and applicative developments of the present work.

# Chapter 1

# Multidisciplinary design optimization survey

## 1.1 Introduction

The design of advanced aeronautical and aerospace vehicles involves many different disciplines due to the intrinsic complexity of such vehicles. Indeed, at least aerodynamic and structural tasks have to be considered, but for a more detailed design one cannot be regardless of others disciplines like, ad example, flight stability, propulsion and control systems. Furthermore, as the reliability of the design improves, there are further essential issues like low computing time, overall life-cost effectiveness and manufacturability, that have to be added as well. Hence, it becomes more and more apparent how complex the design project can be and how a new figure of engineer is necessary for connecting all the specialized tasks coming out from the updating of whichever other discipline and then from any specialized engineering branch.

The concept of Multidisciplinary Design Optimization (MDO) typically resumes all these issues in the design process since it is a formal methodology and a mathematical description that takes into account the synergistic and intrinsical coupling existent in physical complex systems enabling the optimal design of complex multidisciplinary engineering systems. Hence a designer that wants to take into account the relevant scientific and technological developments achieved in the field of aerospace engineering during the last decades, cannot be irrespective of the concept of MDO as well.

It is worth to point out that optimal problems have very old roots (it is inherent to the human nature

to find the best in problem's solutions, Ref.[1]) but it is only in the last three decades that MDO problems and concepts had assumed a more delineated essence Ref.[2],[3]. As known, the MDO concept founds its origin on the field of structural optimization [2],[3]. Since then, it has been developed in several engineering fields and it has took deep roots also in aeronautical and aerospace applications where the weight reduction is a critical issue and where interdisciplinarity is a topic intrinsic to the statement of the problems.

In Refs.[4],[5] it was underlined how the two main challenges in MDO are computational costs and organizational complexity. Furthermore, such a sentence well includes the more recent challenge of MDO: solutions methodology and/or architectures and its software frameworks. These aspects will be widely discussed in the course of this chapter. Indeed, while it is easy to understand how the interdisciplinary coupling inherent to MDO can heavily improve the computational burden respect to the computational burden of a single discipline optimization, the complexity of implementing the necessary coupling in software systems has to be widely discussed. The heavy improvement of the computational costs is actually due to the increased size of the MDO problem since each added discipline will involve a certain number of design variables and analysis variables. Moreover, the overall multidisciplinary computational cost is higher than the sum of the costs of a single discipline optimization and even if a linear analysis method is used for each discipline, for the coupled multidisciplinary system there may be the needing of a nonlinear analysis. On the other side, the organizational complexity is much more challenging since even a different choice in the design variables or in the single-level optimization formulation instead of the multi-level one can cause deep changes in the coordination and transferring of the data between the analysis code and the optimization loop and hence in the overall optimization process. Therefore, it is also evident how the human interaction can really make the difference in a MDO process and hence it is worth to underline how the MDO field is becoming every day more clearly a new field of research with its own experts and engineers meanwhile the MDO strategies are useful in every engineering field.

Finally, the optimization of a complete aircraft showed later on, is a contribution that permits to appreciate the complexity and the multi-tasks of the MDO approach since the analysis of a complete aircraft is one of the principal issues of MDO research.

## 1.2 Current state of the art of the MDO architectures: monolithic approach vs decomposition methods

Since the MDO approach took roots in the field of aerospace engineering, its first applications have been the evaluation of structural, aerodynamics and flight performances analysis codes nested in a single loop of optimization. Thus, consistently with computer technology limitations in terms of time and

computing resources, the codes were processing mathematical model of variable fidelity and they were operating on few design variables in order to optimize an objective function, such as the weight or the flight range. The objective function was also the system level objective.

Subsequently, since the aim of the designers is to give a more realistic representation of the model, the number of accounted disciplines increased, making evident the needing of maintaining a good level of the model fidelity besides the improved complexity of the code. Such development in the number of disciplines accounted led to the implementation of codes that were invoking in a single optimization loop a broad number of disciplinary mathematical models. Thus, this kind of MDO approach has been defined like a *monolithic* one [3] (or *single-level* [6]).

The monolithic approach showed an intrinsic limitation as it can scale poorly when a broad number of discipline is involved in order to solve a large problem. Hence, it became apparent the needing of decomposing large problems into smaller ones without injure the intrinsic coupling of the disciplines accounted. Furthermore, the decomposition of the problem that will yield a system level optimization and a subsystem one, has to be performed considering that for a nonlinear objective function the optimal system-level design is not equivalent to a simple collection of the optimization of the subsystems objective functions.

Referring to the MDO approaches, a clear explanation is given in Ref: [7]: *"The fundamental approaches to MDO formulations vary in two aspects. First is the distinction between single-level optimization and multi-level optimization. In multi-level optimization approaches, the disciplinary design variables are determined by disciplinary optimizers and the system design variables are determined by the system optimizer. In single-level optimization approaches, both disciplinary and system design variables are determined by the system optimizer. Second is the choice between simultaneous analysis and design (SAND) and nested analysis and design (NAND). This distinction can be made at both the system and the discipline levels. At the discipline level, SAND implies that the disciplinary design and state variables are determined simultaneously by the optimizer whereas NAND implies that the optimizer determines only the disciplinary design variables and requires determination of the state variables at each iteration. Thus, at each iteration of the optimizer, disciplinary evaluators are called or SAND, whereas disciplinary analyzers are called for NAND. At the system level, SAND implies that system design variables and coupling variables are determined simultaneously by the system optimizer, whereas NAND implies that the system optimizer determines only the system design variables and requires determination of the coupling variables at each iteration by calling a system analyzer."* Hence, in Ref. [7] Balling and Sobieszczanski suggested to categorize the MDO approaches adopting a three part name the first part being indicative of whether the approach is single or multi level, while the second and third indicate SAND vs NAND at system or discipline levels respectively.

Although the classification of Ref. [7] is exhaustive and compact, with time the MDO formulations have

assumed a well-delineated aspect and a set of new decompositions procedures has been widely developed. Thus, in the following of the chapter, besides the monolithic formulations, the multi-level approaches known as *Collaborative Optimization (CO)* and *Bi-level Integrated System Synthesis (BLISS)* will be discussed in detail.

## 1.3 Monolithic formulations

The distinctive feature of the monolithic formulations is the introduction of a single system-level optimizer acting on the whole problem. In Ref. [8] some alternative single-level formulations to formulate MDO problems are presented in detail, while in Refs. [9] and [6] a more synthetic discussion is provided. It is worth to underline that single-level formulations are well suited for systems that own very strong interactions, but they are not too effective for large dimensions problems where multi-level formulations can be preferred[6]. Before introducing some different kind of monolithic formulations, it is worth to define some terms to understand what they convey and to define some relevant concepts used in the formulations statements.

A key term is the concept of *feasibility*. According to [8] for a single discipline *feasibility* means that the equations the discipline code is intended to solve are satisfied. To better understand this sentence can be useful to refer to a specific problem like the problem of a steady flight of a flexible wing where two disciplines are involved that is structures and aerodynamics. As known the pressure of the air on the wing causes a deflection of it while the effect of the changing of the wing shape causes a change in the aerodynamic pressures field as well. This process continues till when an equilibrium is reached in static aeroelasticity. Usually, the disciplines are solved by individual analysis codes like a finite element (FEM) code for the structures and a boundary element method (BEM) or a computational fluid dynamics (CFD) for the aerodynamics. Hence, according to this example, there is a *single discipline feasibility* for structures when the FEM code has solved the structural analysis equations, once the input forces are given, to produce deflections. Similarly, there is a *single discipline feasibility* for aerodynamics when the BEM or CFD code has solved for the pressures field once the input wing shape is given.

It is then necessary to introduce the concept of *multidisciplinary feasibility*. Still according with [8] the *multidisciplinary analysis feasibility* corresponds to the achievement in the multidisciplinary analysis and it conveys that

- there is already single discipline feasibility (i.e. both in structures and in the aerodynamics there is single discipline feasibility according to the given example)
- the input to each corresponds to the output of the other via the interdisciplinary mappings

where the multidisciplinary mappings represents the coupling between the disciplines. Following the previous example it is evident that the two analysis codes solve their problems on different grids and that they interact only at a specific interface. Also there will be the needing of converting values of pressures from the aerodynamics into values of forces for the structures and of deflections from structures into changes of the aerodynamic shape. Those concepts are conveyed in the concept of interdisciplinary mapping.

Even if there is individual discipline feasibility in each discipline it is possible that there is not multidisciplinary feasibility. This situation occurs when the equations in each code are satisfied but the input to one discipline does not correspond to the output of the other.

In Ref.[8], where three fundamental monolithic approaches for MDO formulations *MultiDisciplinary Feasible* MDF, *All At Once* AAO, and *Individual Discipline Feasible* IDF are presented, is underlined that the kind of feasibility that has to be maintained at each optimization is the key issue between those different formulations. Specifically in the MDF approach the multidisciplinary analysis problem is solved multiple times at each optimization iteration, at least once everytime any problem function or constraint or derivative is evaluated. In the AAO feasibility is guaranteed only at optimization convergence. Finally, the IDF approach relies in[1] *"maintaining feasibility of the individual analysis discipline at each optimization iteration while allowing the optimizer to drive the computation toward multidisciplinary feasibility as convergence is approached"*.

Single-level approaches relies in understanding the structures of the problem for exploiting synergistically the existing coupling between the disciplines. Indeed, when there are multiple interactions, each subsystem may be requested to sacrifice its own needs in order to assure the success of the overall system objective. As reference nomenclature to introduce the different monolithic formulations, we will refer to the one adopted in Ref. [6] that is also the one more widely adopted in the optimization field.
Hence, $\mathbf{x}$ represents the design vector for the whole system; the components of $\mathbf{x}$ that are input to subsystem $i$ form the vector $\mathbf{x_i}$. Some components of $\mathbf{x_i}$ are design variables that are inputs only to subsystem $\mathbf{i}$ that is they are local variables $\mathbf{x_{li}}$. Some others components of $\mathbf{x_i}$ are design variables that are inputs to subsystem $\mathbf{i}$ and at least to one other subsystem that is they are shared variables $\mathbf{x_{si}}$. Each subsystem analysis requires as input pertinent design variable values and eventually some analysis outputs from others subsystems. The interactions quantities, that is the coupling variables, are given by the collection of analysis outputs generated by the subsystem $j$ and input to subsystem $i$ and they are indicated as $\mathbf{y_{ij}}$. The equality and inequality design constraints computed by system $i$ are respectively termed $\mathbf{h_i}$ and $\mathbf{g_i}$. Thus, the collections of equality and inequality constraints are respectively $\mathbf{h} = [\mathbf{h_1}, \mathbf{h_2}, ..., \mathbf{h_N}]$ and $\mathbf{g} = [\mathbf{g_1}, \mathbf{g_2}, ..., \mathbf{g_N}]$. The system objective function is indicated ad $f$ and it is computed by subsystem N. Every subsystem analysis, usually performed by computer-aided engineering tools, conveys taking in values for $\mathbf{x_i}$ and $\mathbf{y_{ij}}$ and evaluating values for $\mathbf{y_{ji}}$, $\mathbf{h_i}$, $\mathbf{g_i}$ and $f$, if $i = N$. The collection of all the

[1] Quoting [8]

coupling variables input to all subsystems form a vector named $\mathbf{y} = [\mathbf{y_1}, \mathbf{y_2}, ...\mathbf{y_N}]$ while the vector $\mathbf{y_i} = [\mathbf{y_{ij_1}}, \mathbf{y_{ij_2}}, ...\mathbf{y_{ij_{N-1}}}]$ represents the coupling variables input to subsystem $i$. A vector analysis function $\mathbf{a_{ij}}(\mathbf{x_j}, \mathbf{y_j})$ is needed in order to compute the value of each corresponding coupling variable $\mathbf{y_{ij}}$, hence, the quantities computed by subsystem $j$ and passed to subsystem $i$ are $\mathbf{y_{ij}} = \mathbf{a_{ij}}(\mathbf{x_j}, \mathbf{y_j})$. Finally, $\mathbf{a}(\mathbf{x}, \mathbf{y})$ represents the vector of all analysis functions that are adopted to evaluate the coupling variables values. The components of such vector correspond directly to the components of $\mathbf{y}$. When fixed values for the coupling variables and for the design variables are given, the evaluation of $\mathbf{a}(\mathbf{x}, \mathbf{y})$ give back computed values for $\mathbf{y}$. However, computed values for $\mathbf{y}$ may not match the original input values for $\mathbf{y}$. A system analysis consists in finding, for a given $\mathbf{x}$, the input values for $\mathbf{y}$ so that the computed coupling variable values agree with the corresponding input coupling variable values. A system in this state is said to be a *consistent* one. Hence, the system analysis problem consists in finding $\mathbf{y}$ such that the consistency equations (that is the system analysis equations)

$$\mathbf{y} - \mathbf{a}(\mathbf{x}, \mathbf{y}) = \mathbf{0} \tag{1.1}$$

are satisfied. A solution to the problem 1.1 is called a *fixed point* and it is denoted as $\mathbf{y_p}$. Indeed, evaluating $\mathbf{a}(\mathbf{x}, \mathbf{y_p})$ it gives back the original input vector $\mathbf{y_p}$. The fixed points values vary with the system design, hence, $\mathbf{y_p} = \mathbf{y_p}(\mathbf{x})$. Summarizing, a system analysis consists in solving the equilibrium equations 1.1 once an input fixed design $\mathbf{x}$ is given, and in evaluating the system analysis outputs required by the design optimization problem such as $f(\mathbf{x}, \mathbf{y_p}(\mathbf{x})), \mathbf{g}(\mathbf{x}, \mathbf{y_p}(\mathbf{x})), \mathbf{h}(\mathbf{x}, \mathbf{y_p}(\mathbf{x}))$ adopting the resulting $\mathbf{y_p}(\mathbf{x})$.

### 1.3.1 Multidisciplinary feasible (MDF)

In the MDF formulation, a single system-level optimizer is adopted and a separate algorithm performs the system analysis as shown in Figure 1.1. Since the analysis is nested in the design this approach is also called *Nested Analysis aNd Design* (NAND). The optimization algorithm provides the design $\mathbf{x}$ to the system analyzer that in turn gives back the function values $\mathbf{g}, \mathbf{h}$ and $f$. Hence, **whenever a complete system analysis is performed for every optimization iteration, the single-level approach adopted can be classified as MDF**.

The system design optimization problem statement can be settled as

$$\begin{aligned} \min_{\mathbf{x}=[\mathbf{x}_l, \mathbf{x}_s]} \; & f(\mathbf{x}, \mathbf{y}_p(\mathbf{x})) \\ s.t. \quad & \mathbf{g}(\mathbf{x}, \mathbf{y}_p(\mathbf{x})) \leq \mathbf{0} \\ & \mathbf{h}(\mathbf{x}, \mathbf{y}_p(\mathbf{x})) = \mathbf{0} \end{aligned} \tag{1.2}$$

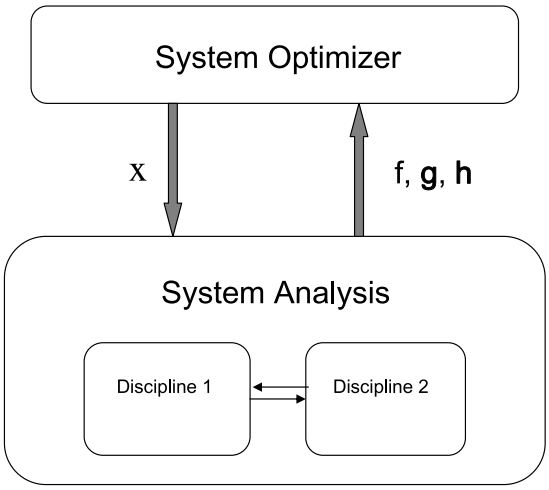


Figure 1.1: The MDF architecture for a two disciplines MDO problem

where $\mathbf{y}_p$ is computed at every step of the optimization process using a system analysis algorithm. Thus, the optimizer has the task of finding the optimal design $\mathbf{x}^*$ while the system analyzer has the role of finding $\mathbf{y}_p(\mathbf{x})$ that is the system analysis solution.

As remarked in [6] the MDF approach is effective when there is a fast system analysis convergence, that means that the subsystems are weakly coupled, and if the subsystem analysis are not expensive from a computational point of view. The wide use of the MDF approach as a traditional MDO architecture in engineering design relies in its intrinsic structure: if a design process performs already a complete system analysis before making a system decision, the MDF formulation is then the natural fit.

A lack related to the MDF approach that must be underlined is the strong dependance that this formulations has to the effectiveness of the system analyzer. Indeed, the optimizer may fail if the analyzer does not converge at any point in the process. Hence, the motivation of searching of approaches that eliminate the needing of repeated system analysis relies in the previous observation that states that the nested analysis and optimization process required by the MDF formulation can be computationally inefficient.

### 1.3.2 Individual disciplinary feasible (IDF)

In the IDF approach, the direct communication between the disciplines is removed: each discipline is solved in isolation and possibly in parallel as shown in Fig. 1.2. A single system-level optimizer is adopted and an analyzer is employed for each subsystem, but the optimizer coordinates only the interactions between the subsystem analysis instead of a system analysis algorithm. In the IDF formulation, thus,

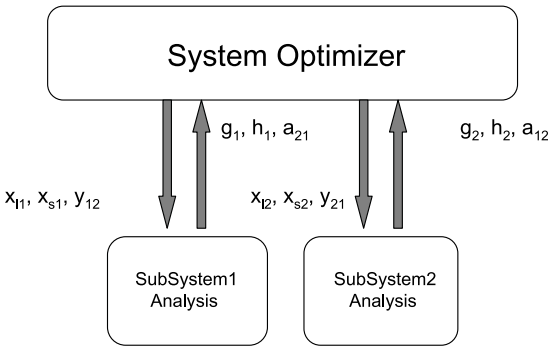


Figure 1.2: The IDF architecture for a two disciplines MDO problem

the optimizer supplies values for both the design variables and the coupling variables since the system analysis and the design are performed at the same time. Also, as previously mentioned, since the optimizer provides all the inputs required for all subsystems concurrently, the subsystem analysis may be performed in parallel.

The IDF formulation can be stated as

$$\begin{aligned} &\min_{\mathbf{x}=[\mathbf{x}_l,\mathbf{x}_s],\mathbf{y}} f(\mathbf{x},\mathbf{y}) \\ &s.t. \quad \mathbf{g}(\mathbf{x},\mathbf{y}) \leq \mathbf{0} \\ &\qquad \mathbf{h}(\mathbf{x},\mathbf{y}) = \mathbf{0} \\ &\qquad \mathbf{h}_{aux}(\mathbf{x},\mathbf{y}) = \mathbf{y} - \mathbf{a}(\mathbf{x},\mathbf{y}) = \mathbf{0} \end{aligned} \tag{1.3}$$

where $\mathbf{h}_{aux}$ are auxiliary constraints added in order to assure system consistency without solving for $\mathbf{y}_p(\mathbf{x})$ at each optimization iteration. Eqs. (1.3) show that in the IDF formulation the decision variable vector includes not only the design variables $\mathbf{x}$ but also the coupling variables $\mathbf{y}$.

Some desirable distinctive features of the IDF approach are explored in [6],[10]. It is appropriate to briefly resume them saying that the increase dimension of the optimization problem, due to the fact that the coupling variables are made decision variables, can pauperize the numerical solution accuracy when the problem size is large. Thus, the MDF formulation may be preferred when the dimension of $\mathbf{y}$ is larger than the dimension of $\mathbf{x}$. Anyhow, the IDF approach shows to improve convergence properties and to drive the design toward better solutions if there is the possibility of multiple analysis solutions. It is also worth to notice that if the solution process is interrupted, the intermediate design may not be consistent or feasible. On the other side, an interrupted MDF solution process yields to a consistent but potentially infeasible design. Furthermore, it is not requested from the IDF approach to achieve system consistency far from the solution, hence the optimization algorithm has a more efficient path toward the solution and the computational expense is drastically reduced through the elimination of repeated system analysis

steps [6].

### 1.3.3 All at once (AAO)

The AAO architecture is usually impractical for MDO since it adds to the optimization problem an excessive number of design variables. Thus, only a short mention of it will be given while in Refs [8] more details can be found. In the AAO formulations the multidisciplinary problem is decomposed setting the governing equations for each discipline as equality constraints in the optimization problem. The purpose of the AAO approach is to do not seek to obtain feasibility for the analysis problem until optimization convergence is reached. Hence, only close to an optimum solution feasibility has to be requested. Respect to the MDF formulation where complete multidisciplinary feasibility is required, in the AAO approach no feasibility is enforced at each optimization iteration. Thus those two mentioned architecture are two extremes ones while the IDF occupies an "in-between" position respect to them.

## 1.4 Multi-level formulations

Due to the intrinsic interdisciplinary nature of the multidisciplinary design optimization problems that makes them very challenging from both a computational and organizational point of view, it is worth to promote discipline autonomy via decomposition methods. Indeed, considering the quality of interaction (weak or strong) between the several design discipline that can affect the MDO problem, decomposition algorithms are often the only feasible solution approach. Quoting Ref.[5] : "*multidisciplinary optimization (MDO) can be described as a methodology for the design of systems where the interaction between several disciplines must be considered, and where the designer is free to significantly affect the system performance in more than one discipline*. Hence, it is evident how the research of the best decomposition algorithm can be sometimes very challenging and why many different formulation can be suggested.

Thus, decomposition algorithms take advantage from the structure of MDO problems trying to promote discipline autonomy by reformulating the problem as a set of independent subproblems, one per discipline, and a coordinating master problem. The master problem task is both to coordinate the subproblems solutions and to find an overall problem minimizer. Even if in general it is possible to think in multi-level formulations, practically the bi-level ones are the most widespread. Hence, only some of the most well-known bi-level approaches will be presented.

### 1.4.1 Collaborative Optimization

The bi-level approach named Collaborative Optimization (CO) is based on solving the MDO problem preserving the autonomy of the disciplinary calculations by removing all the design variables local to an individual disciplinary subsystem from the system level problem. Some detailed references for the CO approach can be found in [11][12] while a wide critical overview of the method is given in [13]. The cited paper [13] is an helpful reference for demonstrating how a problem formulation can have deep and practical algorithmic consequences.

As previously done speaking about the single-level formulations, it can be helpful to refer to a bi-disciplinary problem like the aeroelastic interaction between structural analysis and aerodynamics. Hence, each discipline relies on a disciplinary analysis that takes as its inputs a set of designed variables (some shared with the system-level problem and some local to the disciplinary problem) and parameters, and produces a set of disciplinary outputs. Thus, following the guidelines suggested in [13], the the system-level design variables shared by both the mentioned disciplines can be called $s$ while the disciplinary design variables local to a certain discipline can be indicate as $l_i$. About the parameters $p_i$ it must make known that they cannot be directly modified by the designer in a given discipline $D_i$. Indeed, they are quantities issued from the outputs $a_j, j \neq i$ of the other considered discipline. The outputs of a disciplinary analysis from a given discipline can be indicated as $a_i$. With the previous statement, a disciplinary analysis $A_i$ is such that verifies the following relationship:

$$a_i = A_i(s, l_i, p_i) \tag{1.4}$$

The disciplinary analysis are intended to be independently soluble; thus, disciplinary feasibility is assumed.

Considering a two-discipline problem, the next step is to solve the coupled multidisciplinary analysis system. Indeed, a solution has to simultaneously satisfy the two disciplinary analyses. Hence, the consistent multidisciplinary analysis system can be written as a system of two equation that need to be simultaneously solved

$$\begin{aligned} a_1 &= A_1(s, l_1, a_2) \\ a_2 &= A_2(s, l_2, a_2) \end{aligned} \tag{1.5}$$

It is worth to remind that due to the coupling of the disciplines, the input parameters to a discipline correspond to the outputs from the other disciplinary analysis. Furthermore, via the coupled multidisciplinary analysis, each disciplinary analysis can be regarded as an implicit function of the shared and the

local design variables and each disciplinary analysis describes part of the problem, thus,

$$\begin{aligned} a_1 &= a_1(s, l_1, l_2) \\ a_2 &= a_2(s, l_1, l_2) \end{aligned} \tag{1.6}$$

In the two disciplines of the aeroelastic example considered if the discipline 1 represents the structural analysis and discipline 2 the aerodynamics, then the evaluation of the deformations of the wing $a_1$ needs the information given in $a_2$ about the aerodynamics loads, while the calculation of the flow fields $a_2$ requires the wing shape given from $a_1$. At this point, the standard single-level formulation of the two-disciplines optimization problem would request to add an optimizer over the multidisciplinary analysis problem previously formulated. Hence, the monolithic approach following the nomenclature adopted would be given by:

$$\begin{aligned} \min_{s,l_1,l_2} \quad & f(s, a_1(s, l_1, l_2), a_2(s, l_1, l_2)) \\ s.t. \quad & g_1(s, l_1, a_1(s, l_1, l_2)) \geq 0 \\ & g_2(s, l_2, a_2(s, l_1, l_2)) \geq 0 \end{aligned} \tag{1.7}$$

where $f$ denotes the objective function of the system-level problem. For a given value of the design variables $(s, l_1, l_2)$ it is possible to solve the disciplinary analysis system represented from the equations 1.6 finding then the disciplinary analysis outputs $a_1(s, l_1, l_2), a_2(s, l_1, l_2)$.

In order to focus on the re-formulation of the stated problem according to the lines of the CO approach, some simple simplification can be adopted. In particular, as suggested in [13], it is possible to consider that the constraints $g_1, g_2$ are disciplinary design constraints associated to the disciplines 1 and 2 respectively. The previous statement implies that no constraint involves the disciplinary analysis $a_1$ and $a_2$ jointly and allows to simplify the exposition without affect the statement of the problem. Furthermore, some new disciplinary design variables named[2] $\sigma_1, \sigma_2$ have to be introduced. By these variables it is possible to consider a relaxation of the coupling between the subsystems via the shared design variables at the system-level $s$. Indeed, the variables $\sigma_1, \sigma_2$ are local copies of the shared variables, at the level of the disciplinary sub-problems.

The system-level problem that has to optimize the system-level objective in the CO approach can be set as follows

$$\begin{aligned} &\min_{s,t_1,t_2} f(s, t_1, t_2) \\ &s.t. \quad C(s, t_1, t_2) = 0 \end{aligned} \tag{1.8}$$

[2]Following [13] the Greek letters are used to indicate variables that are auxiliary and that at the subproblem level work like copies of the shared ones.

with $C = c_1, \ldots, c_N$ interdisciplinary consistency constraints (whose meaning will be fully understood as the peculiar CO formulation will be completely introduced) while with $t_1, t_2$ are indicated the values of the system-level targets for the disciplinary inputs and outputs $a_1, a_2$. Thus, the system-level problem controls both the system-level design variables $s$ and the interdisciplinary coupling variables $t_1, t_2$. The CO approach then is distinctively achieved formulating the following disciplinary subproblems that can be solved autonomously

$$\begin{aligned} \min_{\sigma_1, l_1} \quad & \frac{1}{2}\left[\|\sigma_1 - s\|^2 + \|a_1(\sigma_1, l_1, t_2) - t_1\|^2\right] \\ s.t. \quad & g_1(\sigma_1, l_1, a_1(\sigma_1, l_1, t_2)) \geq 0 \end{aligned} \tag{1.9}$$

and similarly

$$\begin{aligned} \min_{\sigma_2, l_2} \quad & \frac{1}{2}\left[\|\sigma_2 - s\|^2 + \|a_2(\sigma_2, l_2, t_1) - t_2\|^2\right] \\ s.t. \quad & g_2(\sigma_2, l_2, a_2(\sigma_2, l_2, t_1)) \geq 0 \end{aligned} \tag{1.10}$$

with $a_1, a_2$ given respectively by the disciplinary analyses

$$\begin{aligned} a_1 &= A_1(\sigma_1, l_1, t_2) \\ a_2 &= A_2(\sigma_2, l_2, t_1) \end{aligned} \tag{1.11}$$

Thus, the system-level problem provides the design targets $(s, t_1, t_2)$ to the constituent disciplines while in the subsystems the disciplines must achieve the given targets. Indeed, concerning the discipline 1 the values of $(s, t_1, t_2)$ are given while the values of $\sigma_1(s, t_1, t_2)$ and $l_1(s, t_1, t_2)$ are computed solving the problem of minimization in $(\sigma_1, l_1)$ 1.9. Similarly concerning the discipline 2 the values of $(s, t_1, t_2)$ are given while the values of $\sigma_2(s, t_1, t_2)$ and $l_2(s, t_1, t_2)$ are computed solving the problem of minimization in $(\sigma_1, l_1)$ 1.10. It is worth to underline that in the disciplinary subproblems the system-level variables $(s, t_1, t_2)$ have both the roles of parameters or targets that have to be achieved.

Once the subproblems are solved, the disciplinary design constraints $g_1, g_2$ can be used to eliminate the disciplinary design variables $l_1, l_2$ from the system level problem and decoupling the evaluation of the disciplinary analysis outputs $a_1, a_2$. Furthermore, the information from the solved subproblems is used to define the system-level consistency constraints $c_1, c_2$ and depending from the type of the system-level constraints, different variant of CO can be obtained.

The most frequently adopted variant of CO is the one that requests as consistency condition to drive to zero the minimum value of the target mismatch objective in the subproblems 1.9, 1.10. Hence, the interdisciplinary consistency constraints $C = (c_1, c_2)$ at the system-level are the optimal values of the

objectives of equations 1.9, 1.10 defined as

$$c_1(s,t_1,t_2) = \frac{1}{2}\left[\|\sigma_1(s,t_1,t_2) - s\|^2 + \|a_1(\sigma_1(s,t_1,t_2), l_1(s,t_1,t_2), t_2) - t_1\|^2\right]$$
$$c_2(s,t_1,t_2) = \frac{1}{2}\left[\|\sigma_2(s,t_1,t_2) - s\|^2 + \|a_2(\sigma_2(s,t_1,t_2), l_2(s,t_1,t_2), t_1) - t_2\|^2\right] \quad (1.12)$$

where the values of $\sigma_1, \sigma_2, l_1, l_2$ are the ones obtained solving the disciplinary optimization subproblems for the given value $(s,t_1,t_2)$ of the system-level variables. Since the interdisciplinary consistency constraints are given by sums of squares, this CO variant is also called $CO_2$.

Alternatively, it can be set that the system-level variables come to agreement directly to their subsystems counterparts computed in 1.9, 1.10. Hence, the consistency constraints will be given by

$$\begin{aligned} c_1(s,t_1,t_2) &= \sigma_1(s,t_1,t_2) - s \\ c_2(s,t_1,t_2) &= a_1(\sigma_1(s,t_1,t_2), l_1(s,t_1,t_2), t_2) - t_1 \\ c_3(s,t_1,t_2) &= \sigma_2(s,t_1,t_2) - s \\ c_4(s,t_1,t_2) &= a_2(\sigma_2(s,t_1,t_2), l_2(s,t_1,t_2), t_1) - t_2 \end{aligned} \quad (1.13)$$

where $c_1, c_2$ are associated to the discipline 1 while $c_3, c_4$ are associated to discipline 2. The variant of CO in this last case is called $CO_1$.

The values of the system-level variables $(s,t_1,t_2)$ that are desirable are the ones that allow the discipline $i$ to match exactly the system-level input-outputs targets without violating the disciplinary design constraints. Such values are called *realizable* and are values of $(s,t_1,t_2)$ that for a given discipline $i$ are such that the optimal objective value in the corresponding optimization problem 1.9 or 1.10 is zero. There can be several realizable values of the system-level variables $(s,t_1,t_2)$ for a given discipline. Thus, a point $(s,t_1,t_2)$ is feasible for the system-level problem when for all the constituent disciplines it is a realizable one.

Several aspects of the CO formulation can be very attractive. First of all, it can be noticed that the flow of the information in the CO decomposition reflects the flow of information characteristic of the engineering organizations. Another mentioned motivation is the keeping of the disciplinary autonomy. This last aspect relies on the intuition that the interaction among the local design variables of different disciplines should be little, hence the system-level coordination problem should be solved in an easier way. Nevertheless, some other aspects of the formulation based on an extended mathematical analysis of the algorithm, show that the CO approach presents some drawbacks. Indeed, it has been widely demonstrate in [14] that adopting the collaborative optimization formulation there are some difficulties that *necessarily* arise at points that are realizable for individual disciplines. Particularly in [14] has been proved that the difficulties that arise are not due to intrinsic properties of the original MDO problem,

but rather to the bi-level representation in $CO$ of the problem and they can be summarized as follows

- the standard Karush-Kuhn-Tucker conditions for a solution do not hold for the $CO_2$ system-level problem; this condition implies that the Lagrange multipliers do not exist for the system-level equality constrained problem that results in $CO_2$;
- the derivatives of the $CO_1$ system-level constraints will be discontinuous at values of the system-level variables that are realizable for a given discipline if the solution of the disciplinary optimization problem is on the boundary of the disciplinary feasible region; unfortunately this means that in general the Jacobian of the system-level constraints is discontinuous at solutions of the system-level optimization problem and the standard Karush-Kuhn-Tucker conditions for a solution do not hold for the $CO_1$ system-level problem;
- the system-level optimization problems in $CO$ are more non-linear than the fully integrated formulation; for instance collaborative optimization transforms linear programs into non-linear programs.

Thus, the $CO$ approach has shown to do not be very effective and the most serious drawback of such formulation can be considered the lack of robustness in using nonlinear programming algorithms in order to solve the $CO$ formulations.

As mentioned, a wide detailed mathematical study about the CO formulation has been carried out by N. Alexandrov in several papers as the cited one [14]. Thus, in the cited paper it is possible to find an exhaustive research about the CO formulation drawbacks. Nevertheless, it seems appropriate in order to complete our survey about the CO architecture, to explain at least the first of the itemized drawbacks for the $CO_2$ formulation as example of the proof procedure also considering that this kind of CO formulation is the more adopted in literature. Thus, the most simple optimization problem to consider is given by a single variable and it is of the kind[3]

$$\begin{aligned} &\min_{s} f(s) = s \\ &s.t.\ 0 \leq s \leq 1 \end{aligned} \tag{1.14}$$

Introducing in 1.14 the CO formulation, two disciplines have to be considered and they are associated with each of the two inequality constraints. Furthermore, $s \geq 0$ and $s \leq 1$ have to be considered as two

[3]This can be the example of a bar of cross-sectional area $A$ (that is the design variable) and fixed length $L$ subject to a longitudinal load $F$. Thus,

$$\begin{aligned} &\min_{A} kLA \\ &s.t.\ F/S \leq A \\ &\quad A \leq W/(\rho L) \end{aligned}$$

where $k$ is the cost per unit volume, $\rho$ is the density of the bar, $w$ its weight and $S$ is some allowable limit.

contending disciplinary design constraints. Hence, the subsystem problems become

$$\begin{aligned}
&\min_{\sigma_1}(1/2)\|\sigma_1 - s\|^2 \\
&s.t.\ \sigma_1 \geq 0 \\
&\min_{\sigma_2}(1/2)\|\sigma_2 - s\|^2 \\
&s.t.\ \sigma_2 \leq 1
\end{aligned} \tag{1.15}$$

Thus, the $CO_2$ reformulation yields

$$\begin{aligned}
&\min_{s} s \\
&s.t.\ c_1(s) = (1/2)\|\bar{\sigma}_1(s) - s\|^2 = 0 \\
&\quad c_2(s) = (1/2)\|\bar{\sigma}_2(s) - s\|^2 = 0
\end{aligned} \tag{1.16}$$

The gradients of the system-level consistency constraints follow from 1.15 and 1.16 thus,

$$\nabla c_1 = \begin{cases} s & \text{if} \quad s \leq 0 \\ 0 & \text{if} \quad s \geq 0 \end{cases}$$

$$\nabla c_2 = \begin{cases} 0 & \text{if} \quad s \leq 1 \\ s & \text{if} \quad s \geq 1 \end{cases}$$

The solution that minimizes the system-level problem 1.14 is $s_* = 0$ and the gradients of the system-level consistency constraints for such value are

$$\nabla c_1(s_*) = \nabla c_2(s_*) = 0$$

Thus, they are linearly dependent. The stationarity conditions for 1.14 would require the existence of Lagrange multipliers $\lambda_1, \lambda_2$ such that

$$\nabla f(s_*) + \lambda_1 \nabla c_1(s_*) + \lambda_2 \nabla c_2(s_*) = 0$$

but for the given system one has

$$\nabla f(s_*) + \lambda_1 \nabla c_1(s_*) + \lambda_2 \nabla c_2(s_*) = \nabla f(s_*) = 1$$

hence, the normal stationarity conditions cannot be satisfied at $s_*$. Thus, the previous relationship proves that the Lagrange multipliers do not exist for the system-level equality constrained problem that results in $CO_2$.

### 1.4.2 Bi-Level Integrated System Synthesis (BLISS)

A valid method for optimization of engineering systems by decomposition is the *Bi-Level Integrated System Synthesis* (BLISS). The method has its origins in [15], [16], [17] and was formulated by J. Sobieszczanski Sobieski et al. in 1998. By the use of the BLISS method, the design of a complex system can be performed considering a single system-level optimization problem with a relatively small number of design variables, and a set of subsystem optimizations problems that potentially have a large number of local design variables.

Before introducing the method, it is worth to underline its benefits. The first advantage of the BLISS method relies in the concept of decomposition itself. Indeed, the method allows to divide a complex optimization problem into smaller problems that are more easy and quick to solve. Furthermore, since the resulting subsystems optimizations are autonomous, adopting the BLISS method it is possible to perform the subsystems optimization by disciplinary experts autonomously thus the evaluation can be conducted concurrently. Finally, it is also possible to use approximate surrogate models in order to reduce the total computational cost, and to compute in parallel the subsystem problems, thus fully utilizing the computing resources available.

Besides the underlined advantages, there is another aspect that is quite attractive in the BLISS formulation. Indeed, the overall architecture of BLISS as a method, does not depend on the fidelity of the analysis performed in each module. As a consequence of that, the method can be used in any design phase starting with the conceptual design trough the preliminary till the detailed one, accounting an appropriate level of analysis in the implemented modules.

Summarizing the main steps of the method it is worth to underline that the two levels of the BLISS optimization are performed in sequence since there is an alternation of subsystems and system-level optimization, linked by sensitivity data, in order to achieve an improvement of the design at each iteration. Thus, posing a best guess initial design, the first step consists in the separate, concurrent and autonomous optimization of the subsystems respect to local design variables specific to each disciplinary black box[4] (BB) module while considering as frozen the system-level variables. Only as a subsequent step, the optimization in the space of the system-level variables is performed by the link of optimization sensitivity data. As seen for the CO formulation, there are different variants of the BLISS method (e.g. BLISS/A and BLISS/B) and in this case they differ for some details concerning the linkage of system-level and subsystems problems by the optimum sensitivity data. Referring to the different versions of BLISS available, it is worth to note that in each of them the BLISS method builds a gradient-guided path between the set of disjoined design subspaces and the common system-level design space. Thus, each segment of the builded path cooperate in an improved design, hence, starting from a feasible state, it is

[4] In the mathematical model of a system each module can be regarded as a black-box as referred in the BLISS nomenclature [15]

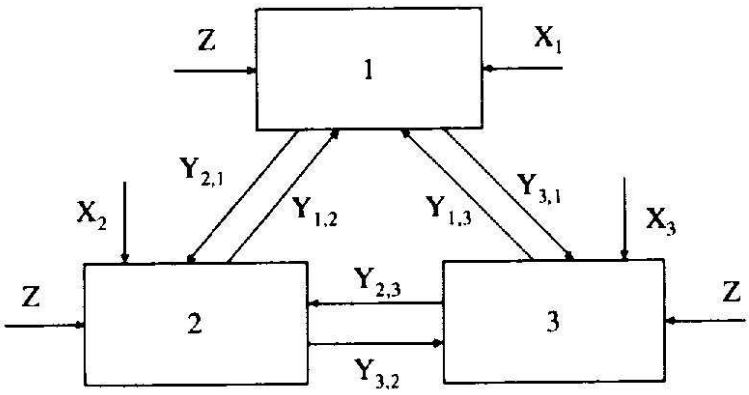


Figure 1.3: System of coupled black-boxes in the BLISS architecture.

possible to preserve that feasibility in each modular design subspace meanwhile minimizing the system-level objective. In case of an infeasible start, the constraints violations are reduced and contemporarily the increase of the objective is minimized. Then, the process can be terminated at any time with the useful information validated by the last system analysis since a system-level analysis is performed at the outset of each segment of the mentioned path. Furthermore, BLISS has been implemented with the idea of allowing the engineers team to exercise judgment at any step in the procedure, by intervening before committing the next successive pass.

Considering the BLISS method more in detail it can be observed that two peculiar features distinguish the BLISS formulation, that is the system-level objective function is adopted as the optimization objective function in each one of the subsystems (besides obviously its adoption in the system-level problem); furthermore, the coupling between the optimization at the system and subsystem levels is accounted by the optimum sensitivity derivatives with respect to parameters.

In Fig. 1.3 an example of the BLISS architecture for three black-boxes (i.e. disciplines) is depicted. In order to get mastery of the BLISS architecture an example of a three disciplines system seems to be enough for the conceptual understanding of the method without burdening to much the mathematical representation. Furthermore, a three black-boxes example allows readily generalization of the BLISS formulation for problems with a larger number of disciplines. From Fig. 1.3 it can be noticed that in the BLISS architecture the variables are split into three categories:

- the $X$ variables are design variables optimized at the local level, hence they are unique and local to each particular black-box, that is to each particular subsystem. In detail, $X_r$ indicates the vector of the design variables local to $BB_r$ while $X$ without subscript indicates a vector of all concatenated

$X_r$;

- the $Y$ variables are state variables that can be regarded as behavior variables since they are output variables from one subsystem and input to another, hence these are coupling variables. In detail $Y$ represents a vector of all concatenated $Y_r$ where $Y_r$ is the vector of the behavior state variables output from a certain $BB_r$. Thus, an element of $Y_r$ is denoted as $y_{r,i}$;
- the $Z$ variables are the system-level design variables, thus, these variables are shared at least from two subsystems. In detail, $Z$ is the vector of the design variables $z_k$ that are shared by two or more $BBs$.

To better understand the BLISS architecture and the role of the variables it is useful to refer to Fig. 1.3 having in mind a specific example like an aircraft optimization. In this case, the three black-boxes ($BB$) can be regarded as $BB_1$ =performance analysis, $BB_2$ =aerodynamics, $BB_3$ =structures. For the mentioned example the system-level objective function $\Phi$ can be the maximum range for given mission characteristics and the depicted variables can be intended as

- $y_{1,2}$ =aerodynamic drag, $y_{1,3}$ =structural weight, $y_{2,1}$ =Mach number, $y_{3,1}$ =take-off gross weight, $y_{2,3}$ =structural deformations that alter the aerodynamic shape, $y_{3,2}$ =aerodynamic loads;
- $x_{1,j}$ =cruise altitude, $x_{2,j}$ =leading edge radius, $x_{3,j}$ =thickness of a given wing skin panel;
- $z_1$ =wing sweep angle, $z_2$ =wing aspect-ratio, $z_3$ =localization of an engine on the wing.

Concerning the constraints local to each $BB$ and named $g_{r,t}$ it can be posed $g_{1,t}$ =noise abatement constraint on the mission profile, $g_{2,t}$ =limit of chord-wise pressure gradient, $g_{3,t}$ =allowable stress.

Since the BLISS method performs the system optimization by means of system decomposition, the algorithm depends on the availability of the derivatives of output with respect to input for each $BB$. That is, the assumption of the differentiability of a $BB$ internal relationship has to be assumed at least at the first order[5].

**$BB$-level optimization**

The first step for achieving the optimization process by the use of the BLISS formulation consists in the local optimization that has to be performed at the single discipline (subsystem) level. In order to do that, after a best guess initialization, the BLISS method starts with a system analysis and sensitivity analysis in which $Y$ and the derivatives of $Y$ with respect to $Z$ and $X$ are evaluated. Then, the basis

[5]The differentiation can be performed by finite differences or by more efficient analytical techniques.

of the algorithm consists in the formulation of an objective function unique for each $BB$ such that the minimization of that function in each single $BB$ results in the minimization of the system-level objective function. Hence, for the given example of the aircraft optimization, the system-level objective function has been assumed to be $\Phi = y_{1,i}$ =maximum range for a given mission characteristics. Then the for the given system-level objective function, considering for example the $BB_2$, its specific objective function $\phi_2$ can be given by

$$\phi_2 = D(y_{1,i}, X_2)^T \Delta X_{2,j}; \quad j = 1..NX_2 \tag{1.17}$$

where $D(y_{1,i}, X_2)$ is the derivative of the system-level objective function (that has been made coincide with $y_{1,i}$) with respect to the local variable of $BB_2$. Indeed, a fundamental concept in the BLISS methodology is that in a system optimization the contributing disciplines should not optimize themselves for a traditional, discipline-specific objective such as the minimum weight or similar, but they should optimize themselves for a synthetic objective function that measures the influence of the design variables $X_r$ of a specific $BB_r$ on the entire system objective function. In an explicit form Eq. 1.17 can be written as

$$\phi_2 = D(y_{1,i}, x_{2,1})^T \Delta X_{2,1} + D(y_{1,i}, x_{2,2})^T \Delta X_{2,2} + D(y_{1,i}, x_{2,j})^T \Delta X_{2,j}; \quad j = 1..NX_2 \tag{1.18}$$

thus, the $BB_2$ objective function can be regarded as a multi-objective function composed by the sum of the local design variables weighted by their influence on the single objective of the whole system[6]. Hence, after defining the local objective function, a local optimization problem has to be solved for the considered $BB_2$. Analogous procedure has to be adopted for $BB_1$ and $BB_3$. All the three problems are independent, thus they can be solved concurrently. Thus, a first improvement of the given system results from the optimization at the subsystems level. It is worth to remember that this first step in the adoption of the BLISS method has been performed considering frozen the $Z$ variables.

**System-level optimization**

In the second step the BLISS architecture determines the system-level optimization by the use of the $Z$ variables. In particular, the influence of $Z$ on $\Phi = y_{1,i}$ has to be explored, that is, the derivatives $D(y_{1,i}, Z)$ have to be evaluated. The way to calculate such derivatives can differ giving rise to different version of the BLISS method well known in literature (see [15]). Thus, in summary, an improvement in the second step is achieved through the system-level variables $Z$, then this improvement is linked to the previous first step performed by the use of the derivatives of optimum with respect to parameters $Z$ and $Y$. The obtained derivatives are adopted to extrapolate each subsystem optimum as a function of $Z$ and $Y$. The functional relationship $Y = Y(Z)$ can be approximated by extrapolation that are based on

[6]This is true also in the particular $BB_r$ where $\Phi$ has been computed. Indeed has been chosen $\Phi = y_{1,i}$ but in $BB_1$ the expression of $\phi_1$ will have an analogous form of Eq. 1.18.

the system-level sensitivity analysis. The summarized procedure has to be performed till convergence. As mentioned, since its first version, several have been the studies and the test performed in literature addressed to the BLISS methodology and that prove its efficiency in the field of the optimization methods by decomposition (e.g. see [18], [16], [15], [19], [20]).

Finally, it is worth to underline that the modularity of the BLISS architecture permits the replacement or the addition of black-boxes with large flexibility. Furthermore, tools of different level of fidelity in the considered black-boxes allow the application of the BLISS methodology in different design phases with efficient improvement of detail in the global design.

# Chapter 2

# Multidisciplinary Aircraft desiGn of Innovative Configurations

## 2.1 Introduction

The aim of this chapter is to present an MDO procedure and an associated survey of the work code called MAGIC, (Multidisciplinary Aircraft desiGn of Innovative Configurations), for conceptual design of aircraft configurations in civil aviation. The algorithms used in MAGIC for modeling structures, aerodynamics, and aeroelasticity are first-principles based, since for innovative configurations the designer cannot rely upon past experience. In addition, the conceptual design is emphasized: thus, the algorithms used must be accurate and efficient, so as to produce accurate predictions with a relatively small computational effort. In other words, the numerical algorithms used should be very efficient and at the same time adequately accurate and apt to be refined as much as necessary.

A second crucial aspect is that the code MAGIC is at the moment geared specifically towards civil aviation applications; hence, advantage is taken of this aspect whenever possible, for instance in the use of potential flows (*i.e.*, flows that are potential everywhere except for a zero–thickness wake surface emanating from the trailing edge), which are combined with integral boundary layers for the analysis of viscous effects. In summary, the physical models chosen must be able to capture the essence of the phenomenon within the specific application of interest, thereby avoiding any unnecessary sophistication.

Another crucial aspect in developing the code MAGIC is that strong emphasis has to be given to the integration of the various disciplines. This implies not only that a special care has to be given to

the interfaces, but also that the concurrency of certain types of analysis has to be exploited whenever possible. For instance, the fact that the natural modes of vibration must be evaluated for the dynamic aeroelastic analysis implies that a modal analysis may be used for the stress and buckling analyses as well. Similar considerations hold for steady and unsteady aerodynamics algorithms.

Furthermore, the optimization algorithm implemented in MAGIC has to be introduced and discussed as well as the efficiency and the potentiality[1]of the code as an MDO tool has to be explained. Thus, in the following of the chapter, after an overview of the code architecture, a section about the insertion of MAGIC in the MDO broad field of formulation scenario will be considered. In addition, some results concerning the use of MAGIC for the multidisciplinary design optimization of aircraft configuration, with emphasis on the preliminary design stages, will be addressed.

## 2.2 Structure of the code

A concise presentation of the structure of the code MAGIC accounting the main modules implemented will be given meanwhile explaining the theoretical fundamentals adopted. Furthermore, a brief general overview of its potentiality will be addressed as well.

### 2.2.1 MAGIC optimizer

The optimization core implemented in MAGIC numerically solves a sequential unconstrained minimization problem SUMT (*Sequential Unconstrained Minimization Thecnique*) by the use of the method of the quadratic extended interior penalty function.

A detailed exposition of the penalty function method is referred in Ref. [2], however it seems appropriate to give some guidelines about it in order to provide a more precise overview of the code MAGIC. Hence, a general problem of constrained optimization can be stated as

$$\begin{aligned} &\min f(x) \\ &s.t. \quad h_i(x) = 0 \quad i = 1, .., n_h \\ &\qquad g_j(x) \geq 0 \quad j = 1, .., n_g \end{aligned} \tag{2.1}$$

where $f(x)$ represents the objective function, $x$ is the design variable vector, $n_h$ and $n_g$ are the numbers of equality constraints $h_i$ and of inequality constraints $g_j$ respectively. Thus, the penalty function method

[1]Such as the different kind of foils profile that can be rated or as the interaction of the fuselage and engines that can be taken int account since the complete aircraft is considered.

in its more general version substitutes to the general stated problem in eq. 2.1 an unconstrained problem of the kind

$$\begin{aligned} &\min \phi(x,r) = f(x) + r\sum_{i=1}^{n_h} h_i^2(x) + r\sum_{j=1}^{n_g}\langle -g_j\rangle^2 \\ &r = r_1, r_2, .. \quad r_i \to \infty \end{aligned} \tag{2.2}$$

being $\phi$ the so-called penalty function, $r$ the penalty factor and indicating by $\langle a\rangle$ the positive part of $a$. The basic idea of the method is to associate a penalty to any violation of a constraint. More precisely, the mentioned method is called *exterior penalty function* since the penalties are added only in the exterior of the feasible domain. As shown in Eq. 2.2 the most common version of the exterior penalty function associates a penalty that is proportional to the square of the violation. The inequality terms are treated separately from the equality ones since the penalty applies only for constraint violations. The penalty factor $r$ is a positive multiplier that controls the magnitude of the penalty terms. However, the exterior penalty function method can produce a design that moves in the unfeasible domain since the constraints contribute to the penalty terms only when they are violated. To overcome this drawback it is possible to define an *interior penalty function* that holds the design in the feasible domain. An expression of the interior penalty function that is applicable when there are only inequality constraints can be found in Ref. [2]. The idea of the interior penalty function method is to define a penalty term proportional to $1/g_j$ that becomes infinitely large at the boundary of the feasible domain defining a barrier to the feasible domain itself. A combination of the exterior and interior penalty function is implemented in MAGIC and is called quadratic extended interior penalty function an its expression can be stated as

$$\begin{aligned} &\phi(x,r) = f(x) + r\sum_{j=1}^{n_g} p[g_j(x)] \\ &r = r_1, r_2, .. \quad r_i \to 0 \quad r_i > 0 \end{aligned} \tag{2.3}$$

where

$$p(g_j) = \begin{cases} \frac{1}{g_j} & g_j \geq g_0 \\ \frac{1}{g_0}[3 - 3(g_j/g_0) + (g_j/g_0)^2] & g_j < 0 \end{cases} \tag{2.4}$$

The term $g_0$ is a transition parameter that defines the limit between the exterior and interior part of the penalty terms and it has to be chosen such that the penalty represented by $rp(g_j) \to \infty$ for $g_j < 0$ and $r \to 0$. The subroutine of MAGIC that allows to evaluate the objective, the penalty and the pseudo-objective functions referring to the updated value of the project variables is called *FEVAL (Function EVALuation)*.

Then, the multi-dimensional unconstrained minimization of the pseudo-objective function is achieved by a quasi-Newton method like, for example, the BFGS (Broyden-Fletcher-Goldfarb-Shanno) algorithm.

The subroutine implemented in MAGIC for evaluating the minimum of an unconstrained multi-variable function is named *UFMIN (Unconstrained Function Minimization)*. For such evaluation several methods are listed in UFMIN and can be selected by switching the value of the parameter called IBFGS. The methods considered are

- Davidon-Fletcher-Powell(DFP),
- Broyden-Fletcher-Goldfarb-Shanno (BFGS),
- conjugate gradient,
- steepest descent,
- univariate search.

Hence, once the search direction has been identified, the mono-dimensional minimization is performed along the direction indicated by one of the previous proposed methods adopting an uni-variant method of zero order, like the quadratic interpolation. The subroutine of MAGIC that allows the mono-dimensional minimization is *ONED (ONE Dimensional)*. The interface between the optimizer and the analysis modules is managed by the subroutine *ANALYS (ANALYSis)*. Hence, ANALYS allows to formulate the objective function and the constraints.

**Design variables**

The code MAGIC is capable of performing the multidisciplinary integrated optimization even of innovative aeronautical configurations. Furthermore, even considering very complex geometries, the code is able to account in the optimization the conventional system wing-tail. Indeed, the total aerodynamic surface is defined by different component portions then, at each portion is assigned a set of independent design variables and a connection vector indicative of the position of the considered aerodynamic portion respect to the others portions and to the fuselage. Some congruence equations assure the connection between contiguous parts. The design variables of each portion can be chosen between the following listed variables:

- $(1, 2, 3)$ leading edge coordinates of the first border[2] $x_{LE}, y_{LE}, z_{LE}$
- $(4, 5)$ chord at the first and second border $C_1, C_2$
- $(6)$ span $B$

[2]First and second border of each portion are considered in sequence on an abscissa defined on the elastic axis.

- $(7, 8)$ airfoil normalized thickness at the first and second border $t/c_1, t/c_2$
- $(9, 10)$ skin thickness at the first and second border $th_{S_1}, th_{S_2}$
- $(11, 12)$ spar thickness at the first and at the second border $th_{SW_1}, th_{SW_2}$
- $(13, 14)$ percentage position of the elastic center on the chord at the first and second border $r_{SC_1}, r_{SC_2}$
- $(15, 16)$ area of the stiffener at the first and second border $x_{LE}, y_{LE}, z_{LE}$
- $(17, 18)$ built-in angle at the first and second border $\alpha_{B_1}, \alpha_{B_2}$
- $(19)$ sweep angle at $1/4$ chord $\Lambda$
- $(20)$ dihedral angle $\Delta$

Besides the mentioned geometrical variables, descriptive of the aerodynamic surfaces, there are other variables that can be considered and that have more general features as:

- weight of the payload $W_{PL}$
- weight of the available fuel $W_{UF}$
- length of the fuselage $L_f$
- diameter of the fuselage $D_f$
- width of the fuselage $W_f$

In the code the design variables are given in input as row vectors. The meaning of each component of the mentioned vector is: the initial value of the considered variable, a switch parameter that allows to consider the variable as an active one or not, the lower boundary, the upper boundary, a scale factor, the step for the evaluation of the finite differences (for the gradient evaluation), the typology of the considered variable (solid geometry or surface geometry or so on). As known, the active variables are the one that can be modified during the optimization process. In Magic they are normalized respect to their starting value[3] and they are listed in a specific vector so that at any step that requires it, the updated value can be easily accessed. Instead, the updated value of the not-active design variables coincides always with their starting value. Regarding the algorithmic structure of the code the design variables are considered as pertaining to two main groups:

[3]If the starting value is zero an automatic process of normalization is available.

- *variables of surface geometry* such as the wing chord or the sweep angle and so on. These kind of variables determine a change in the aerodynamic paneling and in the relative positions of two panels. Thus, the surface geometry variables affect the evaluation of the partial aerodynamic matrices.
- *variables of solid geometry* such as the spar thickness and the skin thickness. The contribution of these variables to the evaluation of the partial aerodynamic matrices is practically equal to zero.

When an active design variable is modified by the optimization process, the aerodynamic matrix is evaluated again only if the variable was pertaining to the surface geometry set, otherwise the same aerodynamic matrix of the previous step is maintained for the updated value as well.

**Constraints**

Several kinds of constraints are currently listed in the code MAGIC. It is worth to note that the code allows to include new constraints at any time. The insertion of a new constraint respect to the one already implemented has to be done adding a parameter indicative of the activity or not activity of the constraint. For numerical reasons the constraint are considered as normalized. The currently available constraints are:

- performance
  - minimal range $g_1 = 1 - \frac{R}{R_{min}} \leq 0$
  - volume of available fuel $g_2 = \frac{V_F}{V_{AF}} - 1 \leq 0$
  - minimal aerodynamic efficiency $g_3 = 1 - \frac{E}{E_{min}} \leq 0$
  - maneuverability $g_4 = \frac{C_{m\alpha}}{C_{m\alpha max}} \leq 0$
  - limitation on the load factor $g_5 = \frac{\Delta n}{\Delta n_{max}} - 1 \leq 0$
- structural
  - maximum normal stress $g_6 = \frac{\sigma}{\sigma_{max}} - 1 \leq 0$
  - maximum shear stress $g_7 = \frac{\tau}{\tau_{max}} - 1 \leq 0$
  - buckling $g_8 = 1 - \frac{\lambda}{\lambda_{cr}} \leq 0$
- aeroelastic
  - minimum flutter speed $g_9 = 1 - \frac{U_F}{U_{Fmin}} \leq 0$
  - minimum divergence speed $g_{10} = 1 - \frac{U_D}{U_{Dmin}} \leq 0$
- vertical equilibrium

– right lift-weight constraint $g_{11} = -1 - a\frac{L-W}{L} \leq 0$

– left lift-weight constraint $g_{12} = b\frac{L-W}{L} - 1 \leq 0$

**Objective function**

Only a brief reminder about the objective function will be given since in the code MAGIC it is possible to consider a broad variety of objective functions. Most generally a multi-objective function is considered and it can be given for example by the weighted average of the empty aircraft weight, the useful fuel weight, the payload weight, the range, and the aerodynamic efficiency. In the application that will follow the objective function will be always previously introduced. The code allows also to consider any kind of functional relationship for the objective function that is not only a weighted average functional relationship can be adopted.

### 2.2.2 MAGIC modeling and analysis modules

Thus, the optimizer of MAGIC interfaces itself with several different modules variously coupled. The modules can be subdivided in *modeling modules* and *disciplinary analysis modules*. The modeling modules concern the geometry generation and the discretization and they can be listed as

- Surface geometry generator: the wing surface is topologically generated relying on geometrical design variables and geometrical parameters previously fixed in the subroutine called *SURFGEOM (SURFace GEOMetry)*.
- Solid geometry generator: is the modeling module that constitutes the pre-processor for the finite element method. Thus, the geometrical and inertial features of the structural elements of the wing are evaluated in a subroutine called *FEMPREPROC-RC*. The subroutine shows also some flags to take into account the contribution of the engines and of the fuel stored in the wing.
- FE (finite element) and BEM (boundary element) mesh generator: the code MAGIC can both adopt the implemented procedure for the finite element method relying on a subroutine called FEM-RC, or interface the commercial code MSC -NASTRAN for the finite element analysis. Particularly, the MSC-NASTRAN analysis that actually the code can interface are the dynamical solution *(SOL*103*)* that gives the frequencies of vibration and the modal deformations, the statical solution *(SOL*101*)* that gives the displacements and the stresses, and the buckling solution *(SOL*105*)*.

Then, the disciplinary analysis modules are the analysis modules capable to give an evaluation of the updated objective function and of the constraints. The disciplinary analysis are managed by the

subroutine *ANAMDLN (ANAlysis MoDuLes)* that administrates the input and output variables of each disciplinary module as well as the interconnection between the disciplines and the updated data needed for the evaluation of the constraints and of the objective function. Thus, in the following are listed the blocks that constitute the disciplinary analyses accounted in MAGIC. For some of them will be given some brief information. The others will be more widely discussed in the following of the chapter since they have been studied in deeper detail for obtaining the numerical result of the optimization runs performed in the applicative part of this thesis. Thus, the disciplinary analysis modules implemented in the code are given by:

- static and dynamic structural analysis,
- buckling analysis,
- aircraft weights and centers of gravity estimation: in the subroutine *WEST (Weight ESTimator)* the aircraft weights and the weight at the take-off are evaluated by a recursive procedure due to Corning for the preliminary design of subsonic aircraft. The subroutine is capable to evaluate also the centers of gravity of each component as well as the center of gravity of the whole aircraft,
- steady and unsteady potential aerodynamics analysis,
- steady viscous aerodynamics: in the subroutine called *EDET (Empirical Drag Estimation Technique)* are evaluated the total drag coefficient in cruise as well as the aerodynamic efficiency by a built-up technique called DELTA method that consists in a semi-empirical method (viscous correction) ,
- steady and unsteady aeroelastic analysis,
- performances analysis: this module provides the evaluation of the range by the use of the Breguet formula. The subroutine that performs this evaluation is called *XRANGE*.
- static longitudinal stability analysis: the static longitudinal stability of the whole aircraft is evaluated mainly in two subroutines called *STDER (STability DERivatives)* and *FLYMECH (FLIght MECHanics)* by the evaluation of any stability derivatives,
- gust response analysis: the subroutine *GUST* utilizes the Pratt formula for the maximum increase of the load factor due to a vertical gust.

### 2.2.3 Static and dynamic structural analysis

The model utilized in the applicative section of this chapter for the structural analysis is that given by a Finite Element (FE) commercial code[21, 22] and it consists of a set of various beam, rod, and plate

elements that built a final wing-box or wing model. The input/output files for the FE modeling are actually the interface with the MDO optimizer.

Using the Galerkin method, *i.e.*, setting

$$\mathbf{u}(\xi^\alpha, t) = \sum_{j=1}^{N} u_j(t)\boldsymbol{\psi}_j(\xi^\alpha), \tag{2.5}$$

where $\xi^\alpha$ are the material curvilinear coordinates and $\boldsymbol{\psi}_j(\xi^\alpha)$ are the base functions, and projecting in the direction of the base function $\boldsymbol{\psi}_j(\xi^\alpha)$, one obtains

$$\mathsf{M}\ddot{\mathsf{u}} + \mathsf{K}\mathsf{u} = \mathsf{f}, \tag{2.6}$$

where $\mathsf{u} = \{u_i\}$ is the state vector, whereas $\mathsf{f} = \{f_j\}$ is the external load vector, with

$$f_j := -\oint_{S_B} p\mathbf{n} \cdot \boldsymbol{\psi}_j d\mathcal{S} \tag{2.7}$$

(note that $\mathsf{f}$ depends upon $\mathsf{u}$ in aeroelastic applications). Equation 2.6 is used for both statics (in stress analysis) and dynamics (in the aeroelastic analysis; divergence and flutter are dealt with the same algorithm). In the first case, the inertial terms vanish, and Eq. 2.6 is used to determine the displacement vector $\mathsf{u}$, and from this the maximum stress. Furthermore, as concerning the buckling analysis, when a static load is assigned (*e.g.*, the aerodynamic static load on a wing), following a linear buckling analysis procedure,[21] the static load $\mathsf{f}_s$ can be rewritten as function of state-space vector $\mathsf{u}$ as $\mathsf{f}_s = \mathsf{K}_d\mathsf{u}$ where $\mathsf{K}_d$ is the so called differential matrix. Thus, the linear buckling analysis consist to solve the eigenproblem

$$(\mathsf{K} - \lambda\mathsf{K}_d)\,\mathsf{u}_b = 0 \tag{2.8}$$

giving as critical load multiplier $\lambda_c$ the smallest eigenvalue $\lambda$ between those evaluated.

In the second case, Eq. 2.6 is used to determine the natural modes. In this case, the forcing term vanishes and the associated eigenproblem is given by

$$-\omega_n^2\mathsf{M}\mathsf{z}_n + \mathsf{K}\mathsf{z}_n = \mathbf{0}. \tag{2.9}$$

where $\omega_n$ $(n = 1, ..., N)$ denotes the $n$th natural frequency, corresponding to the eigenvector $\mathsf{z}_n = \{z_{n_i}\}$, here assumed to be normalized. The approximate normalized modes of vibration are given by (according to Eq. 2.5)

$$\boldsymbol{\Phi}_n(\xi^\alpha) = \sum_{j=1}^{N} z_{n_j}\boldsymbol{\psi}_j(\xi^\alpha). \tag{2.10}$$

The solution of the above eigenproblem is used to model the wing dynamics using a modal approach. The material–point displacement field is expressed in terms of the approximate modes of vibration as

$$\mathbf{u}(\xi^\alpha, t) = \sum_{m=1}^{M} q_m(t) \mathbf{\Phi}_m(\xi^\alpha). \tag{2.11}$$

[Note that typically $M \ll N$ (*i.e.*, the modes required are much less than the finite–element degrees of freedom necessary to evaluate the modes). This is the main reason to prefer an expansion in terms of approximate modes, instead of the finite–element shape functions, $\boldsymbol{\psi}_j(\xi^\alpha)$ (for a deeper analysis of this point, see Ref. [23]). The corresponding Galerkin equations (which coincide with the Lagrange equations of motion) are

$$\ddot{\mathsf{q}} + \Omega^2 \mathsf{q} = \mathsf{e}, \tag{2.12}$$

where $\mathsf{q}$ denotes the Lagrangian–coordinate vector, $\Omega^2$ the square of the diagonal matrix of the wing natural frequencies, and $\mathsf{e} = \{e_n\}$ the vector of the generalized forces,

$$e_n = -\oint_{S_B} p\mathbf{n} \cdot \mathbf{\Phi}_n d\mathcal{S}. \tag{2.13}$$

Note that Eq. 2.12 may be also obtained by diagonalization and truncation of Eq. 2.6. Indeed, comparing Eqs. 2.5, 2.10 and 2.11, we see that $\mathsf{e} = \mathsf{Z}^{\mathrm{T}}\mathsf{f}$, where $\mathsf{Z} = [z_{jn}]$ (with $z_{jn} = z_{n_j}$) is the so–called modal matrix.

### 2.2.4 Aerodynamic modeling

As mentioned above, the basic physical model used for aerodynamics is that of quasi–potential flows, *i.e.*, flows that are potential everywhere except for the wake surface, $\mathcal{S}_W$, which is the locus of the points emanating from the trailing edge. [The effects of viscosity are included through an elementary boundary–layer model (based on the Blasius flat plate solution), which gives an adequate estimate for the viscous drag; for more sophisticated viscous models in MAGIC, not included here for simplicity, see Ref. [23].]

For the sake of simplicity the quasi–potential formulation is outlined here only for incompressible flows (for details, see Refs. [24] and [25]). The extension of the formulation which includes the effects of compressibility is available (Refs. [26] and [24]), is included in MAGIC (Ref. [27]).

An inviscid, incompressible, initially–irrotational flow remains, at all times, quasi–potential, as defined above. In this case, the velocity field, $\mathbf{v}$, may be expressed as $\mathbf{v} = \nabla\varphi$ (where $\varphi$ is the velocity potential).

Combining with the continuity equation for incompressible flows, $\nabla \cdot \mathbf{v} = 0$, yields

$$\nabla^2 \varphi = 0. \tag{2.14}$$

The boundary conditions for this equation are as follows. The boundary surface (surface of the aircraft) $\mathcal{S}_B$ is assumed to be impermeable. This implies $(\mathbf{v} - \mathbf{v}_B) \cdot \mathbf{n} = 0$, *i.e.*,

$$\frac{\partial \varphi}{\partial n} =: \chi = \mathbf{v}_B \cdot \mathbf{n} \qquad (\mathbf{x} \in \mathcal{S}_B), \tag{2.15}$$

where $\partial/\partial n = \mathbf{n} \cdot \nabla$, whereas $\mathbf{v}_B$ is the velocity of a point $\mathbf{x} \in \mathcal{S}_B$, and $\mathbf{n}$ is the outward unit normal to $\mathcal{S}_B$. At infinity, in a frame of reference fixed with the unperturbed air, we set $\varphi = 0$. The boundary conditions on the wake surface, $\mathcal{S}_W$, are obtained from the conservation of mass and momentum across a surface of discontinuity, and are: $(i)$ the wake surface is impermeable, and $(ii)$ the pressure, $p$, is continuous across it. These imply: $(i)$ $\Delta(\partial\varphi/\partial n) = 0$ (where $\Delta$ denotes discontinuity across $\mathcal{S}_W$), and $(ii)$ $\Delta\varphi =$ constant in time following a wake point $\mathbf{x}_W$, the velocity of which is, by definition, the average of the fluid velocity on the two sides of the wake. Thus, $\Delta\varphi(\mathbf{x}_W, t)$ equals the value it had when $\mathbf{x}_W$ left the trailing edge:

$$\Delta\varphi(\mathbf{x}_W, t) = \Delta\varphi(\mathbf{x}_{TE}, t - \tau) \tag{2.16}$$

where $\tau$ is the convection time from $\mathbf{x}_{TE}$ to $\mathbf{x}_W$. The value of $\Delta\varphi$ at the trailing edge is obtained by imposing the trailing–edge condition that, at the trailing edge, $\Delta\varphi$ on the wake equals $\varphi_2 - \varphi_1$ on the body, where the subscripts 1 and 2 denote the two sides of the wing surface (for a detailed analysis of this issue, see Ref. [25]).

In the methodology used in the code MAGIC, the above problem for the velocity potential is solved by boundary elements. In formulating unsteady aerodynamics (used for flutter analysis), the problem is linearized: this implies that the wake surface is considered as fixed in the body frame of reference (specifically, composed of vortex lines parallel to the undisturbed velocity; accordingly $\tau = (x_W - x_{TE})/U_\infty$). Traditionally, the problem is then formulated in the frequency domain, *i.e.*, by assuming that the aerodynamic input is of the $e^{i\omega t}-$type, so that one may assume that $\varphi(\mathbf{x}, t) = \tilde{\varphi}(\mathbf{x})\ e^{i\omega t}$. We prefer to conceive the formulation in terms of the Laplace transform, using an approach introduced in Ref. [28]. It may shown that the Laplace–transform solution is the analytic continuation in the complex $s$–plane of the frequency–domain solution (along the imaginary axis; see Ref. [29]). Thus, in the two cases one obtains the same expressions – however, the use of the Laplace transform allows one to have a solution even off the imaginary axis. Then, the boundary integral representation for the above problem is given by (here $\tilde{}$ denotes Laplace–transformed functions)

$$\tilde{\varphi}(\mathbf{x}) = \int_{\mathcal{S}_B} \left( G\tilde{\chi} - \tilde{\varphi}\frac{\partial G}{\partial n} \right) d\mathcal{S}(\mathbf{y}) + \int_{\mathcal{S}_W} \Delta\tilde{\varphi}_{TE} e^{-s\tau} \frac{\partial G}{\partial n} d\mathcal{S}(\mathbf{y}), \tag{2.17}$$

where $\tilde{\chi}$ denotes the Laplace transform of the unsteady portion of $\mathbf{v}_B \cdot \mathbf{n}$, whereas $G = -1/4\pi\|\mathbf{y} - \mathbf{x}\|$. Note that, by applying the trailing–edge condition, $\Delta\tilde{\varphi}_{TE}$ may be expressed in terms of $\tilde{\varphi}$ over the body. Thus, Eq. 2.17, in the limit as $\mathbf{x}$ tends to $\mathcal{S}_B$, represents a boundary integral equation for $\tilde{\varphi}$ on $\mathcal{S}_B$, with $\chi$ on $\mathcal{S}_B$ known from the boundary condition. Once $\tilde{\varphi}$ on $\mathcal{S}_B$ is known, $\tilde{\varphi}$ (and hence $\mathbf{v}$ and, by using Bernoulli's theorem, $p$) may be evaluated everywhere in the field.

In MAGIC, this boundary integral equation is solved numerically by discretizing the body and wake surfaces with quadrilateral elements, assuming $\tilde{\varphi}$, $\tilde{\chi}$, and $\Delta\tilde{\varphi}$ to be constant within each element, and imposing that the integral equation be satisfied at the center of each surface element (zeroth–order boundary–element collocation method). This yields

$$\tilde{\mathsf{f}}_{\varphi} = \mathsf{E}_{IE}\tilde{\mathsf{f}}_{\chi} \tag{2.18}$$

where $\tilde{\mathsf{f}}_{\varphi} = \{\tilde{\varphi}_j\}$ and $\tilde{\mathsf{f}}_{\chi} = \{\tilde{\chi}_j\}$ are the vectors of the values of $\tilde{\varphi}$ and $\tilde{\chi}$ at the centers of the elements (see Ref. [30] for details).

### 2.2.5 Aeroelastic analysis

It is known that in linear unsteady aerodynamics, the frequency $\omega$ always appears together with the air speed $U_\infty$, through the dimensionless parameter $k = \omega\ell/U_\infty$, known as the reduced frequency ($\ell$ is a reference length). Accordingly, in our case, we formulate the problem in terms of the dimensionless Laplace parameter $\check{s} = s\ell/U_\infty$, also known as complex reduced frequency; for, if $\omega = Imag(s)$, then $k = Imag(\check{s})$ (here, the symbol $p$ typically used for the complex reduced frequency is avoided, since it is used to denote pressure). Then, we have

$$\tilde{\mathsf{e}} = q_D \; \mathsf{E}(\check{s}) \; \tilde{\mathsf{q}} \tag{2.19}$$

where $q_D$ is the dynamic pressure. [Again, it may be shown that $\mathsf{E}\,(\check{s})$ is the analytic continuation of $\mathsf{E}\,(ik)$ from the imaginary axis to the complex plane.] The specific expression for the matrix of the generalized aerodynamic forces, $\mathsf{E}(\check{s})$, in Eq. 2.19 may be obtained as

$$\mathsf{E}(\check{s}) = q_D \; \mathsf{E}_{GF}\mathsf{E}_{BT}(\check{s})\mathsf{E}_{IE}(\check{s})\mathsf{E}_{BC}(\check{s}) \tag{2.20}$$

where:

($i$) the matrix $\mathsf{E}_{BC}(\check{s})$ is obtained from the boundary condition (Eq. 2.15, *i.e.*, $\chi = (U_\infty\mathbf{i} + \sum_n \dot{q}_n\mathbf{\Phi}_n)\cdot(\mathbf{n}_0 + \sum_m \Delta\mathbf{n}_m q_m)$, where $\mathbf{n}_0$ is the unit normal to the undeformed surface and $\Delta\mathbf{n}_m$ is the variation of $\mathbf{n}$ due to $q_m$), and relates the Laplace–transformed vector $\tilde{\mathsf{f}}_{\chi} = \{\tilde{\chi}_n/U_\infty\}$ of the dimensionless

linear unsteady portion of the normalwash, evaluated at the element centers, to the Laplace–transformed Lagrangian–coordinate vector $\tilde{\mathsf{q}} = \{\tilde{q}_n\}$, as $\tilde{\mathsf{f}}_\chi = \mathsf{E}_{BC}\,\tilde{\mathsf{q}}$;

(*ii*) the matrix $\mathsf{E}_{IE}(\check{s})$ is obtained from the discretization of the integral equation, and relates the Laplace–transformed vector of the dimensionless velocity potential, $\tilde{\mathsf{f}}_\varphi = \{\tilde{\varphi}_n/U_\infty\ell\}$, evaluated at the element centers, to $\tilde{\mathsf{f}}_\chi$, as $\tilde{\mathsf{f}}_\varphi = \mathsf{E}_{IE}\tilde{\mathsf{f}}_\chi$ (see Eq. 2.17);

(*iii*) the matrix $\mathsf{E}_{BT}(\check{s})$ is obtained from the discretization of the linearized Bernoulli theorem, $c_p = -2(\dot{\varphi} - U_\infty\partial\varphi/\partial x)/U_\infty^2$, and relates the Laplace–transformed vector of the pressure coefficient evaluated at the element centers, $\tilde{\mathsf{f}}_{c_p}$, to $\tilde{\mathsf{f}}_\varphi$, as $\tilde{\mathsf{f}}_{c_p} = \mathsf{E}_{BT}\tilde{\mathsf{f}}_\varphi$;

(*iv*) the matrix $\mathsf{E}_{GF}$ is obtained from the discretization of Eq. 2.13, and relates the Laplace–transformed vector of the generalized aerodynamic forces, $\tilde{\mathsf{e}}$, to $\tilde{\mathsf{f}}_{c_p}$, as $\tilde{\mathsf{e}} = q_D\mathsf{E}_{GF}\tilde{\mathsf{f}}_{c_p}$.[4]

In order to perform the aeroelastic analysis in the framework of the optimization procedure, a finite–state approximation (reduced order model, ROM) for the aerodynamic matrix $\mathsf{E}(\check{s})$ is considered. Specifically, following Ref. [29], the transcendental function $\mathsf{E}(\check{s})$ is approximated as

$$\mathsf{E}(\check{s}) \simeq \mathsf{E}_2\check{s}^2 + \mathsf{E}_1\check{s} + \mathsf{E}_0 + (\check{s}\mathsf{I} - \mathsf{P})^{-1}\,\mathsf{R}, \tag{2.21}$$

where all the matrices on the right hand side are evaluated by a least–square procedure on a suitable set of aerodynamic data. Substituting Eq. 2.21 into Eq. 2.12, setting $\tilde{\mathsf{r}} := -(\check{s}\mathsf{I} - \mathsf{P})^{-1}\,\mathsf{R}\tilde{\mathsf{q}}$, and introducing the matrices $\mathsf{M}_e := \mathsf{I} - \frac{1}{2}\rho_\infty\ell^2\mathsf{E}_2$, $\mathsf{C}_e := -\frac{1}{2}\rho_\infty U_\infty\ell\mathsf{E}_1$, and $\mathsf{K}_e := \Omega^2 - q_D\mathsf{E}_0$ one obtains, in the time domain,

$$\left\{\begin{array}{c}\dot{\mathsf{x}}_1\\ \dot{\mathsf{x}}_2\\ \dot{\mathsf{x}}_3\end{array}\right\} = \left[\begin{array}{ccc}\mathsf{I} & 0 & 0\\ 0 & \mathsf{M}_e & 0\\ 0 & 0 & \ell\mathsf{I}/U_\infty\end{array}\right]^{-1}\left[\begin{array}{ccc}0 & \mathsf{I} & 0\\ -\mathsf{K}_e & -\mathsf{C}_e & -q_D\mathsf{I}\\ -\mathsf{R} & 0 & \mathsf{P}\end{array}\right]\left\{\begin{array}{c}\mathsf{x}_1\\ \mathsf{x}_2\\ \mathsf{x}_3\end{array}\right\} \tag{2.22}$$

with $\mathsf{x}_1 := \mathsf{q}$, $\mathsf{x}_2 := \dot{\mathsf{q}}$, and $\mathsf{x}_3 := \mathsf{r}$. Thus, the system has been reduced to the standard state–variable format, $\dot{\mathsf{x}} = \mathsf{A}(U_\infty)\mathsf{x}$, where the parametric dependence of the matrix $\mathsf{A}$ on the air speed has been emphasized. This approach allows one to reduce the aeroelastic stability analysis to a root locus for the matrix $\mathsf{A}(U_\infty)$, thereby avoiding standard methods (*e.g.*, $k$ and $p$–$k$ method), which are cumbersome and would unnecessarily complicate the optimization process.

[4]Note that $c_p = 2(p - p_\infty)/\rho_\infty U_\infty^2$ and hence there exists a contribution from $p_\infty$; however, this is steady–state and hence it is not included in the unsteady formulation. In any event, it is typically negligible – and zero for rigid–body modes, since (see Eq. 2.13) $\int_{\mathcal{S}} p_\infty\mathbf{n}\cdot\mathbf{\Phi}_j d\mathcal{S} = p_\infty\int_{\mathcal{V}_\mathcal{S}}\mathrm{div}\,\mathbf{\Phi}_j d\mathcal{V}$.

## 2.3 The code MAGIC in the MDO formulations scenario

Before placing the code MAGIC in the broad scenario of the MDO formulations that have been briefly introduced in the first chapter, it is worth to underline some current challenges and try to understand the future trends of the MDO field. Indeed, such considerations will help also in understanding the relevance of the code MAGIC and in deeper perceiving the potentiality of the mentioned code.

The observations that follow are mainly based on what stated in an interesting MDO colloquium hosted by the *German Aerospace Center* in Goettingen, Germany in May 2006 (see Ref. [3]). About seventy participants from industry, academia and government attended the workshop and enriched it carrying their own point of view but also focusing some aspects that are objective. Thus, the workshop featured a valuable set of presentations, contributions and discussions. Furthermore, rather than dwelling extensively on the accomplishments made in the past in the MDO field, or in the current capabilities of such topic, the focus of the meeting has been posed in the needs and in some identified shortcomings which lead to potential future research directions.

Hence, a first drawback enlightened in that contest is the lack of education about the MDO topics not only at the university level but also within industry and research organizations as well. Regarding the university level, it has been reported that in the past ten years a relatively conspicuous growth has been observed in the number of dedicated MDO courses taught to graduate level students. Nevertheless, quoting [3] *"many of these classes are taught as applied math courses whose target audiences are limited in scope and often do not include design engineers."* Furthermore, even in the case of industry and research the MDO practices are not often realized in the early stages of design or research development. Thus, this aspect shows a lack of education between and within these respective institutes where the engineers who can benefit most from MDO applications are often not aware of what is available in the MDO field until after preliminary design phases are complete.

Another concern pertains the consideration that an adequate number of real-world test cases to which the MDO methods can be applied in an academic setting are still missing from the educational toolbox. The reason of that may partially be due to the fact that the relationship between industry and academia has not yet reached its full potential. Indeed, the models required for worthwhile MDO analysis (that means for example applying an MDO method to a complete real-world aircraft configuration) are commercially sensitive data that the industry does not intend to release to external parties. Furthermore the inherent "multi-disciplinary" of the MDO field means that the required models cannot be limited to few components, but rather must provide a relatively comprehensive representation of the designed system. Hence, this leads often the university to depend on self-developed test cases that generally are quite simplified and do not adequately represent the real-world complexities of industrial applications.

Then, a central problem inherent to the successful application of MDO is that it requires a broad

range of discipline engineers who understand MDO concept and methods. Quoting [3]: *"It is not enough to integrate an MDO specialist into an organization and expect this person to exercise the necessary discipline expertise to correctly formulate the design problem, make adjustments when necessary, and evaluate the results at the end. The amount of information and the complexity of the problem are simply too large. To remedy this, there are several recommendations that may improve the education of upcoming design engineers such that the MDO mindset diffuses down to even the lowest levels of the design organization."* It seems appropriate to underline that this instruction should approach the MDO field from a physical perspective rather than a mathematical one and should not focus so much on details of the algorithms but rather on their use.

Respect to the underlined consideration the code MAGIC can offer some interesting cues. Indeed, as previously mentioned, MAGIC presents the possibility of accounting the whole aircraft during the optimization process. Thus, even if it is still far from a real-world test case wished by the industry fields, the code MAGIC is able to give a more sensible sensation of what a real-world optimization process is. Furthermore, the desired physical perspective in approaching the code MAGIC is intrinsic to the algorithmic formulation of the code, as referred in the section concerning the introduction of the code. In addition, it can be noticed that in order to approach the code and improve it, there is the needing of engineers not only professionally qualified about the single discipline implemented, but who are meanwhile aware of the MDO concepts and practices, reflecting and fulfilling the needs mentioned above.

### 2.3.1 MAGIC's algorithmic formulation classification

In the first chapter, a survey on the currently available algorithmic formulation for MDO has been presented. It is then worth to place the code MAGIC in that formulation scenario and explore its standard classification.

The code MAGIC can be situated in the set of the monolithic or single-level formulations since a single system-level optimizer is adopted. Then, between the monolithic formulations it can be recognized that the code MAGIC belong to the class of the multidisciplinary feasible (MDF) formulations since before starting the optimization process, a complete system-analysis is needed. Indeed, referring to the MDF formulation has been asserted in the first chapter that **whenever a complete system-analysis is performed for every optimization iteration, the single-level approach can be classified as MDF**.

More precisely, referring to the quoting of Ref. [7] reported in section 1.2 of the previous chapter, the structure of MAGIC can be classified as *Single NAND NAND*. Indeed,

- *Single* implies that a single-level optimization is performed

- *NAND* (at the discipline level) conveys that the optimizer determines only the disciplinary design variables and requires determination of the state variables at each iteration
- *NAND* (at the system-level) conveys that the system optimizer determines only the system design variables and requires determination of the coupling variables at each iteration by calling a system analyzer.

Thus, it seems appropriate to explore more widely in literature the features of the MDF formulation among the single-level or monolithic formulation in the MDO field. In the effort of doing that, it is worth to mention an interesting work of Hulme and Bloebaum [31]. The cited paper presents a rigorous numerical comparison of the three main monolithic formulations (i.e. MDF, IDF, AAO) over a wide variety of problem sizes and complexities. Before introducing the important results obtained in [31] it is worth to briefly remind the basic idea of the three single-level formulation cited.

Thus, the MDF (Multidisciplinary Feasible) approach stems its name from the fact that complete multidisciplinary feasibility is maintained in each and every design cycle and is the most commonly used monolithic formulation. Nevertheless, the primary drawback of the MDF approach is that is potentially very time and cost consuming. Indeed, as mentioned in the previous chapter, at each optimization iteration the complete multidisciplinary feasibility is enforced. Thus, at each design cycle there could be a great deal of inefficient time consumption spent for achieving the re-convergence of the system analysis portion of a design that is still far from its optimal solution.

On the other hand the AAO (All-At-Once) formulation has been developed converting the system analysis equations in equality constraints and treating both the system design variables and the sub-systems outputs (behavior variables) as optimization variables. Hence, the main advantage of the AAO approach is the elimination of an iterative design cycle for obtaining an optimal design by the elimination of costly iterative analysis evaluations. However, the AAO formulation shows some drawbacks. First of all a more complicated optimization problem results by the adoption of such formulation. Indeed, this aspect is due to the intrinsic larger number of optimization variables and equality constraints of the AAO formulation. Furthermore, in the AAO approach the disciplinary feasibility is only attained at a relative or at an absolute extremum (indeed the AAO formulation only enforces disciplinary feasibility at the final solution that can be a local or global optimum). Thus, this aspects conveys a reduction in the possibility of attaining a valid design solution if the optimizer is unsuccessful in obtaining the global optimum solution.

Finally, the IDF (Individual Discipline Feasible) approach can be classified in between the MDF and the AAO approaches. In the IDF formulation at every optimization iteration each individual discipline (that is each subsystem) is independently feasible. In order to drive all the individual disciplines towards multidisciplinary feasibility, the optimizer controls the interdisciplinary data. Thus, in this formulation

all coupling variables are considered to be optimization variables by temporarily substituting a replacement "surrogate" variable for each coupling variable in the optimization problem statement. To ensure that each variable is equal to its corresponding surrogate variable, some equality constraints (called "equilibrium" constraints) have to be added to the problem formulation.

Thus, referring to the comparison of the three mentioned formulations performed in [31] it has to be noticed that in the authors' theory for any given MDO problem at some initial starting point an improved local (or hopefully global) optimum solution can be found no matter of the solution strategy adopted. Furthermore, in their idea, the real issue is the "ease" with which the best found solution is attained, with each of the strategies. This, was the aim of their paper. In their results, the MDF approach consistently arrived at the "best found" design point on one of the first trial executions and with minor modifications of the default optimizer settings, or no modifications at all. On the contrary, the IDF and AAO approaches were requiring many more trial executions to attain the corresponding "best found" solution for each of these strategies. Moreover, some substantial modifications to the default optimizer settings were required. Hence, the research presented in [31] concerning a numerical comparison of the MDF, IDF, AAO solution strategies across simulated multidisciplinary design systems of varying sizes and complexity has indicated the MDF approach, besides its costly solution strategy, as the strategy that can achieve the "best found" solution for a broad majority of the test problems considered.

More references in literature confirm the robustness of the MDF formulation. The most typical assertion consider that the MDF approach can be regarded as a "traditional" one. As previously mentioned the Multi-Disciplinary Feasible formulation ensures that all disciplines are evaluated and all inter-disciplinary dependencies are satisfied. It has been widely used in the field of MDO, hence it has been also widely tested. Thus, it has been recognized as the most robust, although can be computationally expensive (see [31],[32],[33],[9]).

### 2.3.2 More considerations about the MDF monolithic formulation implemented in MAGIC

The confirmation of the efficiency of the MDF formulation can be indirectly meet even in some recent studies that focuses in searching new efficient monolithic formulations.

In Ref. [33] a new algorithmic formulation for MDO of aero-structural problems has been introduced by Prof. J. Martins. The new formulation considers the insertion of the structural optimizer within the aerodynamic solver. The new proposed formulation can be regarded as a multi-level one since a nested structural optimizer is considered in the aerodynamic solver. The authors of [33] affirm in their paper that the new formulation simplifies the system-level problem since a fewer number of calls of the aerodynamic solver will be needed and since the structural design variables and the structural constraints

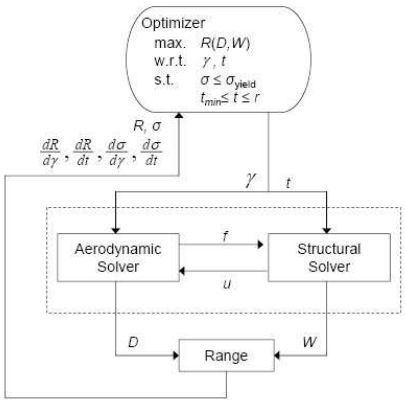


Figure 2. MDF formulation

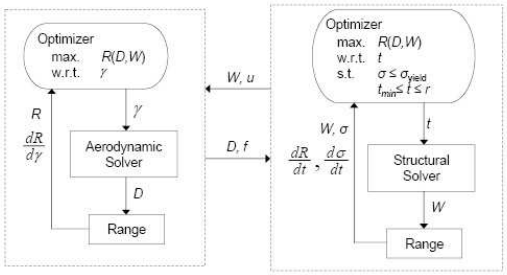


Figure 3. Sequential optimization

Figure 2.1: The MDF formulation and a sequential optimization

are removed from the system-level problem. Then, they introduced a semi-analytical approach for the evaluation of the post-optimality sensitivities that are due to the structural optimization routine. Even if at each call of the aerodynamic solver a structural optimization has to be performed as well, increasing the computational burden of the multi-disciplinary analysis, the new formulation's advantage consists in the elimination of the evaluation of the aerodynamic parameter's derivatives respect to the structural design variables and structural constraints.

In [33] the new algorithmic formulation has been applied to a simple model of a single wing spar modeled by the finite element method to represent a tube-shaped spar and the work was based on low-fidelity aero-structural optimization. The objective function considered was the range and the constraints were acting on the maximum stress and the thickness of the elements. Furthermore, in order to test the new formulation, a comparison between a single level and a bi-level algorithmic formulation has been performed. Thus, in Fig. 2.1, extrapolated from the cited paper, is depicted the optimization problem proposed adopting the traditional MDF approach or a bi-level sequential approach. In the MDF approach the disciplines are connected by the coupling variables that in the simple model adopted are only the external forces and the displacement vector. In the sequential bi-level approach the two disciplines are optimized in sequence thus it is a less precise optimization strategy since it is not possible to account the coupling between the disciplines. Indeed, the aerodynamic optimization is unaware of the structural optimization. Due to this fact, the structural optimization is then limited to a design space dictated by the aerodynamic state converging to an aerodynamic optimum that can not coincide with the true system optimum.

The new formulation proposed by Prof. Martins in [33] is in between the two presented and it is

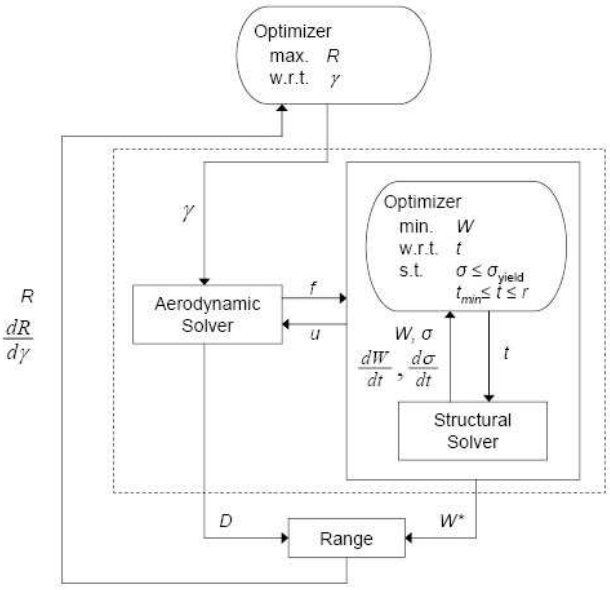


**Figure 5. The new subspace optimization method**

Figure 2.2: The new subspace optimization method by Prof. Martins

depicted in Fig. 2.2. Due to the nesting of the structural optimizer, a post-optimality analysis is needed. The authors underline in [33] that the results that they obtained were confirming the new formulation as a valid one with features similar to the MDF approach but with the advantage of the elimination of the structural variables and constraints from the system-level optimizer. Nevertheless, the evaluation time needed for performing the optimization by the new approach has been considerably longer than the time needed by the MDF approach. In their opinion that was due to the finite difference evaluation, thus, they proposed the use of the Coupled Post-Optimality Sensitivity Analysis (CPOS) that involve the evaluation of the residuals from the aerodynamic and structural analysis[5]. The results shown in [33] and depicted in Fig. 2.3 are about the optimization performed adopting the new formulation and they need to be carefully interpreted. Thus, it is worth to mention them and explain what they convey. In the table the new formulation is indicated by *ARCH* and the results are compared with the ones obtained by the traditional approach MDF adopting the CPOS for the sensitivity evaluation. Nine test were performed (Trial $1-9$) based on four parameters:

- the number of aerodynamic design variables (nxA)
- the number of structural design variables (nxS)

[5]The laborious calculation of the aerodynamic and structural residuals and of the aerodynamic and structural sensitivities is referred in detail in the cited paper [33]

| | | | | | | Iteration Statistics | | | Time Statistics (seconds) | | | | | |
|---|---|---|---|---|---|---|---|---|---|---|---|---|---|---|
| Trial | nxA | nxS | nPanel | nElem | Method | Total MDA Evaluations | Total MDA Iterations | Avg. MDA Iter. per Eval. | Elapsed Time | Total Struct. Time | Total Aero. Time | Total MDA Sens. Time | Aero. Time Delay Required | t_aero / t_struct Required |
| 1 | 5 | 5 | 30 | 30 | MDF | 27 | 934 | 34.59 | 1850.71 | 362.59 | 84.78 | 1399.79 | 3.57 | 9.43 |
| | | | | | ARCH | 14 | 215 | 15.36 | 4417.14 | 2360.32 | 19.58 | 2035.50 | | |
| 2 | 5 | 10 | 30 | 30 | MDF | 29 | 1003 | 34.59 | 2041.32 | 386.67 | 90.12 | 1560.37 | 6.35 | 16.71 |
| | | | | | ARCH | 13 | 211 | 16.23 | 7071.77 | 3956.02 | 19.10 | 3095.01 | | |
| 3 | 5 | 15 | 30 | 30 | MDF | 32 | 1104 | 34.50 | 2330.09 | 425.84 | 99.49 | 1799.69 | 8.09 | 21.20 |
| | | | | | ARCH | 12 | 196 | 16.33 | 9673.34 | 5376.61 | 18.22 | 4276.95 | | |
| 4 | 10 | 5 | 30 | 30 | MDF | 53 | 1870 | 35.28 | 3699.11 | 721.76 | 169.65 | 2800.16 | 2.14 | 5.78 |
| | | | | | ARCH | 23 | 339 | 14.74 | 6973.03 | 3578.46 | 30.75 | 3360.98 | | |
| 5 | 15 | 5 | 30 | 30 | MDF | 79 | 2737 | 34.65 | 5541.25 | 1057.60 | 247.69 | 4223.98 | 1.21 | 3.36 |
| | | | | | ARCH | 28 | 410 | 14.64 | 8349.74 | 4211.37 | 36.94 | 4097.95 | | |
| 6 | 5 | 5 | 30 | 60 | MDF | 28 | 981 | 35.04 | 4815.62 | 783.07 | 90.59 | 3937.57 | 5.77 | 7.34 |
| | | | | | ARCH | 14 | 206 | 14.71 | 9284.43 | 4452.38 | 18.62 | 4809.77 | | |
| 7 | 5 | 5 | 30 | 90 | MDF | 29 | 1010 | 34.83 | 9037.80 | 1223.90 | 91.54 | 7717.38 | 9.37 | 7.81 |
| | | | | | ARCH | 14 | 209 | 14.93 | 16543.53 | 6859.87 | 18.97 | 9672.96 | | |
| 8 | 5 | 5 | 60 | 30 | MDF | 27 | 906 | 33.56 | 4529.02 | 398.33 | 301.70 | 3822.43 | 3.14 | 7.89 |
| | | | | | ARCH | 14 | 214 | 15.29 | 6699.66 | 2293.92 | 71.07 | 4329.67 | | |
| 9 | 5 | 5 | 90 | 30 | MDF | 28 | 990 | 35.36 | 10318.96 | 461.86 | 724.47 | 9121.31 | -0.48 | 0.54 |
| | | | | | ARCH | 14 | 204 | 14.57 | 9942.80 | 2122.70 | 147.80 | 7662.31 | | |

Table 4. Trial summaries for the MDF and new architectures

Figure 2.3:

- the number of aerodynamic panel (nPanel)
- the number of structural elements(nElem).

**Reference test**

The trial 1, with 5 aerodynamic and structural design variables and 30 panels and elements, was selected as the reference test. The results show that the number of the evaluation of the Multidisciplinary Analysis Module (MDA) is approximately halved adopting the new architecture as well as the number of iteration within any disciplinary module. The reduced number of calls of the MDA module was something expected since the structural optimization nested in the aerodynamic module simplify the system-level problem. Instead, the reduction of the iteration within each MDA module was an unexpected result[6]. Nevertheless, the reviewing of the evaluation elapsed time is not supportive of the new architecture because even if the iteration number is reduced, complexity is added by the evaluation of the CPOS sensitivities. Thus, a sensible reduction of the evaluation elapsed time is found only in the aerodynamic module but in our opinion, it could depend from the low-fidelity aerodynamic model adopted. Finally, the total time needed for the optimization process is found to be longer for the new architecture respect to the time needed for the traditional MDF approach[7].

**Test based on the structural design variables**

Trials 2, 3 show the effect of the increase of the structural design variables number. In the traditional MDF approach this increase causes an increase in the number of evaluation and iteration of the MDA module. On the other side, the new architecture there is no increase of the evaluation and iteration

[6]The authors in [33] affirm that this could depend from the presence of the structural optimization in the aerodynamic module that limits the displacements of the wing by preventing the stress constraints from being violated

[7]That is already known as an approach time-consuming.

of the MDA module since the structural optimizer does not interfere anymore with the system-level problem. Nevertheless, once again the reviewing of the evaluation elapsed time does not promote the new architecture. The nesting of the structural analysis in the aerodynamic module aggravate the evaluation of the sensitivity thus, even the adoption of the CPOS does not help in shortening the evaluation elapsed time.

**Test based on the aerodynamic design variables**

Trials 4, 5 show the effect of an increase in the number of the aerodynamic design variables. In the traditional MDF approach this increase causes an increase in the number of evaluation and iteration of the MDA module. In this case, a similar, even if less sensible, increase in the number of evaluation and iteration of the MDA module can be found also adopting the new architecture. Concerning the evaluation elapsed time, the new architecture shows an effective reduction of the elapsed time for the aerodynamic analysis but once again the total elapsed time does not promote the new architecture.

**Test based on the dimension of the structural model**

Trials 6, 7 show the effect of an increase in the number of the structural elements. This parameter increases both the fidelity of the structural analysis and the amount of structural constraints. In the MDF approach the increase of the dimension of the structural model produces a modest increase of the number of optimizer iterations. Furthermore, since these trials are referred to a structural parameter, there is no increase of the number of optimizer iterations for the new architecture that nests the structural optimizer in the aerodynamic module. Nevertheless, also in this case the evaluation of the elapsed time does not promote the new architecture since the complexity is added by the evaluation of the CPOS sensitivities.

**Test based on the dimension of the aerodynamic model**

Trials 8, 9 show the effect of an increase in the number of the aerodynamic panels. In both the architectures adopted the increase of the aerodynamic panels produces a modest increase of the number of iteration of the MDA analysis. Only if the number of panels is really high (trial 9) the new architecture shows to be slightly more efficient of the traditional MDF approach also in the total evaluation elapsed time. Nevertheless, it is worth to remind that the aerodynamic analysis performed is a low-fidelity one.

The same problem solved adopting MAGIC would have been as depicted in Fig. 2.4. Unfortunately, the descriptions of the structural and aerodynamic model adopted in [33] were incomplete in order to reproduce the test with the code magic. Nevertheless, the qualitatively survey performed is still worth for confirming the potentiality of the formulation adopted in MAGIC.

Indeed, the following conclusions can be formulated. Even if the cited paper has the goal to show a simplification of the aerodynamic analysis, there is no feedback for assuming that a more detailed model, not only for the aerodynamics but also of the structural model, will not lead to some unexpected

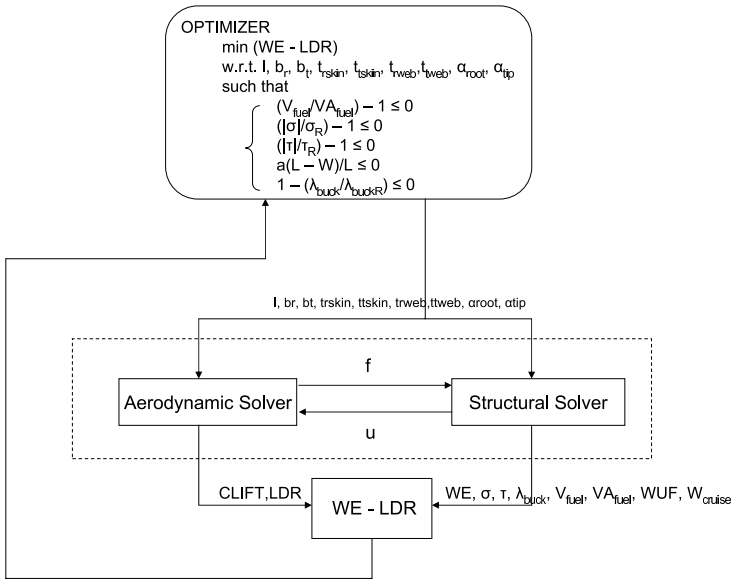


Figure 2.4: The MDF architecture implemented in MAGIC

disadvantages in the new proposed algorithmic formulation or in the sensitivities evaluation. It is also worth to remark that the new architecture does not seem to produce any improvement in the elapsed time needed for the evaluations or neither in the reliability of the obtained results. Indeed, the results are comparable to the ones obtained adopting the traditional MDF approach while the evaluation elapsed time with the new formulation are even doubled respect to the time needed with the MDF approach. This is essentially due to the more complex sensitivity derivatives that the new formulation conveys. Hence, the advantage of the elimination of the structural module from the system-level problem is then canceled by the disadvantage of a more complex evaluation of the sensitivities with no real improvement. Thus, the robustness of the MDF approach can be once again underlined.

## 2.4 Preliminary design of Aircraft configurations adopting the MDO code MAGIC

As mentioned above, MAGIC is in a state of evolution. Thus, it seems appropriate to present some numerical results simply to clarify the extent of the applicability of the current version of the code MAGIC, which although not fully developed, is nonetheless already quite a useful tool for conceptual design.

The results presented in this section pertain to two different steps of design difficulty improvement.

Indeed, the first subsection concerns the structural optimization of a wing-box structure while in the second subsection the more complex optimization of a wing mounted on a conventional plane configuration is presented. More extended results of this kind have been shown also in Ref. [34].

### 2.4.1 Wing Box Optimization

A first test has been performed on a simple wing box as proposed in Ref. [35]. As mentioned, the heart of the optimization code MAGIC adopts a Quasi-Newton method with Penalty Function, hence, it is worth to explore its potentialities when the optimization analysis becomes a multi-disciplinary one. The simple example of the wing box is then appropriate to reach our goal. Furthermore, the role of a shape optimization parameter such as the sweep angle that can modify the geometry of the wing box has been analyzed. More precisely, concerning the shape optimization parameter, it has been considered a slipping of the wing box in the abscissa direction leaving the other two directions unchanged. Thus, the effect of a shifting of the wing box section along the abscissa consists in an extension of the structure length that is it consists in a weight improvement. Hence, the expected result from the optimization process is to bring back to zero the sweep angle variable.

The multi-disciplinary test was performed on the simple wing box mentioned subjected to a bending stress on the wing tip. The bending load accounted was $3000\,N$ and the objective function was the structural weight. Two kind of constraints were considered: the constraint on the maximum tip displacement ($1\,cm$) and the buckling constraint. The two constraints were applied in two different steps, hence, at first only the displacement constraint was adopted and then the buckling constraint was added and the results were compared. Eleven design variables were adopted: the rod area, the skins of the shells and the sweep angle. Several test were performed for the same wing box with different starting sweep angles, but for shortness only the results for $\lambda = 5$ and $\lambda = 20$ degrees will be shown.

**Case** $\lambda = 5deg$

Starting with an initial sweep angle $\lambda_i = 5\,deg$, it is possible to note that when only the maximum displacement constraint is imposed, the optimizer reaches the un-sweep configuration, as shown in the following pictures and tables. The negative value obtained for the final sweep angle has no relevant meaning since no aerodynamic discipline was considered.

Introducing the buckling constraint, the optimization becomes more severe and the sweep angle cannot approach the zero value. Consequently, the objective function assumes an higher value as summarized in Table 2.1. Indeed, a light structure was considered to better underline the relevance of the insertion of the buckling constraint on such a structure. Thus, the buckling constraint can be regarded as a critical

constraint that deeply interfere with the optimization of the wing box structure.

Table 2.1: Optimized values for $\lambda = 5\,deg$.

| | **Initial Value** | **Optimal Value (no Buckling Constr.)** | **Optimal Value (Buckling Constr.)** |
|---|---|---|---|
| $[Kg]$ Objective function | 152.095 | 1156.689 | 2266.143 |
| $[deg]$ Sweep angle | 5.0 | $-0.372$ | 3.75 |

The design variables more interested in the optimization process are the sweep angle and the rod area since the buckling constraint is imposed. The comparative trends are depicted in graphics b) and c) in Fig. 2.5.

It is worth to note that the buckling constraint is violated at the beginning of the optimization process. Hence, the Penalty Function method implemented works to bring back the process into the feasible domain.

In Table 2.2 are summarized the values of each design variable both without and with imposing the buckling constraint.

Table 2.2: Design Variables for $\lambda = 5\,deg$.

| **Variable** | **Initial Value** | **Optimal Value (no Buckling Constr.)** | **Optimal Value (Buckling Constr.)** |
|---|---|---|---|
| $[m^2]$ Rod Area | 0.002 | 0.006 | 0.042 |
| $[m]$ Shell Thickness | 0.002 | 0.019 | 0.001 |
| $[m]$ Shell Thickness | 0.001 | 0.093 | 0.009 |
| $[m]$ Shell Thickness | 0.002 | 0.019 | 0.007 |
| $[m]$ Shell Thickness | 0.001 | 0.049 | 0.004 |
| $[m]$ Shell Thickness | 0.002 | 0.019 | 0.007 |
| $[m]$ Shell Thickness | 0.001 | 0.004 | 0.0006 |
| $[m]$ Shell Thickness | 0.001 | 0.0003 | 0.001 |
| $[m]$ Shell Thickness | 0.001 | 0.0005 | 0.001 |
| $[m]$ Shell Thickness | 0.001 | 0.0002 | 0.003 |
| $[rad]$ Sweep Angle | 0.0873 | $-0.006$ | 0.065 |

**Case** $\lambda = 20\,deg$

As the previous case, also starting with an initial sweep angle $\lambda_i = 20\,deg$ it is possible to note that when only the maximum displacement constraint is imposed, the optimizer reaches the un-sweep configuration. Once again the negative value obtained for the final sweep angle has no relevant meaning since, also in this case, no aerodynamic discipline was considered.

As previously pointed out, adding the buckling constraint, the optimization becomes more severe and the sweep angle cannot approach anymore the zero value and the buckling constraint is once again critical

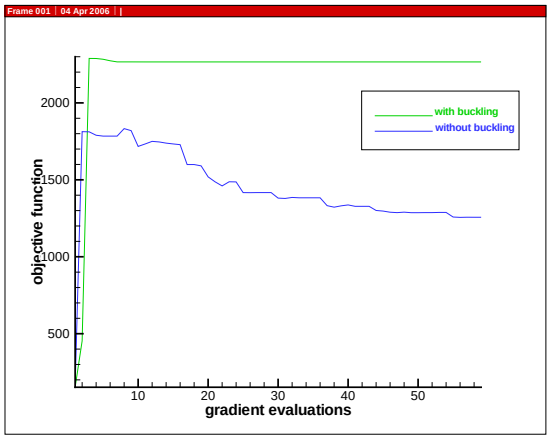


(a) Objective functions

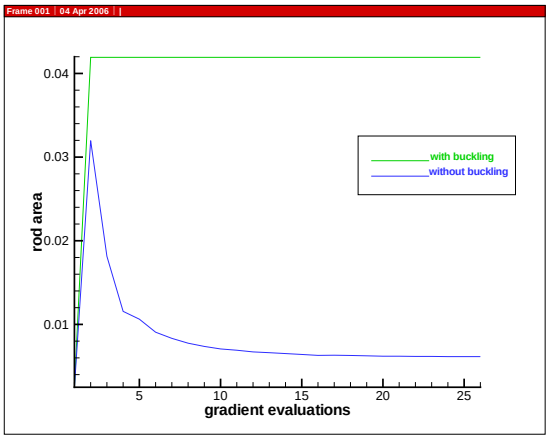


(b) Rod areas

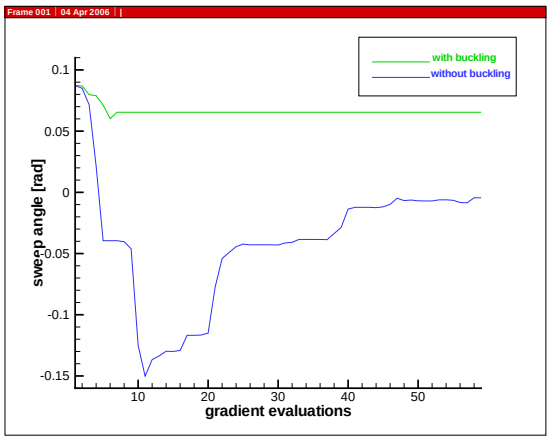


(c) Sweep angles

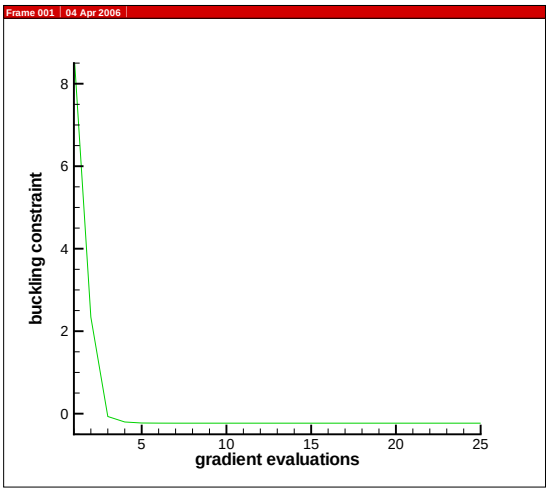


(d) Trend of buckling constraint

Figure 2.5: Comparison between the trends with and without buckling constraint for $\lambda_i = 5\,deg$.

for the wing box structure. Consequently, the objective function assumes an higher value as shown in the following Table 2.3.

Table 2.3: Optimized values for $\lambda = 20\,deg$.

| | **Initial Value** | **Optimal Value (no Buckling Constr.)** | **Optimal Value (Buckling Constr.)** |
|---|---|---|---|
| $[Kg]$ Objective function | 159.779 | 1156.965 | 1685.448 |
| $[deg]$ Sweep angle | 20.0 | $-0.15$ | 9.39 |

The design variables more interested in the optimization process are the sweep angle and the rod area since the buckling constraint is imposed. Thus, the comparative trends are depicted in the following graphics b) and c) of Figure 2.6.

It is worth to note that also in this case the buckling constraint is violated at the beginning of the optimization process. Hence, the Penalty Function method implemented works to bring back the process into the feasible domain, as the graphic d) of Figure 2.6 shows clearly.

In Table 2.4 are summarized the values of each design variable both without and with the imposition of the buckling constraint.

Table 2.4: Design Variables for $\lambda = 20\,deg$.

| **Variable** | **Initial Value** | **Optimal Value (no Buckling Constr.)** | **Optimal Value (Buckling Constr.)** |
|---|---|---|---|
| $[m^2]$ Rod Area | 0.002 | 0.007 | 0.028 |
| $[m]$ Shell Thickness | 0.002 | 0.019 | 0.013 |
| $[m]$ Shell Thickness | 0.001 | 0.090 | 0.026 |
| $[m]$ Shell Thickness | 0.002 | 0.019 | 0.013 |
| $[m]$ Shell Thickness | 0.001 | 0.046 | 0.007 |
| $[m]$ Shell Thickness | 0.002 | 0.018 | 0.011 |
| $[m]$ Shell Thickness | 0.001 | 0.002 | 0.0009 |
| $[m]$ Shell Thickness | 0.001 | 0.0005 | 0.002 |
| $[m]$ Shell Thickness | 0.001 | 0.0002 | 0.0014 |
| $[m]$ Shell Thickness | 0.001 | 0.0001 | 0.0015 |
| $[rad]$ Sweep Angle | 0.349 | $-0.003$ | 0.164 |

The two cases here considered are exemplifying of a relevant aspect of the optimization process. Indeed, the addition of disciplines yields to a more complex problem and the interaction between the disciplines can lead the solution to a suboptimal value since the solution falls into a suboptimal area from where the optimizer cannot quit anymore. Actually, starting with an initial sweep angle $\lambda = 5\,deg$ and considering active both constraints, the reduction of the sweep angle is exiguous and the solution falls in a field from where any further weight reduction is impossible since the rod area cannot be much more reduced due to the buckling constraint. Hence, the final weight obtained is higher than the one obtained starting with an initial sweep angle $\lambda = 20\,deg$. In this last case, indeed, the abatement of the sweep angle is bigger and it allows at the rod area and the sweep variables to work jointly in order to satisfy the constraints and optimize the weight.

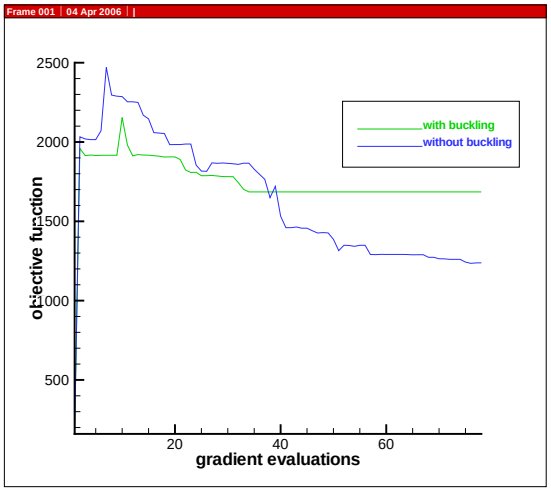


(a) Objective functions

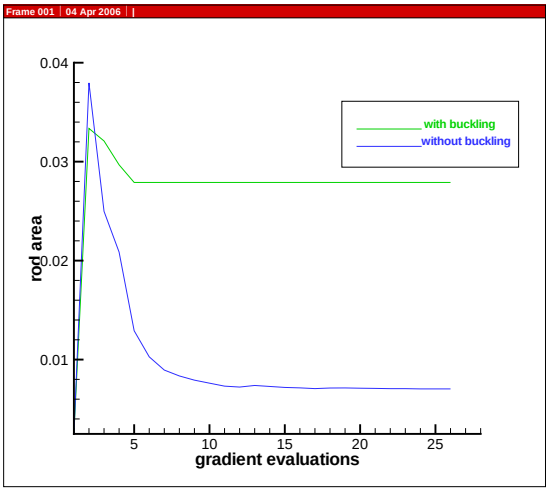


(b) Rod areas

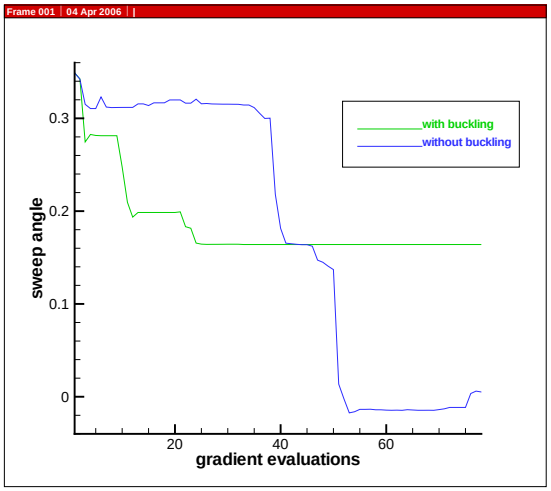


(c) Sweep angles

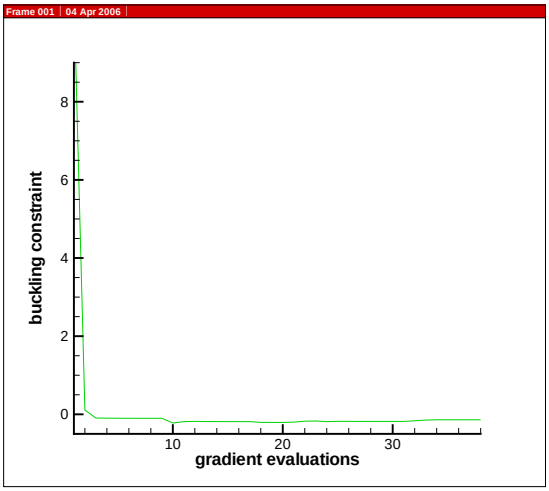


(d) Trend of buckling constraint

Figure 2.6: Comparison between the trends with and without buckling constraint for $\lambda_i = 20\,deg$.

The simple example considered for the wing box structure is anyway indicative of the indispensable needing of a buckling analysis procedure overall if considering the structural optimization of a complete aircraft. Thus, one of the first innovative addition to the code MAGIC that has been considered is the insertion of a buckling module analysis. Hence, the number of disciplines considered in the code MAGIC has been improved allowing the code to provide more reliable results.

The improvements in terms of disciplines added on the code and improved features of it are addressed in the next section while discussing the results obtained for the optimization process of a wing adopting the code MAGIC.

### 2.4.2 Optimization of a Wing

The results presented in this section have been obtained using for the wing a F.E. model (for stress analysis and buckling analysis as well as the evaluation of the natural modes of vibration). The aerodynamic formulation presented in section 2.2.4 is used for steady as well as unsteady aerodynamics. For the evaluation of the steady–state potential–aerodynamics loads (lift and induced drag), we use the formulation of Ref. [36] – an exact extension of the work in Ref. [37]. The unsteady quasi–potential aerodynamics formulation is used for flutter analysis. The finite–state reduced order model for the generalized forces is used in the aeroelastic analysis. The two–dimensional integral boundary–layer formulation, used as 'strip–theory' in three–dimensional applications, has been validated by comparison with experimental results available in literature, in the case of: *(i)* isolated wing, *(ii)* biplane, and *(iii)* box–wing configuration (see Ref. [38], which presents in particular the polar at $Re = 5.1 \cdot 10^5$ of a box–wing configuration; the results are in good agreement with the experimental and numerical results in Ref. [39]. On the basis of these results, we used the strip–theory approach, which we believe to be a better candidate for MDO in that yields results comparable to the three–dimensional ones, with less computational effort. For the sake of conciseness, the results presented are limited to a standard 622–passenger configuration, a cruise altitude of 30.000 ft and a cruise Mach number of $M_\infty = 0.75$. As mentioned above, in the present version of the code, the fuselage is prescribed (in other words, the optimization pertains solely the wing system). The fuselage is $73.0m$ long, $8.41m$ wide, and $7.142m$ high. Also, the aircraft span is set to be $b = 70m$. The propulsion system consists of four underwing–mounted turbo–fan engines. A vertical tail has been considered as well as an horizontal one.

We decided to concentrate on empty weight and useful fuel weight, giving only a lower boundary for the range. Hence, the objective function considered for the results presented in the following is a combination of: *(i) empty weight, $W_e$ (as indicative of manufacturing costs)* , *(ii) useful fuel weight, $W_{uf}$ (as indicative of operative costs)*,

$$J = W_{uf}/W_{uf_{ref}} + W_e/W_{e_{ref}}$$

where subscript *ref* denotes reference values of the above variables (for a deeper analysis of this point, see the life–cycle cost analysis of Ref. [40]). The design variables considered were the wing span, the root and tip chords, the root and tip panel thickness, the root and tip spar thickness the root and tip built-in angle and the sweep angle. The structural mesh coincides with the aerodynamic one and it is composed by 8 panels in the chord direction and 5 panels in the span direction. Thus, the modeled wing has 89 grids, 80$ROD$ elements, 240$CTRIA3$ elements.

The evaluation of the aircraft empty weight, $W_e$, is based on a standard recursive algorithm (see Ref. [41]) for conceptual design.

The comparison between two optimization methods has been performed. Specifically, the *BFGS* method implemented in MAGIC and the *Sequential Quadratic Programming SQP* from the commercial code SNOPT 6.0 were investigated. The comparison has been possible since in the considered test the commercial optimizer has been made interface with the code MAGIC. The insertion of the SNOPT 6.0 optimizer in the code MAGIC adds value to the current version of the code since it allows comparisons of optimization strategies. Thus, the current version of MAGIC leaves to the user the possibility to chose between the PF optimization strategy or the SQP optimization algorithm. Further results of this kind have been also presented in Ref. [34] emphasizing how different approaches can influence the final result of an optimization process. Furthermore, the comparison becomes more interesting as the number of disciplines, and hence the number of constraints, increases. Indeed, the addition of the buckling constraints has been considered separately besides the fuel volume, normal and shear stress, flutter and divergence speed, right lift-weight constraints in order to give more emphasis to what mentioned at the end of the previous section and to the addition of a further discipline. In order of a possible comparison of the results, the starting values of the variables have been chosen congruently with Ref. [34] even if they do not properly apply to a large vehicle of the investigated kind.

As the following results show, adding the buckling constraint the optimized shape of the wing is quite modified. Nevertheless, it is important to note that when more disciplines are involved in the optimization process it is always more useful an adequate multi-disciplinary optimization strategy since it is always more difficult to conceive *a priori* the interaction between the disciplines and hence the final design. This remark could seem a simple one, but its relevance can be appreciated analyzing the obtained results.

Before showing the results obtained it has to be remarked that for the present test the code MAGIC has been made interface with the commercial code NASTRAN for the F.E. analysis. Indeed, as mentioned presenting the code, MAGIC can both perform an "hand-made" F.E. structural analysis or interface for the same analysis the code MSC NASTRAN (particularly for the solutions $SOL101, SOL103, SOL105$).

Thus, the assertion MAGIC/NASTRAN means that the F.E. analysis has been performed interfacing the commercial code MSC NASTRAN. Furthermore, the possibility of interfacing the code NASTRAN for the F.E. analysis adds value to the current version of the code MAGIC.

Thus, the application of the buckling constraint gives rise to an heavier wing, but the optimal value obtained adopting the Penalty Function Method (i.e. *MAGIC/NASTRAN*) and the Sequential Quadratic Programming Method (i.e. *MAGIC-SNOPT/NASTRAN*) show relevant differences for example between the root chords and the tip chords. Other relevant differences can be observed, for example, on the useful fuel weight.

From the obtained values the MAGIC/NASTRAN code seems to give the best results. The reason of such a behavior grows from the optimizers strategy adopted and explains the previous assertion.

Hence, it is possible to observe that the MAGIC-SNOPT/NASTRAN optimizer holds less results accuracy for optimization problems that have a limited number of design variables even if the computational times are small. The results of the application of the buckling constraints using the SNOPT/NASTRAN optimizer show respect when this constraint is not added, that the optimization process attempts to reach the side constraints of the design variables. Thus, it is also possible to appreciate the relevance of the insertion of the buckling constraints since its addition gives a more detailed explanation of which design variables can be considered active or not in such optimization process.

On the other hand it is appropriate to note that the optimization process performed by the MAGIC/NASTRAN code gives rise to a few revisions of the optimal design once that the buckling constraint is added. The most relevant change in this sense is the increased wing weight due essentially to the tip chord extension. At the same time, it is important to underline how the addition of the buckling constraint yields to a more accurate and safe project in terms for examples of the needing of a careful estimation of the flutter speed.

Therefore, it is worth to note that the results obtained allow once again (see also Ref. [34]) to underline how the *SQP* method is not very appropriate for an optimization process that is already close to the optimal solution. Indeed, the configuration adopted was practically conceived on the basis of an existing operating aircraft. Nevertheless, overall if there is a quite large number of design variables, the *SQP* method can be used as a first step of optimization, taking advantage from its reduced time of estimations.

Tables 8 and 9 summarize the results of the optimization analysis without and with the buckling constraint, and make possible the comparison of the obtained values.

Thus, the code MAGIC, in the last updated version reported here, has showed improved performances since it can interface itself with the FE commercial code *NASTRAN*, since the *SQP* optimization method

| Active variables | Optimal Values | |
|---|---|---|
| | MAGIC-NASTRAN without Buckling Constr. | MAGIC-NASTRAN with Buckling Constr. |
| Wing span $[m]$ | 36.2483469138 | 36.248038 |
| Root chord $[m]$ | 15.0696802166 | 15.055609 |
| Tip chord $[m]$ | 6.1105617907 | 6.781101 |
| Root panel thickness $t_{skin}$ $[m]$ | 0.0016627524 | 0.001694 |
| Tip panel thickness $t_{skin}$ $[m]$ | 0.0009684175 | 0.000970 |
| Root spar thickness $t_{web}$ $[m]$ | 0.0129102905 | 0.013244 |
| Tip spar thickness $t_{web}$ $[m]$ | 0.0048946437 | 0.004886 |
| Root built-in-angle $\alpha_{root}$ | 7.0179379117 | 6.391605 |
| Tip built-in-angle$\alpha_{tip}$ | 3.3324792169 | 3.156474 |
| Sweep Angle $\Lambda$ | 26.7827981973 | 25.434219 |
| Performances | | |
| Take off weight $[Kg]$ | 396149.820 | 398843.974 |
| Empty weight $[Kg]$ | 127810.677 | 128311.515 |
| Useful Fuel Weight $[Kg]$ | 196339.143 | 198532.460 |
| Structural wing weight$[Kg]$ | 13989.992 | 14255.579 |
| Lift coefficient | 0.4371 | 0.3995 |
| Induced drag coefficient | 0.0084 | 0.0072 |
| Efficiency | 16.8114 | 16.6338 |
| Flutter speed $[m/s]$ | 356.00 | 338.00000 |
| Divergence speed $[m/s]$ | 550.00 | 550.00 |
| Incremental load factor | 2.59779 | 2.35764 |
| Objective Function | 0.576595107 | 0.581480824 |
| Constraints | | |
| Fuel Volume | -0.739495209 | -0.761612503 |
| Direct Stress | -0.865778700 | -0.836327875 |
| Shear Stress | -0.534626850 | -0.217431500 |
| Flutter Speed | -0.078787879 | -0.024242424 |
| Divergence Speed | -0.447368421 | -0.447368421 |
| Right Lift-Weight | -0.091573148 | -0.029732070 |
| Buckling Constraint | | -12.818900000 |

Table 2.5: Comparison of optimization processes using *MAGIC/NASTRAN* without and with buckling constraint.

| Active variable | Optimal Values | |
|---|---|---|
| | snopt-nastran without Buckling Constr. | snopt-nastran with Buckling Constr. |
| Wing span $[m]$ | 35.07050 | 36.37973 |
| Root chord $[m]$ | 17.06117 | 20.00000 |
| Tip chord $[m]$ | 7.01082 | 4.00000 |
| Root panel thickness $t_{skin}$ $[m]$ | 0.00101 | 0.00100 |
| Tip panel thickness $t_{skin}$ $[m]$ | 0.00080 | 0.00080 |
| Root spar thickness $t_{web}$ $[m]$ | 0.01204 | 0.01200 |
| Tip spar thickness $t_{web}$ $[m]$ | 0.00303 | 0.00334 |
| Root built-in-angle $\alpha_{root}$ | 6.31511 | 7.99154 |
| Tip built-in-angle$\alpha_{tip}$ | 3.21215 | 3.99546 |
| Sweep Angle $\Lambda$ | 30.02061 | 29.36263 |
| Performances | | |
| Take off weight $[Kg]$ | 410422.51 | 435669.143 |
| Empty weight $[Kg]$ | 127642.380 | 131083.026 |
| Useful Fuel Weight $[Kg]$ | 210780.130 | 232586.117 |
| Structural wing weight $[Kg]$ | 12485.540 | 13478.482 |
| Lift coefficient | 0.378 | 0.4894 |
| Induced drag coefficient | 0.0073 | 0.0122 |
| Efficiency | 15.9928 | 15.3432 |
| Flutter speed $[m/s]$ | 353.00 | 369.00000 |
| Divergence speed $[m/s]$ | 550.00 | 550.00 |
| Incremental load factor | 2.61354 | 2.56427 |
| Objective Function | 0.601459115 | 0.642930191 |
| Constraints | | |
| Fuel Volume | -0.777617 | -0.657762 |
| Direct Stress | -0.851012 | -0.760922 |
| Shear Stress | -0.544423 | -0.007950 |
| Flutter Speed | -0.069697 | -0.118182 |
| Divergence Speed | -0.447368 | -0.447368 |
| Right Lift-Weight | -0.013834 | -0.219359 |
| Buckling Constraint | | -14.046570 |

Table 2.6: Comparison of optimization processes using snopt-nastran without and with buckling constraint.

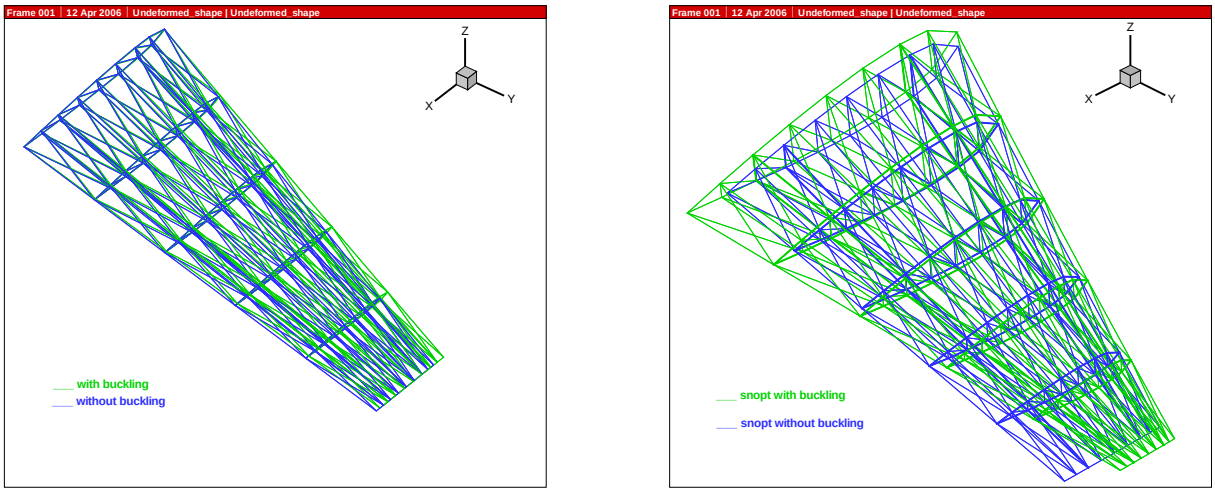


(a) *MAGIC/NASTRAN* (b) *SNOPT/NASTRAN*

Figure 2.7: Optimization results compared with and without the application of the buckling constraint.

implemented in the code allows to compare the performances of two different kind of optimizer, and since the number of disciplines was improved. Its relevance in the field of multidisciplinary design optimization for aircraft configurations has been currently verified and tested.

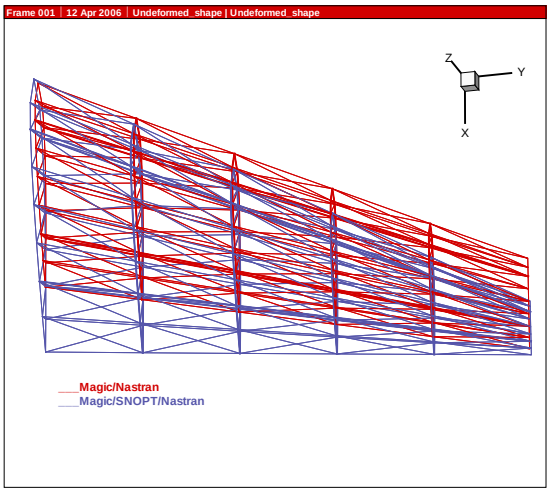


Figure 2.8: Comparison between the optimization results using two different optimization methods: the Penalty Function (MAGIC-NASTRAN) and the Sequential Quadratic Programming (MAGIC/SNOPT-NASTRAN). In both cases the application of the buckling constraint was considered.

# Chapter 3

# Modeling of steady and unsteady aerodynamic systems in ground effect

## 3.1 Introduction: Aerodynamics in ground effect

The aerodynamic ground effect is a phenomenon that has been experienced since the very early manned flight and that causes an improving of the aerodynamic performances of a wing when it operates close to a ground plane. Indeed, just before landing an aircraft the first pilots were having the feeling that the vehicle was resisting to the imposed maneuver 'floating' in a sort of air cushion due to the air trapped between the wing and the ground. For aircraft with a large wing surface the perception of the air cushion was more evident. Even during take off the early pilots were experiencing the ground effect. Accordingly to the low power of the engines mounted at that age, the vehicle was indeed able to lift off exploiting the reduced induced drag in the ground proximity, but once lifted, having not enough engine thrust, it was lowering again the altitude showing the characteristic skipping take off of the early flights. It is possible to suppose that the Wright brothers had flown always in ground effect conditions in their early flights, taking advantages from the ground effect phenomenon without even knowing it. The main benefits of a craft operating within ground effect are that speed, payload and fuel economies are considerably more efficient than with traditional craft transport.

More specifically, ground effect is a phenomenon composed by two different aspects both responsible for the aerodynamic efficiency $E = L/D$ improvement but acting on different aerodynamic terms. Thus,

it is worth to distinguish between a *span* dominated and a *chord* dominated ground effect. Indeed, the denomination adopted underlines the main parameter acting in the pertinent aspect of the ground effect considered that is: the term $h/b$ (height/span) is the main responsible parameter in the span dominated ground effect case while the term $h/c$ (height/chord) is the main one in the corresponding chord dominated ground effect case. As mentioned both aspects improve the aerodynamic efficiency, the former acting on a reduction of induced drag (D) and the latter resulting in an increasing of lift (L). Since in stationary flight thrust is equal to drag and weight is equal to lift, the aerodynamic efficiency ratio also express the amount of thrust required to propel an aircraft of a certain weight; hence it also represents the improvement of thrust to impose in order to obtain a certain improvement of weight. Thus, since decreasing the ground clearance the aerodynamic efficiency of the wing improves, less power is needed to propel an aircraft flying in ground effect conditions.

### 3.1.1 Span dominated ground effect

The span dominated ground effect is the contribution of the ground effect more usually meant when ground effect is mentioned. As previously told, the denomination span dominated is referred to the main parameter acting in this case. Indeed, this aspect of the ground effect is due to the finite spanwise of a wing. In order to explain the expressed concept it is worth to briefly remind some notions about the drag of an aircraft. Thus, the two main contributions of an aircraft's drag are friction and lift induced drag.

The friction drag is due by the friction of the air on the skin of the aircraft and is therefore dependent on its wetted area. The lift induced drag is a contribution of drag intrinsic to the generation of lift. As known, the generation of lift on the wing is the result of a static pressure difference between the two sides of the wing. Particularly, the pressure on the lower wing side is higher than the one on the upper side. Consequently, the lift force is proportional to the mentioned pressure difference times the wing surface area. Due to the finite spanwise of the wing a complication arises at the wingtip. Indeed at the wingtip the high pressure area of the lower side meets the low pressure area of the upper side causing an air flow around the wingtip. Thus, this flow from the lower side to the upper side of the wingtip originates some vortices called wingtip vortices. The energy stored in those vortices is lost and is then experienced as a contribution of drag that is dependent on the spanwise lift distribution and the aspect ratio of the wing. Thus is evident that high aspect ratio wings generate a lower induced drag respect to the one generated by a low aspect ratio wing since their wingtip vortices are weaker. Indeed, for high aspect ratio wings the high and low pressure areas at the tip are smaller since the rest of the wing is extended 'further away' from the tip.

As shown in Figure 3.1 when a wing approaches the ground the wingtip vortices have not enough space for fully developing. Hence, at the ground proximity the vortices become weaker and they are also

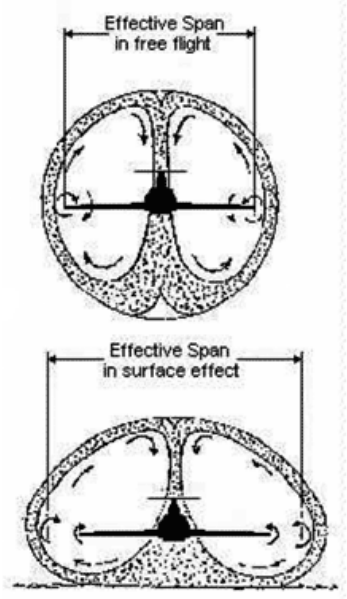


Figure 3.1: *Span dominated ground effect: comparison between the effective span in free flight and the effective span in ground effect. Figure from PacificSeaflight.com*

pushed outward making the effective aspect ratio of the wing appear higher than the geometric one.

Some theoretical studies and results about the spanwise dominated ground effect were carried on from Wieselsberger already in early 1920's developing the Prandtl lifting line theory. It was found that the lift induced drag at a ground clearance of 10% of the wingspan reduces approximately to the 50% of its free flight value.

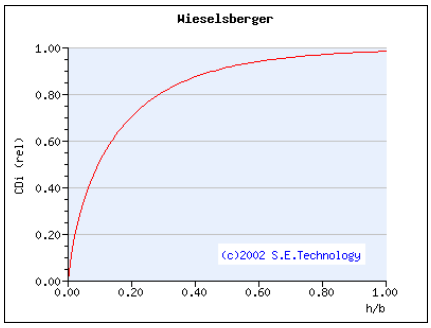


Figure 3.2: *Wieselsberger results about the influence of ground effect on induced drag*

### 3.1.2 Chord dominated ground effect

While the span dominated ground effect improves the aerodynamic efficiency acting on a reduction of the drag, the chord dominated ground effect is directly responsible of an improvement of the lift force. At a small clearance from the ground the air trapped under the wing creates a kind of high pressure air cushion. The lower part of the wing is then in a condition of higher pressure respect to the free flight condition, hence the lift force of the configuration is notably improved. At a very small ground clearance the air can even stagnate determining the highest pressure condition ever, pressure coefficient unity. It is worth to remind that the peak of the suction force at the leading edge is more pronounced in ground effect, hence the separation of the flow is more possible in that area. The effect of the air cushion in ground effect is shown in Figure 3.3 where the red color indicates the high pressure, the blue is the low pressure value and the green color the ambient pressure one. Besides the high pressure air cushion depicted in red at the lower part of the wing, it is possible also to note in the figure a blue area around the profile nose. That blue area indicates the mentioned peak of the suction force on the leading edge of the wing and remarks that separation in ground effect is likely to occur at the nose as confirmed by wind tunnel tests.

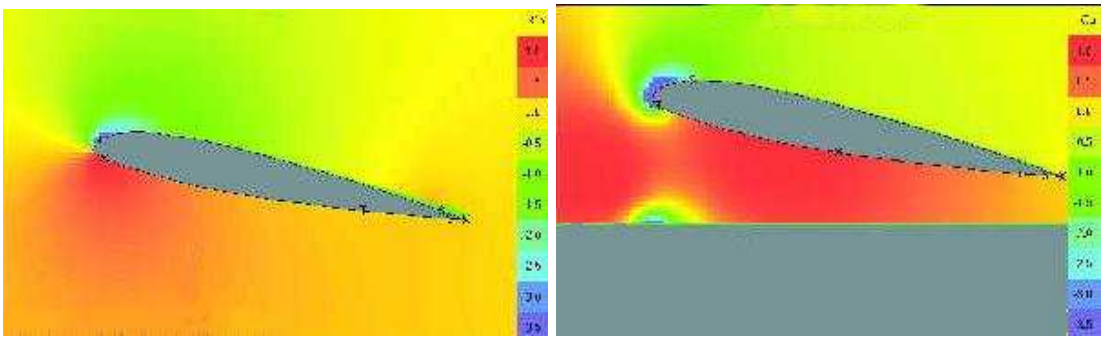

Figure 3.3: *Pressure field for a wing in free flight and a wing in ground effect at a clearance of* 1/10 *of the spanwise*

### 3.1.3 Brief remark on the aerodynamic ground effect

The ground effect phenomenon is not always intended to improve the lift force of a certain configuration. Indeed, if the lower side of the airfoil has a convex shape and if the angle of attack is small, then a kind of Venturi tube effect is established between the foil and the ground. Thus, the air flowing at a very high speed and low pressure 'sucks' the airfoil toward the ground. This feature of the ground effect is the one adopted for designing racing cars.

## 3.2 Ground effect vs free surface effect for a submerged foil

For sake of completeness it is worth to briefly deal with the symmetric case of the ground effect mentioning the influence due to the air/water interface on the pressure and velocity fields around a submerged hydrofoil. Hence, some considerations, that without any lost of generality will be done for a two-dimensional hydrofoil, have to be remarked.

The interest that the free surface problem raises can be understood later on in the paragraph concerning the free surface boundary condition. Indeed, it is worth to underline that the free surface problem is a more general one, that can contain the airfoil problem as a special case. Furthermore, the interest of the free surface effect conjuncted to the ground effect one concerns vehicles that fly in ground effect and that are still in development for their desirable features like the *Wing-In-Ground Effect* craft or more precisely an hybrid version of the WIG craft with piercing struts for controlling of the vehicle that have fins submerged in water. The *SEABUS HYDAER* is an example of such vehicles and it has been designed in an European project called *Brite- Euram*.

It is worth to underline that for submerged foils, the hypothesis of incompressible fluid leads to the omission of the phenomena due to the air compressibility. Nevertheless, a different and peculiar phenomenon called *cavitation* can be observed. The cavitation is due to the establishing, growing and convection of air bubbles generated on the foil surface. Indeed, both an airfoil and a hydrofoil create lift by creating a low pressure on the upper surface. In the case of the hydrofoil though, the pressure can become so low that the liquid water transforms into a gaseous water (cavity) since the static pressure of the liquid's flow field is equal to, or less than, the saturation (vapor) pressure of the liquid. The cavitation can occur even for deeply submerged foils, but it is more frequently observed for hydrofoils at a small clearance from the water free surface since the hydrostatic pressure, due to the air column overlying the foil, has a smaller value.

Another phenomenon called *ventilation* can occur for hydrofoils shallowly submerged, overall if piercing struts are adopted. Thus, some air bubbles can be trapped from the foil. Hence, the air gets sucked down the lifting surface of the foil.

Cavitation and ventilation are both ordinarily undesirable. While both cavitation and ventilation increase the section drag of the hydrofoil, cavitation is also barometrically unstable and can lead to problems such as vibration, excessive noise and erosion of the hydrofoil surface.

A submerged hydrofoil deforms the free surface by generating transversal waves (for the two-dimensional foil case considered). The originated waves system leads to the introduction of a new form of foil drag: thus the waves system absorb part of the energy due to the hydrofoil. The evaluation of this mentioned kind of drag does not request the introduction of the viscosity effects till when the *waves*

*breaking* occurs. The viscosity effects then are similar to the ones observed in air.

In general, the lift force generated by submerged foils decreases for decreasing free surfaces clearances. Nevertheless, the relationship between lift force and submerging distances is more complex for decreasing velocities of the foil. Thus, the *Froude* number, expression of the gravity and inertial forces ratio, has to be introduced in the hydroelastic field in order to effectively describe the mentioned phenomenon.

## 3.3 Lifting surfaces in steady two-dimensional aerodynamics in bounded and unbounded domain

### 3.3.1 Case of unbounded domain

It is useful to mention the main steps of the Potential Flow theory since the nomenclature and the concepts there introduced are the fundamentals of the subsequent analytical study.

Hence, considering the incompressible irrotational flow of an inviscid fluid past a two-dimensional thin airfoil in an unbounded domain, the basic law of fluid mechanics about conservation of mass (called continuity equation) in a lagrangian differential form can be written as

$$\frac{D\rho}{Dt} + \rho \cdot \mathrm{div}\boldsymbol{v} = 0 \tag{3.1}$$

being $D\,\boldsymbol{.}\,/Dt$ the substantial derivative, $\rho$ the fluid density and $\boldsymbol{v}$ the velocity vector. The hypothesis of incompressible fluid can be explained as $\rho = \text{cost}$, thus, $D\rho/Dt = 0$ hence the continuity equation becomes straightforwardly

$$\mathrm{div}\boldsymbol{v} = 0 \tag{3.2}$$

Naming $\boldsymbol{T}$ the viscous stress tensor term, the punctual conservation of the momentum is given by

$$\rho\frac{D\boldsymbol{v}}{Dt} = \mathrm{div}\boldsymbol{T} \tag{3.3}$$

It is well-known that for inviscid fluids $\boldsymbol{T} = -p\boldsymbol{I}$ hence the equation 3.3 yields

$$\rho\frac{D\boldsymbol{v}}{Dt} = -\mathrm{div}(\boldsymbol{I}p) \qquad \Rightarrow \qquad \frac{D\boldsymbol{v}}{Dt} = -\bigtriangledown p \tag{3.4}$$

that is also called Euler equation.

The integration of the equations 3.2, 3.4 with proper boundary and initial (for the unsteady case) conditions gives the values of the velocity vector and of the pressure in the whole flow field. Nevertheless,

a synthetic formulation and solution of the problem can be achieved profiting by the irrotationality of the flow field and using the concept of potential flows. Since the flow is irrotational then rot$\boldsymbol{v} = 0$ everywhere. Thus, the Stokes Theorem assures that being $S$ be an oriented (with outgoing normal $\boldsymbol{n}$) smooth surface that is bounded by a simple, closed, smooth boundary curve $CM$ for the vector field $\boldsymbol{v}$ it is possible to state that

$$\oint_{CM} \boldsymbol{v} d\boldsymbol{x} = \iint_S \text{rot}\boldsymbol{v} \cdot \boldsymbol{n} dS \tag{3.5}$$

It is known that an irrotational flow field can be considered the gradient of a scalar quantity and vice versa[1] Hence, introducing the scalar $\varphi$ called *velocity potential* the following relationship is everywhere satisfied in the flow field

$$\boldsymbol{v} = \boldsymbol{\nabla}\varphi \tag{3.6}$$

that for the continuity equation 3.2 gives

$$\boldsymbol{\nabla} \cdot (\boldsymbol{\nabla}\varphi) = 0 \tag{3.7}$$

that is the Laplace equation

$$\nabla^2 \varphi = 0 \tag{3.8}$$

For an inviscid and irrotational flow is indeed useful to adopt the potential function, $\varphi$, to represent the velocity field since this assumption reduces the number of unknown quantities. Furthermore, the Laplace equation is linear, thus, being $\varphi_1, \varphi_2$ two different solutions, even their linear combination[2] is still a valid solution. Once some fundamentals solutions of the Laplace equation are given, a linear combination of them is adopted in order to satisfy the boundary conditions.

### 3.3.2 The ground effect boundary condition

The steady two-dimensional flow of an inviscid fluid past a thin airfoil at a small clearance from the ground is now considered. As stated in the previous paragraph, it is possible to introduce a scalar velocity potential function such that $\boldsymbol{v} = \boldsymbol{\nabla}\varphi$ for solving the Laplace equation 3.8. Calling $\phi$ the perturbation on the velocity potential due to the airfoil, the potential becomes

$$\varphi = Ux + \phi \tag{3.9}$$

[1]For the scalar quantity $\varphi$ it is always possible to write rotgrad$\varphi = 0$ Indeed, interchanging j,k it yields $\varepsilon_{ijk} \frac{\partial^2 \varphi}{\partial x_k \partial x_j} = \varepsilon_{ikj} \frac{\partial^2 \varphi}{\partial x_j \partial x_k} = -\varepsilon_{ijk} \frac{\partial^2 \varphi}{\partial x_j \partial x_k}$.

[2]As well as a partial derivative of a solution is still a valid solution.

The perturbation of the potential has to verify on turn the Laplace equation. In the following the boundary conditions will be considered in their linearized form since we will assume that the components $u, v$ of the velocity perturbation are small compared to the uniform stream $U$.

Thus, the boundary conditions are applied in $y = 0$ considering the solid boundary of the wall and in $y = h$ instead of the foil boundary since the assumed linearized conditions.

Hence, omitting quantities of the second order in $\phi, u, v$ the boundary conditions in ground effect can be stated as

$$\frac{\partial \phi}{\partial y} = 0 \qquad y = 0 \tag{3.10}$$

$$\frac{\partial \phi}{\partial y} = U\left(\frac{dy}{dx} + \alpha\right) \qquad y = h, |x| \leq b \tag{3.11}$$

where $y = y(x)$ defines the airfoil equation.

**The free surface boundary condition**

The boundary condition needed for evaluating the fluid dynamic field around a submerged hydrofoil close to the free surface is now investigated for completeness since it represents a symmetric problem respect to the ground effect case. Assuming to consider an inviscid fluid and an irrotational flow, for a bi-dimansional foil the Laplace equation 3.8 can be written. Adopting the same notation of the previous section for the velocity components and the potential perturbation term, the equation that solves the fluid dynamic field is given by

$$\nabla^2 \phi = 0 \tag{3.12}$$

The boundary condition has to take into account that an heavy fluid is now considered, thus the gravity constant $g$ will appear. Furthermore, the boundary condition on the free surface will be considered as given in their linearized form. Hence, the free surface boundary assumed will be $y = 0$ instead of $y = \eta(x)$ (being the function $\eta(x)$ representative of the exact shape of the free surface boundary) while the foil boundary condition will be given in $y = -h$ as follows

$$\frac{\partial \phi}{\partial y} + \left(\frac{U^2}{g}\right)\frac{\partial^2 \phi}{\partial x^2} = 0 \qquad y = 0 \tag{3.13}$$

$$\frac{\partial \phi}{\partial y} = U\left(\frac{dy}{dx} + \alpha\right) \qquad y = -h, |x| \leqslant b \tag{3.14}$$

where $y = y(x)$ defines the hydrofoil shape.

The adimensionalization of the boundary condition 3.13, addressed in the appendix, leads to interesting considerations. Thus,3.13 can be written adimensionally[3] as

$$\frac{\partial \hat{\phi}}{\partial \hat{y}} + \left(\frac{U^2}{gb}\right) \frac{\partial^2 \hat{\phi}}{\partial \hat{x^2}} = 0 \qquad\qquad \hat{y} = 0 \tag{3.15}$$

Introducing the *Froude* number $F = U/\sqrt{g \cdot b}$ that is the ratio between the inertial and gravitational forces. Thus, Eq. 3.15 becomes

$$\frac{\partial \hat{\phi}}{\partial \hat{y}} + \left(F^2\right) \frac{\partial^2 \hat{\phi}}{\partial \hat{x^2}} = 0 \qquad\qquad \hat{y} = 0 \tag{3.16}$$

It is worth to note that if $F \to 0$ the contribution of the gravitational force can be neglected since the gravity does not have any influence on the problem. Thus, $F \to 0$ coincides with the aerodynamic case where the weight of the fluid is negligible.

The boundary condition 3.16 can be investigated for $F \to \infty$ and for $F \to 0$. For $F \to \infty$ in order to satisfy Eq. 3.16 it has to be

$$\frac{\partial^2 \hat{\phi}}{\partial \hat{x^2}} = 0 \qquad \text{in} \qquad \hat{y} = 0 \qquad \Rightarrow \frac{\partial \hat{\phi}}{\partial \hat{x}} = \text{cost} \qquad \text{in} \qquad \hat{y} = 0 \tag{3.17}$$

where the constant value has to be such as the free stream velocity value is finally obtained, thus,

$$\frac{\partial \hat{\phi}}{\partial \hat{x}} = \text{cost} = 0 \qquad \text{in} \qquad \hat{y} = 0 \tag{3.18}$$

Hence, for $F \to \infty$ dimensionally one has

$$\frac{\partial \phi}{\partial x} = 0 \qquad\qquad y = 0 \tag{3.19}$$

that shows that the horizontal component of the velocity perturbation has to be identically zero $\hat{u} = 0, \forall\, \hat{x}$. Considering instead $F \to 0$ Eq. 3.16 simply gives

$$\frac{\partial \phi}{\partial y} = 0 \qquad\qquad y = 0 \tag{3.20}$$

that coincides with the ground effect boundary condition requesting that the vertical component of the velocity perturbation is identically zero.

[3]The lengths have to be adimensionalized respect to the half-chord value $b$ as $\hat{y} = \frac{y}{b}$ and $\hat{x} = \frac{x}{b}$ while the dimensionless potential is defined as $\hat{\varphi} = \frac{\varphi}{U}$.

### 3.3.3 Brief survey on the singularity and the images methods

The well known solutions, source and vortex, of the Laplace equation are the ones mentioned in the present work, thus it seems worth to address some remarks more about the singularity and image methods.

For two-dimensional potential flows, the potential and the stream[4] functions of a source singularity are given by

$$\begin{aligned} \varphi &= \frac{m}{2}\log(x^2+y^2) = m\log r \\ \psi &= m\tan^{-1}\frac{y}{x} = -m\vartheta \end{aligned} \tag{3.21}$$

where $m = Q/2\pi$ is the flowing rate of the fluid for angle unity and the referred frame is depicted in fig 3.4. For the source singularity solution the equipotential lines, that is lines everywhere orthogonal to the

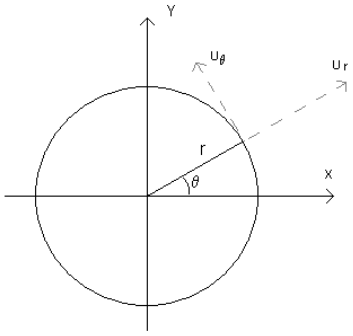


Figure 3.4: *Source singularity reference frame.*

velocity, are circumferences centered in the origin while the streamlines, that is lines everywhere tangent to the velocity, are rays from the origin of coordinates.

Interchanging the roles between stream function and potential function of the source solution, the fluid dynamics field of a vortex is achieved. Hence, for the vortex singularity the equipotential lines are rays from the origin while the streamlines are circumferences centered in the origin. The vortex solution is then given by

$$\begin{aligned} \varphi &= -A\,\vartheta \\ \psi &= -A\,\log r \end{aligned} \tag{3.22}$$

[4]The stream function instead of potential function can be used as it is slightly more intuitive to consider a line that is everywhere tangent to the velocity. Streamline function is represented by $\psi$. Lines of constant $\psi$ are perpendicular to lines of constant $\varphi$, except at a stagnation point.

where $A$ indicates the circuitation positive in the anticlockwise direction.

It is known that a two-dimensional Eulerian flow can be described by a function of complex variable such that its real part coincides with the potential function $\varphi(x, y)$ while the coefficient of the imaginary unit is the stream function $\psi(x, y)$. That is the *complex potential* has been introduced as follows

$$\Phi(z) = \varphi(x, y) + i\psi(x, y) \tag{3.23}$$

Then the complex velocity is given by:

$$W(z) = \Phi'(z) = \frac{\partial \varphi}{\partial x} + i\frac{\partial \psi}{\partial x} = u - i\, v \tag{3.24}$$

with $u, v$ horizontal and vertical components of the velocity.

The Image method adopts the complex potential in order to simulate the ground effect (or the free surface) condition by the appropriate use of the source and vortex singularities explored. These considerations aiding to understand what schematically referred in Figs. 3.3.3. Thus, in an unbounded domain

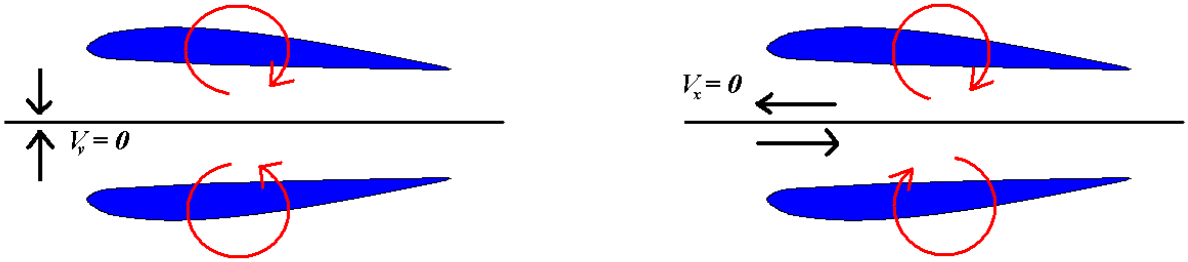


(a) Ground Effect

(b) Free Surface

a foil is simulated by a distribution of vortexes, that simulates its camber and incidence, and sources, that simulates its thickness. If a bounded domain, as in the ground effect case, is considered, then the same distribution of vortexes and sources has to be placed at a distance $y = -h$; $|x| \leq c/2$ with $c$ chord of the airfoil. The image vortexes have to show an opposite circulation in order to verify that the vertical component of the velocity is identically zero, as requested by the physics of not crossing of the ground. Similarly, for the free surface case the distribution of vortexes and sources will be placed at a distance $y = h$; $|x| \leq c/2$ and the circulation of the image vortexes has to be the same of the ones simulating the lifting surface in order to assure the zero value of the horizontal component of the velocity on the free

surface[5].

### 3.3.4 Case of bounded domain: general description of the linearized approach of Keldysh-Lavrentiev for a thin airfoil

In order to investigate the potential flow of an uniform stream past a thin airfoil at a small clearance from the ground, the linearized method of Keldysh and Lavrentiev (dated around 1949) will be introduced and adopted. It is worth to underline that the method in the beginning has been developed for studying the case of a foil submerged in an heavy fluid. Nevertheless, since its versatility and since the symmetry of the thin airfoil problem in ground effect respect to the hydrofoil problem, it can be easily adopted for solving the airfoil in ground effect problem.

The full description of the method can be found in [42]. In early $70's$ Professor Allen Plotkin issued some papers [43], [44], [45], [46] relying on the Keldysh and Lavrentiev approach working and developing the original ideas. In this context, the statement of the method in the case of the submerged hydrofoil will be presented in the appendix while for detailed references the previous work [47] is suggested. Hence, only a short general description of the method will be given caring of its main aspects and pertaining the notions useful in order to give an extension of it in the unsteady case.

Before introducing the Keldysh-Lavrentiev methodology for the steady aerodynamics in bounded domain it is worth to underline and remark that the proposed methodology concerns only the *moderate* ground effect case, hence it is applicable to ground clearances $\geq b$ where $b$ is the half chord of the airfoil. Smaller clearances pertain to the case of *extreme* ground effect and need different peculiar methodology.

#### Thin airfoil in ground effect: problem with angle of attack

Thus, the two-dimensional potential flow of an uniform stream past a symmetric thin airfoil at an angle of attack $\alpha$ and at a distance $hb$ (being $b$ the half-cord of the foil) from the ground is considered. Indicating with $U$ the free steam velocity and with $c = 2b$ the airfoil chord, it is useful to state the problem from an adimensional, and hence more general, point of view. Furthermore, all the length will be considered normalized respect to the half-chord value $b$ while the velocities will be normalized respect $U$. The frame reference has the $x$ axis aligned with the uniform stream with origin in the middle of the foil chord while the $y$ axis is orthogonal and pointing the upper side. Then, indicating with $\varepsilon$ the airfoil

[5]The boundary condition for the free surface case explored for $F \to 0$ and for $F \to \infty$ can be easily understood observing Figs. 3.3.3.

thickness, the airfoil equation is given by

$$y = -\alpha x \pm \varepsilon T(x) \tag{3.25}$$

and represents the boundary condition that has to be imposed on the airfoil.

The method relies on the definition of an appropriate complex potential function by using the image method with an appropriate distribution of sources and vortices along the chord, for solving the Laplace equation, so that the presence of the foil can be considered and such that the linearized boundary condition on the foil and on the ground are both satisfied. The complex potential is normalized respect to $U\,b$ and setting $z = x + i\,y$ it can be expressed as

$$\Phi(z,\varepsilon) = z + \varepsilon\Phi_1(z) + \mathcal{O}(\varepsilon^2) \tag{3.26}$$

where only terms of order $\mathcal{O}(\varepsilon)$ will be considered and where $\Phi_1(z)$ is the perturbation on the potential. Thus, the most the thickness is small ($\varepsilon \to 0$), the most accurate the theory presented will be. The sources and vortices intensities, normalized by $U$, are denoted by $\sigma(x)$ and $\gamma(x)$ respectively. The perturbation on the potential is then

$$\begin{aligned}\Phi_1(z) = &\int_{-1}^{1} \sigma(\xi)\left\{\log(z-\xi) + \log(z-\xi-2ih)\right\}\frac{d\xi}{2\pi} + \\ &+ i\int_{-1}^{1} \gamma(\xi)\{\log(z-\xi) + \log(z-\xi-2ih)\}\frac{d\xi}{2\pi}\end{aligned} \tag{3.27}$$

Similarly, for the complex velocity term $W(z) = \Phi'(z)$ the expansion in the term $\varepsilon$ is

$$W(z,\varepsilon) = 1 + \varepsilon W_1(z) + \mathcal{O}(\varepsilon^2) \tag{3.28}$$

and for the previous relationship given for $\Phi_1(z)$ it yields

$$\begin{aligned}W_1(z) = &\int_{-1}^{1} \sigma(\xi)\left\{\frac{1}{z-\xi} - \frac{1}{z-\xi-2ih}\right\}\frac{d\xi}{2\pi} + \\ &+ i\int_{-1}^{1} \gamma(\xi)\left\{\frac{1}{z-\xi} - \frac{1}{z-\xi-2ih}\right\}\frac{d\xi}{2\pi}\end{aligned} \tag{3.29}$$

Applying the tangency condition in $z = x \pm 0i$ with $-1 \leqslant x \leqslant 1$ one has

$$\begin{aligned} W_1(x \pm 0i) = & \int_{-1}^{1} \sigma(\xi) \left\{ \frac{1}{x-\xi} - \frac{x-\xi}{(x-\xi)^2 + 4h^2} \right\} \frac{d\xi}{2\pi} \pm \\ & \pm \frac{\gamma(x)}{2} + \int_{-1}^{1} \gamma(\xi) \left\{ \frac{-2h}{(x-\xi)^2 + 4h^2} \right\} \frac{d\xi}{2\pi} \mp \\ & + i \frac{\sigma(x)}{2} + i \int_{-1}^{1} \sigma(\xi) \left\{ \frac{-2h}{(x-\xi)^2 + 4h^2} \right\} \frac{d\xi}{2\pi} + \\ & + i \int_{-1}^{1} \gamma(\xi) \left\{ \frac{1}{x-\xi} - \frac{x-\xi}{(x-\xi)^2 + 4h^2} \right\} \frac{d\xi}{2\pi} \end{aligned} \tag{3.30}$$

The boundary condition that has to be imposed is

$$W_1(x \pm 0i) = -\alpha x \mp T'(x) \tag{3.31}$$

and setting then for the sources intensities $\sigma = 2T'(x)$ it is possible to determine $\gamma(x)$ and to obtain the relationship

$$\int_{-1}^{1} \gamma(\xi) K(x-\xi) d\xi = 2\,\pi\,\alpha - 2 \int_{-1}^{1} T'(\xi) H(x-\xi) d\xi \tag{3.32}$$

with

$$\begin{aligned} H(x) &= \frac{-2h}{x^2 + 4h^2} \\ K(x) &= \frac{1}{x} - \frac{x}{x^2 + 4h^2} \end{aligned} \tag{3.33}$$

Once the kernel functions of the vorticity and thickness problems have been evaluated, an asymptotic expansion of such functions is given respect to the adimensional parameter $\frac{1}{h}$, with $h$ clearance of the airfoil from the ground adimensionalized respect the foil half-chord, that is

$$\begin{aligned} H(x) &= \frac{1}{h} \sum_{0}^{\infty} H_n \left( \frac{x}{h} \right)^n \\ K(x) &= \frac{1}{x} + \frac{1}{h} \sum_{0}^{\infty} K_n \left( \frac{x}{h} \right)^n \\ \gamma(x) &= \sum_{0}^{\infty} h^{-n} \gamma_n(x) \end{aligned} \tag{3.34}$$

Introducing the previous expansion in the integral equation 3.32 and collecting the terms of the same magnitude of the expansion parameter, a set of problems to solve in sequence in the unknown $\gamma_i(\xi)$ is

achieved [6]

$$\begin{aligned}
\oint_{-1}^{1} \frac{\gamma_0(\xi)}{(x-\xi)} d\xi &= 2\,\pi\,\alpha \\
\oint_{-1}^{1} \frac{\gamma_1(\xi)}{(x-\xi)} d\xi &= -\oint_{-1}^{1} \left[K_0 \gamma_0(\xi) + 2T'(\xi) H_0\right] d\xi \\
&\vdots \\
\oint_{-1}^{1} \frac{\gamma_n(\xi)}{(x-\xi)} d\xi &= -\oint_{-1}^{1} \left[\sum_{m=0}^{m=n-1} K_m (x-\xi)^m \gamma_{n-m-1}(\xi) + 2H_{n-1} T'(\xi)(x-\xi)^{n-1}\right] d\xi
\end{aligned} \tag{3.35}$$

The uniqueness of the solution has to be imposed, thus, the Kutta condition fulfillment has to be considered at the trailing edge. Calling $F_n(x)$ the right hand side of equations (3.35) the imposition of the Kutta condition coincides with the satisfaction of the Söhngen equation. Thus, at the trailing edge must be imposed [7]:

$$\gamma_n(x) = \frac{1}{\pi^2} \left(\frac{1-x}{1+x}\right)^{1/2} \oint_{-1}^{1} \left(\frac{1+\xi}{1-\xi}\right)^{1/2} \frac{F_n(\xi)}{(\xi - x)} d\xi \tag{3.36}$$

In the following, terms till the third order magnitude of the expansion parameter will be considered. The exposed method allows to easily evaluate the vorticity at each order as function of the coefficients $H_n, K_n$ resulting from the expansions of the Kernel functions according to Keldysh-Lavrentiev. The evaluation of the coefficients $H_n, K_n$ is referred in the appendix[8]. With the proposed method once the vorticity at each order is evaluated, the aerodynamic quantities such as the lift force have to be calculated by superimposing the different order contribution such as

$$\mathcal{L} = \rho c U^2 \int_{-1}^{1} \left(\gamma_0(\xi) + \frac{1}{h}\gamma_1(\xi) + \frac{1}{h^2}\gamma_2(\xi) + \ldots + \frac{1}{h^n}\gamma_n(\xi)\right) d\xi \tag{3.37}$$

***Zero order solution***

Considering $n = 0$ one has:

$$\oint_{-1}^{1} \frac{\gamma_0(\xi)}{(x-\xi)} d\xi = 2\,\pi\,\alpha \qquad \Rightarrow \qquad F_0(x) = 2\,\pi\,\alpha \tag{3.38}$$

$$\Rightarrow \gamma_0(x) = 2\,\alpha \left(\frac{1-x}{1+x}\right)^{1/2} \tag{3.39}$$

***First order solution***

[6] See appendix for details, the same procedure will be carried on for a submerged foil.

[7] Note that the integrals in equations (3.35) wherever singular have to be intended in their Cauchy principal value, as meant by the integral symbol adopted. For the solution of the singular integrals see the list of the notable integrals referred in the appendix and [48].

[8] The evaluation will be carried on for the submerged foil case.

The equation that has to be solved is in this case is :

$$\oint_{-1}^{1} \frac{\gamma_1(\xi)}{(x-\xi)} d\xi = -\oint_{-1}^{1} \left[K_0 \gamma_0(\xi) + 2T'(\xi) H_0\right] d\xi \tag{3.40}$$

where $\gamma_0(\xi)$ is the one evaluated at the previous step of the zero order problem. Thus:

$$\oint_{-1}^{1} \frac{\gamma_1(\xi)}{(x-\xi)} d\xi = -\oint_{-1}^{1} K_0 \cdot 2\alpha \cdot \left(\frac{1-\xi}{1+\xi}\right)^{1/2} d\xi - 2H_0 \oint_{-1}^{1} T'(\xi) d\xi \tag{3.41}$$

but $\int_{-1}^{1} T'(\xi) d\xi = 0$ hence:

$$\begin{aligned} \oint_{-1}^{1} \frac{\gamma_1(\xi)}{(x-\xi)} d\xi \qquad &= -2\,\alpha\, K_0 \oint_{-1}^{1} \left(\frac{1-\xi}{1+\xi}\right)^{1/2} d\xi = -2\,\alpha\,\pi\, K_0 \\ &\Rightarrow F_1(x) = -2\,\pi\,\alpha\, K_0 \end{aligned} \tag{3.42}$$

that gives:

$$\gamma_1(x) = -2\,\alpha\, K_0 \left(\frac{1-x}{1+x}\right)^{1/2} \tag{3.43}$$

***Second order solution***

Setting $n = 2$ one has:

$$\oint_{-1}^{1} \frac{\gamma_2(\xi)}{(x-\xi)} d\xi = -\oint_{-1}^{1} \left[\gamma_0(\xi) K_1(x-\xi) + \gamma_1(\xi) K_0 + 2T'(\xi) H_1(x-\xi)\right] d\xi \tag{3.44}$$

Following the same solving procedures of the previous steps the following solution is achieved[9]

$$\gamma_2(x) = \frac{1}{\pi} \left(\frac{1-x}{1+x}\right)^{1/2} \left[2\pi\alpha \left(K_0^2 - \frac{3}{2} K_1 - K_1 x\right) - 2H_1 s\right] \tag{3.45}$$

being $s = \int_{-1}^{1} T(\xi) d\xi$ a quantity proportional to the airfoil area.

***Third order solution***

In case of $n = 3$ the equation that has to be solved is:

$$\begin{aligned} \oint_{-1}^{1} \frac{\gamma_3(\xi)}{x-\xi} d\xi \quad &= \quad -\oint_{-1}^{1} \big[\gamma_0(\xi) K_2 (x-\xi)^2 + \gamma_1(\xi) K_1 (x-\xi) + \\ &\quad + \gamma_2(\xi) K_0 + 2T'(\xi) H_2 (x-\xi)^2\big] d\xi \end{aligned} \tag{3.46}$$

The evaluation of the third order contribution of the vorticity is referred in the appendix[10] in order to

[9] See the appendix for details.

[10] Instead of the ground effect, the case of the submerged foil is considered in the appendix. Nevertheless, the versatility of the Keldysh-Lavrentiev methodology consists in having the same procedure for both cases.

do not weigh down the current exposition. Hence, only the final result is presented:

$$\gamma_3(x) = \frac{1}{\pi}\left(\frac{1-x}{1+x}\right)^{1/2}\Bigg\{(4H_2p - 4H_2s + 2K_0H_1s - 2\pi\alpha K_0^3 + 5\pi\alpha K_0K_1 - 4\pi\alpha K_2) + \\ + x(-4H_2s + 2\pi\alpha K_0K_1 - 4\pi\alpha K_2) + x^2(-2\pi\alpha K_2)\Bigg\} \tag{3.47}$$

where $p$ is given by $\int_{-1}^{1} T(\xi)\xi d\xi$.

***Lift evaluation***

The lift generated from the airfoil is given by

$$\mathcal{L} = \rho c U^2 \int_{-1}^{1} \gamma(\xi) d\xi \tag{3.48}$$

where the different contribution of the vorticity till the third order have to be superimposed being

$$\gamma(\xi) = \gamma_0(\xi) + \frac{1}{h}\gamma_1(\xi) + \frac{1}{h^2}\gamma_2(\xi) + \frac{1}{h^3}\gamma_3(\xi) + \dots \tag{3.49}$$

Hence

$$\begin{aligned}\gamma(x) = {} & 2\alpha\left(\frac{1-x}{1+x}\right)^{1/2} + \frac{1}{h}\cdot(-2\alpha K_0)\left(\frac{1-x}{1+x}\right)^{1/2} + \\ & \frac{1}{h^2}\cdot\frac{1}{\pi}\left(\frac{1-x}{1+x}\right)^{1/2}\left[2\pi\alpha\left(k_0^2 - \frac{3}{2}K_1 - K_1x\right) - 2H_1s\right] + \\ & + \frac{1}{h^3}\cdot\frac{1}{\pi}\left(\frac{1-x}{1+x}\right)^{1/2}\Bigg\{(4H_2p - 4H_2s + 2K_0H_1s - 2\pi\alpha K_0^3 + 5\pi\alpha K_0K_1 - 4\pi\alpha K_2) + \\ & + x(-4H_2s + 2\pi\alpha K_0K_1 - 4\pi\alpha K_2) + x^2(-2\pi\alpha K_2)\Bigg\}\end{aligned} \tag{3.50}$$

The previous equation can be re-arranged isolating the terms independent from $x$ or proportional to $x, x^2, \dots ...$ yielding

$$\begin{aligned}\gamma(x) = {} & \left(\frac{1-x}{1+x}\right)^{1/2}\Bigg\{\Bigg[2\alpha - \frac{1}{h}2\alpha K_0 + \frac{1}{h^2\pi}\left(2\pi\alpha\left(K_0^2 - \frac{3}{2}K_1\right) - 2H_1s\right) + \\ & + \frac{1}{h^3\pi}(4H_2(p-s) + 2K_0H_1s - 2\pi\alpha K_0^3 + 5\pi\alpha K_0K_1 - 4\pi\alpha K_2)\Bigg]_{\mathcal{A}} + \\ & + x\cdot\left[\frac{1}{h^2\pi}(-2\pi\alpha K_1) + \frac{1}{h^3\pi}(-4H_2s + 2\pi\alpha K_0K_1 - 4\pi\alpha K_2)\right]_{\mathcal{B}} + \\ & + x^2\cdot\left[\frac{1}{h^3\pi}(-2\pi\alpha K_2)\right]_{\mathcal{C}}\Bigg\}\end{aligned} \tag{3.51}$$

that has to be integrated as follows[11]

$$\int_{-1}^{1}\gamma(\xi)d\xi=\int_{-1}^{1}\left(\frac{1-\xi}{1+\xi}\right)^{1/2}\left\{\left[\dots\right]_{\mathcal{A}}+\left[\dots\right]_{\mathcal{B}}+\left[\dots\right]_{\mathcal{C}}\right\}d\xi \tag{3.52}$$

Integrating the terms $\mathcal{A},\mathcal{B},\mathcal{C}$ the remarkable integrals listed in the appendix have to be used obtaining:

$$\begin{aligned}\int_{-1}^{1}\left(\frac{1-\xi}{1+\xi}\right)^{1/2}\left[\dots\right]_{\mathcal{A}} &= \pi\cdot\left[2\alpha-\frac{1}{h}2\alpha K_0+\frac{1}{h^2\pi}\left(2\pi\alpha\left(K_0^2-\frac{3}{2}K_1\right)-2H_1s\right)+\right.\\ &\left.+\frac{1}{h^3\pi}(4H_2(p-s)+2K_0H_1s-2\pi\alpha K_0^3+5\pi\alpha K_0K_1-4\pi\alpha K_2)\right] \qquad (3.53)\\ \int_{-1}^{1}\left(\frac{1-\xi}{1+\xi}\right)^{1/2}\left[\dots\right]_{\mathcal{B}} &= -\frac{\pi}{2}\cdot\left[\frac{1}{h^2\pi}(-2\pi\alpha K_1)+\frac{1}{h^3\pi}(-4H_2s+2\pi\alpha K_0K_1-4\pi\alpha K_2)\right]_{\mathcal{B}} \qquad (3.54)\\ \int_{-1}^{1}\left(\frac{1-\xi}{1+\xi}\right)^{1/2}\left[\dots\right]_{\mathcal{C}} &= \frac{\pi}{2}\cdot\left[\frac{1}{h^3\pi}(-2\pi\alpha K_2)\right] \qquad (3.55)\end{aligned}$$

Collecting the terms in the same order of $1/h$ one has:

$$\begin{aligned}(1/h)^0 &: \quad C_{L0}=2\pi\alpha \qquad (3.56)\\ (1/h)^1 &: \quad C_{L1}=2\pi\alpha(-K_0)\\ (1/h)^2 &: \quad C_{L2}=2\pi\alpha(K_0^2-K_1)-2H_1s\\ (1/h)^3 &: \quad C_{L3}=2\pi\alpha\left(-K_0^3+2K_0K_1-\frac{3}{2}K_2\right)+2H_2(2p-s)+2K_0H_1s\end{aligned}$$

As previously mentioned, the extreme versatility of the proposed methodology due to the symmetry between the wall-effects in air/water environment allows to adopt the obtained result even for a submerged hydrofoil[12]. The only difference will be in the value of the Keldysh-Lavrentiev coefficient adopted due to the different direction of the vorticity distributions introduced for simulating the image foil presence: counter-rotating vorticity distribution for the ground effect case, co-rotating vorticity distribution for the free surface effect one as previously shown in Figure 3.3.3. Summarizing the Keldysh-Lavrentiev coefficient for the airfoil problem are

$$H(x)=\frac{-2h}{x^2+4h^2} \tag{3.57}$$

$$K(x)=\frac{1}{x}-\frac{x}{x^2+4h^2} \tag{3.58}$$

[11]The integration will give directly the adimensional lift coefficient since it coincides with the adimensionalization of the equation (3.48).

[12]Nevertheless, the hydrofoil case demonstration of the method is a more general one since the Froude number influence is considered. For such reason the main steps that delineates the method for the hydrofoil problem are referred to the appendix

while in the hydrofoil case they are

$$\begin{aligned} H(x) &= \frac{-2h}{x^2+4h^2} - 2F^{-2} Re\left[I[iF^{-2}(x-2ih)]\right] \\ K(x) &= \frac{1}{x} + \frac{x}{x^2+4h^2} - 2F^{-2} Im\left[I[iF^{-2}(x-2ih)]\right] \end{aligned} \tag{3.59}$$

The Taylor series expansion till the ninth order for the airfoil coefficients has produced

$$\begin{aligned} K_0 &= 0 & H_0 &= -\tfrac{1}{2} \\ K_1 &= -\tfrac{1}{4} & H_1 &= 0 \\ K_2 &= 0 & H_2 &= \tfrac{1}{8} \\ K_3 &= \tfrac{1}{16} & H_3 &= 0 \\ K_4 &= 0 & H_4 &= -\tfrac{1}{32} \\ K_5 &= -\tfrac{1}{64} & H_5 &= 0 \\ K_6 &= 0 & H_6 &= \tfrac{1}{128} \\ K_7 &= \tfrac{1}{256} & H_7 &= 0 \\ K_8 &= 0 & H_8 &= -\tfrac{1}{512} \\ K_9 &= -\tfrac{1}{1024} & H_9 &= 0 \end{aligned}$$

with evident alternating of zeros and powers of two.

Imposing the proper value of the Keldysh-Lavrentiev coefficients for the airfoil problem and setting $\alpha = \pi/8$ for the angle of attack value, the ratio between the lift coefficient in ground effect and the lift coefficient in free flight

$$\frac{C_{Lh}}{C_{L\infty}} = \frac{C_{L0} + h^{-1} C_{L1} + h^{-2} C_{L2}}{C_{L0}} \tag{3.60}$$

considered while varying the ground clearance is depicted in Figure 3.5

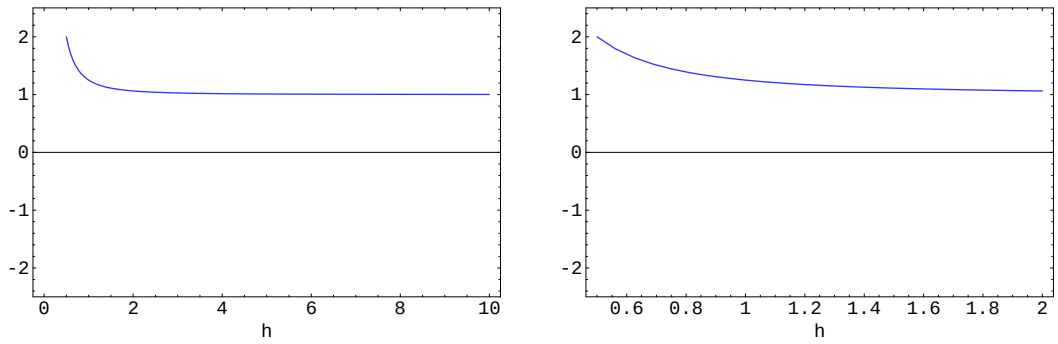


Figure 3.5: *Trend of ratio between the steady lift coefficient in ground effect and the steady lift coefficient in free flight at different adimensional distances expressed as half-chords from the ground.*

The depicted trend shows that the remarkable lift improvement typical of the ground effect condition

is obtained for ground clearances minor or equal to one half-chord.

## 3.4 Lifting surfaces in bounded domain: problems related to the unsteady aerodynamics extension

Drawing on the ground effect model based on the asymptotic expansion proposed by Keldysh-Lavrentiev and adopted by Plotkin in steady aero-hydrodinamics problems, it seems convenient to explore how the mentioned model can be used in order to take into account the ground effect flying condition in case of unsteady flows. Practically, such a study concerns the estimation of the possibility of an extension of the well-known Theodorsen theory for bounded domains. The lack of studies in literature about the applicability of the ground effect modeling proposed by Plotkin for unsteady aero-hydrodynamic problems represents the peculiarity and the vanguard interest of the present work.

Thus, for sake of simplicity and pursuing the studies of Theodorsen, will be considered from now on a flat plate model originated by a proper distribution of two-dimensional vortices along the chord and placed in the same reference frame adopted in the previous section for the airfoil in ground effect case. Thus, the flat plate is placed in $y = 0$ and extended in $x \in [-1, 1]$. The hypothesis of unsteady aerodynamics yields to a time dependency for the total circulation around the lifting surface, therefore a wake of two-dimensional shed vortices along the $x$-axis extending from the trailing edge to infinity had to be added to the flat plate model.

Hence, for the mentioned flat plate in unsteady aerodynamics and in an unbounded domain the following adimensional fundamental integral equation can be written[13]

$$w_a(x,t) = -\frac{1}{2\pi}\oint_{-1}^{1} \frac{\gamma_a(\xi,t)}{x-\xi}\,d\xi - \frac{1}{2\pi}\int_{1}^{\infty} \frac{\gamma_w(\xi,t)}{x-\xi}\,d\xi \tag{3.61}$$

being $w_a$ the vertical component of the velocity of the body normalized respect to the uniform stream velocity $U$ that has the direction of the positive $x$-axis. Furthermore, the subscript $_a$ denotes quantities pertinent to the lifting surface[14] while the subscript $_w$ denotes the ones pertinent to the wake domain.

As assumed in the steady case, considering a bounded domain the fundamental solutions of the image method are meaningless and the kernel function $K$ is then the one given by the series expansion of

[13] See also [49] eq. $5 - 313a$.

[14] Considering a flat plate instead of an airfoil, the effects of thickness and cumber have to be intended as uncoupled. Thus, $\gamma_a$ denotes directly the sum of the upper and lower side of the lifting surface that is $\gamma_a = \gamma_U + \gamma_L$.

Keldysh-Lavrentiev, hence:

$$w_a\,(x,t) = -\frac{1}{2\pi}\oint_{-1}^{1}\gamma_a(\xi,t)\,K(x-\xi)\,d\xi\;-\;\frac{1}{2\pi}\int_{1}^{\infty}\gamma_w(\xi,t)\,K(x-\xi)\,d\xi \tag{3.62}$$

Thus, according to the Keldysh-Lavrentiev expansion and to the previous work of Plotkin in steady flow, the integral equation for an airfoil taking into account the ground effect condition in unsteady aerodynamics can be written in the frequency domain as:

$$\bar{w}_a(x) = -\frac{1}{2\pi}\oint_{-1}^{1}\bar{\gamma}_a(\xi)\,K(x-\xi)\,d\xi\;-\;\frac{1}{2\pi}\int_{1}^{\infty}\bar{\gamma}_w(\xi)\,K(x-\xi)\,d\xi \tag{3.63}$$

since with the assumption of harmonic motion each function can be decoupled in as $f(x,t) = \bar{f}(x)\cdot e^{i\omega t}$ where $^-$ denotes the harmonic component.

The boundary condition is given by

$$w_a\,(x,t) = \bar{w}_a(x)\cdot e^{i\omega t} = \left[i\omega\bar{z}_a(x) + U\,\frac{d\bar{z}_a}{dx}\right]\cdot e^{i\omega t} \tag{3.64}$$

As known, the quantity $\bar{\gamma}_w(\xi)$ acting on the wake, can be expressed in terms of the lifting surface circulation $\Gamma$. In order to do that it is useful to define the integral $\Gamma\,(x,t) := \int_{-1}^{x}\gamma(\xi,t)\,d\xi$.

Considering the Kutta condition as referred in [50],[49],[51] and with the harmonic motion assumption the vorticity intensity[15] on the wake in terms of the total circulation on the lifting surface is

$$\bar{\gamma}_w\,(x) = -\frac{\bar{\Gamma}(1)}{b}\,ik\,e^{-ik(x-1)} \tag{3.65}$$

where $k = \frac{\omega b}{U}$ denotes the reduced frequency. Substituting Eq. 3.65 into Eq. 3.62 and moving the term $\bar{\gamma}_a$ on the left hand side, the following relationship is achieved:

$$\frac{1}{2\pi}\oint_{-1}^{1}\bar{\gamma}_a(\xi)\,K(x-\xi)\,d\xi = -\bar{w}_a(x) + \frac{ik}{2\pi}\frac{\bar{\Gamma}(1)}{b}\int_{1}^{\infty}e^{-ik(\xi-1)}K(x-\xi)\,d\xi \tag{3.66}$$

It is proper to remark[16] that in the Theodorsen Theory the term $\bar{\Gamma}(1)/b$ is given by

$$\frac{\bar{\Gamma}(1)}{b} = \frac{4e^{-ik}}{\pi\,ik\left[H_1^{(2)}(k) + iH_0^{(2)}(k)\right]}\cdot\oint_{-1}^{1}\sqrt{\frac{1+\xi}{1-\xi}}\,\bar{w}_a(\xi)\,d\xi \tag{3.67}$$

Introducing the Keldysh-Lavrentiev asymptotic expansion given in 3.34 in the left hand side of Eq. 3.66 and omitting the subscript $_a$ since all the terms are now referred to quantities evaluated on the lifting

[15] Note that the given expression for $\bar{\gamma}_w$ is adimensional hence the term $\bar{\Gamma}(1)$ denotes that the quantity $\bar{\Gamma}$ is evaluated at the trailing edge that is $b/b = 1$.

[16] See also [50],[49],[51]

surface the following is achieved

$$\frac{1}{2\pi}\oint_{-1}^{1}\sum_{0}^{\infty}\bar{\gamma}_n(\xi)\left(\frac{1}{h}\right)^n\left[\frac{1}{x-\xi}+\frac{1}{h}\sum_{0}^{\infty}K_n\left(\frac{x-\xi}{h}\right)^n\right]d\xi=-\bar{w}(x)+\frac{ik}{2\pi}\frac{\bar{\Gamma}(1)}{b}\int_{1}^{\infty}e^{-ik(\xi-1)}K(x-\xi)d\xi \quad (3.68)$$

The previous relationship has been written considering that $\bar{\Gamma}(1)$ is already an integral quantity hence, a further series expansion of it would only add more complexity to the exposition of the problem without likely adding any relevant result.

Furthermore, some fundamental hypothesis and remarks have to be done in order to account in steady aerodynamics the presence of a bounded domain. The former aspect to remark respect to the approach previously investigated about the Keldysh-Lavrentiev methodology in the steady case, is that Eq.3.66 (and then Eq. 3.68) in the unknown $\bar{\gamma}_a$ is an integral equation that is not invertible since an analytical inversion is known only for Kernel function of the kind $K(x-\xi)=1/(x-\xi)$ while in the bounded domain the Kernel function has a more general expression as referred in 3.58. The latter aspect pertains to the advantage of performing an asymptotic expansion and to the observation that the right hand side of Eq. 3.68 is a known quantity once the ground clearance $h$ is known. Indeed, the expansion suggested by Keldysh-Lavrentiev on the airfoil in the steady case for the terms of vorticity and for the Kernel function was having the advantage to lead to an expression of the lift coefficient that could be evaluated at any clearance $h$ from the ground. The consideration of unsteadiness, though, introduces a dependency from the time and the dependency of the lift coefficient from the ground clearance will happen through function that are time dependent. Thus, the same asymptotic expansion of Keldysh-Lavrentiev is adopted here with a different meaning respect to the steady case. Indeed, in the steady aerodynamics the asymptotic expansion was presenting the advantage of giving an analytical expression of the lift coefficient at any changing of the ground clearance $h$ while in the unsteady case a specific value of the ground clearance is assigned, since in the unsteady case also the known term depends from $h$. Thus, in the unsteady case the lift coefficient will not have an analytical expression generally valid for any $h$ and always a specific given $h$ value will be adopted. The subscript $_*$ denotes then the given $h$ value. Hence, the asymptotic expansion performed in Eq. 3.68 does not involve the wake terms. With the exposed hypothesis Eq. 3.68 becomes

$$\begin{aligned}&\frac{1}{2\pi}\oint_{-1}^{1}\sum_{0}^{\infty}\bar{\gamma}_n(\xi)\left(\frac{1}{h}\right)^n\left[\frac{1}{x-\xi}+\frac{1}{h}\sum_{0}^{\infty}K_n\cdot\left(\frac{x-\xi}{h}\right)^n\right]d\xi=-\bar{w}(x)+\\&+\frac{ik}{2\pi}\frac{\bar{\Gamma}(1)}{b}e^{ik}\int_{1}^{\infty}e^{-ik\xi}\left[\frac{1}{x-\xi}-\frac{x-\xi}{(x-\xi)^2+4h_*^2}\right]d\xi\end{aligned} \quad (3.69)$$

Collecting the terms of the same magnitude in the parameter $1/h$, a collection of problems to solve in

cascade is obtained as follows

$$\begin{aligned}
\oint_{-1}^{1} \frac{\bar{\gamma}_0(\xi)}{(x-\xi)} d\xi &= -\bar{w}(x) + \frac{ik}{2\pi} \frac{\bar{\Gamma}(1)}{b} e^{ik} \int_1^{\infty} e^{-ik\xi} \left[ \frac{1}{x-\xi} - \frac{x-\xi}{(x-\xi)^2 + 4h_*^2} \right] d\xi \qquad (3.70)\\
\oint_{-1}^{1} \frac{\bar{\gamma}_1(\xi)}{(x-\xi)} d\xi &= -\frac{1}{2\pi} \oint_{-1}^{1} [K_0 \bar{\gamma}_0(\xi)]\, d\xi \\
\oint_{-1}^{1} \frac{\bar{\gamma}_2(\xi)}{(x-\xi)} d\xi &= -\frac{1}{2\pi} \oint_{-1}^{1} [K_0 \bar{\gamma}_1(\xi) + K_1(x-\xi)\bar{\gamma}_0(\xi)] d\xi
\end{aligned}$$

where for conciseness and for the purposes of this work only terms till the second order have been considered.

Thus, the achieved equation of the zero order in the frequency domain is:

$$\oint_{-1}^{1} \frac{\bar{\gamma}_0(\xi)}{x-\xi} d\xi = -2\,\pi\,\bar{w}(x) + i\,k\,\frac{\bar{\Gamma}(1)}{b} e^{i\,k} \int_1^{+\infty} e^{-i\,k\,\xi} \left[ \frac{1}{x-\xi} - \frac{x-\xi}{(x-\xi)^2 + 4\,h_*^2} \right] d\xi \qquad (3.71)$$

Following the steps of the steady case, the application of the Söhngen inversion formula[17]

$$\bar{\gamma}_n(x) = \frac{1}{\pi^2} \left( \frac{1-x}{1+x} \right)^{1/2} \oint_{-1}^{1} \left( \frac{1+\xi}{1-\xi} \right)^{1/2} \frac{\mathcal{F}_n(\xi)}{\xi - x} d\xi \qquad (3.72)$$

gives

$$\begin{aligned}
\bar{\gamma}_0(x) &= \frac{2}{\pi} \left( \frac{1-x}{1+x} \right)^{1/2} \oint_{-1}^{1} \left( \frac{1+\xi}{1-\xi} \right)^{1/2} \frac{\bar{w}(\xi)}{x-\xi}\, d\xi + \\
&- \frac{i\,k}{\pi^2} \frac{\bar{\Gamma}(1)}{b}\, e^{ik} \left( \frac{1-x}{1+x} \right)^{1/2} \oint_{-1}^{1} \left( \frac{1+\xi}{1-\xi} \right)^{1/2} \left[ \int_1^{+\infty} e^{-i\,k\,t} \frac{dt}{\xi - t} \right] \frac{d\xi}{x-\xi} + \\
&+ \frac{i\,k}{\pi^2} \frac{\bar{\Gamma}(1)}{b}\, e^{ik} \left( \frac{1-x}{1+x} \right)^{1/2} \oint_{-1}^{1} \left( \frac{1+\xi}{1-\xi} \right)^{1/2} \left[ \int_1^{+\infty} \frac{e^{-i\,k\,t}(\xi - t) dt}{(\xi - t)^2 + 4\,h_*^2} \right] \frac{d\xi}{x-\xi} \qquad (3.73)
\end{aligned}$$

Setting

$$\mathcal{I}_n(\xi, h_*) = \int_1^{+\infty} \frac{e^{-i\,k\,t}(\xi - t)\, dt}{(\xi - t)^2 + 4\,h_*^2}$$

it yields

$$\begin{aligned}
\bar{\gamma}_0(x) &= \frac{2}{\pi} \left( \frac{1-x}{1+x} \right)^{1/2} \oint_{-1}^{1} \left( \frac{1+\xi}{1-\xi} \right)^{1/2} \frac{\bar{w}(\xi)}{x-\xi}\, d\xi + \\
&- \frac{i\,k}{\pi^2} \frac{\bar{\Gamma}(1)}{b}\, e^{ik} \left( \frac{1-x}{1+x} \right)^{1/2} \oint_{-1}^{1} \left( \frac{1+\xi}{1-\xi} \right)^{1/2} \left[ \int_1^{+\infty} e^{-i\,k\,t} \frac{dt}{\xi - t} \right] \frac{d\xi}{x-\xi} + \\
&+ \frac{i\,k}{\pi^2} \frac{\bar{\Gamma}(1)}{b}\, e^{ik} \left( \frac{1-x}{1+x} \right)^{1/2} \oint_{-1}^{1} \left( \frac{1+\xi}{1-\xi} \right)^{1/2} \frac{[\mathcal{I}_n(\xi, h_*)]}{x-\xi}\, d\xi \qquad (3.74)
\end{aligned}$$

[17]Where $\mathcal{F}_n(\xi)$ denotes the right hand side of Eq. 3.71.

Following the procedure referred in [49] pgg.275/276 and setting

$$\bar{\Omega} = \frac{\bar{\Gamma}}{b} e^{ik}$$

the following is achieved

$$\begin{aligned}
\bar{\gamma}_0(x) &= \frac{2}{\pi}\left(\frac{1-x}{1+x}\right)^{1/2} \oint_{-1}^{1} \left(\frac{1+\xi}{1-\xi}\right)^{1/2} \frac{\bar{w}(\xi)}{x-\xi}\, d\xi + \\
&- \frac{i\,k}{\pi^2}\,\bar{\Omega}\left(\frac{1-x}{1+x}\right)^{1/2} \int_{1}^{+\infty} e^{-i\,k\,t}\, \frac{\pi}{x-t}\sqrt{\frac{1+t}{1-t}}\, dt + \\
&+ \frac{i\,k}{\pi^2}\,\bar{\Omega}\left(\frac{1-x}{1+x}\right)^{1/2} \oint_{-1}^{1} \left(\frac{1+\xi}{1-\xi}\right)^{1/2} \frac{[\mathcal{I}_n(\xi, h_*)]}{x-\xi}\, d\xi
\end{aligned} \tag{3.75}$$

Integrating between $x = [-1, 1]$

$$\begin{aligned}
\int_{-1}^{1} \bar{\gamma}_0(x) dx &= \bar{\Omega}\, e^{-ik} = \\
&= \int_{-1}^{1} \frac{2}{\pi}\left(\frac{1-x}{1+x}\right)^{1/2} \oint_{-1}^{1} \left(\frac{1+\xi}{1-\xi}\right)^{1/2} \frac{\bar{w}(\xi)}{x-\xi}\, d\xi\, dx + \\
&- \frac{i\,k}{\pi}\,\bar{\Omega} \int_{-1}^{1} \left(\frac{1-x}{1+x}\right)^{1/2} \int_{1}^{+\infty} e^{-i\,k\,t}\, \frac{1}{x-t}\sqrt{\frac{1+t}{1-t}}\, dt\, dx + \\
&+ \frac{i\,k}{\pi^2}\,\bar{\Omega} \int_{-1}^{1} \left(\frac{1-x}{1+x}\right)^{1/2} \oint_{-1}^{1} \left(\frac{1+\xi}{1-\xi}\right)^{1/2} \frac{[\mathcal{I}_n(\xi, h_*)]}{x-\xi}\, d\xi\, dx
\end{aligned} \tag{3.76}$$

and then interchanging the integration orders it yields

$$\begin{aligned}
\int_{-1}^{1} \bar{\gamma}_0(x) dx &= \bar{\Omega}\, e^{-ik} = \\
&= \frac{2}{\pi} \oint_{-1}^{1} \left(\frac{1+\xi}{1-\xi}\right)^{1/2} \bar{w}(\xi) \int_{-1}^{1} \left(\frac{1-x}{1+x}\right)^{1/2} \frac{dx}{x-\xi}\, d\xi + \\
&- \frac{i\,k}{\pi}\,\bar{\Omega} \int_{1}^{+\infty} e^{-i\,k\,t} \sqrt{\frac{1+t}{1-t}} \int_{-1}^{1} \left(\frac{1-x}{1+x}\right)^{1/2} \frac{dx}{x-t}\, dt + \\
&+ \frac{i\,k}{\pi^2}\,\bar{\Omega} \oint_{-1}^{1} \left(\frac{1+\xi}{1-\xi}\right)^{1/2} [\mathcal{I}_n(\xi, h_*)] \int_{-1}^{1} \left(\frac{1-x}{1+x}\right)^{1/2} \frac{dx}{x-\xi}\, d\xi
\end{aligned} \tag{3.77}$$

Thus, rearranging the terms:

$$\begin{aligned}\int_{-1}^{1}\bar{\gamma}_0(x)dx &= \bar{\Omega}\,e^{-ik} = \\ &= -2\oint_{-1}^{1}\left(\frac{1+\xi}{1-\xi}\right)^{1/2}\bar{w}(\xi)d\xi + \\ &- i\,k\,\bar{\Omega}\int_{1}^{+\infty}e^{-i\,k\,t}\left[\sqrt{\frac{t+1}{t-1}}-1\right]dt + \\ &- i\,k\,\bar{\Omega}\oint_{-1}^{1}\left(\frac{1+\xi}{1-\xi}\right)^{1/2}[\mathcal{I}_n(\xi,h_*)]d\xi \end{aligned} \tag{3.78}$$

Solving respect to the $\bar{\Omega}$ term the following is achieved:

$$\begin{aligned}\bar{\Omega}\quad & e^{-ik}+i\,k\,\bar{\Omega}\left\{-\frac{\pi}{2}[H_1^{(2)}(k)+iH_0^{(2)}(k)-\frac{e^{-ik}}{ik}]\right\}+ \\ +\quad & i\,k\,\bar{\Omega}\oint_{-1}^{1}\left(\frac{1+\xi}{1-\xi}\right)^{1/2}[\mathcal{I}_n(\xi,h_*)]d\xi = -2\oint_{-1}^{1}\left(\frac{1+\xi}{1-\xi}\right)^{1/2}\bar{w}(\xi)d\xi \end{aligned} \tag{3.79}$$

Thus,

$$\begin{aligned}\bar{\Omega}\quad & \left\{[H_1^{(2)}(k)+iH_0^{(2)}(k)]-\frac{2}{\pi}\oint_{-1}^{1}\left(\frac{1+\xi}{1-\xi}\right)^{1/2}[\mathcal{I}_n(\xi,h_*)]d\xi\right\}= \\ =\quad & \frac{4}{\pi\,i\,k}\oint_{-1}^{1}\left(\frac{1+\xi}{1-\xi}\right)^{1/2}\bar{w}(\xi)d\xi \end{aligned} \tag{3.80}$$

that gives

$$\bar{\Omega} = \frac{4}{\pi\,i\,k}\frac{\oint_{-1}^{1}\left(\frac{1+\xi}{1-\xi}\right)^{1/2}\bar{w}(\xi)d\xi}{\left\{[H_1^{(2)}(k)+iH_0^{(2)}(k)]-\frac{2}{\pi}\oint_{-1}^{1}\left(\frac{1+\xi}{1-\xi}\right)^{1/2}[\mathcal{I}_n(\xi,h_*)]d\xi\right\}} \tag{3.81}$$

As shown in the steady case, the asymptotic expansion proposed by Keldysh-Lavrentiev was allowing to easily evaluate the vorticity at each order of the parameter $1/h$. The total vorticity was then given by a sum of the kind $\gamma(x)=\gamma_0(x)+(1/h)\gamma_1(x)+(1/h^2)\gamma_2(x)+....$ Thus, it is worth to remind that the aerodynamic coefficient of pressure, lift, momentum will be evaluated with the same procedure. Hence, in order to obtain an expression for the lift coefficient, the pressure coefficient must be evaluated following the steps of the Theodorsen Theory[18] and considering that for the Keldysh-Lavrentiev approach one

[18] See [50],[49],[51].

has[19]

$$\frac{\Delta\bar{p}(x)}{\rho U^2} = -\left[\bar{\gamma}_0(x) + h^{-1}\bar{\gamma}_1(x) + \ldots\right] - i\,k\int_{-1}^{x}(\bar{\gamma}_0(\xi) + h^{-1}\bar{\gamma}_1(\xi) + \ldots)\,d\xi \tag{3.83}$$

Hence, the pressure coefficient that represents the difference between the pressure of the upper and lower side[20] of the lifting surface at the zero order can be adimensionally written as

$$\frac{\Delta\bar{p}_0(x)}{\rho U^2} = \Delta\bar{C}_{p_0}(x) = -\bar{\gamma}_0(x) - i\,k\int_{-1}^{x_*}\bar{\gamma}_0(s)\,ds \tag{3.84}$$

Hence, the value of equation 3.75 must be calculated for $x = s$, and then integrate the obtained value in the range $[-1, x_*]$.

Thus, setting $x = s$

$$\begin{aligned}
\bar{\gamma}_0(s) &= \frac{2}{\pi}\left(\frac{1-s}{1+s}\right)^{1/2}\oint_{-1}^{1}\left(\frac{1+\xi}{1-\xi}\right)^{1/2}\frac{\bar{w}(\xi)}{s-\xi}\,d\xi + \\
&- \frac{i\,k}{\pi}\,\bar{\Omega}\left(\frac{1-s}{1+s}\right)^{1/2}\int_{1}^{+\infty}e^{-i\,k\,t}\,\frac{1}{s-t}\sqrt{\frac{1+t}{1-t}}\,dt + \\
&+ \frac{i\,k}{\pi^2}\,\bar{\Omega}\left(\frac{1-s}{1+s}\right)^{1/2}\oint_{-1}^{1}\left(\frac{1+\xi}{1-\xi}\right)^{1/2}\frac{[\mathcal{I}_n(\xi, h_*)]}{s-\xi}\,d\xi
\end{aligned} \tag{3.85}$$

Integrating in the range $[-1, x_*]$ and interchanging the integration order it yields

$$\begin{aligned}
\int_{-1}^{x_*}\bar{\gamma}_0(s) &= \frac{2}{\pi}\oint_{-1}^{1}\left(\frac{1+\xi}{1-\xi}\right)^{1/2}\bar{w}(\xi)\int_{-1}^{x_*}\left(\frac{1-s}{1+s}\right)^{1/2}\frac{ds}{s-\xi}d\xi + \\
&- \frac{i\,k}{\pi}\,\bar{\Omega}\int_{1}^{+\infty}e^{-i\,k\,t}\sqrt{\frac{1+t}{1-t}}\int_{-1}^{x_*}\left(\frac{1-s}{1+s}\right)^{1/2}\frac{ds}{s-t}dt + \\
&+ \frac{i\,k}{\pi^2}\,\bar{\Omega}\oint_{-1}^{1}\left(\frac{1+\xi}{1-\xi}\right)^{1/2}[\mathcal{I}_n(\xi, h_*)]\int_{-1}^{x_*}\left(\frac{1-s}{1+s}\right)^{1/2}\frac{ds}{s-\xi}d\xi
\end{aligned} \tag{3.86}$$

[19] Where

$$\begin{aligned}
\frac{\Delta\bar{p}_0(x)}{\rho U^2} &= -\bar{\gamma}_0(x) - i\,k\int_{-1}^{x}\bar{\gamma}_0(\xi)d\xi \\
\frac{\Delta\bar{p}_1(x)}{\rho U^2} &= -\bar{\gamma}_1(x) - i\,k\int_{-1}^{x}\bar{\gamma}_1(\xi)\,d\xi \\
\frac{\Delta\bar{p}_2(x)}{\rho U^2} &= -\bar{\gamma}_2(x) - i\,k\int_{-1}^{x}\bar{\gamma}_2(\xi)\,d\xi
\end{aligned} \tag{3.82}$$

and so on.

[20] In the current section the pressure difference will be intended as given by the difference between the upper and lower side of the lifting surface for better showing the analogy with the analytical steps of Ref.[49], but in the next section the pressure coefficient will be considered as given by the difference between the lower and the upper side of the lifting surface determining a changing of sign.

Thus,

$$\begin{aligned}\int_{-1}^{x_*}\bar{\gamma}_0(s) &= -\frac{2}{\pi}\oint_{-1}^{1}\left(\frac{1+\xi}{1-\xi}\right)^{1/2}\bar{w}(\xi)\int_{-1}^{x_*}\left(\frac{1-s}{1+s}\right)^{1/2}\frac{ds}{\xi-s}d\xi + \\ &- \frac{i\,k}{\pi}\,\bar{\Omega}\int_{1}^{+\infty}e^{-i\,k\,t}\sqrt{\frac{t+1}{t-1}}\int_{-1}^{x_*}\left(\frac{1-s}{1+s}\right)^{1/2}\frac{ds}{t-s}dt + \\ &- \frac{i\,k}{\pi^2}\,\bar{\Omega}\oint_{-1}^{1}\left(\frac{1+\xi}{1-\xi}\right)^{1/2}[\mathcal{I}_n(\xi,h_*)]\int_{-1}^{x_*}\left(\frac{1-s}{1+s}\right)^{1/2}\frac{ds}{\xi-s}d\xi \end{aligned} \tag{3.87}$$

that can be written as

$$\begin{aligned}\int_{-1}^{x_*}\bar{\gamma}_0(s) &= -\frac{2}{\pi}\oint_{-1}^{1}\Lambda_1(x_*,\xi)\bar{w}(\xi)d\xi - \frac{\bar{\Omega}}{\pi}\int_{1}^{+\infty}\frac{\partial\Lambda_2}{\partial t}(x_*,t)e^{-i\,k\,t}\,dt + \\ &- \frac{i\,k}{\pi^2}\,\bar{\Omega}\oint_{-1}^{1}\Lambda_1(x_*,\xi)[\mathcal{I}_n(\xi,h_*)]d\xi \end{aligned} \tag{3.88}$$

Furthermore, it is worth to note that

$$\frac{\partial\Lambda_2}{\partial t} = \sqrt{\frac{1-x_*}{1+x_*}}\left[\frac{1}{\sqrt{t^2-1}} + \sqrt{\frac{t+1}{t-1}}\,\frac{1}{x_*-t}\right] \tag{3.89}$$

Hence, from Eqs. 3.75,3.88 it follows for the pressure coefficient

$$\begin{aligned}\Delta\bar{C}_{p_0}(x_*) &= -\bar{\gamma}_0(x) - i\,k\int_{-1}^{x_*}\bar{\gamma}_0(s)\,ds = \\ &= -\frac{2}{\pi}\left(\frac{1-x_*}{1+x_*}\right)^{1/2}\oint_{-1}^{1}\left(\frac{1+\xi}{1-\xi}\right)^{1/2}\frac{\bar{w}(\xi)}{x_*-\xi}\,d\xi + \\ &- \frac{i\,k}{\pi}\,\bar{\Omega}\left(\frac{1-x_*}{1+x_*}\right)^{1/2}\int_{1}^{+\infty}e^{-i\,k\,t}\sqrt{\frac{t+1}{t-1}}\,\frac{dt}{x_*-t} + \\ &- \frac{i\,k}{\pi^2}\,\bar{\Omega}\left(\frac{1-x_*}{1+x_*}\right)^{1/2}\oint_{-1}^{1}\left(\frac{1+\xi}{1-\xi}\right)^{1/2}\frac{[\mathcal{I}_n(\xi,h_*)]}{x_*-\xi}\,d\xi + \\ &+ \frac{2\,i\,k}{\pi}\oint_{-1}^{1}\Lambda_1(x_*,\xi)\bar{w}(\xi)d\xi + \\ &+ \frac{i\,k\,\bar{\Omega}}{\pi}\int_{1}^{+\infty}\left(\frac{1-x_*}{1+x_*}\right)^{1/2}\frac{1}{\sqrt{t^2-1}}e^{-i\,k\,t}\,dt + \\ &+ \frac{i\,k\,\bar{\Omega}}{\pi}\int_{1}^{+\infty}\left(\frac{1-x_*}{1+x_*}\right)^{1/2}e^{-i\,k\,t}\sqrt{\frac{t+1}{t-1}}\,\frac{dt}{x_*-t} + \\ &+ \frac{(i\,k)^2}{\pi^2}\,\bar{\Omega}\oint_{-1}^{1}\Lambda_1(x_*,\xi)[\mathcal{I}_n(\xi,h_*)]d\xi \end{aligned} \tag{3.90}$$

That is[21]

$$\begin{aligned}\Delta\bar{C}_{p_0}(x_*) &= \frac{i\,k}{\pi}\,\bar{\Omega}\int_1^{+\infty}\sqrt{\frac{1-x_*}{1+x_*}}\frac{1}{\sqrt{t^2-1}}e^{-i\,k\,t}\,dt + \\ &- \frac{2}{\pi}\oint_{-1}^{1}\left[\left(\frac{1-x_*}{1+x_*}\right)^{1/2}\left(\frac{1+\xi}{1-\xi}\right)^{1/2}\frac{1}{x_*-\xi} - i\,k\,\Lambda_1(x_*,\xi)\right]\bar{w}(\xi)d\xi + \\ &- \frac{i\,k}{\pi^2}\bar{\Omega}\oint_{-1}^{1}\left[\left(\frac{1-x_*}{1+x_*}\right)^{1/2}\left(\frac{1+\xi}{1-\xi}\right)^{1/2}\frac{1}{x_*-\xi} - ik\Lambda_1(x_*,\xi)\right][\mathcal{I}_n(\xi,h_*)]d\xi\end{aligned} \tag{3.91}$$

Since[22]

$$\int_1^{+\infty}\frac{e^{-i\,k\,t}}{\sqrt{t^2-1}}\,dt = -\,i\,\frac{\pi}{2}H_0^{(2)}(k) \tag{3.92}$$

the term $\Delta\bar{C}_{p_0}(x_*)$ can be written as

$$\begin{aligned}\Delta\bar{C}_{p_0}(x_*) &= \frac{k}{2}\,\bar{\Omega}\left(\frac{1-x_*}{1+x_*}\right)^{1/2}H_0^{(2)}(k) + \\ &- \frac{2}{\pi}\oint_{-1}^{1}\left[\left(\frac{1-x_*}{1+x_*}\right)^{1/2}\left(\frac{1+\xi}{1-\xi}\right)^{1/2}\frac{1}{x_*-\xi} - i\,k\,\Lambda_1(x_*,\xi)\right]\bar{w}(\xi)d\xi + \\ &- \frac{i\,k}{\pi^2}\bar{\Omega}\oint_{-1}^{1}\left[\left(\frac{1-x_*}{1+x_*}\right)^{1/2}\left(\frac{1+\xi}{1-\xi}\right)^{1/2}\frac{1}{x_*-\xi} - ik\Lambda_1(x_*,\xi)\right][\mathcal{I}_n(\xi,h_*)]d\xi\end{aligned} \tag{3.93}$$

Substituting the relationship obtained for $\bar{\Omega}$ 3.81

$$\begin{aligned}\Delta\bar{C}_{p_0}(x_*) &= \frac{k}{2}\,\frac{4}{\pi\,i\,k}\,\frac{H_0^{(2)}(k)\oint_{-1}^{1}\left(\frac{1+\xi}{1-\xi}\right)^{1/2}\bar{w}(\xi)d\xi}{\{[H_1^{(2)}(k)+i\,H_0^{(2)}(k)] - (2/\pi)\oint_{-1}^{1}\left(\frac{1+\xi}{1-\xi}\right)^{1/2}[\mathcal{I}_n(\xi,h_*)]d\xi\}}\left(\frac{1-x_*}{1+x_*}\right)^{1/2} + \\ &-\frac{2}{\pi}\oint_{-1}^{1}\left[\left(\frac{1-x_*}{1+x_*}\right)^{1/2}\left(\frac{1+\xi}{1-\xi}\right)^{1/2}\frac{1}{x_*-\xi} - i\,k\,\Lambda_1(x_*,\xi)\right]\bar{w}(\xi)d\xi + \\ &-\frac{i\,k}{\pi^2}\,\frac{4}{\pi\,i\,k}\,\frac{\oint_{-1}^{1}\left(\frac{1+\xi}{1-\xi}\right)^{1/2}\bar{w}(\xi)d\xi}{\{[H_1^{(2)}(k)+i\,H_0^{(2)}(k)] - (2/\pi)\oint_{-1}^{1}\left(\frac{1+\xi}{1-\xi}\right)^{1/2}[\mathcal{I}_n(\xi,h_*)]d\xi\}}\cdot \\ &\cdot\oint_{-1}^{1}\left[\left(\frac{1-x_*}{1+x_*}\right)^{1/2}\left(\frac{1+\xi}{1-\xi}\right)^{1/2}\frac{1}{x_*-\xi} - i\,k\,\Lambda_1(x_*,\xi)\right][\mathcal{I}_n(\xi,h_*)]d\xi\end{aligned} \tag{3.94}$$

[21] See also [49] for comparison, Eq.$(5-341)$

[22] See [49].

The lift force, then, would be given (at the zero order) by

$$\bar{\mathcal{L}}_0 = b\,\rho\,U^2\left\{ -\int_{-1}^{1} \bar{\gamma}_0(x)\,dx \;-\; i\,k\,\int_{-1}^{1}\int_{-1}^{x} \bar{\gamma}_0(\xi)d\xi\,dx \right\} \tag{3.95}$$

Nevertheless, the difficulties related to the integration of Eq. 3.94 are quite evident. Indeed, it is easy to understand that the contemporary dependence of the previous equation by $k, h_*, x_*$ complicates its inversion. Thus, it is not possible do determine an analytical solution even renouncing to the general variation of $h$ and assigning it, as the initial hypothesis was requesting. Hence, further simplification and assumptions have to be done in order of considering the unsteady aerodynamics condition in ground effect.

### 3.4.1 Considerations about the ground effect modeling for unsteady flow

Before suggesting another possible formulation for taking into account the ground effect condition in unsteady aerodynamics, it is worth to explore the capability and the limits of the asymptotic expansion introduced by Keldysh-Lavrentiev as well as the validity of the hypothesis adopted in the previous section.

Resuming the main initial steps that were leading to the introduction of the Keldysh-Lavrentiev approach in unsteady flow and adopting the notation previously mentioned, the integral equation for an airfoil can be written in the frequency domain as:

$$\bar{w}_a(x) = -\frac{1}{2\pi}\oint_{-1}^{1} \bar{\gamma}_a(\xi)\,K(x-\xi)\,d\xi \;-\; \frac{1}{2\pi}\int_{1}^{+\infty} \bar{\gamma}_w(\xi)\,K(x-\xi)\,d\xi \tag{3.96}$$

where the Kernel of the vorticity problem is given[23] by

$$K(x-\xi) = K_\infty(x-\xi) + K_h(x-\xi) = \frac{1}{x-\xi} - \frac{x-\xi}{(x-\xi)^2 + 4\,h^2} \tag{3.97}$$

The main difficulty related to the introduction of the wake term in ground effect is due to the base of function adopted by Keldysh-Lavrentiev in their asymptotic expansion. Indeed, the simple introduction of the asymptotic expansion suggested by Keldysh-Lavrentiev and given by

$$K_{h_a}(x-\xi) \simeq \frac{1}{x-\xi} + \frac{1}{h}\sum_{n=0}^{N} K_{h_n}\left[\frac{(x-\xi)}{h}\right]^n \tag{3.98}$$

$$\bar{\gamma}_a(x) \simeq \sum_{n=0}^{N} h^{-n}\,\bar{\gamma}_{a_n}(x) \tag{3.99}$$

into the integral equation in ground effect 3.96 is meaningless. A detailed investigation of the series

[23] The term $h$ is now considered as general without any specific value.

expansion adopted shows that while on the airfoil, *i.e.* a bounded interval, the term $(x-\xi)$ is always bounded too and the whole term vanishes for $h \to \infty$, on the wake the term $(x-\xi)$ is unbounded and the expansion suggested is no more representative of the physics of the shedding vorticity on the wake since there would be an increasing shedding of vorticity for increasing distances from the trailing edge.

In order to explain the previous assertion let the term

$$f = \frac{x}{x^2+1} \tag{3.100}$$

be representative of the ground effect term on the wake. Thus, In this case $x$ will be representative of a generic distance $(x-\xi)$ and the term $+1$ will synthetically take into account the effect of the ground clearance. Then, let the terms *taylorf* and *taylorz* represent the Taylor series expansion of the stated function $f$ respect to $x$ and $z = 1/x$ respectively. Hence, *taylorf*$= (x - x^3 + x^5)$ and *taylorz*$= (z - z^3 + z^5)$.

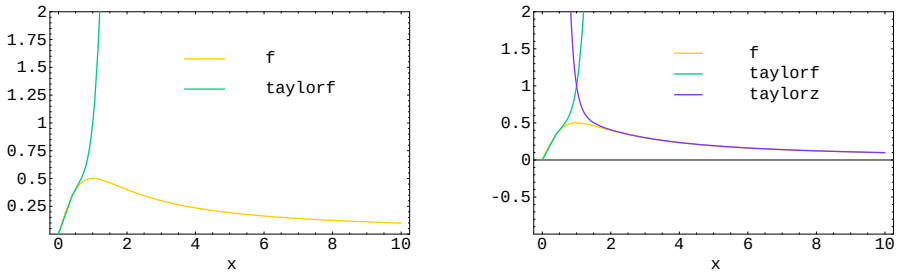


Figure 3.6: *Trends of f, taylorf and taylorz.*

Figure 3.6 shows that none of the suggested expansion can take into account the right trend of the function for $x \in (0, +\infty)$. Moreover, the maximum of $f$ will depend from the ground clearance $h$, hence its position is not univocally determined.

Adding the term that represents the single airfoil problem in the unbounded domain, the function $f$ can be stated as

$$ftot = \frac{1}{x} - \frac{x}{x^2+1} \tag{3.101}$$

Figure 3.7 shows that even taking into account the whole function and considering as previously its Taylor series expansions (with *taylorftot*$= (\frac{1}{x}) - x + x^3 - x^5$ and *taylorzftot*$= (\frac{1}{z}) - z + z^3 - z^5$), the trend is not correctly depicted and only a proper mix (depending still from the ground clearance $h$) of the two Taylor expansions can approximate the $ftot$ trend.

The Figures 3.4.1(a,b,c,d,e,f) show the trends obtained adding the contribution of the ground clearance

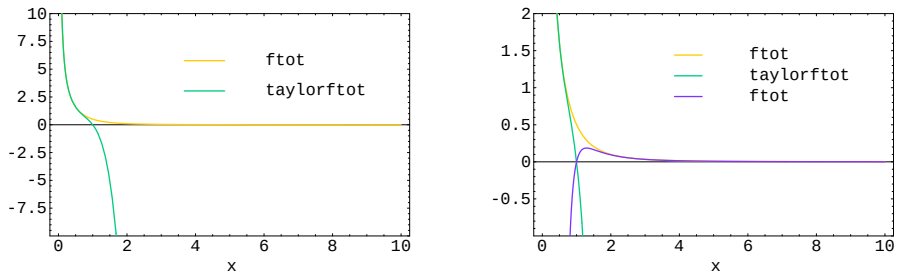


Figure 3.7: *Trends of ftot, taylorftot and taylorztot.*

for $h = 2, 4, 8$ half-chord respectively, hence the function considered[24] is

$$fhtot = \frac{1}{x} - \frac{x}{x^2 + 4h^2} \tag{3.102}$$

It is evident in this case, how the peak of the function is related to the wall clearance. This is obviously another complication in order to find an extension of the vorticity Kernel function on the wake.

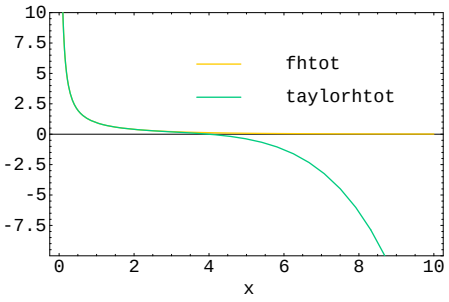


(a) h=2

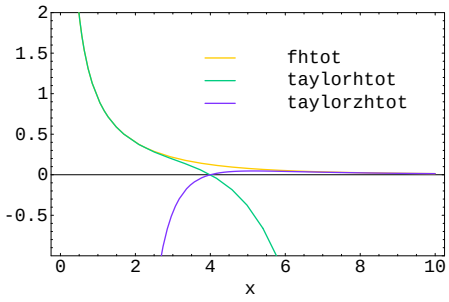


(b) h=2

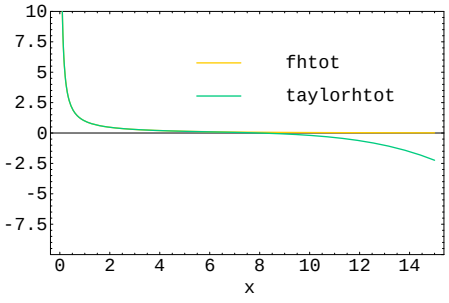


(c) h=4

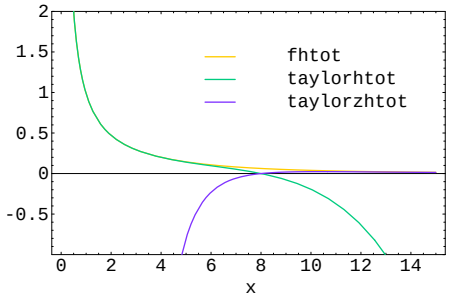


(d) h=4

Before ending this section a further remark has to be done about the cascade of equations 3.70. As

[24]Hence, *taylorfhtot*= $(\frac{1}{x}) - (\frac{x}{4h^2}) + (\frac{x^3}{16h^4}) - (\frac{x^5}{64h^6})$ and *taylorzfhtot*= $(\frac{1}{z}) - (\frac{z}{4h^2}) + (\frac{z^3}{16h^4}) - (\frac{z^5}{64h^6})$.

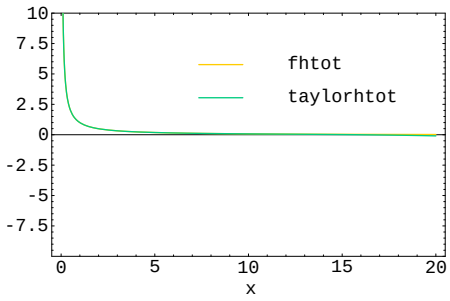


(e) h=8

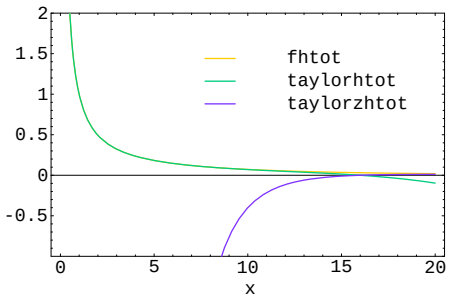


(f) h=8

evident from the application of the Keldysh-Lavrentiev expansion adopted by Plotkin in the steady case, the problems at different orders of the ground clearance parameter $h$, show to be independent from $h$ at each order (see Eq. 3.35). Hence, the zero order equation of the previous section, here referred for clarity as follows

$$(1/h)^0 : \frac{1}{2\pi}\oint_{-1}^{1}\frac{\bar{\gamma}_0(\xi)}{x-\xi}d\xi = -\bar{w}(x)+\frac{ik}{2\pi}\frac{\bar{\Gamma}(1)}{b}e^{ik}\int_1^{+\infty}e^{-ik\xi}\left[\frac{1}{x-\xi}-\frac{(x-\xi)}{(x-\xi)^2+4h_*^2}\right]d\xi \tag{3.103}$$

shows the problem, or better the inconsistency, of the dependance from $h_*$ even in the uncoupled problems.

### 3.4.2 Analytical solution by the omission of the image wake term

An analytical solution can be obtained neglecting the image term that simulated the presence of the ground on the wake. Even if this assumption could seem too reductive, actually it is instead very useful in order to understand the participation and the relevance of the wake term in the bounded unsteady problem. Furthermore, this kind of solution has the advantage to maintain the structure of the ground effect modeling suggested by Plotkin[25] and to rightly describe the physics of the wake shedding of vorticity that tends to vanish far from the trailing edge of the airfoil.

Hence, in Eq. 3.66 only the vorticity and the Kernel vorticity function on the left hand side will be expanded following the assumption of Keldysh-Lavrentiev obtaining in this case:

$$\begin{aligned}&\frac{1}{2\pi}\oint_{-1}^{1}\sum_0^{\infty}\bar{\gamma}_n(\xi)\left(\frac{1}{h}\right)^n\left[\frac{1}{x-\xi}+\frac{1}{h}\sum_0^{\infty}K_n\cdot\left(\frac{x-\xi}{h}\right)^n\right]d\xi = -\bar{w}(x)+\\&+\frac{ik}{2\pi}\frac{\bar{\Gamma}(1)}{b}e^{ik}\int_1^{\infty}e^{-ik\xi}\frac{d\xi}{x-\xi}\end{aligned} \tag{3.104}$$

[25]That, as mentioned, has to be independent from $h$ at each order of the uncoupled problems.

Thus, the uncoupled problems at different $1/h$ orders are

$$
\begin{aligned}
(1/h)^0 \quad &: \frac{1}{2\pi}\oint_{-1}^{1}\frac{\bar{\gamma}_0(\xi)}{(x-\xi)}d\xi = -\bar{w}(x) + \frac{ik}{2\pi}\frac{\bar{\Gamma}(1)}{b}\,e^{ik}\int_1^{\infty} e^{-ik\xi}\frac{d\xi}{x-\xi} \\
(1/h)^1 \quad &: \oint_{-1}^{1}\frac{\bar{\gamma}_1(\xi)}{x-\xi}\,d\xi = -\oint_{-1}^{1}\bar{\gamma}_0(\xi)\,K_0\,d\xi \\
(1/h)^2 \quad &: \oint_{-1}^{1}\frac{\bar{\gamma}_2(\xi)}{x-\xi}\,d\xi = -\oint_{-1}^{1}\left[\,\bar{\gamma}_0(\xi)\,K_1\cdot(x-\xi) \;+\; \bar{\gamma}_1(\xi)\,K_0\,\right]d\xi
\end{aligned}
\tag{3.105}
$$

For the purposes of the actual work a study till the first order could be considered satisfying, but since the coefficient of Keldysh-Lavrentiev that appears in the first order problem is only $K_0$ and for it it has been found in the steady case section that $K_0 = 0$, a study till the second order is needed.

***Zero order solution***

It follows from Eq. 3.105 that the zero order problem coincides with the Theodorsen problem in the unbounded domain, problem that has a well-known analytical solution. Applying the Söhngen inversion formula 3.72 the following is obtained

$$
\begin{aligned}
\bar{\gamma}_0(x) \quad = \quad & \frac{2}{\pi}\left(\frac{1-x}{1+x}\right)^{1/2}\left\{\oint_{-1}^{1}\left(\frac{1+\xi}{1-\xi}\right)^{1/2}\frac{[-\bar{w}(\xi)]}{\xi-x}\,d\xi + \right. \\
& \left. + ik\,\frac{\bar{\Gamma}(1)}{b}\,e^{ik}\oint_{-1}^{1}\left(\frac{1+\xi}{1-\xi}\right)^{1/2}\left[\int_1^{\infty}\frac{e^{-ik\lambda}d\lambda}{\xi-\lambda}\right]\frac{d\xi}{\xi-x}\right\}
\end{aligned}
\tag{3.106}
$$

The main steps to solve the difficulties related to the evaluation of the right hand side integral are given in detail in [50],[49],[51]. Following the Theory of Theodorsen in the referred bibliography, it is worth to give an expression for the pressure difference between the lower and the upper side[26] of the lifting

[26] As mentioned the pressure difference in the current section will be considered as given by the difference by the lower and upper side of the lifting surface.

surface, that is in adimensional terms[27]:

$$\frac{\Delta\bar{p}_0(x)}{\rho U^2} = \bar{\gamma}_0(x) + i\,k\int_{-1}^{x}\bar{\gamma}_0(\xi)\,d\xi \tag{3.112}$$

The final well-known expression is then given by

$$\begin{aligned} -\frac{\Delta\bar{p}_0(x)}{\rho U^2} &= \frac{2}{\pi}[1-\mathcal{C}(k)]\sqrt{\frac{1-x}{1+x}}\int_{-1}^{1}\left(\frac{1+\xi}{1-\xi}\right)^{1/2}\bar{w}(\xi)\,d\xi + \\ &+\frac{2}{\pi}\oint_{-1}^{1}\left[\sqrt{\frac{1-x}{1+x}}\sqrt{\frac{1+\xi}{1-\xi}}\,\frac{1}{x-\xi} - ik\,\Lambda_1(x,\xi)\right]\bar{w}(\xi)\,d\xi \end{aligned} \tag{3.113}$$

where $\mathcal{C}(k)$ is the Theodorsen function denoted by

$$\mathcal{C}(k) = \frac{H_1^{(2)}(k)}{H_1^{(2)}(k) \;+\; ik\,H_0^{(2)}(k)} \tag{3.114}$$

with $H_n^{(2)}$ Hankel functions of the second kind given by a proper combination of the Bessel functions of the first and second kind
$H_n^{(2)} := J_n - iY_n$.

[27] As mentioned the adoption of the Keldysh -Lavrentiev expansion implies

$$\frac{\Delta\bar{p}(x)}{\rho U^2} = \bar{\gamma}_0(x) + h^{-1}\bar{\gamma}_1(x) + \ldots + i\,k\int_{-1}^{x}(\bar{\gamma}_0(\xi) + h^{-1}\bar{\gamma}_1(\xi) + \ldots)\,d\xi \tag{3.107}$$

Thus,

$$\frac{\Delta\bar{p}(x)}{\rho U^2} = \frac{\Delta\bar{p}_0(x)}{\rho U^2} + h^{-1}\frac{\Delta\bar{p}_1(x)}{\rho U^2} + h^{-2}\frac{\Delta\bar{p}_2(x)}{\rho U^2} \tag{3.108}$$

with

$$\begin{aligned} \frac{\Delta\bar{p}_0(x)}{\rho U^2} &= \bar{\gamma}_0(x) + i\,k\int_{-1}^{x}\bar{\gamma}_0(\xi)d\xi \\ \frac{\Delta\bar{p}_1(x)}{\rho U^2} &= \bar{\gamma}_1(x) + i\,k\int_{-1}^{x}\bar{\gamma}_1(\xi)\,d\xi \\ \frac{\Delta\bar{p}_2(x)}{\rho U^2} &= \bar{\gamma}_2(x) + i\,k\int_{-1}^{x}\bar{\gamma}_2(\xi)\,d\xi \end{aligned} \tag{3.109}$$

Similarly for the Keldysh-Lavrentiev approach also the lift force will be given by the sum of the contribution of each order as follows

$$\bar{\mathcal{L}} = \bar{\mathcal{L}}_0 + \frac{1}{h}\bar{\mathcal{L}}_1 + \frac{1}{h^2}\bar{\mathcal{L}}_2 \tag{3.110}$$

with

$$\begin{aligned} \bar{\mathcal{L}}_0 &= b\,\rho\,U^2\int_{-1}^{1}\frac{\Delta\bar{p}_0(x)}{\rho U^2}\,dx \\ \bar{\mathcal{L}}_1 &= b\,\rho\,U^2\int_{-1}^{1}\frac{\Delta\bar{p}_1(x)}{\rho U^2}\,dx \\ \bar{\mathcal{L}}_2 &= b\,\rho\,U^2\int_{-1}^{1}\frac{\Delta\bar{p}_2(x)}{\rho U^2}\,dx \end{aligned} \tag{3.111}$$

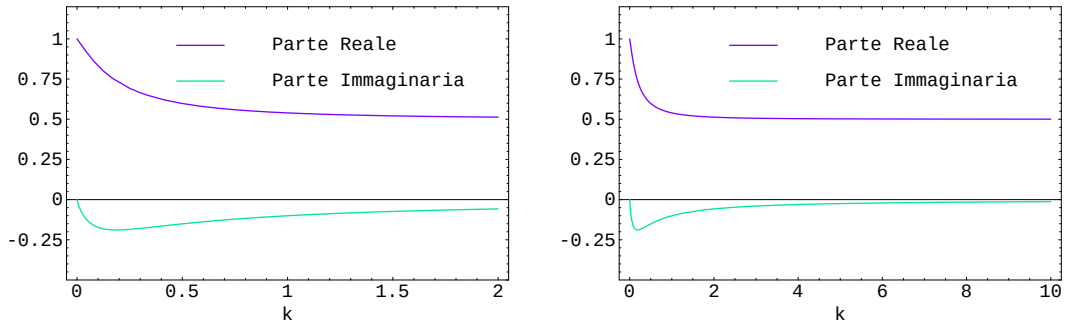


Figure 3.8: *The Theodorsen function $\mathcal{C}(k)$ in its real and imaginary parts plotted at different value of the reduced frequency.*

### The boundary condition

For evaluating the lift at the zero order a specification of the boundary condition is needed, it is worth to assign it in the current section since it will be useful even for the next order solutions of the 'cascade' problems. As for the Theodorsen theory two degrees of freedom will be considered:

- plunge motion positive downward
- plunge rotation positive clockwise

Hence, the cinematic expression in the vertical direction is given by

$$\hat{z} = \hat{z}_0 - \hat{\zeta} - \alpha(\hat{x} - b\,a) \tag{3.115}$$

where $\hat{z}_0$ indicates a constant ground clearance that verifies $\frac{\partial \hat{z}_0}{\partial t} = 0$. The symbol $\hat{}$ denotes dimensional terms.

Thus, for the velocity it is possible to write

$$\hat{w}(\hat{x}, t) = \frac{D\hat{z}}{Dt} = \frac{\partial \hat{z}}{\partial t} + U\frac{\partial \hat{z}}{\partial \hat{x}} \tag{3.116}$$

that for what previously mentioned gives

$$\hat{w}(\hat{x}, t) = -\frac{\partial \hat{\zeta}}{\partial t} - \frac{\partial \alpha}{\partial t}(\hat{x} - \hat{a}) - U\alpha = -\dot{\hat{\zeta}} - \dot{\alpha}(\hat{x} - b\,a) - U\alpha \tag{3.117}$$

Dividing by $U$ and considering the adimensionalization of the variables [28] $\zeta = \hat{\zeta}/b, x = \hat{x}/b$, the following is achieved

$$w(x,t) = \frac{\hat{w}(\hat{x},t)}{U} = -\frac{\dot{\zeta} b}{U} - \frac{\dot{\alpha}}{U}(b\,x - b\,a) - \alpha \tag{3.118}$$

Introducing the hypothesis of harmonic motion one has

$$\bar{w}(x) \cdot e^{i\omega t} = -i\frac{\omega b}{U}\bar{\zeta} \cdot e^{i\omega t} - i\frac{\omega b}{U}\bar{\alpha}(x-a) \cdot e^{i\omega t} - \bar{\alpha} \cdot e^{i\omega t} \tag{3.119}$$

Finally, since the reduced frequency is defined as $k = \frac{\omega b}{U}$ the desired relationship is simply

$$\bar{w}(x) = -ik\,\bar{\zeta} - ik\,\bar{\alpha}(x-a) - \bar{\alpha} \tag{3.120}$$

For sake of simplicity in the calculation, as will be evident later on, it is useful to separate the terms independent from $x$ and the terms proportional to $x$. Thus, the adimensional boundary condition in the frequency domain assumes the following final expression

$$\bar{w}(x) = -[ik\,(\bar{\zeta} - a\bar{\alpha}) + \bar{\alpha}] - ik\,\bar{\alpha}x \tag{3.121}$$

***Zero order solution: determination of the lift force***

In order to obtain the lift force expression for the zero order problem, the integration of Eq. 3.113 has to be performed. Thus, the solution suggested by Theodorsen will be achieved and two kind of contribution can be remarked *not-circulatory* and *circulatory* respectively that are dimensionally given in the frequency domain by

$$\bar{\mathcal{L}}_0^{(NC)} = \pi\,\rho\,b^2\,[-\omega^2\,\hat{\bar{\zeta}} + i\,\omega\,U\,\bar{\alpha} + b\,a\,\omega^2\,\bar{\alpha}] \tag{3.122}$$

$$\bar{\mathcal{L}}_0^{(C)} = 2\,\pi\,\rho\,b\,U\,\mathcal{C}(k)\left[i\,\omega\,\hat{\bar{\zeta}} + U\,\bar{\alpha} + b\left(\frac{1}{2} - a\right) i\,\omega\,\bar{\alpha}\right] \tag{3.123}$$

Considering the adimensionalization respect to the dynamic pressure times the chord $\frac{1}{2}\rho U^2 c$ and adopting the reduced frequency definition $k = \frac{\omega b}{U}$, it yields the following

$$\begin{aligned} \bar{C_L}_0^{(NC)} &= \pi\left[-k^2\bar{\zeta} + ik\,\bar{\alpha} + k^2 a\bar{\alpha}\right] \\ \bar{C_L}_0^{(C)} &= 2\pi\mathcal{C}(k)\left[ik\,\bar{\zeta} + \bar{\alpha} + ik\,\left(\frac{1}{2} - a\right)\bar{\alpha}\right] \end{aligned} \tag{3.124}$$

[28] The adimensional plunge in literature is commonly indicated by $\xi$ but since that symbol has been repetitively adopted for the variables of integration in the Keldysh-Lavrentiev methodology, it seems convenient to adopt the symbol $\zeta$.

***First order solution***

From Eqs.3.105 it follows that the first order problem is given by

$$\oint_{-1}^{1} \frac{\bar{\gamma}_1(\xi)}{x-\xi}\, d\xi = -K_0 \oint_{-1}^{1} \bar{\gamma}_0(\xi)\, d\xi \tag{3.125}$$

Considering what referred[29] and from the definition of $\bar{\Gamma}$ it is possible to set:

$$\oint_{-1}^{1} \bar{\gamma}_0(\xi)\, d\xi = \frac{\bar{\Gamma}(1)}{b} \tag{3.126}$$

where the result given in [49] has been adopted assuming a series expansion for the vorticity and taking only the zero order term of the expansion. From the definition of $\frac{\bar{\Gamma}(1)}{b}$ stated in Eq.3.67 it follows

$$\oint_{-1}^{1} \bar{\gamma}_0(\xi)\, d\xi = \frac{4e^{-ik}}{\pi\, ik\left[H_1^{(2)}(k) + iH_0^{(2)}(k)\right]} \cdot \oint_{-1}^{1} \left(\frac{1+\xi}{1-\xi}\right)^{1/2} \bar{w}(\xi)\, d\xi \tag{3.127}$$

Setting

$$\mathcal{H}(k) = \frac{-2\, e^{-ik}}{\pi\, i\, k[H_1^{(2)}(k) + i\, H_0^{(2)}(k)]} \tag{3.128}$$

synthetically can be obtained

$$\oint_{-1}^{1} \bar{\gamma}_0(\xi)\, d\xi = -2\,\mathcal{H}(k) \oint_{-1}^{1} \left(\frac{1+\xi}{1-\xi}\right)^{1/2} \bar{w}(\xi)\, d\xi \tag{3.129}$$

The function $\mathcal{H}(k)$ has been defined in analogy with the Theodorsen function $C(k)$, thus, the limit of $\mathcal{H}(k)$ is 1 for $k \to 0$ and 0 for $k \to \infty$.

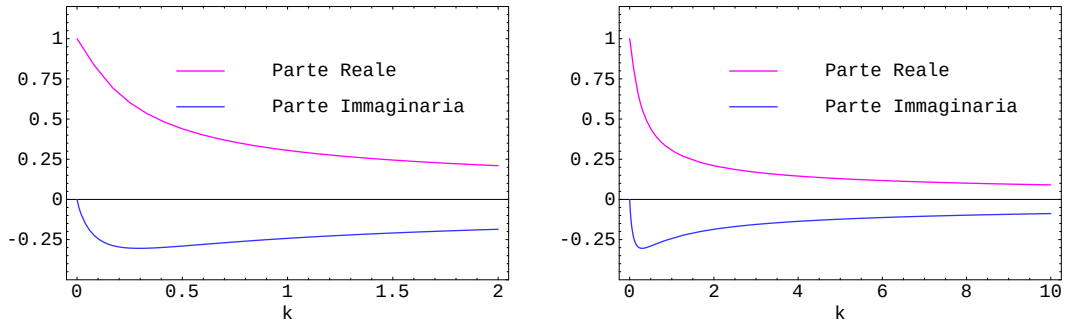


Figure 3.9: *Trend of the function $\mathcal{H}(k)$ in its real and imaginary parts plotted at different value of the reduced frequency.*

[29] Particularly Eq.$(5-332)$ in [49].

Finally, the first order problem is given by

$$\oint_{-1}^{1} \frac{\bar{\gamma}_1(\xi)}{x-\xi}\, d\xi = 2\, K_0\, \mathcal{H}(k) \oint_{-1}^{1} \left(\frac{1+\xi}{1-\xi}\right)^{1/2} \bar{w}(\xi)\, d\xi \tag{3.130}$$

The obtained relationship has to be inverted by using the Söhngen formula 3.72 in order to evaluate the term $\bar{\gamma}_1(x)$: thus[30],

$$\bar{\gamma}_1(x) = \frac{1}{\pi^2} \left(\frac{1-x}{1+x}\right)^{1/2} \oint_{-1}^{1} \left(\frac{1+\xi}{1-\xi}\right)^{1/2} \frac{\bar{F}_1(\xi)}{(\xi-x)} d\xi \tag{3.131}$$

Once the value of $\bar{\gamma}_1(x)$ will be calculated, the pressure difference between the lower-upper side of the lifting surface will be given by

$$\frac{\Delta \bar{p}_1(x)}{\rho U^2} = \bar{\gamma}_1(x) + i\, k \int_{-1}^{x} \bar{\gamma}_1(\xi)\, d\xi \tag{3.132}$$

The boundary condition given in Eq. 3.121 allows to determine the right hand side of Eq. 3.130 being

$$\oint_{-1}^{1} \frac{\bar{\gamma}_1(\xi)}{x-\xi} d\xi = 2\, K_0 \mathcal{H}(k) \oint_{-1}^{1} \left(\frac{1+\xi}{1-\xi}\right)^{1/2} \{-[ik\,(\bar{\zeta} - a\,\bar{\alpha}) + \bar{\alpha}] - ik\,\bar{\alpha}\,\xi\}\, d\xi \tag{3.133}$$

Solving the integral (using the remarkable integrals list reported in the appendix) one has,

$$\oint_{-1}^{1} \frac{\bar{\gamma}_1(\xi)}{x-\xi} d\xi = -\,2\,\pi\, K_0\, \mathcal{H}(k) \left\{ ik \left[\bar{\zeta} + \left(\frac{1}{2} - a\right) \bar{\alpha}\right] + \bar{\alpha} \right\} \tag{3.134}$$

The previous equation has to be inverted using the Söhngen inversion formula 3.72 and obtaining

$$\bar{\gamma}_1(x) = -2\, K_0\, \mathcal{H}(k) \left(\frac{1-x}{1+x}\right)^{1/2} \left[ik\,\bar{\zeta} + ik \left(\frac{1}{2} - a\right) \bar{\alpha} + \bar{\alpha}\right] \tag{3.135}$$

It is worth to note that the limit[31] for $k \to 0$ of the Eq. 3.135 supplies the same result of the steady case (see Eq. 3.43). Knowing the $\bar{\gamma}_1(x)$ term and reminding the relationship 3.132, the pressure coefficient can be determined. Thus, the lift will follow using the second Eq. in 3.111. Nevertheless, for simplifying

[30] Where $\bar{F}_1(\xi)$ is the right hand side of Eq. 3.130.

[31] Indeed, for the definition of $\mathcal{H}(k)$ in Eq.3.128 one has

$$\lim_{k\to 0} \mathcal{H}(k) = 1 \qquad \Rightarrow \lim_{k\to 0} \bar{\gamma}_1(x) = -2\bar{\alpha} K_0 \left(\frac{1-x}{1+x}\right)^{1/2} \tag{3.136}$$

the notation, the direct integration that allows to evaluate the lift force will be considered[32]. Thus,

$$\bar{\mathcal{L}}_1 = b\,\rho\,U^2\left\{\int_{-1}^{1}\bar{\gamma}_1(x)\,dx\;+\;i\,k\int_{-1}^{1}\int_{-1}^{x}\bar{\gamma}_1(\xi)d\xi\,dx\right\} \tag{3.137}$$

or adimensionally[33]

$$\bar{C_{L1}} = \int_{-1}^{1}\bar{\gamma}_1(x)\,dx\;+\;i\,k\int_{-1}^{1}\int_{-1}^{x}\bar{\gamma}_1(\xi)d\xi\,dx \tag{3.138}$$

Solving for the obtained $\bar{\gamma}_1(x)$ evaluated in Eq.3.135 the following is achieved

$$\bar{C_{L1}}^{(C)} \;=\; -2\,\pi\,K_0\,\mathcal{H}(k)\left(1+\frac{3}{2}i\,k\right)\left[ik\,\bar{\zeta}+ik\,\left(\frac{1}{2}-a\right)\bar{\alpha}+\bar{\alpha}\right] \tag{3.139}$$

where for analogy with the Theodorsen Theory the contribution of the lift depending from the function $\mathcal{H}(k)$ has been considered as circulatory. Note that at the first order only a circulatory contribution for the lift force has been highlighted.

***Second order solution***

The second order problem mentioned in Eq.3.105 can be written as:

$$\oint_{-1}^{1}\frac{\bar{\gamma}_2(\xi)}{x-\xi}\,d\xi = \underbrace{-K_1\,x\oint_{-1}^{1}\bar{\gamma}_0(\xi)d\xi}_{A}\underbrace{+K_1\oint_{-1}^{1}\bar{\gamma}_0(\xi)\cdot\xi\,d\xi}_{B}\underbrace{-K_0\oint_{-1}^{1}\bar{\gamma}_1(\xi)d\xi}_{C} \tag{3.140}$$

where $\bar{\gamma}_0(x)$ and $\bar{\gamma}_1(x)$ are the ones evaluated in the previous steps. From Eqs.3.126, 3.67 and 3.121 follows

$$A = -2\,\pi\,K_1\,\mathcal{H}(k)\,x\left\{i\,k\,\bar{\zeta}+i\,k\,\left(\frac{1}{2}-a\right)\bar{\alpha}+\bar{\alpha}\right\} \tag{3.141}$$

For evaluating the term $B$, it has to be considered the value of $\bar{\gamma}_0(x)$ of Eq. 3.106 obtaining

$$B = -\pi\,K_1\,[\,i\,k\,(\bar{\zeta}-\;a\,\bar{\alpha})+\;\bar{\alpha}] \tag{3.142}$$

[32]Indeed, the integration of $\int_{-1}^{x}\bar{\gamma}_1(\xi)d\xi$ is tedious and difficult, while it is more easily possible to directly evaluate the following integral

$$\int_{-1}^{1}\int_{-1}^{x}\bar{\gamma}_1(\xi)d\xi\,dx = \frac{3\,\pi}{2}(-2K_0\mathcal{H}(k))\left[ik\,\bar{\zeta}+ik\,\left(\frac{1}{2}-a\right)\bar{\alpha}+\bar{\alpha}\right]$$

since

$$\int_{-1}^{1}\int_{-1}^{x}\left(\frac{1-\xi}{1+\xi}\right)^{1/2}d\xi\,dx = \frac{3\,\pi}{2}$$

.

[33]Note that in order to obtain the adimensional lift coefficient, the dimensional lift force terw should be divided by $c\,\rho\,U^2$, thus, it is evident that $\int_{-1}^{1}\bar{\gamma}_1(x)\,dx\;+\;i\,k\int_{-1}^{1}\int_{-1}^{x}\bar{\gamma}_1(\xi)d\xi\,dx$ coincides already with $\bar{C_{L1}}$.

The term $C$ can be the calculated substituting the obtained value of $\bar{\gamma}_1(x)$ from Eq.3.135, thus,

$$C = 2\,\pi\,K_0^2\,\mathcal{H}(k)\left\{i\,k\,\bar{\zeta} + i\,k\,\left(\frac{1}{2} - a\right)\bar{\alpha} + \bar{\alpha}\right\} \tag{3.143}$$

Hence for the right hand side of Eq.3.140 one has

$$\begin{aligned}\bar{F}_2(x) \;&=\; A + B + C = -2\,\pi\,K_1\,\mathcal{H}(k)\,x\left\{i\,k\,\bar{\zeta} + i\,k\,\left(\frac{1}{2} - a\right)\bar{\alpha} + \bar{\alpha}\right\} + \\ &-\pi K_1[\,i\,k\,(\bar{\zeta} - \,a\,\bar{\alpha}) + \,\bar{\alpha}] + 2\,\pi\,K_0^2\,\mathcal{H}(k)\left\{i\,k\,\bar{\zeta} + i\,k\,\left(\frac{1}{2} - a\right)\bar{\alpha} + \bar{\alpha}\right\}\end{aligned} \tag{3.144}$$

Adopting the Söhngen inversion formula 3.72 for solving Eq. 3.140, considering that 3.144, it is possible to obtain for the term $\bar{\gamma}_2(x)$

$$\begin{aligned}\bar{\gamma}_2(x) \;&=\; \left(\frac{1-x}{1+x}\right)^{1/2}\left\{-\,2\,K_1\,\mathcal{H}(k)\left[i\,k\,\bar{\zeta} + i\,k\,\left(\frac{1}{2} - a\right)\bar{\alpha} + \bar{\alpha}\right] + \right. \\ &-2\,K_1\,\mathcal{H}(k)\,x\left[i\,k\,\bar{\zeta} + i\,k\,\left(\frac{1}{2} - a\right)\bar{\alpha} + \bar{\alpha}\right] - K_1\,[\,i\,k\,(\bar{\zeta} - \,a\,\bar{\alpha}) + \,\bar{\alpha}] + \\ &\left.+2\,K_0^2\,\mathcal{H}(k)\,\left[i\,k\,\bar{\zeta} + i\,k\,\left(\frac{1}{2} - a\right)\bar{\alpha} + \bar{\alpha}\right]\right\}\end{aligned} \tag{3.145}$$

It is worth to note that also for the second order problem if $k \to 0$ it is possible to obtain the same second order vorticity contribution of the steady case[34]. As issued for the first order problem, will be currently considered the double integration that defines directly the lift contribution, thus,

$$\bar{C}_{L2} = \underbrace{\int_{-1}^{1}\bar{\gamma}_2(x)\,dx}_{I_1}\;\underbrace{+\,i\,k\,\int_{-1}^{1}\int_{-1}^{x}\bar{\gamma}_2(\xi)d\xi\,dx}_{I_2} \tag{3.146}$$

where the two contribution will be evaluated separately. Substituting the value obtained in Eq. 3.145 for $\bar{\gamma}_2(x)$ one has

$$\begin{aligned}I_1 \;&=\; -\pi\,K_1\,\mathcal{H}(k)\left[i\,k\,\bar{\zeta} + i\,k\,\left(\frac{1}{2} - a\right)\bar{\alpha} + \bar{\alpha}\right] - \pi\,K_1\,[\,i\,k\,(\bar{\zeta} - \,a\,\bar{\alpha}) + \,\bar{\alpha}] + \\ &+2\,\pi\,K_0^2\,\mathcal{H}(k)\,\left[i\,k\,\bar{\zeta} + i\,k\,\left(\frac{1}{2} - a\right)\bar{\alpha} + \bar{\alpha}\right]\end{aligned} \tag{3.147}$$

[34]Indeed, $\lim_{k\to 0}\mathcal{H}(k) = 1$ thus,

$$\begin{aligned}\lim_{k\to 0}\bar{\gamma}_2(x) \;&=\; \left(\frac{1-x}{1+x}\right)^{1/2}(-3K_1 + 2K_0^2 - 2K_1 x)\,\bar{\alpha} \\ &\Rightarrow\;\; \lim_{k\to 0}\bar{\gamma}_2(x) = 2\,\bar{\alpha}\,\left(\frac{1-x}{1+x}\right)^{1/2}\left[K_0^2 - \frac{3}{2}\,K_1 - K_1\,x\right]\end{aligned}$$

that coincides with the result found in Eq. 3.45. once the thickness terms (meaningless for a flat plate) are omitted

For the term $I_2$ it is possible to obtain[35]

$$\begin{aligned} I_2 &= -\pi K_1 \mathcal{H}(k) i k \left[ i k \bar{\zeta} + i k \left( \frac{1}{2} - a \right) \bar{\alpha} + \bar{\alpha} \right] + \\ &\quad -\frac{3}{2} \pi K_1 i k \left[ i k \left( \bar{\zeta} - a \bar{\alpha} \right) + \bar{\alpha} \right] + \\ &\quad +3\pi K_0^2 \mathcal{H}(k) i k \left[ i k \bar{\zeta} + i k \left( \frac{1}{2} - a \right) \bar{\alpha} + \bar{\alpha} \right] \end{aligned} \tag{3.148}$$

Finally considering that $\bar{C_L}_2 = I_1 + I_2$ and splitting the circulatory and not-circulatory contributions it yields

$$\begin{aligned} \bar{C_L}_2^{(NC)} &= -\pi K_1 \left[ i k \left( \bar{\zeta} - a \bar{\alpha} \right) + \bar{\alpha} \right] \left( 1 + \frac{3}{2} i k \right) \\ \bar{C_L}_2^{(C)} &= -\pi K_1 \mathcal{H}(k) \left[ i k \bar{\zeta} + i k \left( \frac{1}{2} - a \right) \bar{\alpha} + \bar{\alpha} \right] (1 + i k) + \\ &\quad +2 \pi K_0^2 \mathcal{H}(k) \left[ i k \bar{\zeta} + i k \left( \frac{1}{2} - a \right) \bar{\alpha} + \bar{\alpha} \right] \left( 1 + \frac{3}{2} i k \right) \end{aligned} \tag{3.149}$$

**Lift force expression**

In adimensional terms, the lift coefficient due to the Keldysh-Lavrentiev expansion will be given by

$$\bar{C_L} = \bar{C_L}_0 + \frac{1}{h} \bar{C_L}_1 + \frac{1}{h^2} \bar{C_L}_2 \tag{3.150}$$

Substituting the contribution of each order, thus, Eqs. 3.124, 3.139, 3.149 and considering separately the circulatory and not-circulatory part, the following is achieved:

$$\begin{aligned} \bar{C_L}^{(NC)} &= 2\pi \left\{ -\left( \frac{1}{2} - \frac{1}{h^2} \frac{3}{4} K_1 \right) k^2 \bar{\zeta} - \frac{1}{h^2} \frac{K_1}{2} i k \bar{\zeta} + \right. \\ &\quad + \left( \frac{1}{2} - \frac{1}{h^2} \frac{3}{4} K_1 \right) k^2 a \bar{\alpha} + \frac{1}{h^2} \frac{K_1}{2} i k a \bar{\alpha} + \\ &\quad \left. + \left( \frac{1}{2} - \frac{1}{h^2} \frac{3}{4} K_1 \right) i k \bar{\alpha} - \frac{1}{h^2} \frac{K_1}{2} \bar{\alpha} \right\} \end{aligned} \tag{3.151}$$

[35] Being $\int_{-1}^{1} \int_{-1}^{x} \left( \frac{1-\xi}{1+\xi} \right)^{1/2} d\xi \, dx = \frac{3\pi}{2}$ e $\int_{-1}^{1} \int_{-1}^{x} \left( \frac{1-\xi}{1+\xi} \right)^{1/2} \cdot \xi \, d\xi \, dx = -\pi$.

$$
\begin{aligned}
\bar{C_L}^{(C)} = 2\,\pi \Bigg\{ & \left( \mathcal{C}(k) - K_0\,\mathcal{H}(k)\frac{1}{h} - \frac{1}{2}K_1\,\mathcal{H}(k)\frac{1}{h^2} + K_0^2\mathcal{H}(k)\frac{1}{h^2} \right) \cdot ik\,\bar{\zeta} + \\
& + \left[ \left( \mathcal{C}(k) - K_0\,\mathcal{H}(k)\frac{1}{h} - \frac{1}{2}K_1\,\mathcal{H}(k)\frac{1}{h^2} + K_0^2\mathcal{H}(k)\frac{1}{h^2} \right) \cdot ik \left( \frac{1}{2} - a \right) \bar{\alpha} \right] + \\
& + \left( \mathcal{C}(k) - \, K_0\,\mathcal{H}(k)\,\frac{1}{h} - \, \frac{1}{2}\,K_1\,\mathcal{H}(k)\,\frac{1}{h^2} + \, K_0^2\,\mathcal{H}(k)\frac{1}{h^2} \right) \cdot \bar{\alpha} + \\
& + \left( \frac{3}{2}\,K_0\,\mathcal{H}(k)\,\frac{1}{h} + \frac{1}{2}\,K_1\,\mathcal{H}(k)\,\frac{1}{h^2} - \, \frac{3}{2}\,K_0^2\,\mathcal{H}(k)\,\frac{1}{h^2} \right) \cdot k^2\,\bar{\zeta} + \\
& + \left[ \left( \frac{3}{2}\,K_0\,\mathcal{H}(k)\,\frac{1}{h} + \frac{1}{2}\,K_1\,\mathcal{H}(k)\,\frac{1}{h^2} - \, \frac{3}{2}\,K_0^2\,\mathcal{H}(k)\,\frac{1}{h^2} \right) \cdot k^2 \, \left( \frac{1}{2} - a \right) \bar{\alpha} \right] + \\
& - \left( \frac{3}{2}\,K_0\,\mathcal{H}(k)\,\frac{1}{h} + \frac{1}{2}K_1\,\mathcal{H}(k)\frac{1}{h^2} - \frac{3}{2}K_0^2\mathcal{H}(k)\,\frac{1}{h^2} \right) \cdot i\,k\,\bar{\alpha} \Bigg\}
\end{aligned}
\tag{3.152}
$$

### 3.4.3 The Wagner problem in ground effect

**Reminding of the statements of the Wagner problem in the unbounded domain**

The Wagner problem represents a typical aeroelastic application useful to better understand the features of the Theodorsen function. Certainly, the Wagner problem has been widely explored in literature as the Refs. [50], [49], [51] show, hence, only a brief remark on its fundamental topics will be given. Indeed, a natural consequence of having considered the Theodorsen Theory extension to the ground effect condition, is to account the mentioned extension even to the Wagner problem.

The Wagner analysis consists in determining the transient lift response due to an assigned step of incidence applied to the same lift surface adopted in the Theodorsen Theory. Thus, a two dimensional profile with no angle of attack is considered. At the starting time a step on incidence named $\alpha_0$ is assigned. The Wagner problem can then be stated as

$$
\begin{cases}
\alpha = 0 \quad \text{per} \quad t < 0 \Rightarrow \dot{\alpha}, \ddot{\alpha} = 0 \\
\alpha = \alpha_0 \quad \text{per} \quad t > 0 \Rightarrow \dot{\alpha}, \ddot{\alpha} = 0
\end{cases}
$$

assuming that $\dot{\zeta}, \ddot{\zeta} = 0 \; \forall t$. Thus, it follows that the not-circulatory part of the lift expression determined by the Theodorsen Theory and given in Eq. 3.122 will be equal to zero since it is determined only by first or second derivatives of the pitch and plunge terms. Regarding the circulatory part in dimensional notation it can be written

$$
\mathcal{L} = -2\,\pi\,\rho\,U\,b \left[ \frac{1}{2\,\pi} \int_{-\infty}^{+\infty} \mathcal{C}(k)\,f(\omega)\,e^{i\,\omega\,t} d\omega \right] \tag{3.153}
$$

where

$$\begin{aligned} f(\omega) &= -\left[ i\,\omega\, b\,\bar{\zeta} + U\,\bar{\alpha} + b\left(\frac{1}{2} - a\right) i\,\omega\,\bar{\alpha}\right] = \\ &= \int_{-\infty}^{+\infty} -\left[ b\,\dot{\zeta} + U\,\alpha + b\left(\frac{1}{2} - a\right)\dot{\alpha}\right] e^{-i\,\omega\,t} dt = \\ &= \int_{-\infty}^{+\infty} w_{3/4\,c}(t)\, e^{-i\,\omega\,t} dt \end{aligned} \tag{3.154}$$

being $w_{3/4\,c}$ the vertical component of the velocity (thus, the *downwash*) of a point placed at 3/4 of the chord of the profile. The demonstration of the validity of the previous equation can be found in Refs. [50], [49], [51]. Hence, for the Wagner problem (still assuming $\dot{\zeta}, \ddot{\zeta} = 0$) one has

$$w_{3/4\,c} = \begin{cases} 0 & \text{per} \quad t < 0 \Rightarrow \dot{\alpha}, \ddot{\alpha} = 0 \\ -\,U\,\alpha_0 & \text{per} \quad t > 0 \Rightarrow \dot{\alpha}, \ddot{\alpha} = 0 \end{cases}$$

where $f(\omega)$ can be expressed as

$$f(\omega) = \int_0^{+\infty} -\,U\,\alpha_0\, e^{-i\,\omega\,t} dt = -\,\frac{U\,\alpha_0}{i\,\omega} \tag{3.155}$$

Hence, in the time domain, considering the adimansionalization of the time terms as $\tau = t\frac{U}{b}$ the adimensional response to the Wagner problem is then given by

$$\mathcal{L}(\tau) = 2\,\pi\,\rho\,U^2\,\alpha_0\,b\left[\frac{1}{2\,\pi}\int_{-\infty}^{+\infty} \frac{\mathcal{C}(k)}{i\,k} e^{i\,k\,\tau} dk\right] \tag{3.156}$$

Setting

$$\varphi(\tau) := \frac{1}{2\,\pi}\int_{-\infty}^{+\infty} \frac{\mathcal{C}(k)}{i\,k} e^{i\,k\,\tau} dk \tag{3.157}$$

and naming $\varphi(\tau)$ the Wagner function, it is possible to demonstrate (see [49]) the following relationship

$$\varphi(\tau) = \frac{2}{\pi}\int_0^{\infty} \frac{F(k)}{k}\,\sin(k\,\tau) dk = 1 + \frac{2}{\pi}\int_0^{\infty} \frac{G(k)}{k}\,\cos(k\,\tau) dk \tag{3.158}$$

with $F(k)$ and $G(k)$ real and imaginary part of the Theodorsen function respectively. The final expression for the lift is then

$$\mathcal{L}(\tau) = 2\,\pi\,\rho\,U^2\,b\,\alpha_0\,\varphi(\tau) \tag{3.159}$$

The trend of $\varphi(\tau)$ depicted[36] in Fig. 3.10 shows that the Wagner function tends to the unit value at the growing of the time. Thus, for a sudden start of a given incidence value, the steady value of lift is obtained for advanced values of time. Hence, the Wagner function is the response to an initial step of incidence assigned to a system represented by the Theodorsen function. That means that the function

[36] The software Mathematica 5.0 has been used.

$\varphi(\tau)$ can be regarded as the indicial response to the transferring function $\mathcal{C}(k)$.

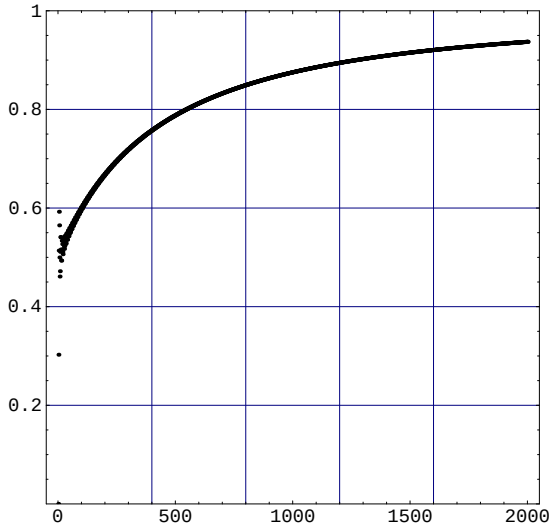


Figure 3.10: *Wagner function plotted respect to the adimensional time.*

**Statements of the Wagner problem in ground effect**

The addressed preamble to the Wagner problem in the unbounded domain jointly with the extension of the Theodorsen Theory obtained omitting the wake image term, can be adopted in order to extend the Wagner problem to the ground effect flying condition. Starting from the general statements of the problem, as shown in the unbounded domain, it can be set $\dot{\zeta}, \ddot{\zeta} = 0 \; \forall t$

$$\begin{cases} \alpha = 0 \quad \text{per} \quad t < 0 \Rightarrow \dot{\alpha}, \ddot{\alpha} = 0 \\ \alpha = \alpha_0 \quad \text{per} \quad t > 0 \Rightarrow \dot{\alpha}, \ddot{\alpha} = 0 \end{cases}$$

In the bounded case considered the lift term contributes are the one adimensionally evaluated in Eqs. 3.151, 3.152 In those mentioned equations repeatedly occurs the term given in 3.121 and identified as the boundary condition. It is still possible to show that that boundary condition coincides with the downwash at 3/4 of the chord. Thus, setting $a = -(1/4)c$ and $x = (c/2) = b$, the relationship[37] 3.121 becomes

$$\begin{aligned} \bar{w}(x) &= -ik\,\bar{\zeta} + \frac{b}{2} i\,k\,\bar{\alpha} - \bar{\alpha} - ik\,\bar{\alpha} b = \\ &= -\left[ i\,k\,\left( \bar{\zeta} + \frac{b}{2}\bar{\alpha} \right) + \bar{\alpha} \right] \end{aligned} \tag{3.160}$$

[37]Note that Eq. 3.121 is adimensional. Nevertheless, the adimensional notation is still maintained since the analogy with the similar dimensional expression given in [50], [49], [51], is evident.

that coincides with $\bar{w}_{3/4\,c}$ as evident considering the reference frame previously introduced. Hence, similarly to the unbounded domain case, it is possible dimensionally to write

$$f(\omega) = \int_{-\infty}^{+\infty} - \left[ b\,\dot{\zeta} + U\,\alpha + b\,\dot{\alpha} \right] e^{-i\,\omega\,t}\,dt = \int_{-\infty}^{+\infty} w_{3/4\,c}(t)\,e^{-i\,\omega\,t}\,dt \tag{3.161}$$

thus the Wagner problem is still given by

$$w_{3/4\,c} = \begin{cases} 0 & \text{per} \quad t < 0 \;\Rightarrow\; \dot{\alpha}, \ddot{\alpha} = 0 \\ -\,U\,\alpha_0 & \text{per} \quad t > 0 \;\Rightarrow\; \dot{\alpha}, \ddot{\alpha} = 0 \end{cases}$$

and it is still valid

$$f(\omega) = \int_{0}^{+\infty} -U\,\alpha_0\,e^{-i\,\omega\,t}\,dt = -\frac{U\,\alpha_0}{i\,\omega} \tag{3.162}$$

Considering the expression of the lift coefficient in ground effect Eqs. 3.151, 3.152 in their dimensional form and in analogy with the term 3.153, the lift in ground effect can be expressed as

$$\begin{aligned} \mathcal{L} \;=\; & -2\,\pi\,\rho\,U\,b \left[ \frac{1}{2\,\pi} \int_{-\infty}^{+\infty} \mathcal{C}(k)\,f(\omega)\,e^{i\,\omega\,t} d\omega \right] + \\ & -2\,\pi\,\rho\,U\,b \left( -\frac{K_0}{h} - \frac{K_1}{2}\frac{1}{h^2} + \frac{K_0^2}{h^2} \right) \left[ \frac{1}{2\,\pi} \int_{-\infty}^{+\infty} \mathcal{H}(k)\,f(\omega)\,e^{i\,\omega\,t} d\omega \right] + \\ & +2\,\pi\,\rho\,U^2\,b \left( -\frac{K_1}{2}\frac{1}{h^2} \right) \alpha_0 \end{aligned} \tag{3.163}$$

Substituting Eq. 3.162, the following relationship for the lift force in terms of the adimensional time $\tau = t\frac{U}{b}$ is obtained:

$$\begin{aligned} \mathcal{L}(\tau) \;=\; & 2\,\pi\,\rho\,U^2\,\alpha_0\,b \left[ \frac{1}{2\,\pi} \int_{-\infty}^{+\infty} \frac{\mathcal{C}(k)}{i\,k} e^{i\,k\,\tau} dk \right] + \\ & +2\,\pi\,\rho\,U^2\,\alpha_0\,b \left( -\frac{K_0}{h} - \frac{K_1}{2}\frac{1}{h^2} + \frac{K_0^2}{h^2} \right) \left[ \frac{1}{2\,\pi} \int_{-\infty}^{+\infty} \frac{\mathcal{H}(k)}{i\,k} e^{i\,k\,\tau} dk \right] + \\ & +2\,\pi\,\rho\,U^2\,b \left( -\frac{K_1}{2}\frac{1}{h^2} \right) \alpha_0 \end{aligned} \tag{3.164}$$

It is still possible to define the Wagner function given by

$$\varphi(\tau) := \frac{1}{2\,\pi} \int_{-\infty}^{+\infty} \frac{\mathcal{C}(k)}{i\,k} e^{i\,k\,\tau} dk \tag{3.165}$$

that as shown verifies

$$\varphi(\tau) = \frac{2}{\pi} \int_{0}^{\infty} \frac{F(k)}{k}\,\sin(k\,\tau) dk = 1 + \frac{2}{\pi} \int_{0}^{\infty} \frac{G(k)}{k}\,\cos(k\,\tau) dk \tag{3.166}$$

being $F(k)$ and $G(k)$ the real and imaginary part of the Theodorsen function repectively.

Furthermore, it is possible to define a function named $\Phi(\tau)$ that attends to the ground effect case given by

$$\Phi(\tau) := \frac{1}{2\,\pi}\int_{-\infty}^{+\infty}\frac{\mathcal{H}(k)}{i\,k}e^{i\,k\,\tau}dk \tag{3.167}$$

Calling $\hat{F}(k)$ and $\hat{G}(k)$ the real and imaginary part of the function $\mathcal{H}(k)$ respectively, an analogous expression of Eq. 3.166 can be written as follows

$$\Phi(\tau) = \frac{2}{\pi}\int_0^{\infty}\frac{\hat{F}(k)}{k}\,\sin(k\,\tau)dk = 1 + \frac{2}{\pi}\int_0^{\infty}\frac{\hat{G}(k)}{k}\,\cos(k\,\tau)dk \tag{3.168}$$

Thus, the lift will be expressed as

$$\mathcal{L}(\tau) = 2\pi\rho U^2 b\alpha_0\left[\varphi(\tau) + \left(-\frac{K_0}{h} - \frac{K_1}{2}\frac{1}{h^2} + \frac{K_0^2}{h^2}\right)\Phi(\tau)\right] + 2\pi\rho U^2 b\left(-\frac{K_1}{2}\frac{1}{h^2}\right)\alpha_0 \tag{3.169}$$

Hence, the adimensional lift coefficient is

$$C_L(\tau) = 2\,\pi\,\alpha_0\left[\varphi(\tau) + \left(-\frac{K_0}{h} - \frac{K_1}{2}\frac{1}{h^2} + \frac{K_0^2}{h^2}\right)\Phi(\tau)\right] + 2\,\pi\,\alpha_0\left(-\frac{K_1}{2}\frac{1}{h^2}\right) \tag{3.170}$$

The limit for $k \Longrightarrow 0\,;\,\tau \Longrightarrow \infty$ of the previous equation coincides with the steady lift coefficient in ground effect mentioned in Eq. 3.56. Nevertheless, it has to be underlined that a contribution to the lift force is due to the not-circulatory lift term and it is adimensionally given by $\left[2\,\pi\,\alpha_0\,\left(-\frac{K_1}{2}\frac{1}{h^2}\right)\right]$. The mentioned contribution seems to be due only to the ground presence: that accounting the ground effect configuration a starting higher value of lift has to be considered respect to the unbounded case.

**Results of the extension of the Wagner problem to the ground effect condition**

The numerical evaluation of the Wagner function in ground effect introduced in the previous subsection has been performed adopting the Software *Mathematica* 5.1. The Keldysh-Lavrentiev coefficient in ground effect are the ones evaluated once for all in the steady case. Different ground clearances conditions have been considered. Specifically, clearances of $1, 2, 10$ half-chords have been progressively investigated. The results concerning the comparison between the several considered trends are depicted in Fig. 3.11 The trends show the fact that in ground effect the steady lift value is higher respect to the unbounded domain case, thus the curves have different staring point values. The results show a trend at each ground clearance that seems to be practically the same of the unbounded domain, but the steady final values are higher for smaller distances from the ground, as expected.

An interesting plot can be obtained by normalizing the lift force at each ground clearance by its steady value. Thus, the normalized indicial functions in unbounded domain and in the bounded domain at different clearances are depicted in Fig. 3.12 Zooming the trends as referred in pictures 3.4.3 shows

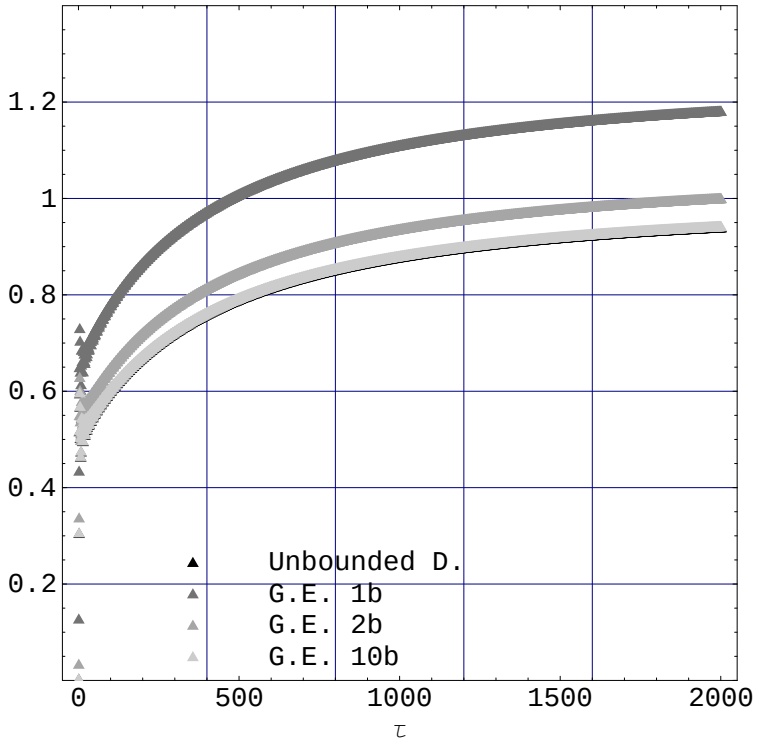


Figure 3.11: *Comparison of the Wagner function trends plotted respect to the adimensional time. Case of: unbounded domain and ground effect with clearances* 1*half-chord,* 2*half-chords,* 10*half-chords.*

that the trend of the indicial function in ground effect for $h = 1$ is slightly more rapid than the trend of the indicial response of the unbounded domain.

It is worth to remark that a similar trend of the Wagner indicial response in the unbounded domain has been obtained in the bounded domain too since the wake image term has been neglected. Thus, an underestimation of the wake contribution analytically obtained should be expected once comparing the depicted trends with experimental results. Nevertheless, even with the simplificative hypothesis adopted, the introduced methodology is still capable to partially estimate the wake contribution. The not-circulatory part of the lift force that appears in the definition of the Wagner problem in the bounded domain is responsible for such behavior and shows that the ground effect configurations owns itself an increased lift.

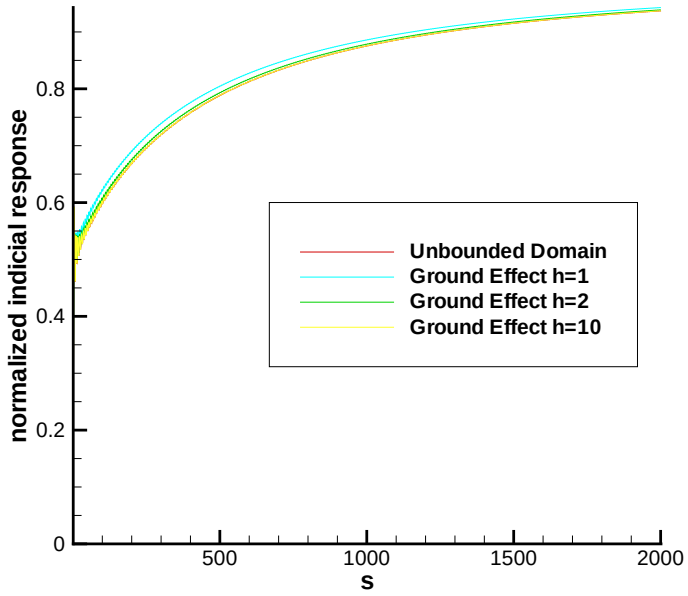


Figure 3.12: *Normalization of the indicial functions.*

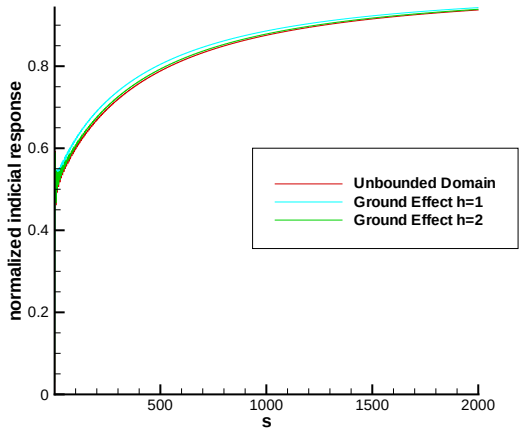


(a) Wagner indicial response and normalized indicial response in ground effect for $h = 1$

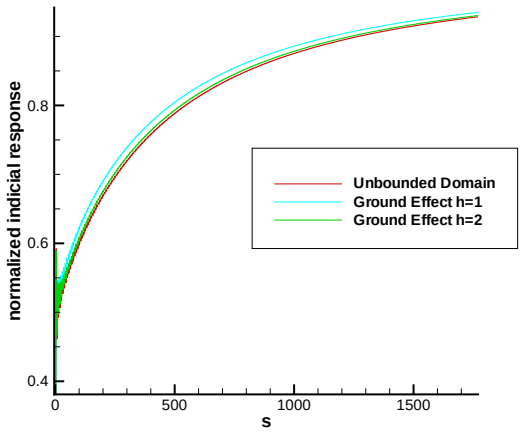


(b) Wagner indicial response and normalized indicial response in ground effect for $h = 1, 2$

### 3.4.4 Remarks on the ground effect modeling

Few remarks have still to be done respect to the ground effect modeling adopted in the previous sections. Indeed, Fig. 3.13 shows the plot of $1/x$ and $ftot = [1/x - (x/(x^2 + 4h^2)]$ that are representative

of the Theodorsen wake term in the unbounded domain and the image wake terms in the ground effect case respectively. The $ftot$ term has been evaluated for increasing value of the ground clearances of $0.5b, 1b, 2b, 10b$ where $b$ represents the airfoil half-chord. The case $0.5b$ can be considered extreme ground effect, thus it can not be investigated by the Keldysh-Lavrentiev approach. Nevertheless, that case has been depicted in order to show how the extreme case is totally separated from the others and need special solving methodologies. Respect the trends depicted for $h = 1b, 2b, 10b$ it is possible to remark that the higher differences between the free flight condition and the moderate ground effect condition is obtained for ground clearances comparable with one half-chord. Thus, the underestimation of the wake effects due to the simplified model adopted are rapidly more negligible for increasing values of the ground distances.

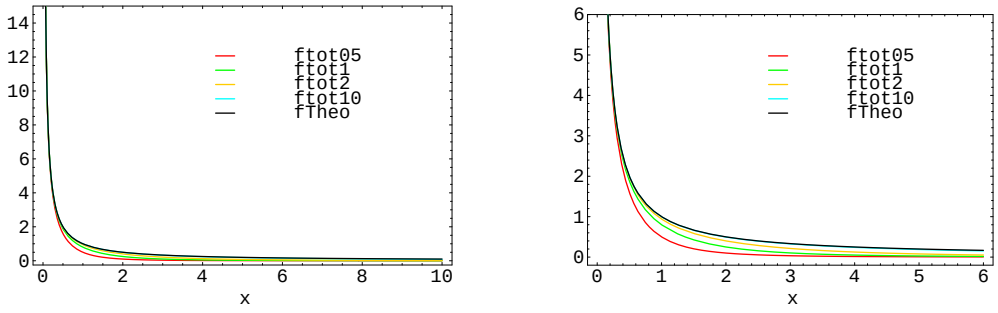


Figure 3.13: *Theodorsen wake term vs the ground effect image wake terms.*

Furthermore, another interesting trend is shown in Fig. 3.14. The functions depicted have been evaluated setting $h = 1b$ and *taylorftot* is the Taylor series expansion of the $ftot$ term previously introduced. As evident from the depicted figures, the error committed moving along the $taylorftot$ function

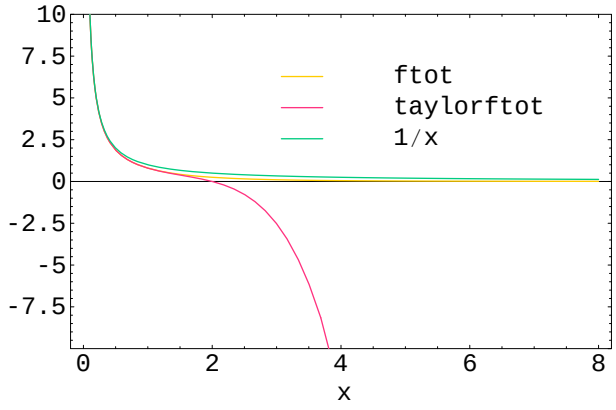


Figure 3.14: *Trends of* $ftot, taylorftot, 1/x$

is less than the error committed moving along the $1/x$ curve (that is an hyperbola and coincides with the unbounded domain case investigated by Theodorsen) till the point where the $taylorftot$ function

leaves the $ftot$ trend. This behavior has to be intended only for small ground clearances. Indeed, for large ground clearances the trend of the $ftot$ function will be similar to the $1/x$ one. Thus, in order to better accounting the wake term the best solution would be to follow the $taylorftot$ trend and then go to zero (for the extreme ground effect case) or follow the hyperbola trend (for moderate the ground effect case). Nevertheless, for different values of the ground clearance $h$, the point where the $taylorftot$ trend abruptly leaves the $ftot$ trend changes, hence the consideration of the wake term should be repeated at each ground distance without being univocally determined.

Finally, a plot of the errors committed considering the $taylorftot$ trend or the $1/x$ trend is shown in figure 3.15 for $h = 1b$. The trends depicted resume the previous assertions.

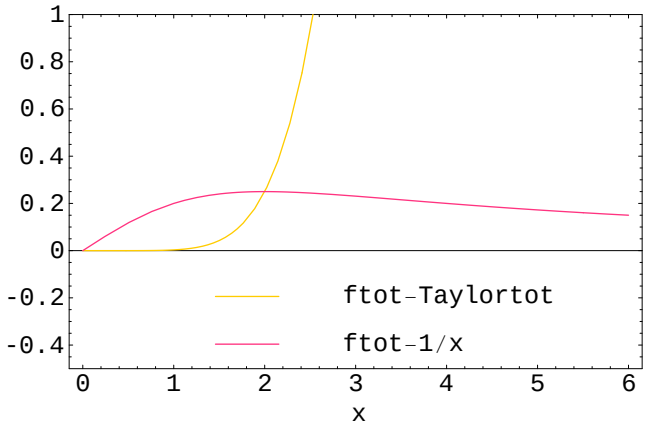


Figure 3.15: *Comparison of the trends of the functions* $ftot - taylorftot$ *and* $ftot - 1/x$

# Chapter 4

# Preliminary design of Amphibious Aircraft configurations adopting the MDO code MAGIC

## 4.1 Introduction

In the past few decades, since the aeronautical and aerospace engineering have assumed a leadership role in the industry of transportation, the requirement of improving aircraft performances and features, and the need of craft performing special missions were growing meanwhile. Hence, the possibility of unconventional or innovative configurations for aircraft design was pointed out. As known, a broad number of disciplines like aerodynamics, structural statics and dynamic analysis, thermal analysis, propulsion and performances are involved in aircraft design. Furthermore, considering new aircraft configurations, an 'extra'-problem besides the multi-disciplinary coupling, arises. Indeed, developing unconventional or innovative configurations, the reference data extrapolated by known standard configurations are useless. Thus, the concept of Multidisciplinary Design Optimization, MDO, for the preliminary design of aeronautical and aerospace structures is the natural answer to the challenge that aeronautical and aerospace structures represent above all if new configurations of craft are requested. Indeed, MDO offers the feasibility of an appropriate preliminary design of a vehicle, since it is possible to include into the project the constraints and project variables representative of the whole system investigating and taking into account the existing link among the involved disciplines. Hence, the aim of this chapter is to present an MDO procedure for preliminary design of non-conventional aircraft configurations in civil aviation by the use

of the code MAGIC.

Accordingly, the relevance of an adequate modeling is indispensable in order to obtain meaningful designing results. Thus, the intimate link between MDO, modeling, and simulations fields is evident. The demonstration of the previous assertions is one of the purposes of this chapter, meaning by 'appropriate' a design of the craft that can offer accurate and robust predictions with a relatively moderate computational effort.

The optimization code MAGIC adopted for the computational part of this work relies on these aspects. As mentioned in the second chapter, the code has been developed having as primary criterion the aim to work out algorithms based on first-principles overall for the structural and aerodynamical modules, as described later, besides other relevant properties of the code MAGIC (see also [52]).

Therefore, MAGIC is conceived for evaluating the multidisciplinary design optimization of a fixed-wing both in steady and the unsteady aerodynamics. The basic physical model used in MAGIC for modeling the aerodynamics is that of quasi–potential flows, *i.e.*, flows that are potential everywhere except for the wake surface, $\mathcal{S}_W$, which is the locus of the points emanating from the trailing edge.

Since we will focus this application of the code on the preliminary design of an aircraft able to perform its cruise in ground effect, *i.e.*, a special flight condition not generally accounted, the steady aerodynamics will be considered. Thus, the potential flows theory will be adopted, while for the wing structure we will use, in a first modeling stage, a linear elastic finite-element beam model.

Indeed, the goal of this chapter is also to explore the capability of an MDO analysis for aircraft performing special mission, like for example amphibious fire-extinguisher craft approaching the ground for watering or like the Wing In Ground effect craft (WIG). In the preliminary design phase of such vehicles, it is important to determine the loads acting on the wing in ground effect. Hence, for evaluating the lift we have adopted the specific methodology introduced by Keldysh-Lavrentiev (KL) and available in the steady aerodynamic case for airfoils in bounded domain that has been mentioned in chapter 3.

The scientific and applicative emphasis of the KL approach for the evaluation of the aerodynamical coefficients in moderate ground effect in case of thin airfoil and the method can be find in Ref. [44]. As shown in Refs.[44],[43] the KL method was tested adopting a thin Joukowski symmetric profile nevertheless, the relevance of this kind of airfoils is merely conceptual.

The main limit of the Joukowski foils is the difficult achievement of their cuspidate trailing edge. This problem can be overcome using the Karman-Trefftz airfoils. Hence, it seemed appropriate to generate the wing using a Karman-Trefftz profile furthermore a rectangular wing will be considered in order to extend the foil results to the finite wing, as itemized later.

A finite-element model of the wing is further developed adopting the commercial code MSC Nastran. Moreover, the code MAGIC has been allowed to interface the code MSC Nastran so that to perform the structural wing analysis and evaluate the statically deformed configuration. Once the structural analysis is fully accomplished, the optimization section starts. Some remarks on the optimizer and the results obtained will be widely dealt in the pertinent sections.

## 4.2 Structural Analysis

For the structural analysis adopted in the current application of the code MAGIC one can rely on the structural analysis presented when referring to the applicative part of the second chapter. Thus, see paragraph 2.2.3 for details.

## 4.3 Aerodynamic Modeling for the Ground Effect: testing of the Keldysh-Lavrentiev methodology on a Karman-Trefftz profile

As mentioned in the Introduction, in the following we will focus on the steady formulation for incompressible flows. Hence, we will address in this section only some remarks on the method adopted for the aerodynamic modeling in ground effect focusing on the basis of the Keldysh-Lavrentiev (KL) methodology that has been introduced in the previous chapter.

The method introduced by KL[1] for evaluating the steady aerodynamical coefficients of a foil operating in a bounded domain, was originally worked out for naval problems, *i.e.*, for hydrofoils approaching the free surface. Nevertheless, one of the advantages of the KL procedure is its own versatility that, under appropriate hypothesis, allows to use it also in case of airfoils in ground effect.

It is worth to remark that the method relies on the definition of an appropriate complex potential function by using the image method so that the presence of the foil can be considered and such that the linearized boundary condition on the foil and on the ground are both satisfied. Hence, let us consider the two-dimensional potential flow of a uniform stream of speed $V_\infty$ past a thin airfoil chord $c = 2b$ located at distance $\hat{h}$ from the ground.

Following reference [44] and the theory introduced in the previous chapter, the non-dimensional (the

[1] As pointed out later it is more appropriate to speak about the KL *expansion* more than the KL *method*, since the innovative contribution due to KL consists in an asymptotic expansion.

adimensionalization is achieved normalizing all the length by the half chord $b$ and all the speeds by $V_\infty$) integral equation [2] for such airfoil in a steady potential flow is

$$\oint_{-1}^{1} \gamma(\xi)\, K(x-\xi)\, d\xi = 2\,\pi\,\alpha \;-\; 2\oint_{-1}^{1} T'(\xi)\, H(x-\xi)\, d\xi \tag{4.1}$$

being $\alpha$ the angle of attack, $\gamma$ the vorticity, $T$ a function defining the shape of the airfoil while $H, K$ are the kernel functions of thickness and vorticity problems respectively expressible as

$$\begin{aligned} H(x) &= \frac{-2h}{x^2+4h^2} \\ K(x) &= \frac{1}{x} - \frac{x}{x^2+4h^2} \end{aligned} \tag{4.2}$$

being $h$ a non dimensional parameter representing the distance between the airfoil and the ground (the adimensionalization is obtained using as reference length the midchord of the foil hence, $h = \hat{h}/b$). It is worth to point out that the function $T(x)$ is properly adopted to take into account also the effect of the camber of the foil (as will be shown later on in evaluating the meanline).

Once the kernel function of the vorticity and thickness problems are introduced, the KL method consists of performing an asymptotic expansion of these kernel functions respect to $h$ as follows

$$\begin{aligned} H(x) &= \frac{1}{h}\sum_{0}^{\infty} H_n \left(\frac{x}{h}\right)^n \\ K(x) &= \frac{1}{x} + \frac{1}{h}\sum_{0}^{\infty} K_n \left(\frac{x}{h}\right)^n \\ \gamma(x) &= \sum_{0}^{\infty} h^{-n}\gamma_n(x) \end{aligned} \tag{4.3}$$

Inserting the previous expansion in the corresponding terms of the equation (4.1) and collecting the terms of the same order respect to the expansion parameter, a sequence of simpler problems is obtained. Hence, after evaluating at each order the corresponding vorticity adopting the Söhngen inversion formula[3], the lift coefficient follows by integration

$$C_L = \int_{-1}^{+1} \left[\gamma_0(\xi) + \frac{1}{h}\gamma_1(\xi) + \frac{1}{h^2}\gamma_2(\xi)\cdots + \frac{1}{h^n}\gamma_n(\xi)\right] d\xi = C_{L0} + \frac{1}{h}C_{L1} + \frac{1}{h^2}C_{L2} + \cdots + \frac{1}{h^n}C_{Ln} \tag{4.5}$$

In the pursuance of the thesis has been considered an expansion till the third order in $h$, thus, the lift

[2] The integrals are intended in their Cauchy principal value.

[3]
$$\gamma_n(x) = \frac{1}{\pi^2}\left(\frac{1-x}{1+x}\right)^{1/2} \oint_{-1}^{1} \left(\frac{1+\xi}{1-\xi}\right)^{1/2} \frac{F_n(\xi)}{(\xi-x)} d\xi \tag{4.4}$$

coefficient is given by

$$C_L = C_{L0} + h^{-1}C_{L1} + h^{-2}C_{L2} + h^{-3}C_{L3} \tag{4.6}$$

with

$$\begin{aligned}
(1/h)^0 \quad &: \quad C_{L0} = 2\pi\alpha \\
(1/h)^1 \quad &: \quad C_{L1} = 2\pi\alpha(-K_0) \\
(1/h)^2 \quad &: \quad C_{L2} = 2\pi\alpha(K_0^2 - K_1) - 2H_1 s \\
(1/h)^3 \quad &: \quad C_{L3} = 2\pi\alpha\left(-K_0^3 + 2K_0K_1 - \frac{3}{2}K_2\right) + 2H_2(2p - s) + 2K_0H_1 s
\end{aligned} \tag{4.7}$$

where the KL coefficient $K_0, K_1, K_2, H_0, H_1, H_2$ can be evaluated once for all (since the versatility of the KL methodology, as already mentioned, this evaluation can be done once for all either for an airfoil or, obviously with different values, for an hydrofoil as in Ref.[44]), while $y = \pm T(x)$ is the function that defines the shape of the airfoil.

Hence, the terms $p$ and $s$ respectively are defined as

$$\begin{aligned}
s &= \int_{-1}^{1} T(\xi) d\xi \\
p &= \int_{-1}^{1} T(\xi)\, \xi d\xi
\end{aligned} \tag{4.8}$$

Following the procedure outlined in reference [44] for the thin airfoil, the KL coefficients are

$$\begin{aligned}
H_0 &= -\frac{1}{2} \qquad K_0 = 0 \\
H_1 &= 0 \qquad\quad K_1 = -\frac{1}{4} \\
H_2 &= \frac{1}{8} \qquad K_2 = 0
\end{aligned} \tag{4.9}$$

As mentioned in the introductive section, in literature the KL expansion and methodology was tested adopting a thin Joukowski symmetric profile.

Instead of the Joukowski profile, since the difficulties related to its cuspidate trailing edge, we adopted a more achievable foil applying the Karman-Trefftz transformation. Indeed, the extremely cuspidate Joukowski airfoils trailing edge makes almost impossible the placing of stiffening elements in that area suitable to counteract the aerodynamical loads. Figure 4.1 compares the transformation by Joukowski and by Karman-Trefftz of a same circumference showing the heavily cuspidate trailing edge of the Joukowski foil. Thus, the Karman-Trefftz profile has been implemented in the code MAGIC thanks to its versatility. It is also important to remark that the Karman-Trefftz airfoil adopted in this work has some features, such

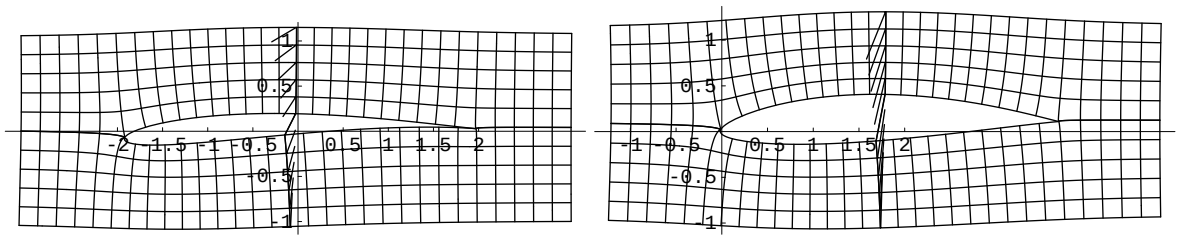


Figure 4.1: *Joukowski (on the left side) and Karman-Trefftz (on the right side) transformations of a same circumference.*

as a flat lower surface, that are needed in order to efficiently take advantage from the ground effect flying conditions. Therefore, the Karman-Trefftz profile used in this thesis has been obtained transforming the circumference centered in $(-0.02975, 0.02895)$ and properly applying (in order to achieve the Karman-Trefftz transformation) what referred in *Complex Analysis Mathematica* 3.0 *Notebooks* 1998 *by J.H. Mathews and R.W. Howell* for the Joukowski transformations.

The conformal transformation of Karman-Trefftz consists of three sequential main steps

- the first step concerns the decomposition of the basics conformal transformation of Joukowski in order to obtain a linear fraction transformation able to expand the Joukowski circle into an unbounded sector
- the second step concerns the modification of the sector amplitude by a power elevation
- the last step concerns another linear fraction transformation in order to go back to the foil.

The three steps itemized can be resumed in the final expression

$$z(\zeta) = f + \frac{k(c-1)}{(\frac{\zeta-1}{\zeta-c})^k - 1} \tag{4.10}$$

where $k$ represents the angle at the trailing edge[4] defined unless a $\pi$ value. For the transformation performed in this work with a trailing edge angle of 18.32 degrees, the value obtained has been $k = 18.89822$. The other terms of the transformation are $c = -(1 + 2b)$ that represents the second critical point of the transformation[5] with $b$ value of the coordinate of the center of the circumference that originates the airfoil[6]. The transformation is determined unless a complex constant $f$ that represents a

[4]For the Joukowski conformal transformation $k$ has always the same value that is $k = 2$; in case of the Karman-Trefftz conformal transformation $k$ can assume different values that is $k(1\text{div}\,2)$.

[5]The first critical point is the one that simulates the trailing edge and fulfills there the Kutta condition. The first critical point is thus always placed in $(a, 0)$ where $a$ is the radius of the fundamental circumference.

[6]It is worth to note that only for the conformal transformation the terms $b, c$ represent respectively the center of the fundamental circumference and the position of the second critical point while in the previous the same terms were adopted for naming the half-chord and the chord of the airfoil respectively, but it seems evident that there is not risk of misunderstanding.

simple translation of the reference frame and coincides with the position of the foil trailing edge in the $\zeta$ plane (for $f = 0$ the trailing edge of the airfoil is placed in the origin of the $\zeta$ plane).

Then, having the purpose of evaluating the lift, it has been necessary to obtain the function $T(\xi)$ (being $\xi$ a non dimensional abscissa moving along the chord) defining the upper and lower parts of the foil. In order to do that, the foil points were sampled as shown in Fig. 4.2 and then the obtained foil shape as been rotated so that the chord became parallel to the abscissa axes. After normalizing the foil (by dividing its points by the midchord value), it has also been translated obtaining the final airfoil in the requested range $\pm 1$ as depicted in Fig. 4.3.

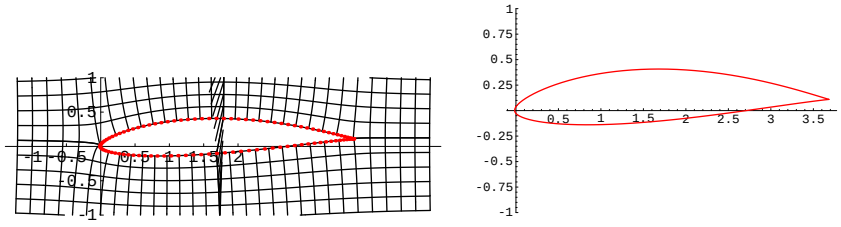


Figure 4.2: *Extrapolation of the Karman-Trefftz profile points.*

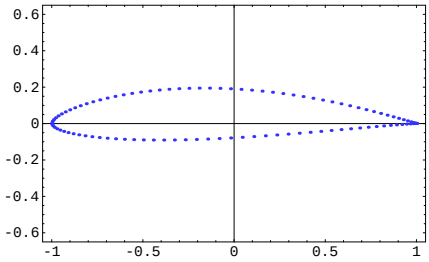


Figure 4.3: *The final profile achieved, rotated and centered.*

The airfoil point were then interpolated in order to obtain an analytical expression for the function $T(\xi)$. Thus, for the interpolation a polynomial basis extended to the fifth order of the kind

$$\mathcal{P} = \left\{ \int \frac{\xi^n}{\sqrt{1-\xi^2}} d\xi; (n, 0, 5) \right\} \tag{4.11}$$

has been adopted and this procedure has been pursued both for the upper $T_u(\xi)$ and for the lower $T_l(\xi)$ surfaces. The obtained expressions are

$$\begin{aligned} T_u(\xi) =& 0.288\sqrt{1-\xi^2} - 0.017\sqrt{1-\xi^2}\left(-\frac{4}{3} - \frac{2\xi^2}{3}\right) + 0.227\sqrt{1-\xi^2}\left(-\frac{8}{15} - \frac{4\xi^2}{15} - \frac{\xi^4}{5}\right) + \\ &+0.022\left[\sqrt{1-\xi^2}\left(-\frac{3\xi}{8} - \frac{\xi^3}{4}\right) + \frac{3\arcsin\xi}{8}\right] + 0.901\left(-\frac{1}{2}\xi\sqrt{1-\xi^2} + \frac{\arcsin\xi}{2}\right) - 0.054\arcsin\xi \end{aligned}$$

$$T_l(\xi) = -0.094\sqrt{1-\xi^2} + 0.001\sqrt{1-\xi^2}\left(-\frac{4}{3} - \frac{2\xi^2}{3}\right) - 0.034\sqrt{1-\xi^2}\left(-\frac{8}{15} - \frac{4\xi^2}{15} - \frac{\xi^4}{5}\right) +$$
$$-0.011\left[\sqrt{1-\xi^2}\left(-\frac{3\xi}{8} - \frac{\xi^3}{4}\right) + \frac{3\arcsin\xi}{8}\right] - 0.102\left(-\frac{1}{2}\xi\sqrt{1-\xi^2} + \frac{\arcsin\xi}{2}\right) + 0.056\arcsin\xi$$

.

Hence, in order to obtain the terms $s = |s_u| + |s_l|$, $p = |p_u| + |p_l|$ the following integrals had to be solved

$$\begin{aligned} s_u &= \int_{-1}^{1} T_u(\xi)d\xi \qquad s_l = \int_{-1}^{1} T_l(\xi)d\xi \\ p_u &= \int_{-1}^{1} T_u(\xi)\,\xi d\xi \qquad p_l = \int_{-1}^{1} T_l(\xi)\,\xi d\xi \end{aligned} \tag{4.12}$$

For the Karman-Trefftz airfoil considered the values obtained gave

$$\begin{aligned} s &= |s_u| + |s_l| = 0.3874 \\ p &= |p_u| + |p_l| = 0.0449 \end{aligned} \tag{4.13}$$

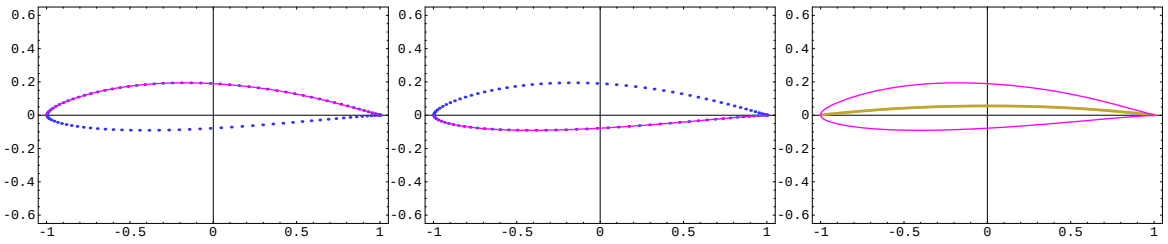


Figure 4.4: *Fitting the profile points the function $T(x)$ is obtained. Subsequently, the mean line is evaluated.*

In order to evaluate the points of the airfoil mean-line we proceeded by sampling, at same spaced steps along the chord, the points of the functions approximating the upper and lower parts of the foils and evaluating then their half-sum. Thus, the point obtained for simulating the mean-line have been interpolated adopting a simple polynomial development of the kind

$$\mathcal{P}_{ml} = \left\{\xi^n\,;\;\; (n, 0, 5)\right\} \tag{4.14}$$

to achieve the analytical expression for the mentioned mean-line shown below

$$ml(x) = 0.0561 + 0.0009\,x - 0.0532\,x^2 - 0.0025\,x^3 - 0.0020\,x^4 + 0.0013\,x^5 \tag{4.15}$$

As shown in the pictures above (Fig. 4.4) and as mentioned before, the lower part of the obtained airfoil is almost flat like the ground effect flight condition requests.

The adoption of the KL procedure arrested to the third order for the Karman-Trefftz airfoil considered, yields the following lift coefficients[7] that can be used for the MDO integrated analysis (some details on obtaining the evaluation of the lift coefficient at each order using the KL methodology are addressed in Ref. [53] and are not listed here for sake of conciseness)

$$\begin{aligned} C_{L0} &= 2\,\pi\,(\alpha - 0.057) \\ C_{L1} &= -2\,\pi\,K_0\,(\alpha - 0.057) \\ C_{L2} &= 2\,\pi\,\left[\left(K_0^2\alpha - K_1\,\alpha\right) + 0.028\,K_1 - 0.057\,K_0^2\right] - 2\,H_1\,s \\ C_{L3} &= 2H_2(2p - s) \end{aligned} \tag{4.18}$$

Finally, the lift coefficient for the airfoil in ground effect can be evaluated as shown in Eq.(4.6). In Fig. 4.5 it is shown the comparison between the lift coefficient of the Karman-Trefftz foil including the ground effect correction evaluated by the KL method, and the lift coefficient of a flat plate. The abscissa value of the plots is the non dimensional (respect to the half chord) clearance from the ground and it is evident that the most relevant contribution of the chord dominated ground effect at the increase of lift is achieved for ground clearance less than one half chord. The figure shows also that when the third order is considered the thickness terms become relevant, hence, the lift correction in ground effect for the Karman-Trefftz airfoil has less authority compared with the trend obtained taking into account only the terms till the second order.

In the methodology used in MAGIC the problem of the velocity potential is solved by boundary elements. Hence, it is highly important to explore whereas the proposed $2D$ correction for the lift in ground effect could be adopted in the code. Practically, it was already investigated in reference [54] where the $2D$ KL correction was inserted in the lifting-line theory of Prandtl and the results were compared with the ones obtained for the same rectangular wing adopting a vortex-lattice method for wings with different aspect ratios. In the cited reference a very good agreement between the two compared methods had been observed for aspect ratio of the order or 4. Furthermore, the case of aspect ratio of the order of 6 was investigated and a better agreement at the larger aspect ratio adopted had been detected (as expected).

[7] In the particular case we are interested in, *i.e.*, the Karman-Trefftz airfoil, besides the angle of attack $\alpha$ we had to consider the local incidence obtained differentiating the analytical expression of the mean-line (for small angle of attack) that is

$$\alpha_{ml}(x) = 0.0009 - 0.0532\,x - 0.0025\,x^2 - 0.0020\,x^3 + 0.0013\,x^4 \tag{4.16}$$

Thus, the zero order problem is the following

$$\oint_{-1}^{1} \frac{\gamma_0(\xi)}{(x-\xi)}\,d\xi = 2\,\pi\,\alpha + 2\,\pi\,\alpha_{ml} \tag{4.17}$$

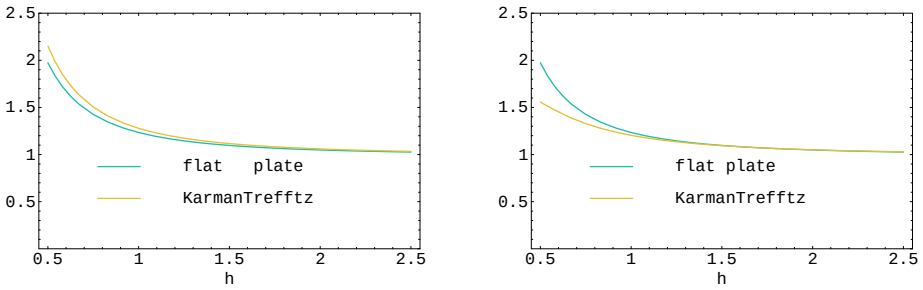


Figure 4.5: *Comparison between the lift coefficients of the Karman-Trefftz airfoil and a flat plate in ground effect for an angle of attack* $\alpha = \pi/\mathbf{20}$ *and at a variable distance from the ground. The left figure shows the second order contribution while the right one takes into account also the third order contribution.*

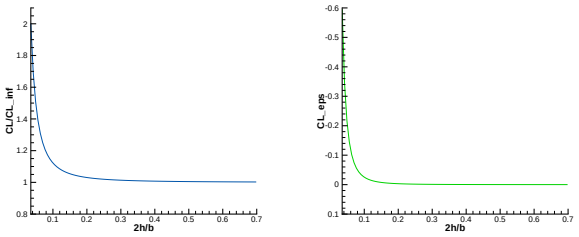


Figure 4.6: *Trends of the lift curve slope (on the right side) and of the slope of lift coefficient vs thickness ratio curve (on the left) for the rectangular wing considering the Karman-Trefftz foil shape. The wing aspect ratio considered is approximately* 8.

In Fig. 4.6 are depicted the trends of the lift curve slope and of the slope of lift coefficient vs thickness ratio curve for the rectangular wing adopted in the optimization code (shaped by the Karman-Trefftz foil).

The trends are qualitatively analogous to the ones obtained in Ref.[54]. Indeed, we considered in our study a rectangular wing in order to avoid the chord dependance of the lift distribution on the wing, and hence be able to use the $2D$ KL correction for the finite wing adopted in MAGIC as shown in the similar results obtained in Ref. [54]. It is also worth to remark that the aspect ratio of the wing considered is of the order of 8.

## 4.4 Remarks on the Optimization Process

Once the structural and aerodynamic analysis are achieved, the optimization process can be performed. Thus, since the optimization procedure covers a wide part of the present work, it is appropriate to

introduce the optimization process adopted.

The optimizer employed in MAGIC has been presented in the second chapter. The code MAGIC contains modeling modules for fixing the physical structure of the aircraft, and analysis modules suitable to evaluate the current values of the objective function and of the structural constraints. The code MAGIC is currently able to submit a finite element commercial code for the finite element analysis and to suitably interface it during the analysis like also the possibility of performing the optimization process using the commercial optimizer code SNOPT 6.0.

The structure analyzed is a complete aircraft. The wing box structure is built using a Karman-Trefftz profile and assembled in a conventional aircraft configuration. Since one of the aims of this work is the optimization of a craft performing its cruise in ground effect conditions, we referred to a fire extinguisher craft of the kind of the Canadair CL415.

Two kind of objective functions has been considered and compared in performing the wing optimization: a *logarithmic* objective function and a *weighted average* one, respectively stated as follows

$$\begin{aligned} OBJ_{log} &= \ln\left(e^{\eta_{WE}\frac{W_E}{W_{ER}}} + e^{\eta_{LD}\frac{LD_R}{LD_{RR}}}\right) \\ OBJ_{wa} &= \eta_{WE}\frac{W_E}{W_{ER}} + \eta_{LD}\frac{LD_R}{LD_{RR}} \end{aligned} \tag{4.19}$$

where $\eta$ are coefficients that weigh the estimated contribution of each term, while $W_E, LD$ are the structure empty weight and the lift to drag ratio (*i.e.*, the aerodynamic efficiency) respectively. The subscript $_R$ indicates reference values. Since the empty weight has to be reduced while the aerodynamic efficiency has to be improved, the coefficients $\eta$, that weigh their relevance, have been set as $\eta_{WE} = 0.5$ ; $\eta_{LD} = -0.5$.

It is worth to note that the choice of the empty weight and of the aerodynamic efficiency as components of the objective function is indicative of the behavior of the manufacturing costs and of the operative costs. Indeed, while it is easy to consider the empty weight as representative of the manufacturing costs, it has to be remarked that an high aerodynamic efficiency conveys a moderate fuel consumption. Hence, the aerodynamic efficiency can be considered as representative of the operative costs, an higher aerodynamic efficiency determines lower operative costs.

In order to underline the "topographic map" of the two different expressions adopted for the multi-objective function, the contour plot of those functional relationships is depicted in Fig. 4.7. The contours join points on the surface that have the same height.

The variables chosen as the active ones in the optimization process are the wing span, the root and tip chords, the thickness of the skin at the root and at the tip, the thickness of the root and tip spars, and

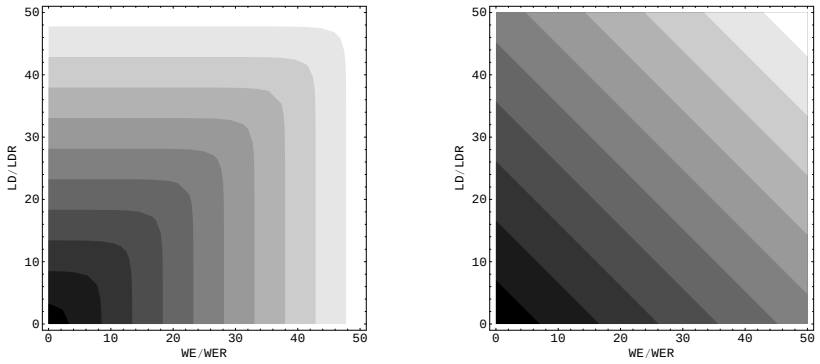


Figure 4.7: Contour plot that shows the topology of the functional relationships adopted in formulating the multi-objective function. Case of logarithmic expression (on the left) and of weighted average expression (on the right).

the root and tip built-in-angles. The wing root is considered as fixed. The starting values of the design variables and the side constraints are depicted in Table 4.1.

| Active variables | Initial value | Lower side constraints | Upper side constraints |
|---|---|---|---|
| Wing span $[m]$ | 14.315 | 13.00 | 15.50 |
| Root chord $[m]$ | 3.54 | 2.80 | 4.50 |
| Tip chord $[m]$ | 3.54 | 2.80 | 4.50 |
| Root panel thickness $t_{skin}$ $[m]$ | 0.002 | 0.001 | 0.005 |
| Tip panel thickness $t_{skin}$ $[m]$ | 0.001 | 0.0008 | 0.004 |
| Root spar thickness $t_{web}$ $[m]$ | 0.015 | 0.012 | 0.050 |
| Tip spar thickness $t_{web}$ $[m]$ | 0.005 | 0.003 | 0.030 |
| Root built-in-angle $\alpha_{root}$ | 6.00 | 0.00 | 8.00 |
| Tip built-in-angle$\alpha_{tip}$ | 6.00 | 0.00 | 8.00 |

Table 4.1: Side constraints.

The constraints adopted can be classified in three different branches:

- *structural*: direct stress, shear stress, and buckling constraints
- *vertical equilibrium*: lift-weight constraint
- *performances*: useful fuel volume constraint

## 4.5 Numerical Results

As previously mentioned, the optimization of the wing was performed adopting two different multi-objective function formulations. Hence, after presenting the results obtained for each kind of objective function adopted, it is useful to compare them in order to explore the advantage or disadvantage of each used formulation. The test were performed considering four flight condition:

- out of ground effect *i.e.*, high-flying condition;
- dimensionless ground clearance $h = 1$ *i.e.*, half-chord clearance flight condition;
- dimensionless ground clearance $h = 2$ *i.e.*, one chord clearance flight condition;
- dimensionless ground clearance $h = 10$ *i.e.*, five chords clearance flight condition.

Even if the flying condition $h = 1$ is a too extreme one, it was seeming appropriate, in order to obtain a more exhaustive overview, to add it into the analysis.

It is worth to remark that the wing we were referring to has been basically dimensioned adopting an efficient existing model. Therefore, small modification from the starting values are expected.

### 4.5.1 Results of the wing optimization using the logarithmic expression for the objective function formulation

The initial values and the results of the optimization process performed adopting the logarithmic formulation of the objective function are accounted in the second and third column of Tables 4.4, 4.5, 4.6, 4.7.

Even if in each case the wing span tends to reach the upper side constraint level, it reaches that value only when the ground clearance is extremely small. This result can be caused by the adoption of the extension of a $2D$ lift correction, even if with the mentioned proper considerations addressed to the $3D$ case, for the finite wing case, as referred in section 4.6.

In all four cases the rectangular plan shape of the wing is well enough maintained. After the optimization process, the root and tip built-in-angles introduce a small twisting of the wing that is more pronounced for $h = 1$ and tends to be minimum getting out from the ground effect flight conditions.

The performances improvements and their percentage values are briefly compared for the four cases tested in Table 4.2. As expectable, the savings in terms of empty weight and useful fuel weight as the

| Performances | Initial value | **Out G.E.** Final (log.obj.) and % Improv. | **h = 1** Final (log.obj.) and % Improv. | **h = 2** Final (log.obj.) and % Improv. | **h = 10** Final (log.obj.) and % Improv. |
|---|---|---|---|---|---|
| Take off w.$[Kg]$ | 21583.630 | 20984.082 | 19906.146 | 20570.804 | 20848.557 |
| | | **2.77%** | **7.77%** | **4.69%** | **3.40%** |
| Empty w. $[Kg]$ | 10934.63 | 10695.57 | 10378.709 | 10566.223 | 10614.021 |
| | | **2.18%** | **5.08%** | **3.37%** | **2.93%** |
| Useful Fuel w.$[Kg]$ | 4649.0 | 4288.512 | 3527.437 | 4004.581 | 4234.535 |
| | | **7.75%** | **24.12%** | **13.86%** | **8.91%** |
| Structural Wing w. $[Kg]$ | 3027.774 | 2866.524 | 2691.918 | 2799.826 | 2802.513 |
| | | **5.32%** | **11.09%** | **7.53%** | **7.44%** |
| Efficiency | 14.51 | 17.85 **23.02%** | | | |
| | 14.60 | | 20.94 **43.42%** | | |
| | 14.54 | | | 18.85 **29.64%** | |
| | 14.51 | | | | 17.97 **23.84%** |

Table 4.2: Percentage values of the improvements achieved performing the multi-disciplinary optimization process. Case of logarithmic objective function formulation adopted.

improvements in aerodynamic efficiency are more remarkable when the ground effect flight condition is attained. The values obtained in the extreme case of $h = 1$ have to be considered as purely qualitative.

It is worth to note that the best advantage from the ground effect condition is achieved for ground clearance approximately about one chord length. Indeed, the performances profits obtained for distances larger than one chord, quickly reach values approximately equal to the values achieved out of the ground effect condition, as shown from the results attained for $h = 10$.

The trends of the design variables optimizations are depicted in Fig. 4.10. The root and tip built-in-angles trends clearly show how the larger twisting of the wing is achieved at very small ground clearance, while for larger clearances their values quickly decrease tending towards the out of ground effect ones.

Analogous consideration can be drawn on from any of the trends depicted in Fig. 4.11, where the objective function and the constraints patterns are considered. Indeed, every pattern shows how after one chord clearance the corresponding trend quickly moves to the one obtained out of the ground effect.

It is worth to remark that the investigated structure is based on the dimension of an existing one, thus, not too extreme changes applying the optimization process have been expected (for the existing craft the dimensions can be already considered as optimized ones). Nevertheless, the relevance of the results rely on the determining the behavior of the optimization process accounting the peculiar condition of the ground effect. The decreasing of the performances for growing values of the ground clearances is in agreement with a correct implementation of the Keldysh-Lavrentiev methodology.

| Performances | Initial value | **Out G.E.** Final (wa.obj.) and % Improv. | **h = 1** Final (wa.obj.) and % Improv. | **h = 2** Final (wa.obj.) and % Improv. | **h = 10** Final (wa.obj.) and % Improv. |
|---|---|---|---|---|---|
| Take off w.$[Kg]$ | 21583.630 | 20589.858 | 19930.567 | 20496.887 | 20760.280 |
| | | **4.60%** | **7.66%** | **5.03%** | **3.81%** |
| Empty w. $[Kg]$ | 10934.63 | 10440.813 | 10399.509 | 10516.152 | 10579.101 |
| | | **4.51%** | **4.89%** | **3.83%** | **3.25%** |
| Useful Fuel w.$[Kg]$ | 4649.0 | 4149.045 | 3531.058 | 3980.735 | 4181.179 |
| | | **10.75%** | **24.05%** | **14.37%** | **10.06%** |
| Structural Wing w. $[Kg]$ | 3027.774 | 2672.181 | 2712.718 | 2758.358 | 2790.654 |
| | | **11.74%** | **10.40%** | **8.90%** | **7.83%** |
| Efficiency | 14.51 | 18.13 **24.95%** | | | |
| | 14.60 | | 20.94 **43.42%** | | |
| | 14.54 | | | 18.90 **29.98%** | |
| | 14.51 | | | | 18.14 **25.02%** |

Table 4.3: Percentage values of the improvements achieved performing the multi-disciplinary optimization process. Case of weighted average objective function formulation adopted.

### 4.5.2 Results of the wing optimization using the weighted average expression for the objective function formulation

In the second and fourth column of Tables 4.4, 4.5, 4.6, 4.7 there are shown the initial values and the results of the optimization process performed adopting the weighted average formulation for the objective function.

In this instance, the wing span tends to reach the upper side constraint level for every case considered highlighting that the wing span does not act like an active variable in the optimization process since it is constrained to its limit value.

In all four cases the rectangular plan shape of the wing is well enough maintained. Also in case of weighted average formulation of the objective function, after the optimization process, the root and tip built-in-angles introduce a small twisting of the wing. However, in this case the twisting is less pronounced for $h = 1$ and tends to be greater getting out from the ground effect flight conditions.

The performances improvements and their percentage values are briefly compared for the four cases tested in Table 4.3. As expectable, once again the savings in terms of empty weight and useful fuel weight as the improvements in aerodynamic efficiency are more remarkable when the ground effect flight condition is attained. As already mentioned, the values obtained in the extreme case of $h = 1$ have to be considered as purely qualitative.

Same considerations about the best advantage from the ground effect condition achieved for ground

clearance of approximately one chord length can be done also when the weighted average objective function is adopted. The trends of the design variables optimizations are depicted in Fig. 4.12 while the objective functions and constraints trends patterns are shown in Fig. 4.13.

### 4.5.3 Comparison of the optimization processes performed adopting the two different objective functions expressions

As pointed out in the previous subsections, the multi-disciplinary design optimization processes performed adopting the two different expressions for the objective function formulations, have shown good results agreement. However, one of the main advantages in using the logarithmic formulation, is the less number of gradient evaluations performed before the convergence value is achieved.

In order to emphasize the assertion above, it is useful to depict for each design variable and for each constraint, the comparison between the trends of the patterns obtained adopting the two different objective function formulations. For sake of completeness, this has been iterated for every one of the four cases considered, as shown in Figs. 4.14, 4.15, 4.16, 4.17, 4.18, 4.19, 4.20, 4.21.

Indeed, every trend shows the needing of a smaller number of gradient evaluations if the logarithmic functional relationship is adopted for the objective function.

Another advantage in using the logarithmic expression is addressable in obtaining an always positive value for the objective function expression (as the values of the objective functions in Tables 4.4, 4.5, 4.6, 4.7 shown). Indeed, the much less than zero values of the weighted average objective function can lead to numerical problems also if the double precision in the evaluations is taken into account.

On the other hand, it is worth to note that adopting the weighted average formulation the values obtained for the empty weight and for the aerodynamic efficiency (terms whose contribution is considered in the multi-objective function settled) are respectively smaller and higher than the ones achieved adopting the logarithmic formulation (except for $h = 1$ where the same values are reached). Furthermore, the weighted average formulation seems to better take advantage from the constraints, making them closer (even if their are never violated) to the critical value.

## 4.6 Remarks

The capability of an MDO analysis for aircraft performing special mission, like for example an amphibious fire-extinguisher craft approaching the ground for watering has been explored.

In order to evaluate the lift we have adopted the specific methodology introduced by Keldysh-Lavrentiev (KL) and available in the steady aerodynamic case for airfoils in bounded domain. In literature, the KL method was tested adopting a thin Joukowski symmetric profile nevertheless, the importance of this kind of airfoils is merely conceptual since their main limit is the difficult achievement of their cuspidate trailing edge. Hence, to overcome this problem, in our work the wing has been generated using a Karman-Trefftz profile furthermore a rectangular wing has been considered in order to extend the foil results to the finite wing.

The finite-element model of the wing has been further developed adopting the commercial code MSC Nastran. Moreover, as addressed in the thesis, the code MAGIC has been allowed to interface the code MSC Nastran so that to perform the structural wing analysis and evaluate the statically deformed configuration.

Once the structural analysis has been fully accomplished, the optimization section has been performed employing the extended interior quadratic penalty function method implemented in MAGIC. Two kind of objective functions functional relationship has been considered and compared in performing the wing optimization: a *logarithmic* objective function and a *weighted average* one, and four flying condition has been taken into account in performing the optimization.

The results obtained adopting the two different functional relationship in stating the multi-objective functions have shown good agreement as also depicted in Fig 4.8. The figure shows that the final wings obtained adopting the two different multi-objective function formulations are practically overlapped. As addressed in the thesis, even if the results are in good agreement, the use of the logarithmic functional relationship has shown to need less gradient evaluations before to reach the convergence values.

Furthermore, it is interesting to point out how the optimization process considered show the tendency to achieve the best wing performances when the wing-shape becomes as much as possible similar to a lifting-line, *i.e.*, how much the span grows while the chord decreases.

This result is clearly in agreement with the procedure adopted of extending the $2D$ KL lift correction in ground effect to the finite wing considered and with Ref. [54]. Obviously, this tendency in a multidisciplinary optimization contest is forbidden for considerations due to the wing structural strength. Indeed, doubling the weight of the water stored in the tank of the fire-extinguisher aircraft[8] and modifying the upper side constraint of the wing span (till $20m$) and the lower side constraint of the wing chord (down to $2m$) it has been observed what depicted in Fig. 4.9.

Practically, the wing span grows till the value of $19m$ and the wing chord approaches the lower side constraint. However, the shear stress constraints becomes a critical design constraint arresting the further

[8]The logarithmic relationship for the multi-objective function has been adopted in performing this test and the ground clearance considered has been the one of $h = 1$.

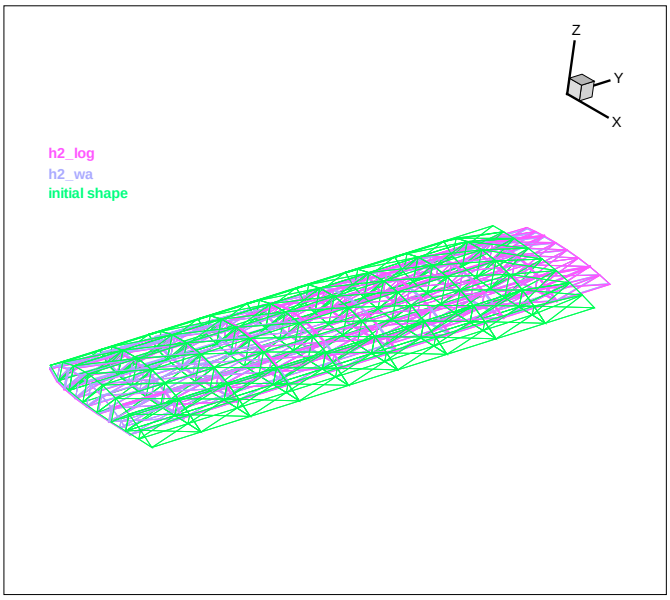


Figure 4.8: Comparison between the starting wing shape and the final one for dimensionless ground clearance $h = 2$. The results obtained for the final wing shape adopting the two different function formulation for stating the objective function show good agreement.

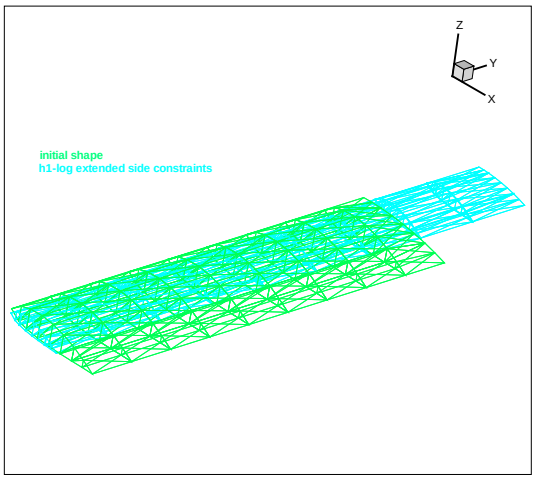


(a) Final wing obtained performing the optimization process with modified side constraints

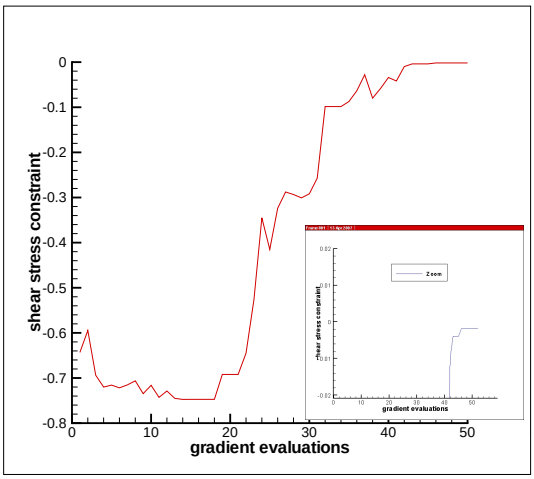


(b) Trend of the shear stress constraint. The violation of the constraints is lightly recovered as shown in the zoomed picture

Figure 4.9: Test of the optimization process with modified side constraints. Case of logarithmic objective function and ground clearance $h = 1$.

growing of the wing span. The penalty function algorithm implemented allows a light recovery of the violated constraints.

Clearly, this last test has only a conceptual value (the doubling of the weight of the stored water is unacceptable in the existing model that has been already considered as fully loaded) in order to better exemplify what previously asserted about the tendency of the wing to the lifting-line condition.

Due to this reason, the final values obtained from this last optimization test have been omitted.

## 4.7 Tables and Results

In the following are presented the tables and the results obtained for the MDO preliminary design of the amphibious aircraft introduced in this chapter.

| **Active variables** | Initial Value | **Values Obtained** Final Value (Log.Obj.Funct.) | Final Value (W.Aver.Obj.Funct.) |
|---|---|---|---|
| Wing span $[m]$ | 14.315 | 15.410 | 15.498 |
| Root chord $[m]$ | 3.54 | 2.83 | 2.80 |
| Tip chord $[m]$ | 3.54 | 2.80 | 2.80 |
| Root panel thickness $t_{skin}$ $[m]$ | 0.002 | 0.001 | 0.001 |
| Tip panel thickness $t_{skin}$ $[m]$ | 0.0010 | 0.0014 | 0.0008 |
| Root spar thickness $t_{web}$ $[m]$ | 0.015 | 0.015 | 0.012 |
| Tip spar thickness $t_{web}$ $[m]$ | 0.005 | 0.008 | 0.007 |
| Root built-in-angle $\alpha_{root}$ | 6.0 | 4.94 | 7.49 |
| Tip built-in-angle$\alpha_{tip}$ | 6.0 | 3.05 | 2.37 |
| **Performances** | | | |
| Take off weight $[Kg]$ | 21583.630 | 20984.082 | 20589.858 |
| Empty weight $[Kg]$ | 10934.630 | 10695.57 | 10440.813 |
| Useful Fuel Weight $[Kg]$ | 4649.0 | 4288.512 | 4149.045 |
| Structural Wing Weight $[Kg]$ | 3027.774 | 2866.524 | 2672.181 |
| Lift coefficient | 0.746 | 0.627 | 0.721 |
| Induced Drag coefficient | 0.021 | 0.011 | 0.014 |
| Total Drag coefficient | 0.051 | 0.035 | 0.039 |
| Efficiency | 14.51 | 17.85 | 18.13 |
| **Objective Function (Logarithmic)** | 0.763 | 0.726 | |
| **Objective Function (Weighted Average)** | -0.059 | | -0.199 |
| **Constraints** | | | |
| Fuel Volume | -0.869 | -0.822 | -0.827 |
| Direct Stress | -0.900 | -0.910 | -0.892 |
| Shear Stress | -0.643 | -0.592 | -0.486 |
| Right Lift-Weight | -0.457 | -0.261 | -0.370 |
| Buckling Constraint | -3.933 | -1.639 | -1.126 |

Table 4.4: Multidisciplinary design optimization process in *out of ground effect* flight condition.

| **Active variables** | Initial Value | **Values Obtained** Final Value (Log.Obj.Funct.) | Final Value (W.Average Obj.Funct.) |
|---|---|---|---|
| Wing span $[m]$ | 14.315 | 15.499 | 15.499 |
| Root chord $[m]$ | 3.54 | 2.80 | 2.80 |
| Tip chord $[m]$ | 3.54 | 2.80 | 2.80 |
| Root panel thickness $t_{skin}$ $[m]$ | 0.002 | 0.001 | 0.001 |
| Tip panel thickness $t_{skin}$ $[m]$ | 0.001 | 0.0008 | 0.0009 |
| Root spar thickness $t_{web}$ $[m]$ | 0.015 | 0.012 | 0.012 |
| Tip spar thickness $t_{web}$ $[m]$ | 0.005 | 0.007 | 0.007 |
| Root built-in-angle $\alpha_{root}$ | 6.0 | 6.65 | 6.78 |
| Tip built-in-angle$\alpha_{tip}$ | 6.0 | 2.02 | 2.43 |
| **Performances** | | | |
| Take off weight $[Kg]$ | 21583.630 | 19906.146 | 19930.567 |
| Empty weight $[Kg]$ | 10934.630 | 10378.709 | 10399.509 |
| Useful Fuel Weight $[Kg]$ | 4649.0 | 3527.437 | 3531.058 |
| Structural Wing Weight $[Kg]$ | 3027.774 | 2691.918 | 2712.718 |
| Lift coefficient | 0.932 | 0.833 | 0.861 |
| Induced Drag coefficient | 0.021 | 0.012 | 0.013 |
| Total Drag coefficient | 0.064 | 0.039 | 0.041 |
| Efficiency | 14.60 | 20.94 | 20.94 |
| **Objective Function (Logarithmic)** | 0.762 | 0.689 | |
| **Objective Function (Weighted Average)** | -0.062 | | -0.294 |
| **Constraints** | | | |
| Fuel Volume | -0.869 | -0.853 | -0.853 |
| Direct Stress | -0.900 | -0.899 | -0.892 |
| Shear Stress | -0.643 | -0.521 | -0.489 |
| Right Lift-Weight | -0.565 | -0.470 | -0.487 |
| Buckling Constraint | -3.933 | -1.159 | -1.221 |

Table 4.5: Multidisciplinary design optimization process *in ground effect* flight condition for dimensionless clearance $\mathbf{h = 1}$.

| **Active variables** | Initial Value | **Values Obtained** Final Value (Log.Obj.Funct.) | Final Value (W.Average Obj.Funct.) |
|---|---|---|---|
| Wing span $[m]$ | 14.315 | 15.489 | 15.499 |
| Root chord $[m]$ | 3.54 | 2.80 | 2.80 |
| Tip chord $[m]$ | 3.54 | 2.84 | 2.81 |
| Root panel thickness $t_{skin}$ $[m]$ | 0.002 | 0.001 | 0.001 |
| Tip panel thickness $t_{skin}$ $[m]$ | 0.001 | 0.0012 | 0.0011 |
| Root spar thickness $t_{web}$ $[m]$ | 0.015 | 0.012 | 0.012 |
| Tip spar thickness $t_{web}$ $[m]$ | 0.005 | 0.008 | 0.007 |
| Root built-in-angle $\alpha_{root}$ | 6.0 | 6.25 | 6.74 |
| Tip built-in-angle$\alpha_{tip}$ | 6.0 | 2.84 | 2.35 |
| **Performances** | | | |
| Take off weight $[Kg]$ | 21583.630 | 20570.804 | 20496.887 |
| Empty weight $[Kg]$ | 10934.630 | 10566.223 | 10516.152 |
| Useful Fuel Weight $[Kg]$ | 4649.0 | 4004.581 | 3980.735 |
| Structural Wing Weight $[Kg]$ | 3027.774 | 2799.826 | 2758.358 |
| Lift coefficient | 0.7929 | 0.7223 | 0.7266 |
| Induced Drag coefficient | 0.0214 | 0.0128 | 0.0128 |
| Total Drag coefficient | 0.054 | 0.038 | 0.038 |
| Efficiency | 14.54 | 18.85 | 18.90 |
| **Objective Function (Logarithmic)** | 0.763 | 0.713 | |
| **Objective Function (Weighted Average)** | -0.060 | | -0.222 |
| **Constraints** | | | |
| Fuel Volume | -0.869 | -0.836 | -0.835 |
| Direct Stress | -0.900 | -0.887 | -0.892 |
| Shear Stress | -0.643 | -0.474 | -0.500 |
| Right Lift-Weight | -0.489 | -0.375 | -0.378 |
| Buckling Constraint | -3.933 | -1.386 | -1.335 |

Table 4.6: Multidisciplinary design optimization process *in ground effect* flight condition for dimensionless clearance $\mathbf{h = 2}$.

| **Active variables** | Initial Value | **Values Obtained** Final Value (Log.Obj.Funct.) | Final Value (W.Average Obj.Funct.) |
|---|---|---|---|
| Wing span $[m]$ | 14.315 | 15.460 | 15.499 |
| Root chord $[m]$ | 3.54 | 2.82 | 2.81 |
| Tip chord $[m]$ | 3.54 | 2.81 | 2.80 |
| Root panel thickness $t_{skin}$ $[m]$ | 0.002 | 0.001 | 0.001 |
| Tip panel thickness $t_{skin}$ $[m]$ | 0.001 | 0.0013 | 0.0013 |
| Root spar thickness $t_{web}$ $[m]$ | 0.015 | 0.012 | 0.012 |
| Tip spar thickness $t_{web}$ $[m]$ | 0.005 | 0.008 | 0.008 |
| Root built-in-angle $\alpha_{root}$ | 6.0 | 5.47 | 7.26 |
| Tip built-in-angle$\alpha_{tip}$ | 6.0 | 2.87 | 2.28 |
| **Performances** | | | |
| Take off weight $[Kg]$ | 21583.630 | 20848.557 | 20760.280 |
| Empty weight $[Kg]$ | 10934.630 | 10614.021 | 10579.101 |
| Useful Fuel Weight $[Kg]$ | 4649.0 | 4234.535 | 4181.179 |
| Structural Wing Weight $[Kg]$ | 3027.774 | 2802.513 | 2790.654 |
| Lift coefficient | 0.7481 | 0.6466 | 0.7079 |
| Induced Drag coefficient | 0.0214 | 0.0116 | 0.0137 |
| Total Drag coefficient | 0.051 | 0.036 | 0.039 |
| Efficiency | 14.51 | 17.97 | 18.14 |
| **Objective Function (Logarithmic)** | 0.763 | 0.722 | |
| **Objective Function (Weighted Average)** | -0.059 | | -0.194 |
| **Constraints** | | | |
| Fuel Volume | -0.869 | -0.825 | -0.827 |
| Direct Stress | -0.900 | -0.897 | -0.893 |
| Shear Stress | -0.643 | -0.522 | -0.497 |
| Right Lift-Weight | -0.458 | -0.290 | -0.354 |
| Buckling Constraint | -3.933 | -1.465 | -1.418 |

Table 4.7: Multidisciplinary design optimization process *in ground effect* flight condition for dimensionless clearance $\mathbf{h = 10}$.

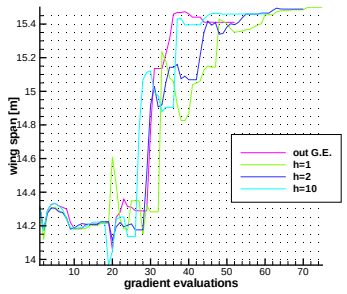


(a) Wing span: trends of the optimization processes

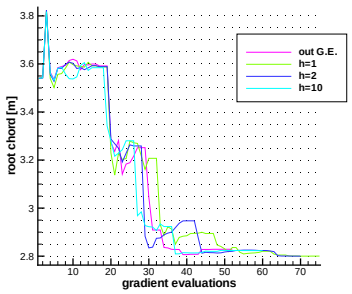


(b) Root chord: trends of the optimization processes

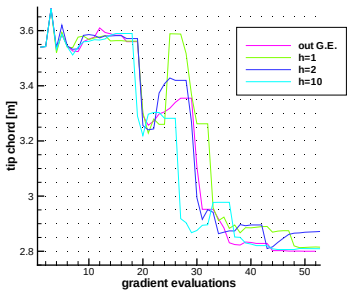


(c) Tip chord: trends of the optimization processes

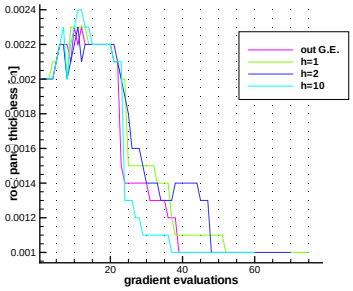


(d) Root panel thickness: trends of the optimization processes

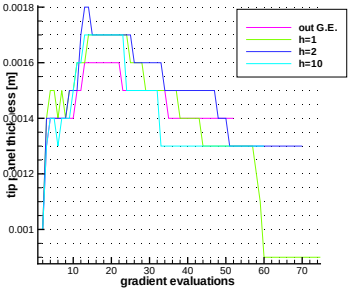


(e) Tip panel thickness: trends of the optimization processes

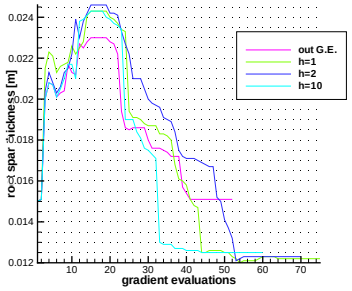


(f) Root spar thickness: trends of the optimization processes

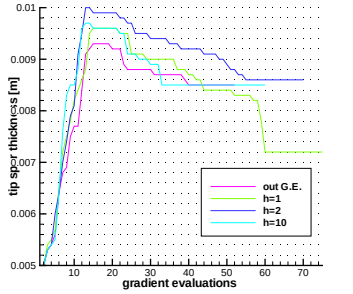


(g) Tip spar thickness: trends of the optimization processes

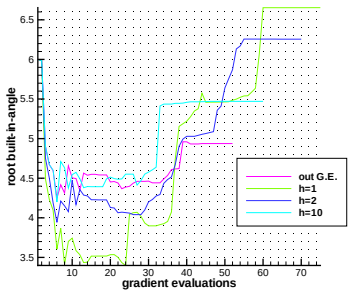


(h) Root built-in-angle: trends of the optimization processes

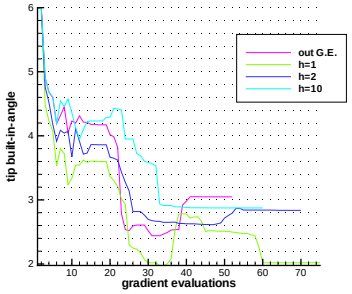


(i) Tip built-in-angle: trends of the optimization processes

Figure 4.10: Design Variables: comparison between the trends of the optimization processes performed out of ground effect and in ground effect flight conditions for dimensionless clearances $\mathbf{h} = \mathbf{1}, \mathbf{2}, \mathbf{10}$ (case of logarithmic objective function).

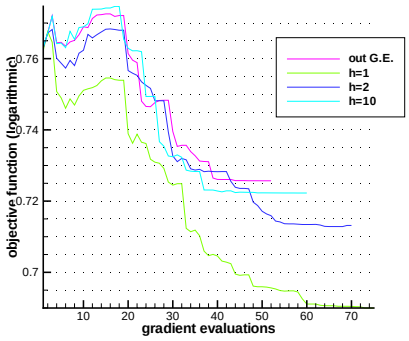


(a) Logarithmic objective function: trends of the optimization processes

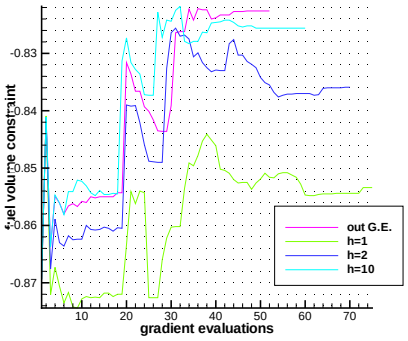


(b) Fuel volume constraint: trends of the optimization processes

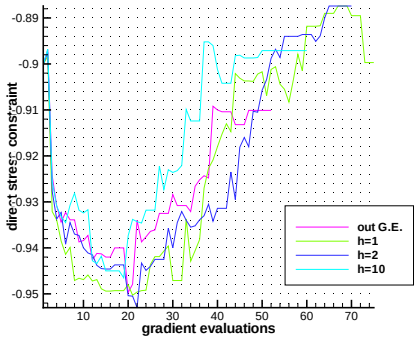


(c) Direct stress constraint: trends of the optimization processes

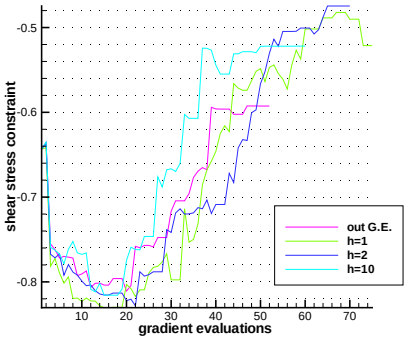


(d) Shear stress constraint: trends of the optimization processes

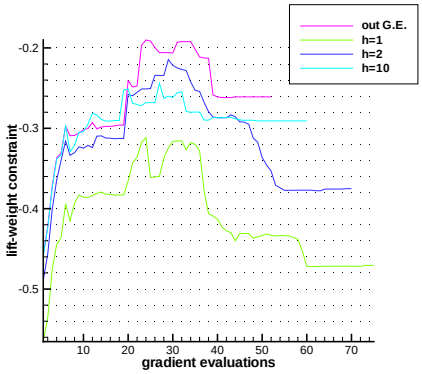


(e) Lift-weight constraint: trends of the optimization processes

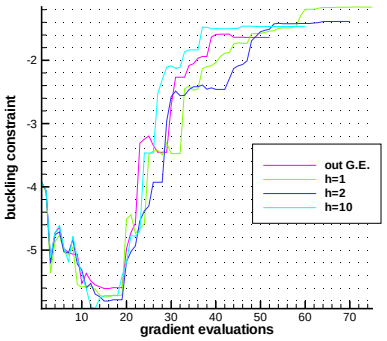


(f) Buckling constraint: trends of the optimization processes

Figure 4.11: Objective function and constraints: comparison between the trends of the optimization processes performed out of ground effect and and in ground effect flight conditions for dimensionless clearances $\mathbf{h} = \mathbf{1}, \mathbf{2}, \mathbf{10}$ (case of logarithmic objective function).

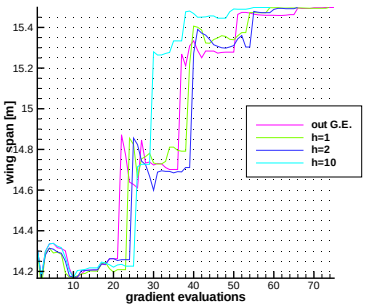


(a) Wing span: trends of the optimization processes

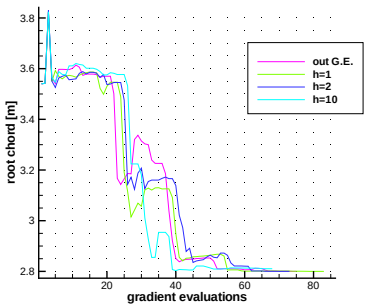


(b) Root chord: trends of the optimization processes

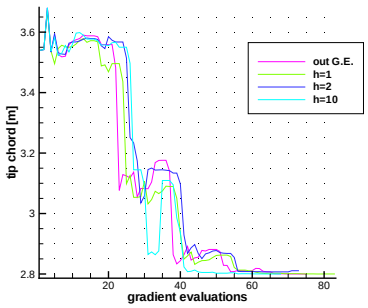


(c) Tip chord: trends of the optimization processes

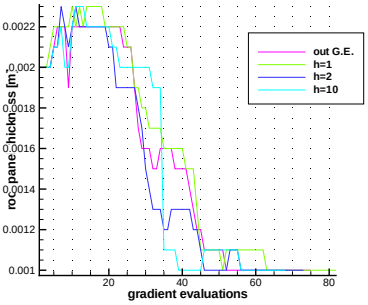


(d) Root panel thickness: trends of the optimization processes

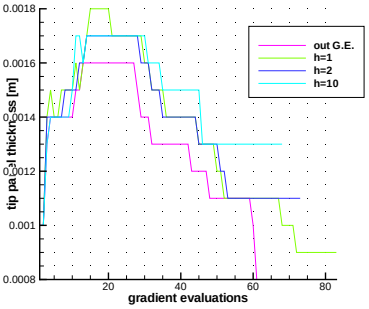


(e) Tip panel thickness: trends of the optimization processes

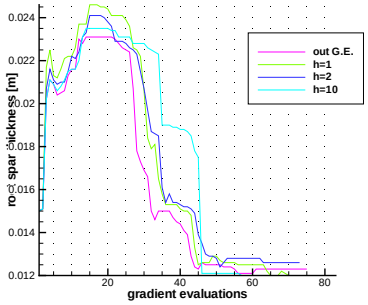


(f) Root spar thickness: trends of the optimization processes

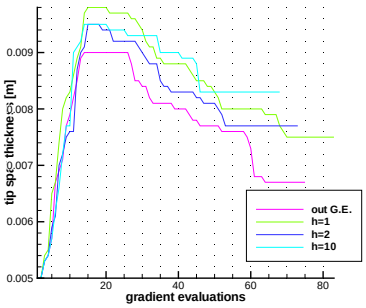


(g) Tip spar thickness: trends of the optimization processes

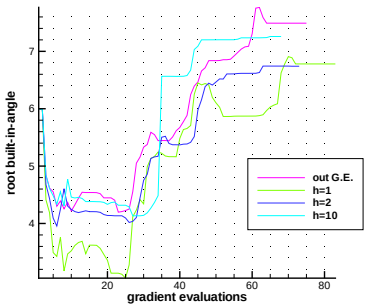


(h) Root built-in-angle: trends of the optimization processes

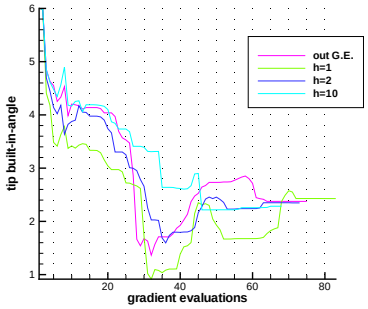


(i) Tip built-in-angle: trends of the optimization processes

Figure 4.12: Design Variables: comparison between the trends of the optimization processes performed out of ground effect and in ground effect flight conditions for dimensionless clearances $\mathbf{h} = \mathbf{1}, \mathbf{2}, \mathbf{10}$ (case of weighted average objective function).

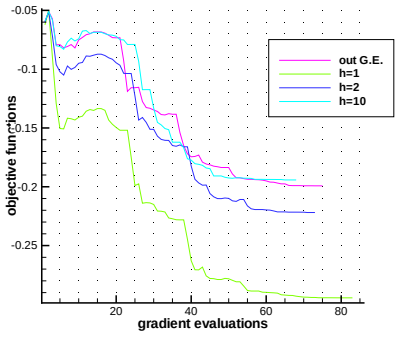


(a) Weighted average objective function: trends of the optimization processes

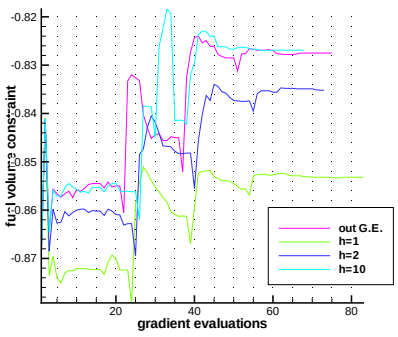


(b) Fuel volume constraint: trends of the optimization processes

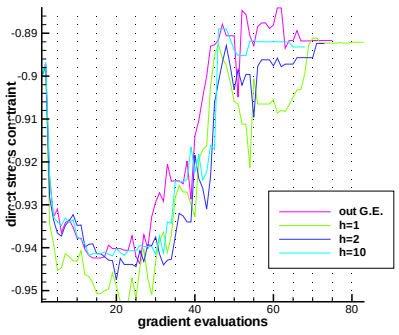


(c) Direct stress constraint: trends of the optimization processes

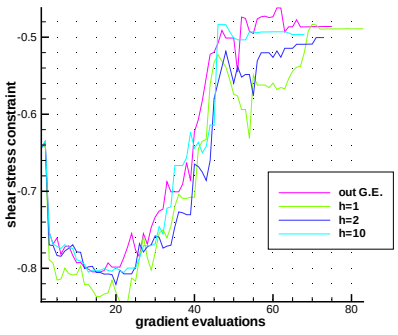


(d) Shear stress constraint: trends of the optimization processes

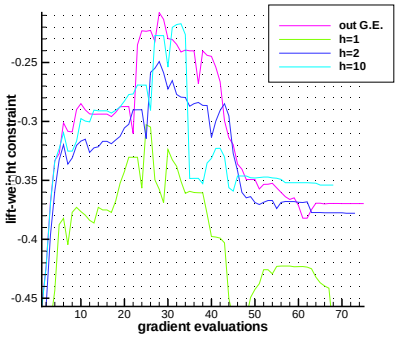


(e) Lift-weight constraint: trends of the optimization processes

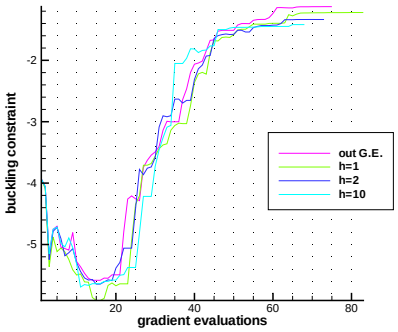


(f) Buckling constraint: trends of the optimization processes

Figure 4.13: Objective function and constraints: comparison between the trends of the optimization processes performed out of ground effect and and in ground effect flight conditions for dimensionless clearances $\mathbf{h} = \mathbf{1}, \mathbf{2}, \mathbf{10}$ (case of weighted average objective function).

**Out of ground effect flight condition**

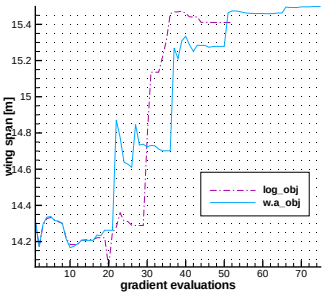


(a) Wing span: trends of the optimization processes

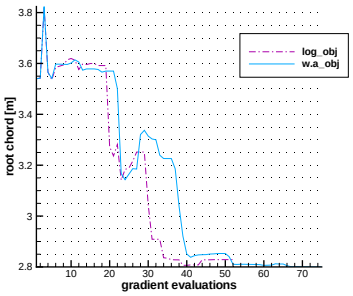


(b) Root chord: trends of the optimization processes

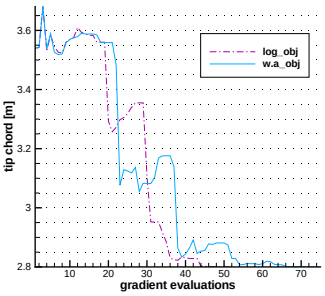


(c) Tip chord: trends of the optimization processes

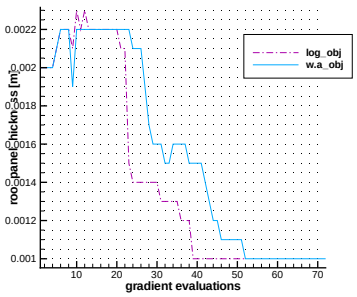


(d) Root panel thickness: trends of the optimization processes

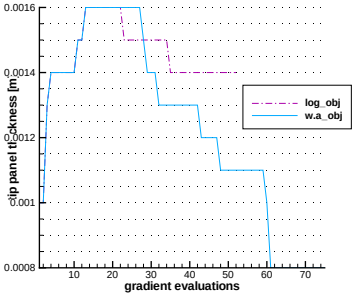


(e) Tip panel thickness: trends of the optimization processes

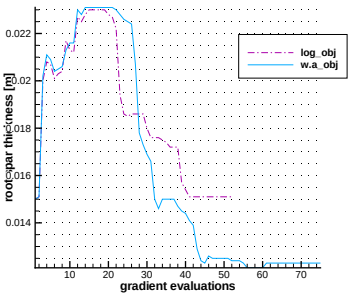


(f) Root spar thickness: trends of the optimization processes

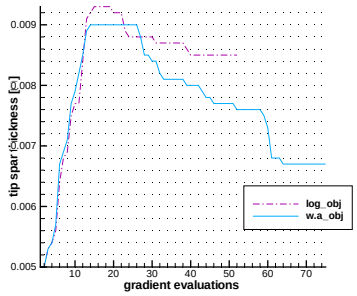


(g) Tip spar thickness: trends of the optimization processes

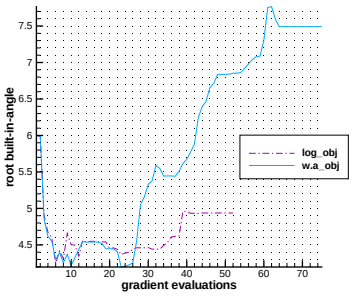


(h) Root built-in-angle: trends of the optimization processes

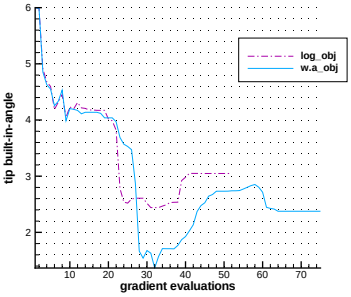


(i) Tip built-in-angle: trends of the optimization processes

Figure 4.14: Design Variables: comparison between the trends of the multidisciplinary optimization processes performed in the *out of ground effect* flight condition adopting a logarithmic objective function and a weighted average objective function.

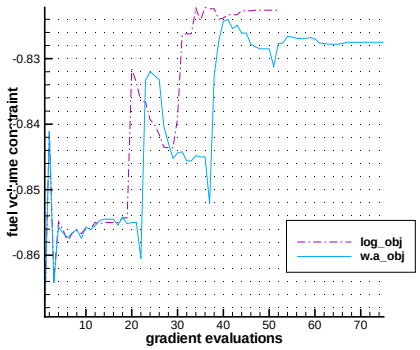


(a) Fuel volume constraint: trends of the optimization processes

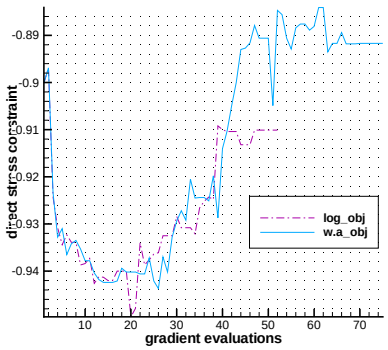


(b) Direct stress constraint: trends of the optimization processes

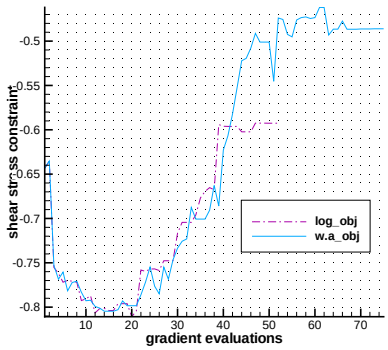


(c) Shear stress constraint: trends of the optimization processes

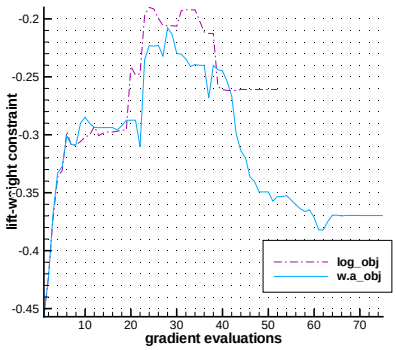


(d) Lift-weight constraint: trends of the optimization processes

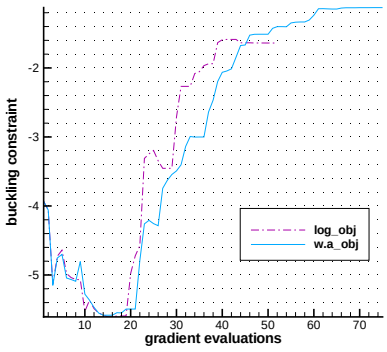


(e) Buckling constraint: trends of the optimization processes

Figure 4.15: Constraints: comparison between the trends of the multidisciplinary optimization processes performed the *out of ground effect* flight condition adopting a logarithmic objective function and a weighted average objective function.

**Case of ground-clearance $h = 1$**

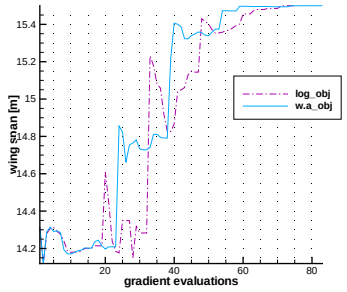


(a) Wing span: trends of the optimization processes

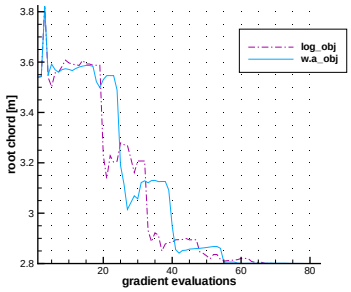


(b) Root chord: trends of the optimization processes

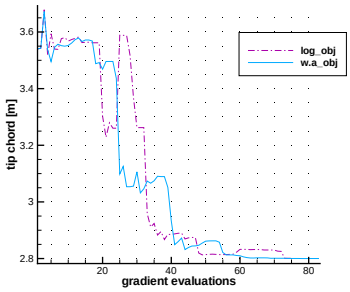


(c) Tip chord: trends of the optimization processes

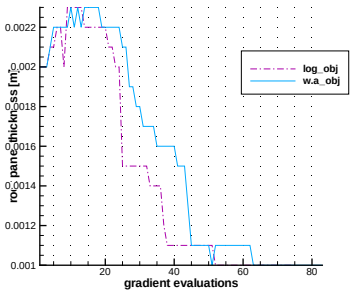


(d) Root panel thickness: trends of the optimization processes

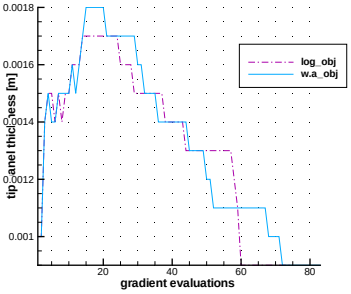


(e) Tip panel thickness: trends of the optimization processes

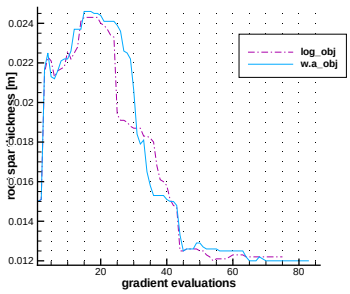


(f) Root spar thickness: trends of the optimization processes

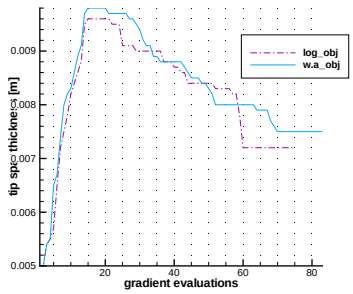


(g) Tip spar thickness: trends of the optimization processes

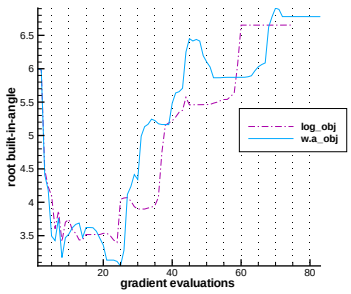


(h) Root built-in-angle: trends of the optimization processes

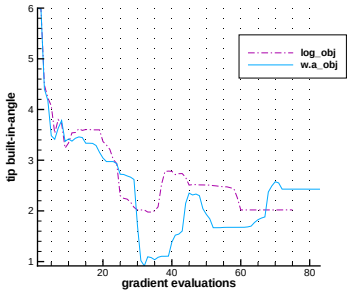


(i) Tip built-in-angle: trends of the optimization processes

Figure 4.16: Design Variables: comparison between the trends of the optimization processes performed adopting a logarithmic objective function and a weighted average objective function in ground effect flight condition. Dimensionless ground clearance $\mathbf{h = 1}$.

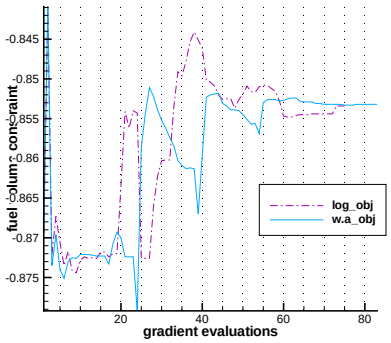


(a) Fuel volume constraint: trends of the optimization processes

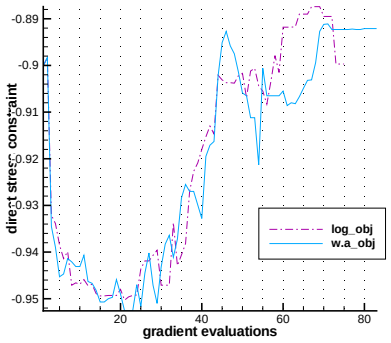


(b) Direct stress constraint: trends of the optimization processes

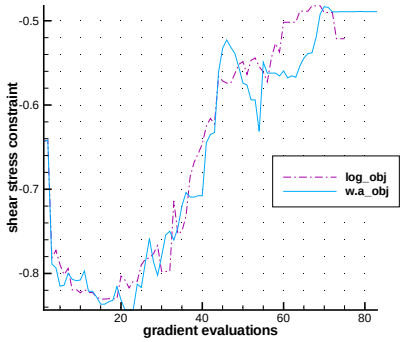


(c) Shear stress constraint: trends of the optimization processes

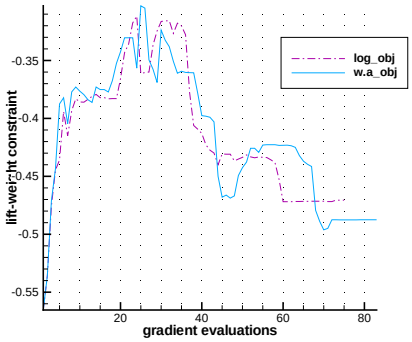


(d) Lift-weight constraint: trends of the optimization processes

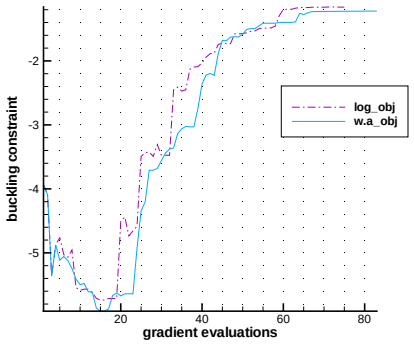


(e) Buckling constraint: trends of the optimization processes

Figure 4.17: Constraints: comparison between the trends of the optimization processes performed adopting a logarithmic objective function and a weighted average objective function in ground effect flight condition. Dimensionless ground clearance $\mathbf{h} = \mathbf{1}$.

**Case of ground-clearance $h = 2$**

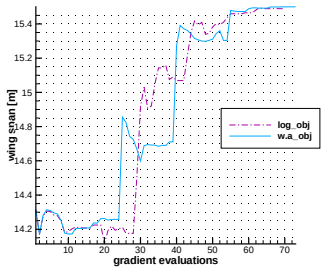


(a) Wing span: trends of the optimization processes

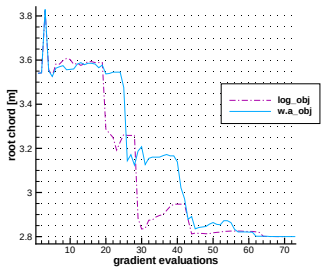


(b) Root chord: trends of the optimization processes

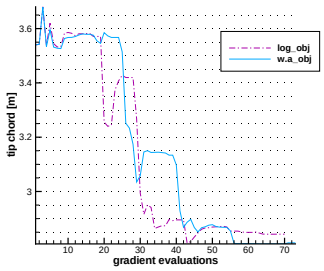


(c) Tip chord: trends of the optimization processes

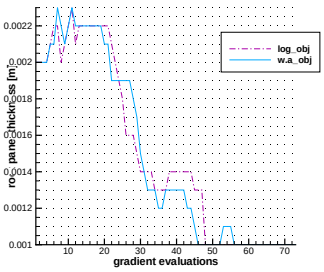


(d) Root panel thickness: trends of the optimization processes

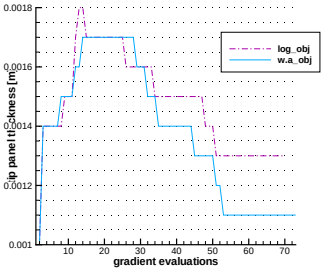


(e) Tip panel thickness: trends of the optimization processes

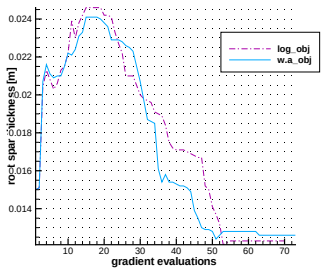


(f) Root spar thickness: trends of the optimization processes

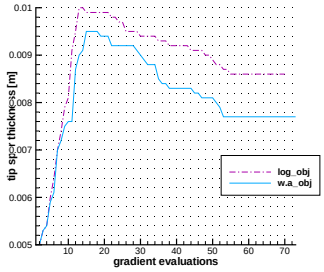


(g) Tip spar thickness: trends of the optimization processes

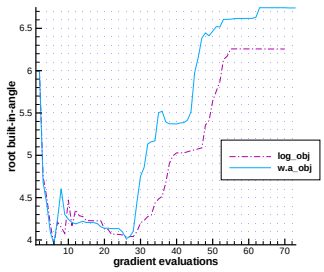


(h) Root built-in-angle: trends of the optimization processes

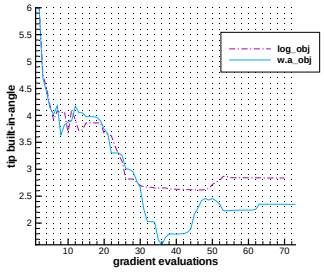


(i) Tip built-in-angle: trends of the optimization processes

Figure 4.18: Design Variables: comparison between the trends of the optimization processes performed adopting a logarithmic objective function and a weighted average objective function in ground effect flight condition. Dimensionless ground clearance $\mathbf{h = 2}$.

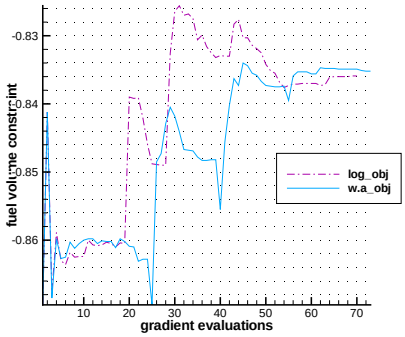


(a) Fuel volume constraint: trends of the optimization processes

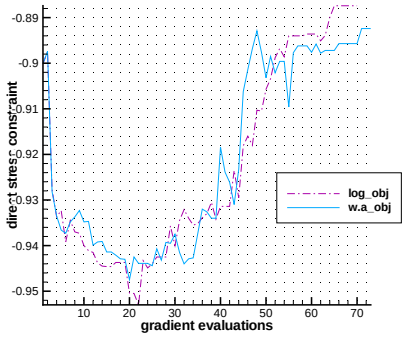


(b) Direct stress constraint: trends of the optimization processes

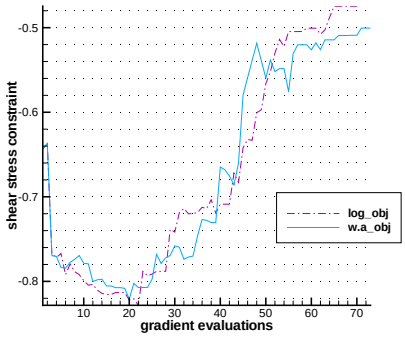


(c) Shear stress constraint: trends of the optimization processes

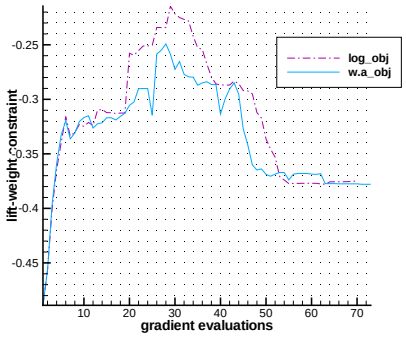


(d) Lift-weight constraint: trends of the optimization processes

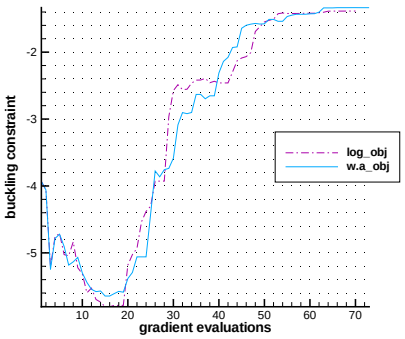


(e) Buckling constraint: trends of the optimization processes

Figure 4.19: Constraints: comparison between the trends of the optimization processes performed adopting a logarithmic objective function and a weighted average objective function in ground effect flight conditions. Dimensionless ground clearance $\mathbf{h = 2}$.

**Case of ground-clearance $h = 10$**

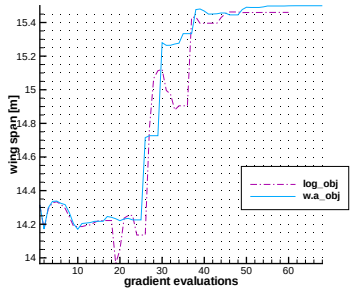


(a) Wing span: trends of the optimization processes

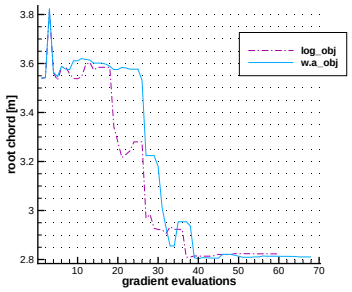


(b) Root chord: trends of the optimization processes

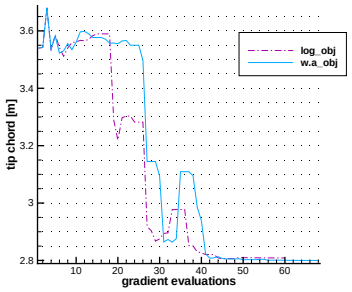


(c) Tip chord: trends of the optimization processes

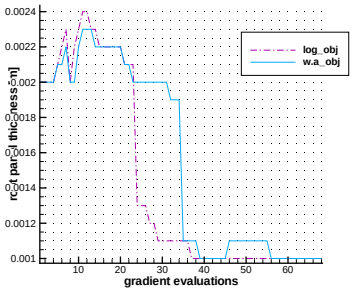


(d) Root panel thickness: trends of the optimization processes

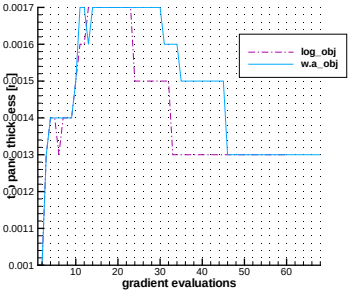


(e) Tip panel thickness: trends of the optimization processes

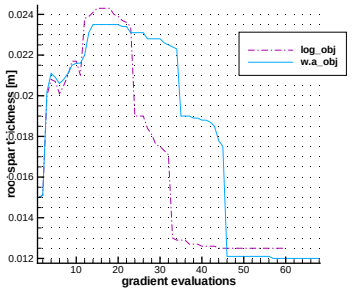


(f) Root spar thickness: trends of the optimization processes

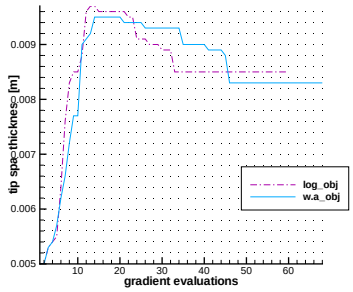


(g) Tip spar thickness: trends of the optimization processes

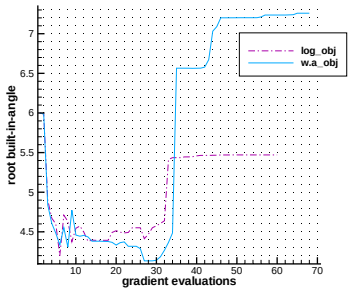


(h) Root built-in-angle: trends of the optimization processes

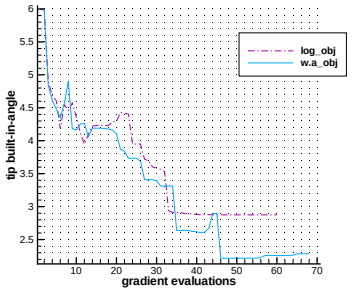


(i) Tip built-in-angle: trends of the optimization processes

Figure 4.20: Design Variables: comparison between the trends of the optimization processes performed adopting a logarithmic objective function and a weighted average objective function in ground effect flight condition. Dimensionless ground clearance $\mathbf{h = 10}$.

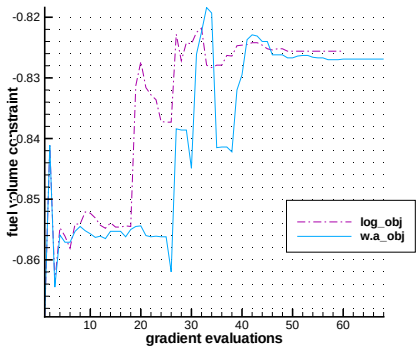


(a) Fuel volume constraint: trends of the optimization processes

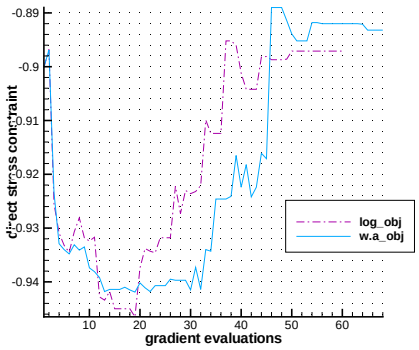


(b) Direct stress constraint: trends of the optimization processes

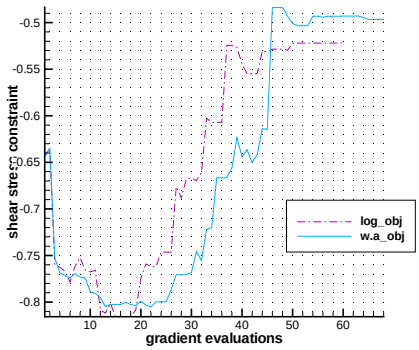


(c) Shear stress constraint: trends of the optimization processes

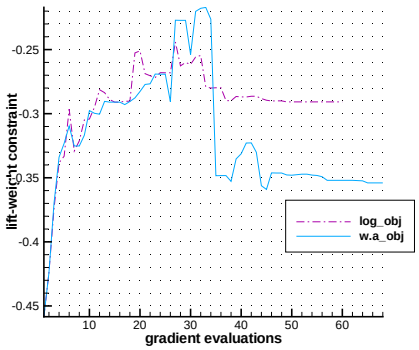


(d) Lift-weight constraint: trends of the optimization processes

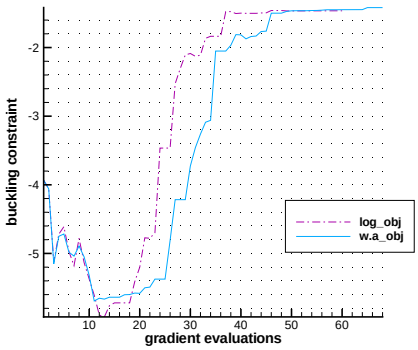


(e) Buckling constraint: trends of the optimization processes

Figure 4.21: Constraints: comparison between the trends of the optimization processes performed adopting a logarithmic objective function and a weighted average objective function. Ground clearance $\mathbf{h = 10}$.

# Concluding remarks

In the thesis the aeroelastic modeling and the MDO analysis of aircraft wings have been considered and explored. The analysis has been performed following a general theoretical approach and finally considering, for the applicative part, a civil large airplane wing for passengers transportation as well as a fire extinguisher aircraft operating in ground effect.

Concerning the aeroelastic modeling, the most significative and innovative theoretical contribution referred in the present work consists in the development of an aerodynamic model of a perturbative kind for the evaluation of the lift coefficient in unsteady case for airfoils operating in ground effect. Such innovative model rely on the theory presented in literature by Theodorsen and valid for unsteady flows in unbounded fluid domains matched with the Keldysh-Lavrentiev approach valid for steady flows in bounded fluid domains.

The main step of the proposed methodology has been the adoption of a series expansion, performed respect to the ground clearance and suggested by the Keldysh-Lavrentiev approach, of the kernel functions obtained by the use of the image method and that appear in the Theodorsen integral equations for the vorticity problem. The difficulties related to the insertion of the Theodorsen theory in bounded domain adopting the Keldysh-Lavrentiev approach have been widely investigated as well as the limits and the applicability of the proposed methodology. An extension in ground effect of the Wagner problem has been considered as well in order to validate the obtained results.

Future developments concerning the aeroelastic modeling presented in the thesis could concern the experimental validation of the proposed theory and its comparison with numerical codes. Another future development could concern the use of a different functional base for the series expansion in order to better account the wake presence in ground effect. Furthermore, considering high angles of attack in ground effect it determines an asymmetric behavior of the airfoil for positive or negative changes in the incidence. Thus, this situation could cause a lost of linearity of the problem involving further hypothesis and assumption in the proposed methodology.

Concerning the MDO analysis, a section on the current state-of-the-art and a detailed overview of the most adopted MDO algorithmic formulations has been presented. Furthermore, the potentiality and the structure of the MDO code MAGIC have been widely discussed and the relevance of the code in the worldwide algorithmic formulation scenario has been validated.

The code has been tested first considering a wing-box structure and then operating on a complete wing structure. Simple tests on the wing-box structure have allowed some considerations on the relevance of the addition of the buckling analysis module in a structural optimization process. Hence, a first indispensable improvement of the code MAGIC has been the insertion of a buckling module analysis for the optimization of a wing of a complete aircraft. Thus, the number of disciplines included in the code has been increased and the new implemented modules have been made interface the commercial code MSC NASTRAN for the finite element analysis. Moreover, the code and the new implemented modules have been made interface with the commercial optimization code SNOPT 6.0. Thus, a comparison between the optimization performed adopting the penalty function method implemented in MAGIC and the same optimization process performed with the commercial optimizer SNOPT 6.0 has been achieved. Hence, the current version of the code has shown improved features.

Furthermore, in order to take into account the theory presented in the aeroelastic modeling section, the possibility of accounting the ground effect flying condition in the aerodynamic module of the code has been validated and a complete different aircraft model has been implemented in the code. As sectional shape of the wing under study, a Karman-Trefftz profile has been considered. Several tests of the optimization process in the ground effect case have been performed. Different functional relationships for the multi-objective function have been considered such as a logarithmic and a weighted average one. The results obtained adopting the mentioned different functional relationships have been compared and discussed.

Several developments could be suggested as the implementation of different algorithmic formulation in order to allow the designer to choose the best formulation for a given problem. New modules, that is further disciplinary analysis, can be added at any time in the code.

# Appendix A

# Remarks on the case symmetric to ground effect: notes on a submerged foil

## A.1 Adimensionalization of the free surface boundary condition

In the third chapter the free surface boundary condition has been written as (see Eq. 3.13)

$$\frac{\partial \phi}{\partial y} + \left(\frac{U^2}{g}\right)\frac{\partial^2 \phi}{\partial x^2} = 0 \qquad y = 0 \tag{A.1}$$

$$\frac{\partial \phi}{\partial y} = U\left(\frac{dy}{dx} + \alpha\right) \qquad y = -h, |x| \leqslant b \tag{A.2}$$

the adimensionalization has to be performed considering as a reference length the half-chord $b$. The adimensional terms are denoted by $\hat{}$, thus for the adimensionalization of the coordinates can be written $\hat{y} = \frac{y}{b}$, $\hat{x} = \frac{x}{b}$. The adimensionalization of the potential is achieved setting $\hat{\varphi} = \frac{\varphi}{U}$, hence, the Laplace equation Laplace can be written as

$$\frac{\partial^2 \hat{\phi}}{\partial \hat{x}^2} + \frac{\partial^2 \hat{\phi}}{\partial \hat{y}^2} = 0 \tag{A.3}$$

The free surface boundary conditions in the adimensional representation are

$$\frac{\partial \hat{\phi}}{\partial \hat{y}} + \left(\frac{U^2}{gb}\right)\frac{\partial^2 \hat{\phi}}{\partial \hat{x^2}} = 0 \qquad \hat{y} = 0 \tag{A.4}$$

## A.2 The Keldysh-Lavrentiev methodology for submerged hydrofoils

The two-dimensional potential flow of an uniform stream $U$ past a thin submerged hydrofoil of given chord $c = 2b$ aligned with the flow and at a clearance $h \cdot b$ under a free surface of an heavy fluid is considered. The problem will be considered referring to adimensional values, thus, all the length will be considered normalized respect to the half-chord $b$ while for the velocities the reference value will be $U$. The reference frame adopted has its origin placed in the half value of the chord, the $x$ axis is aligned with the stream flow and the $y$ axis is as in Fig. A.1

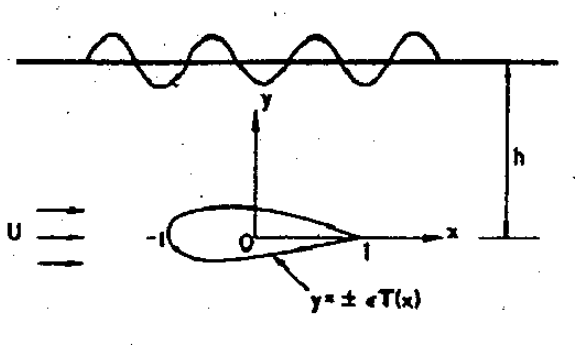


Figure A.1: *Reference frame.*

The hydrofoil is described by the equation

$$y = \pm \varepsilon T(x) \tag{A.5}$$

where $\varepsilon$ is a parameter indicating the thin thickness of the foil.

The complex potential representative of the problem and normalized respect to $U \cdot b$ can be considered in its expanded form as

$$\Phi(z, \varepsilon) = z + \varepsilon \Phi_1(z) + \mathcal{O}(\varepsilon^2) \tag{A.6}$$

with $z = x + iy$ coordinate of a point on the complex plane. Only the terms if the kind $\mathcal{O}(\varepsilon)$ will be considered. Nevertheless, the accuracy of the theory increases as much $\varepsilon \to 0$ that is as much the the foil can be considered thin.

According to the Keldysh-Lavrentiev methodology the solution of the Laplace equation can be stated considering a sources and vortexes distribution along the chord of intensity given respectively by (nor-

malized respect to $U$) $\sigma(x)$ and $\gamma(x)$. The perturbation on the potential is then

$$\begin{aligned}\Phi_1(z)=&\int_{-1}^{1}\sigma(\xi)\left\{\log(z-\xi)+\log(z-\xi-2ih)+2I[iF^{-2}(z-\xi-2ih)]\right\}\frac{d\xi}{2\pi}+\\&+i\int_{-1}^{1}\gamma(\xi)\left\{\log(z-\xi)-\log(z-\xi-2ih)-2I[iF^{-2}(z-\xi-2ih)]\right\}\frac{d\xi}{2\pi}\end{aligned}\tag{A.7}$$

where[1] $I(r)=e^{-r}\int_{-r}^{\infty}e^{-w}\frac{dw}{w}$.

Analogously, for the complex velocity $W(z)=\Phi'(z)$ the expansion in terms of the parameter $\varepsilon$ yields

$$W(z,\varepsilon)=1+\varepsilon W_1(z)+\mathcal{O}(\varepsilon^2)\tag{A.8}$$

and considering the previously mentioned expression of e $\Phi_1(z)$ one has

$$\begin{aligned}W_1(z)=&\int_{-1}^{1}\sigma(\xi)\left\{\frac{1}{z-\xi}-\frac{1}{z-\xi-2ih}-2iF^{-2}I[iF^{-2}(z-\xi-2ih)]\right\}\frac{d\xi}{2\pi}+\\&+i\int_{-1}^{1}\gamma(\xi)\left\{\frac{1}{z-\xi}+\frac{1}{z-\xi-2ih}+2iF^{-2}I[iF^{-2}(z-\xi-2ih)]\right\}\frac{d\xi}{2\pi}\end{aligned}\tag{A.9}$$

Applying on the chord the tangency condition valid on the body, that is considering the tangency condition in $z=x\pm 0i$ with $-1\leqslant x\leqslant 1$ the following is achieved

$$\begin{aligned}W_1(x\pm 0i)=&\int_{-1}^{1}\sigma(\xi)\left\{\frac{1}{x-\xi}-\frac{x-\xi}{(x-\xi)^2+4h^2}+2F^{-2}I[iF^{-2}(x-\xi-2ih)]\right\}\frac{d\xi}{2\pi}\pm\\&\pm\frac{\gamma(x)}{2}+\int_{-1}^{1}\gamma(\xi)\left\{\frac{-2h}{(x-\xi)^2+4h^2}-2F^{-2}Re\left[I[iF^{-2}(x-\xi-2ih)]\right]\right\}\frac{d\xi}{2\pi}\mp\\&+i\frac{\sigma(x)}{2}+i\int_{-1}^{1}\sigma(\xi)\left\{\frac{-2h}{(x-\xi)^2+4h^2}-2F^{-2}Re\left[I[iF^{-2}(x-\xi-2ih)]\right]\right\}\frac{d\xi}{2\pi}+\\&+i\int_{-1}^{1}\gamma(\xi)\left\{\frac{1}{x-\xi}+\frac{x-\xi}{(x-\xi)^2+4h^2}-2F^{-2}Im\left[I[iF^{-2}(x-\xi-2ih)]\right]\right\}\frac{d\xi}{2\pi}\end{aligned}\tag{A.10}$$

where the terms $\Re,\Im$ represent the real and imaginary part respectively.

The boundary condition that has to be imposed is then

$$IW_1(x\pm 0i)=\mp T'(x)\tag{A.11}$$

and following what suggested by Keldysh and Lavrentiev it can be set

$$\sigma(x)=2T'(x)\tag{A.12}$$

[1] With $r,w$ dummy variables.

The Eq. A.11 allows to determine $\gamma(x)$ and t can be written as

$$\int_{-1}^{1} 2T'(x)H(x-\xi)d\xi + \int_{-1}^{1} \gamma(\xi)K(x-\xi)d\xi = 0 \tag{A.13}$$

where

$$\begin{aligned} H(x) &= \frac{-2h}{x^2+4h^2} - 2F^{-2}Re\left[I[iF^{-2}(x-2ih)]\right] \\ K(x) &= \frac{1}{x} + \frac{x}{x^2+4h^2} - 2F^{-2}Im\left[I[iF^{-2}(x-2ih)]\right] \end{aligned} \tag{A.14}$$

Keldysh and Lavrentiev suggested the following series expansion respect to the adimensional parameter $h^{-1}$

$$\begin{aligned} H(x) &= \frac{1}{h}\sum_{0}^{\infty} H_n(hF^{-2})\left(\frac{x}{h}\right)^n \\ K(x) &= \frac{1}{x} + \frac{1}{h}\sum_{0}^{\infty} K_n(hF^{-2})\left(\frac{x}{h}\right)^n \\ \gamma(x) &= \sum_{0}^{\infty} h^{-n}\gamma_n(x) \end{aligned} \tag{A.15}$$

Substituting such expressions in Eq. A.13 and collecting the terms of the same order in $h^{-1}$, the following system of equation in the unknown $\gamma_n(x)$ is achieved

$$\begin{aligned} &\oint_{-1}^{1} \frac{\gamma_0(\xi)}{(x-\xi)}d\xi = 0 \\ &\oint_{-1}^{1} \frac{\gamma_1(\xi)}{(x-\xi)}d\xi = -\oint_{-1}^{1} \left[K_0\gamma_0(\xi) + 2T'(\xi)H_0\right]d\xi \\ &\qquad\vdots \\ &\oint_{-1}^{1} \frac{\gamma_n(\xi)}{(x-\xi)}d\xi = -\oint_{-1}^{1}\left[\sum_{m=0}^{m=n-1} K_m(x-\xi)^m\gamma_{n-m-1}(\xi) + 2H_{n-1}T'(\xi)(x-\xi)^{n-1}\right]d\xi \end{aligned} \tag{A.16}$$

In order to obtain an univocally determined solution, it is necessary to impose the Kutta condition at the trailing edge; naming $F_n(x)$ the right hand side of Eqs.A.16, the Kutta condition is verified if[2]

$$\gamma_n(x) = \frac{1}{\pi^2}\left(\frac{1-x}{1+x}\right)^{1/2}\oint_{-1}^{1}\left(\frac{1+\xi}{1-\xi}\right)^{1/2}\frac{F_n(\xi)}{(\xi-x)}d\xi \tag{A.17}$$

The vorticity at the different orders can then be easily evaluated and it will results to be expressed

[2]The integrals belonging to the Eqs. A.16 if singular have to be intended in their Cauchy principal value as denoted by the peculiar symbol adopted for the integration. Furthermore, for the solution of such integrals it can be useful what referred in [48] and in the section of the appendix where the notable integrals are listed.

in function of the coefficient $H_n$,$K_n$ that appear in the expansion of the kernel function suggested by Keldysh-Lavrentiev. Thus, e.g., for the lift evaluation will be

$$\mathcal{L} = \rho c U^2 \int_{-1}^{1} \left( \gamma_0(\xi) + \frac{1}{h}\gamma_1(\xi) + \frac{1}{h^2}\gamma_2(\xi) + \ldots + \frac{1}{h^n}\gamma_n(\xi) \right) d\xi \tag{A.18}$$

The number of terms that have to be added will depend, obviously, by the particular problem tested.

The evaluation of the coefficients $H_n, K_n$ can be done once for all and in the following has been performed using the mathematical tool Mathematica 5.1.

**Evaluation of the Keldysh-Lavrentiev coefficient for the hydrofoil problem**

It is necessary to provide the terms $H_n, K_n$ appearing in Eqs. A.15 considering the expansion respect to powers of $x/h$ of the functions $H(x), K(x)$ given in A.14. In order to do that the following expansion can be adopted $I(r) = -e^{-r}(\gamma_e + \log r + i\pi + \sum_1^\infty \frac{r^n}{n \cdot n!})$ where $\gamma_e = 0.5772$ is the Euler constant.

The coefficients will be obtained for $n \leq 2$ that coincides with the evaluation of $\gamma_n$ for $n \leq 3$. The result, referred in the original work presented by Keldysh-avrentiev, after simple manipulations can be written as

$$H_0 = -\frac{1}{2} + 2\delta e^{-2\delta} \left[ \gamma_e + \log 2\delta + \sum_1^\infty \frac{(2\delta)^n}{n \cdot n!} \right] \tag{A.19}$$

$$H_1 = 2\pi\delta^2 e^{-2\delta} \tag{A.20}$$

$$H_2 = \frac{1}{8} + 2\delta e^{-2\delta} \Bigg[ -\gamma_e \frac{\delta^2}{2} - \frac{\delta \log 2\delta}{2} - \delta^2 \sum_1^\infty \frac{(2\delta)^n}{n \cdot n!} + \\ + \frac{1}{8} + \sum_1^\infty (2\delta)^n \frac{1-n}{8n!} + \frac{\delta}{2} + \sum_1^\infty \frac{(2\delta)^n}{n \cdot n!} \Bigg] \tag{A.21}$$

$$K_0 = 2\pi\delta e^{-2\delta} \tag{A.22}$$

$$K_1 = \frac{1}{4} + 2\delta e^{-2\delta} \left[ \frac{1}{2} + \sum_1^\infty \frac{(2\delta)^n}{2n!} - \gamma_e\delta - \delta \log 2\delta - \delta \sum_1^\infty \frac{(2\delta)^n}{n \cdot n!} \right] \tag{A.23}$$

$$K_2 = -\pi\delta^3 e^{-2\delta} \tag{A.24}$$

being $\delta = h \cdot F^{-2}$. It is evident that the coefficients $H_0, H_2, K_1$ have order $\mathcal{O}(1)$ respect to $h^{-1}F^2$ while the coefficients $H_1, K_0, K_2$ are $\circ(1)$ respect to the same term, that is, $H_1, K_0, K_2 \to 0$ if $(F^2/h) \to 0$.

**Hydrofoil problem with incidence**

For the same hydrofoil of the previous section placed at a certain incidence $\alpha$, and defined by $y = -\alpha x \pm \varepsilon T(x)$, the integral equation that has to be solved A.13 becomes

$$\oint_{-1}^{1} \gamma(\xi)\, K(x-\xi)\, d\xi = 2\,\pi\,\alpha - 2 \oint_{-1}^{1} T'(\xi)\, H(x-\xi)\, d\xi \tag{A.25}$$

being

$$\begin{aligned} H(x) &= -\frac{2h}{x^2+4h^2} - 2F^{-2} Re\left[I[iF^{-2}(x-2ih)]\right] \\ K(x) &= \frac{1}{x} + \frac{x}{x^2+4h^2} - 2F^{-2} Im\left[I[iF^{-2}(x-2ih)]\right] \end{aligned} \tag{A.26}$$

where $I(r) = e^{-r}\int_{-r}^{\infty} e^{-w} dw/w$.

Considering the expansion respect to $1/h$ suggested by Keldysh-Lavrentiev, that is

$$\begin{aligned} \gamma(x) &= \sum_{0}^{\infty} h^{-n} \gamma_n(x) \\ H(x) &= \frac{1}{h} \sum_{0}^{\infty} H_n(hF^{-2}) \left(\frac{x}{h}\right)^n \\ K(x) &= \frac{1}{x} + \frac{1}{h} \sum_{0}^{\infty} K_n(hF^{-2}) \left(\frac{x}{h}\right)^n \end{aligned} \tag{A.27}$$

and inserting the previous equation in the integral equation A.25, the following is achieved

$$\begin{aligned} &\oint_{-1}^{1} \sum_{0}^{\infty} \gamma_n(\xi) \left(\frac{1}{h}\right)^n \left[\frac{1}{x-\xi} + \frac{1}{h} \sum_{0}^{\infty} K_n \left(\frac{x-\xi}{h}\right)^n\right] = \\ &\qquad = 2\,\pi\,\alpha - 2 \oint_{-1}^{1} T'(\xi) \left[\frac{1}{h} \sum_{0}^{\infty} H_n \left(\frac{x-\xi}{h}\right)^n\right] d\xi \end{aligned} \tag{A.28}$$

Adopting an explicit expression for the sum symbol one has

$$\begin{aligned} &\oint_{-1}^{1} \left(\gamma_0(\xi) + \gamma_1(\xi)\frac{1}{h} + \gamma_2(\xi)\frac{1}{h^2} + \ldots + \gamma_n(\xi)\frac{1}{h^n}\right) \cdot \left\{\frac{1}{x-\xi} + \right. \\ &\left. + \frac{1}{h}\left[K_0 + K_1\frac{(x-\xi)}{h} + K_2\frac{(x-\xi)^2}{h^2} + \ldots + K_n\frac{(x-\xi)^n}{h^n}\right]\right\} d\xi = \\ &= 2\,\pi\,\alpha - 2 \oint_{-1}^{1} T'(\xi)\frac{1}{h}\left[H_0 + H_1\frac{(x-\xi)}{h} + \right. \\ &\left. + H_2\frac{(x-\xi)^2}{h^2} + \ldots + H_n\frac{(x-\xi)^n}{h^n}\right] \end{aligned} \tag{A.29}$$

and collecting the terms of the same order of $1/h$, the following relationships are achieved

$$
\begin{aligned}
(1/h)^0\colon & \oint_{-1}^{1} \frac{\gamma_0(\xi)}{(x-\xi)}\, d\xi = 2\,\pi\,\alpha \\
(1/h)^1\colon & \oint_{-1}^{1} \left(\gamma_0(\xi)K_0 + \frac{\gamma_1(\xi)}{(x-\xi)}\right) d\xi = -2\oint_{-1}^{1} T'(\xi)H_0\, d\xi \\
(1/h)^2\colon & \oint_{-1}^{1} \left(\gamma_0(\xi)K_1(x-\xi) + \gamma_1(\xi)K_0 + \frac{\gamma_2(\xi)}{(x-\xi)}\right) d\xi = \\
& \qquad = -2\oint_{-1}^{1} T'(\xi)H_1(x-\xi)\, d\xi \\
& \vdots \\
(1/h)^n\colon & \oint_{-1}^{1} \left(\sum_{m=0}^{m=n-1} K_m(x-\xi)^m\gamma_{n-m-1}(\xi) + \frac{\gamma_n(\xi)}{(x-\xi)}\right) = \\
& \qquad = -2\oint_{-1}^{1} H_{n-1}T'(\xi)(x-\xi)^{n-1}\, d\xi
\end{aligned}
\tag{A.30}
$$

Isolating at the left hand side the terms of the kind $\int_{-1}^{1} \frac{\gamma_i(\xi)}{(x-\xi)} d\xi$ it is possible to obtain a sequence of problems in the unknown $\gamma_i(\xi)$ that have to be solved in 'cascade'

$$
\begin{aligned}
\oint_{-1}^{1} \frac{\gamma_0(\xi)}{(x-\xi)}\, d\xi &= 2\,\pi\,\alpha \\
\oint_{-1}^{1} \frac{\gamma_1(\xi)}{(x-\xi)}\, d\xi &= -\oint_{-1}^{1} \left[K_0\gamma_0(\xi) + 2T'(\xi)H_0\right] d\xi \\
& \vdots \\
\oint_{-1}^{1} \frac{\gamma_n(\xi)}{(x-\xi)}\, d\xi &= -\oint_{-1}^{1} \left[\sum_{m=0}^{m=n-1} K_m(x-\xi)^m\gamma_{n-m-1}(\xi) + 2H_{n-1}T'(\xi)(x-\xi)^{n-1}\right] d\xi
\end{aligned}
\tag{A.31}
$$

In order to verify the Kutta condition at the trailing edge, it has to be verified[3]

$$
\gamma_n(x) = \frac{1}{\pi^2}\left(\frac{1-x}{1+x}\right)^{1/2} \oint_{-1}^{1} \left(\frac{1+\xi}{1-\xi}\right)^{1/2} \frac{F_n(\xi)}{(\xi-x)} d\xi
\tag{A.32}
$$

where $F_n(\xi)$ represents the right hand side of the Eqs.A.32.

***Zero order solution***[4]

[3]The singular integrals have to be considered in their Cauchy principal value as referred in [48].

[4]For solving the singular integrals from now on the section of the notable integrals referred later on i the appendix, as well as what referred in [48] have to be reminded.

For $n = 0$ one has

$$\oint_{-1}^{1} \frac{\gamma_0(\xi)}{(x-\xi)}\, d\xi = 2\,\pi\,\alpha \qquad \Rightarrow \qquad F_0(x) = 2\,\pi\,\alpha \tag{A.33}$$

$$\gamma_0(x) = \frac{1}{\pi^2}\left(\frac{1-x}{1+x}\right)^{1/2} \oint_{-1}^{1} \left(\frac{1+\xi}{1-\xi}\right)^{1/2} \frac{(2\pi\alpha)}{(\xi-x)} d\xi$$

$$\gamma_0(x) = \frac{1}{\pi^2}\left(\frac{1-x}{1+x}\right)^{1/2} 2\pi\alpha\cdot\pi = 2\,\alpha\left(\frac{1-x}{1+x}\right)^{1/2}$$

$$\gamma_0(x) = 2\alpha\left(\frac{1-x}{1+x}\right)^{1/2} \tag{A.34}$$

***First order solution***

The equation that has to be solved is in this case

$$\oint_{-1}^{1} \frac{\gamma_1(\xi)}{(x-\xi)}\, d\xi = -\oint_{-1}^{1} \left[K_0\,\gamma_0(\xi) + 2\,T'(\xi)\,H_0\right]\, d\xi \tag{A.35}$$

where $\gamma_0(\xi)$ is not identically equal to zero and it is given by the solution of the zero order problem. Thus,

$$\oint_{-1}^{1} \frac{\gamma_1(\xi)}{(x-\xi)}\, d\xi = -\oint_{-1}^{1} K_0\, 2\,\alpha\left(\frac{1-\xi}{1+\xi}\right)^{1/2} d\xi - 2\,H_0 \oint_{-1}^{1} T'(\xi)\, d\xi \tag{A.36}$$

but obviously $\oint_{-1}^{1} T'(\xi) d\xi = 0$ hence,

$$\begin{aligned} \oint_{-1}^{1} \frac{\gamma_1(\xi)}{(x-\xi)}\, d\xi \;&= -2\,\alpha\,K_0 \oint_{-1}^{1} \left(\frac{1-\xi}{1+\xi}\right)^{1/2} d\xi = -2\,\alpha\,\pi\,K_0 \\ &\Rightarrow F_1(x) = -2\,\pi\,\alpha\,K_0 \end{aligned} \tag{A.37}$$

Thus,

$$\gamma_1(x) = \frac{1}{\pi^2}\left(\frac{1-x}{1+x}\right)^{1/2} \oint_{-1}^{1} \left(\frac{1+\xi}{1-\xi}\right)^{1/2} \frac{(-2\pi\alpha K_0)}{(\xi-x)} d\xi \tag{A.38}$$

$$\gamma_1(x) = \frac{1}{\pi^2}\left(\frac{1-x}{1+x}\right)^{1/2} (2\pi\alpha K_0) = -2\alpha K_0\left(\frac{1-x}{1+x}\right)^{1/2}$$

$$\gamma_1(x) = -2\,\alpha\,K_0\,\left(\frac{1-x}{1+x}\right)^{1/2} \tag{A.39}$$

***Second order solution***

For $n = 2$ one has

$$\oint_{-1}^{1} \frac{\gamma_2(\xi)}{(x-\xi)}\, d\xi = -\oint_{-1}^{1} [\gamma_0(\xi) K_1(x-\xi) + \gamma_1(\xi) K_0 + 2T'(\xi) H_1(x-\xi)]\, d\xi \tag{A.40}$$

that is

$$\int_{-1}^{1} \frac{\gamma_2(\xi)}{(x-\xi)} d\xi = \underbrace{-\oint_{-1}^{1} \gamma_0(\xi) K_1(x-\xi) d\xi}_{A} \underbrace{-\oint_{-1}^{1} \gamma_1(\xi) K_0 d\xi}_{B} \underbrace{-\oint_{-1}^{1} 2T'(\xi) H_1(x-\xi) d\xi}_{C} \tag{A.41}$$

and solving separately the three terms one has

$$\begin{aligned}
A &= -2\,\alpha\, K_1 \oint_{-1}^{1} \left(\frac{1-\xi}{1+\xi}\right)^{1/2} (x-\xi)\, d\xi = -2\,\alpha\, K_1 \cdot \frac{1}{2}(1+2x)\pi \\
A &= -\pi\,\alpha\, K_1\,(1+2x) \qquad \text{(A.42)} \\
B &= -K_0 \oint_{-1}^{1} \left[ -2\alpha K_0 \left(\frac{1-\xi}{1+\xi}\right)^{1/2} \right] d\xi = 2\,\alpha\, K_0^2 \oint_{-1}^{1} \left(\frac{1-\xi}{1+\xi}\right)^{1/2} d\xi \\
B &= 2\,\pi\,\alpha\, K_0^2 \qquad \text{(A.43)} \\
C &= -2\, H_1 \oint_{-1}^{1} T'(\xi)(x-\xi)\, d\xi
\end{aligned}$$

Integrating by parts and considering that $-2H_1\,[T(\xi)(x-\xi)]_{-1}^{1} = 0$ it yields

$$C = -2\, H_1 \oint_{-1}^{1} T(\xi)\, d\xi = -2\, H_1\, s \tag{A.44}$$

being $s = \int_{-1}^{1} T(\xi) d\xi$ a quantity proportional to the hydrofoil area.

Hence,

$$F_2(x) = A + B + C = -\pi\alpha K_1(1+2x) + 2\pi\alpha K_0^2 - 2H_1 s \tag{A.45}$$

thus,

$$\gamma_2(x) = \frac{1}{\pi^2} \left(\frac{1-x}{1+x}\right)^{1/2} \oint_{-1}^{1} \left(\frac{1+\xi}{1-\xi}\right)^{1/2} \frac{[-\pi\alpha K_1(1+2\xi) + 2\pi\alpha K_0^2 - 2H_1 s]}{(\xi - x)} d\xi \tag{A.46}$$

that can be written as

$$\begin{aligned}
\gamma_2(x) = \frac{1}{\pi^2} \left(\frac{1-x}{1+x}\right)^{1/2} \Big[ &\pi(2\pi\alpha K_0^2 - 2H_1 s) + \\
&- \pi\alpha K_1 \oint_{-1}^{1} \frac{1+2\xi}{\xi - x} \left(\frac{1+\xi}{1-\xi}\right)^{1/2} d\xi \Big]
\end{aligned} \tag{A.47}$$

and then

$$\gamma_2(x)=\frac{1}{\pi}\left(\frac{1-x}{1+x}\right)^{1/2}\left[2\pi\alpha K_0^2-2H_1 s\underbrace{-\alpha K_1 \oint_{-1}^{1}\left(\frac{1+\xi}{1-\xi}\right)^{1/2}\frac{1+2\xi}{\xi-x}d\xi}_{D}\right] \tag{A.48}$$

where the following statement has been made

$$D\equiv-\alpha K_1\left(\oint_{-1}^{1}\left(\frac{1+\xi}{1-\xi}\right)^{1/2}\frac{1}{\xi-x}d\xi+2\oint_{-1}^{1}\left(\frac{1+\xi}{1-\xi}\right)^{1/2}\frac{\xi}{\xi-x}d\xi\right) \tag{A.49}$$

Hence,

$$\begin{aligned} D &= -\alpha\pi K_1-2\alpha K_1\oint_{-1}^{1}\sqrt{\frac{1+\xi}{1-\xi}\cdot\frac{1+\xi}{1+\xi}}\cdot\frac{\xi}{\xi-x}d\xi= \\ &= -\alpha\pi K_1-2\alpha K_1\oint_{-1}^{1}\frac{(1+\xi)}{\sqrt{1-\xi^2}}\cdot\frac{\xi}{\xi-x}d\xi \end{aligned} \tag{A.50}$$

thus,

$$\begin{aligned} D &= -\alpha\pi K_1-2\alpha K_1\left[\oint_{-1}^{1}\frac{\xi}{\sqrt{1-\xi^2}}\cdot\frac{d\xi}{(x-\xi)}+\oint_{-1}^{1}\frac{\xi^2}{\sqrt{1-\xi^2}}\cdot\frac{d\xi}{(x-\xi)}\right] \\ &\Rightarrow D=-\alpha\pi K_1-2\alpha\pi K_1(1+x) \end{aligned} \tag{A.51}$$

inserting what obtained for $D$ in $\gamma_2(x)$ it is possible to find

$$\begin{aligned} \gamma_2(x) &= \frac{1}{\pi}\left(\frac{1-x}{1+x}\right)^{1/2}\left[2\pi\alpha K_0^2-2H_1 s-\alpha\pi K_1-2\alpha K_1\pi(1+x)\right] \\ \Rightarrow \gamma_2(x) &= \frac{1}{\pi}\left(\frac{1-x}{1+x}\right)^{1/2}\left[2\pi\alpha\left(K_0^2-\frac{K_1}{2}-K_1(1+x)\right)-2H_1 s\right] \end{aligned} \tag{A.52}$$

and finally,

$$\gamma_2(x)=\frac{1}{\pi}\left(\frac{1-x}{1+x}\right)^{1/2}\left[2\pi\alpha\left(K_0^2-\frac{3}{2}K_1-K_1 x\right)-2H_1 s\right] \tag{A.53}$$

***Third order solution***

The equation to solve for $n=3$ is:

$$\oint_{-1}^{1}\frac{\gamma_3(\xi)}{x-\xi}d\xi=-\oint_{-1}^{1}\left[\gamma_0(\xi)K_2(x-\xi)^2+\gamma_1(\xi)K_1(x-\xi)+\gamma_2(\xi)K_0+2T'(\xi)H_2(x-\xi)^2\right]d\xi \tag{A.54}$$

and it is possible to solve separately the different contributions

$$\oint_{-1}^{1} \frac{\gamma_3(\xi)}{x-\xi}\, d\xi = \underbrace{-\oint_{-1}^{1} \gamma_0(\xi)\, K_2(x-\xi)^2\, d\xi}_{A} \underbrace{-\oint_{-1}^{1} \gamma_1(\xi)\, K_1(x-\xi)\, d\xi}_{B}$$
$$\underbrace{-\oint_{-1}^{1} \gamma_2(\xi)\, K_0\, d\xi}_{C} \underbrace{-\oint_{-1}^{1} 2\, T'(\xi)\, H_2(x-\xi)^2\, d\xi}_{D} \tag{A.55}$$

Hence,

$$\begin{aligned} A &= -\oint_{-1}^{1} \gamma_0(\xi)\, K_2(x-\xi)^2\, d\xi = -2\,\alpha\, K_2 \int_{-1}^{1} \left(\frac{1-\xi}{1+\xi}\right)^{1/2} (x-\xi)^2 d\xi = \\ &= -2\alpha K_2 \cdot \frac{1}{2}(1+2x+2x^2)\cdot\pi \\ &\Rightarrow A = -\pi\alpha K_2(1+2x+2x^2) \end{aligned} \tag{A.56}$$

$$\begin{aligned} B &= -\int_{-1}^{1} \gamma_1(\xi) K_1(x-\xi) d\xi = 2\alpha K_0 K_1 \int_{-1}^{1} \left(\frac{1-\xi}{1+\xi}\right)^{1/2} (x-\xi) d\xi = \\ &= 2\alpha K_0 K_1 \cdot \frac{1}{2}(1+2x)\cdot\pi \\ &\Rightarrow B = \pi\alpha K_0 K_1 (1+2x) \end{aligned} \tag{A.57}$$

$$C = -\int_{-1}^{1} \gamma_2(\xi) K_0 d\xi$$

Reminding the expression obtained for $\gamma_2(\xi)$ in A.53 the following can be written

$$C = -K_0 \int_{-1}^{1} \frac{1}{\pi} \left(\frac{1-\xi}{1+\xi}\right)^{1/2} \left\{ \left[ 2\pi\alpha \left( K_0^2 - \frac{3}{2} K_1 \right) - 2H_1 s \right] - 2\pi\alpha K_1 \xi \right\} d\xi \tag{A.58}$$

$$C = -\frac{k_0}{\pi} \left\{ \pi \cdot \left[ 2\pi\alpha \left( K_0^2 - \frac{3}{2} K_1 \right) - 2H_1 s \right] - 2\pi\alpha K_1 \int_{-1}^{1} \left(\frac{1-\xi}{1+\xi}\right)^{1/2} \cdot \xi d\xi \right\}$$

$$C = -\frac{k_0}{\pi} \left\{ \pi \cdot \left[ 2\pi\alpha \left( K_0^2 - \frac{3}{2} K_1 \right) - 2H_1 s \right] - 2\pi\alpha K_1 \left( \frac{-\pi}{2} \right) \right\}$$

that is

$$\begin{aligned} C &= -K_0 \left[ 2\pi\alpha K_0^2 - 3\pi\alpha K_1 - 2H_1 s \right] - K_0 \left[ \pi\alpha K_1 \right] \\ C &= -2\pi\alpha K_0^3 + 3\pi\alpha K_0 K_1 + 2K_0 H_1 s - \pi\alpha K_0 K_1 \\ &\Rightarrow C{=}2\pi\alpha \left( -K_0^3 + K_0 K_1 \right) + 2K_0 H_1 s \end{aligned} \tag{A.59}$$

Finally for the term $D$ one has

$$D = -2H_2 \int_{-1}^{1} T'(\xi)(x-\xi)^2 d\xi \tag{A.60}$$

that integrated by parts gives

$$\begin{aligned} D &= -2H_2\left[T(\xi)(x-\xi)^2\right]_{-1}^{1} - 2H_2\int_{-1}^{1} 2T(\xi)(x-\xi)d\xi \\ D &= -2H_2\left[2\int_{-1}^{1} T(\xi)\cdot x d\xi - 2\int_{-1}^{1} T(\xi)\cdot \xi d\xi\right] \\ &\Rightarrow D = -2H_2\left[2sx - 2p\right] \end{aligned} \tag{A.61}$$

naming $p$ the integral $\int_{-1}^{1} T(\xi)\xi d\xi$.
Obviously, it yields

$$\begin{aligned} F_3(x) &= A + B + C + D = -\pi\alpha K_2(1 + 2x + 2x^2) + \pi\alpha K_0 K_1(1 + 2x) + \\ &+ 2\pi\alpha(-K_0^3 + K_0 K_1) + 2K_0 H_1 s - 4H_2 sx + 4H_2 p \end{aligned} \tag{A.62}$$

Such equation can be written enlightening the terms independent from $x$ or proportional to $x, x^2 \ldots$ achieving at the end

$$\begin{aligned} F_3(x) &= (4H_2 p + 2K_0 H_1 s - 2\pi\alpha K_0^3 + 3\pi\alpha K_0 K_1 - \pi\alpha K_2) + \\ &+ x(-4H_2 s + 2\pi\alpha K_0 K_1 - 2\pi\alpha K_2) + x^2(-2\pi\alpha K_2) \end{aligned} \tag{A.63}$$

Consequently, since $\gamma_3(x) = \frac{1}{\pi^2}\left(\frac{1-x}{1+x}\right)^{1/2} \oint_{-1}^{1}\left(\frac{1+\xi}{1-\xi}\right)^{1/2} \frac{F_3(\xi)}{(\xi-x)}d\xi$ one has

$$\begin{aligned} \gamma_3(x) =& \frac{1}{\pi^2}\left(\frac{1-x}{1+x}\right)^{1/2}\Bigg\{\oint_{-1}^{1}(4H_2 p + 2K_0 H_1 s - 2\pi\alpha K_0^3 + 3\pi\alpha K_0 K_1 - \pi\alpha K_2)\left(\frac{1+\xi}{1-\xi}\right)^{1/2} d\xi + \\ &+ \oint_{-1}^{1}(-4H_2 s + 2\pi\alpha K_0 K_1 - 2\pi\alpha K_2)\left(\frac{1+\xi}{1-\xi}\right)^{1/2}\cdot\frac{\xi}{\xi-x}d\xi + \\ &+ \oint_{-1}^{1}(-2\pi\alpha K_2)\left(\frac{1+\xi}{1-\xi}\right)^{1/2}\cdot\frac{\xi^2}{\xi-x}d\xi\Bigg\} \end{aligned} \tag{A.64}$$

Thus, for $\gamma_3$ one has

$$\begin{aligned} \gamma_3(x) &= \frac{1}{\pi^2}\left(\frac{1-x}{1+x}\right)^{1/2}\Bigg\{\pi(4H_2 p + 2K_0 H_1 s - 2\pi\alpha K_0^3 + 3\pi\alpha K_0 K_1 - \pi\alpha K_2) + \\ &+ \pi(1+x)(-4H_2 s + 2\pi\alpha K_0 K_1 - 2\pi\alpha K_2) + \\ &+ \frac{\pi}{2}(2x^2 + 2x + 1)(-2\pi\alpha K_2)\Bigg\} \end{aligned} \tag{A.65}$$

Collecting once again the terms independent from $x$ or proportional to $x, x^2 \ldots$ the following is achieved

$$\gamma_3(x) = \frac{1}{\pi}\left(\frac{1-x}{1+x}\right)^{1/2}\Bigg\{(4H_2p - 4H_2s + 2K_0H_1s - 2\pi\alpha K_0^3 + 5\pi\alpha K_0K_1 - 4\pi\alpha K_2) + \\ + x(-4H_2s + 2\pi\alpha K_0K_1 - 4\pi\alpha K_2) + x^2(-2\pi\alpha K_2)\Bigg\} \tag{A.66}$$

It is now possible evaluate the lift force produced by such foil being

$$\mathcal{L} = \rho c U^2 \varepsilon \int_{-1}^{1} \gamma(\xi) d\xi \tag{A.67}$$

Nevertheless, reminding that

$$\gamma(\xi) = \gamma_0(\xi) + \frac{1}{h}\gamma_1(\xi) + \frac{1}{h^2}\gamma_2(\xi) + \frac{1}{h^3}\gamma_3(\xi) + \ldots \tag{A.68}$$

Thus, it is possible to evaluate $\int_{-1}^{1}\gamma(\xi)d\xi$ considering for conciseness terms till the third order

$$\begin{aligned}\gamma(x) = {} & 2\alpha\left(\frac{1-x}{1+x}\right)^{1/2} + \frac{1}{h}\cdot(-2\alpha K_0)\left(\frac{1-x}{1+x}\right)^{1/2} + \\ & \frac{1}{h^2}\cdot\frac{1}{\pi}\left(\frac{1-x}{1+x}\right)^{1/2}\left[2\pi\alpha\left(k_0^2 - \frac{3}{2}K_1 - K_1x\right) - 2H_1s\right] + \\ & + \frac{1}{h^3}\cdot\frac{1}{\pi}\left(\frac{1-x}{1+x}\right)^{1/2}\Bigg\{(4H_2p - 4H_2s + 2K_0H_1s - 2\pi\alpha K_0^3 + 5\pi\alpha K_0K_1 - 4\pi\alpha K_2) + \\ & + x(-4H_2s + 2\pi\alpha K_0K_1 - 4\pi\alpha K_2) + x^2(-2\pi\alpha K_2)\Bigg\}\end{aligned} \tag{A.69}$$

Isolating the terms independent from $x$ or proportional to $x, x^2 \ldots$ one has

$$\begin{aligned}\gamma(x) = {} & \left(\frac{1-x}{1+x}\right)^{1/2}\Bigg\{\Bigg[2\alpha - \frac{1}{h}2\alpha K_0 + \frac{1}{h^2\pi}\left(2\pi\alpha\left(K_0^2 - \frac{3}{2}K_1\right) - 2H_1s\right) + \\ & + \frac{1}{h^3\pi}(4H_2(p-s) + 2K_0H_1s - 2\pi\alpha K_0^3 + 5\pi\alpha K_0K_1 - 4\pi\alpha K_2)\Bigg]_{\mathcal{A}} + \\ & + x\cdot\left[\frac{1}{h^2\pi}(-2\pi\alpha K_1) + \frac{1}{h^3\pi}(-4H_2s + 2\pi\alpha K_0K_1 - 4\pi\alpha K_2)\right]_{\mathcal{B}} + \\ & + x^2\cdot\left[\frac{1}{h^3\pi}(-2\pi\alpha K_2)\right]_{\mathcal{C}}\Bigg\}\end{aligned} \tag{A.70}$$

and it yields

$$\int_{-1}^{1}\gamma(\xi)d\xi=\int_{-1}^{1}\left(\frac{1-\xi}{1+\xi}\right)^{1/2}\left\{\left[\dots\right]_{\mathcal{A}}+\left[\dots\right]_{\mathcal{B}}+\left[\dots\right]_{\mathcal{C}}\right\}d\xi \tag{A.71}$$

where for integrating the terms $\mathcal{A},\mathcal{B},\mathcal{C}$ it is necessary to refer to the notable integrals list addressed later on in the appendix. Thus,

$$\int_{-1}^{1}\left(\frac{1-\xi}{1+\xi}\right)^{1/2}\left[\dots\right]_{\mathcal{A}}=\pi\cdot\left[2\alpha-\frac{1}{h}2\alpha K_0+\frac{1}{h^2\pi}\left(2\pi\alpha\left(K_0^2-\frac{3}{2}K_1\right)-2H_1s\right)+\right.$$
$$\left.+\frac{1}{h^3\pi}(4H_2(p-s)+2K_0H_1s-2\pi\alpha K_0^3+5\pi\alpha K_0K_1-4\pi\alpha K_2)\right] \tag{A.72}$$

$$\int_{-1}^{1}\left(\frac{1-\xi}{1+\xi}\right)^{1/2}\left[\dots\right]_{\mathcal{B}}=-\frac{\pi}{2}\cdot\left[\frac{1}{h^2\pi}(-2\pi\alpha K_1)+\frac{1}{h^3\pi}(-4H_2s+2\pi\alpha K_0K_1-4\pi\alpha K_2)\right]_{\mathcal{B}} \tag{A.73}$$

$$\int_{-1}^{1}\left(\frac{1-\xi}{1+\xi}\right)^{1/2}\left[\dots\right]_{\mathcal{C}}=\frac{\pi}{2}\cdot\left[\frac{1}{h^3\pi}(-2\pi\alpha K_2)\right] \tag{A.74}$$

Collecting the terms in the same order of $1/h$ the following is achieved

$$\begin{aligned}
&(1/h)^0 : 2\pi\alpha \\
&(1/h)^1 : 2\pi\alpha(-K_0) \\
&(1/h)^2 : 2\pi\alpha(K_0^2-K_1)-2H_1s \\
&(1/h)^3 : 2\pi\alpha\left(-K_0^3+2K_0K_1-\frac{3}{2}K_2\right)+2H_2(2p-s)+2K_0H_1s
\end{aligned} \tag{A.75}$$

## A.3 Notable Integrals

$$\oint_{-1}^{1} \left(\frac{1+\xi}{1-\xi}\right)^{1/2} \frac{d\xi}{\xi - x} \;=\; \pi \tag{A.76}$$

$$\oint_{-1}^{1} \left(\frac{1+\xi}{1-\xi}\right)^{1/2} \frac{\xi}{\xi - x}\, d\xi = \pi\,(1+x) \tag{A.77}$$

$$\oint_{-1}^{1} \left(\frac{1+\xi}{1-\xi}\right)^{1/2} \frac{\xi^2}{\xi - x}\, d\xi = \frac{\pi}{2}\,(2\,x^2 + 2\,x + 1) \tag{A.78}$$

$$\oint_{-1}^{1} \left(\frac{1+\xi}{1-\xi}\right)^{1/2} d\xi \;=\; \pi \tag{A.79}$$

$$\oint_{-1}^{1} \left(\frac{1+\xi}{1-\xi}\right)^{1/2} \xi\, d\xi \;=\; \frac{\pi}{2} \tag{A.80}$$

$$\int_{-1}^{1} \left(\frac{1-\xi}{1+\xi}\right)^{1/2} d\xi = \pi \tag{A.81}$$

$$\int_{-1}^{1} \left(\frac{1-\xi}{1+\xi}\right)^{1/2} (x-\xi)\, d\xi = \frac{\pi}{2}\,(1+2\,x) \tag{A.82}$$

$$\int_{-1}^{1} \left(\frac{1-\xi}{1+\xi}\right)^{1/2} (x-\xi)^2\, d\xi = \frac{\pi}{2}(1+2\,x+2\,x^2) \tag{A.83}$$

$$\int_{-1}^{1} \left(\frac{1-\xi}{1+\xi}\right)^{1/2} \xi\, d\xi = -\,\frac{\pi}{2} \tag{A.84}$$

$$\int_{-1}^{1} \left(\frac{1-\xi}{1+\xi}\right)^{1/2} \xi^2\, d\xi = \frac{\pi}{2} \tag{A.85}$$

$$\int_{-1}^{1} \left(\frac{1-\xi}{1+\xi}\right)^{1/2} \xi^3\, d\xi = -\,\frac{3}{8}\,\pi \tag{A.86}$$

$$\int_{-1}^{1} \left(\frac{1-\xi}{1+\xi}\right)^{1/2} \xi^4\, d\xi = \frac{3}{8}\,\pi \tag{A.87}$$

$$\tag{A.88}$$

# Bibliography


[1] H. Ashley. "On Making Things the Best-Aeronautical Uses of Optimization ". *Journal of Aircraft*, Vol. 19(no. 1):pp. 5–27, January 1982.

[2] R.T. Haftka and Z. Gürdal. *"Elements of Structural Optimization"*. Kluwer Academic Publishers, Third revised and expanded edition, 1992.

[3] O. de Weck, J. Agte, J. Sobieszczanski-Sobieski, P. Arendsen, A. Morris, and M. Spieck. "State of the Art and Future Trends in Multidisciplinary Design Optimization". In *Proceedings of the* 48*th AIAA/ASME/ASCE/AHS/ASC Structures, Structural Dynamics, and Materials Conference, AIAA* 2007 − 1905*, Honolulu, Hawaii*, 23-26 April 2007.

[4] J. Sobieszczanski-Sobieski and R.T. Haftka. "Multidisciplinary Aerospace Design Optimization: Survey of Recent Developments". *AIAA Journal* 96 − 0711, 1996.

[5] J. Sobieszczanski-Sobieski and R. T. Hafka. "Multidisciplinary Aerospace Optimization: Survey of Recent Developments". *Structural optimization J.*, Vol. 14(No. 1), August 1997.

[6] J.T. Allison, M. Kokkolaras, and P.Y. Papalambros. "On Selecting Single-Level Formulations for Complex System Design Optimization". *Journal of Mechanical Design*, 129(9):898–906, 2007.

[7] R.J. Balling and J. Sobieszczanski-Sobieski. "Optimization of Coupled Systems: A Critical Overview of Approaches". *AIAA Journal*, 34(No.1):pp.6–17, 1996.

[8] E.J. Cramer, J.E. Dennis Jr., P.D. Frank, R.M. Lewis, and G.R. Shubin. "Problem Formulations for Multidisciplinary Optimization". Crpc-tr93334, Center for Research on Parallel Computation, Rice University, Houston, Texas, August 1993.

[9] J. R. R. A. Martins and C. Marriage. "An Object-Oriented Framework for Multidisciplinary Design Optimization". In *Proceedings of the* 48*th AIAA/ASME/ASCE/AHS/ASC Structures, Structural Dynamics, and Materials Conference, AIAA* 2007 − 1906*, Honolulu, Hawaii*, 23-26 April 2007.

[10] N.M. Alexandrov and R.M. Lewis. "Algorithmic Perspective on Problem Formulation in MDO". In *Proceedings of the* 8*th AIAA/USAF/NASA/ISSMO Symposium on Multidisciplinary Analysis and Optimization, YEAR = 6-8 September 2000.*

[11] R.D. Braun and I.M. Kroo. "Development and Application of the Collaborative Optimization Architecture in a Multidisciplinary Design Environment". In *Multidisciplinary Design Optimization: State of the Art*, pages 98–116. SIAM, 1996.

[12] B. Moore, R.D. Braun, and I.M. Kroo. "Use Of The Collaborative Optimization Architecture For Launch Vehicle Design". In *6th AIAA/USAF/NASA/ISSMO Symposium on Multidisciplinary Analysis and Optimization*, pages 306–318, 1996.

[13] N.M. Alexandrov and R.M. Lewis. "Analytical and Computational Aspects of Collaborative Optimization". Tm-210104, NASA, 2000.

[14] N.M. Alexandrov and R.M. Lewis. "Analytical and Computational Aspects of Collaborative Optimization for Multidisciplinary Design". *AIAA Journal*, Vol. 40(no. 2):pp. 301–309, February 2002.

[15] J. Sobiezczanski-Sobieski, J.S. Agte, and R.S. Sandusky Jr. "Bi-Level Integrated System Synthesis". Technical report, NASA TM-1998-208715, 1998.

[16] J. Sobieszczanski-Sobieski and S. Kodiyalam. "BLISS/S: a new method for two-level structural optimization". *Structural Multidisciplinary Optimization*, 21:1–13, 2001.

[17] R.J. Balling and J. Sobieszczanski-Sobieski. "An algorithm for solving the system-level problem in multi-level optimization". *Structural Optimization*, 9:168–177, 1995.

[18] J. Sobieszczanski-Sobieski, M.S. Emiley, J.S. Agte, and R.R. Sandusky Jr. "Advancement of Bi-Level Integrated System Synthesis (BLISS)". In *38th AIAA Aerospace Sciences Meeting and Exhibit, Reno, NV*, 10-13 January 2000.

[19] H. Kim, S. Ragon, J. Mullins, and J. Sobieszczanski-Sobieski. "A Web-based Collaborative Environment for Bi-Level Integrated System Synthesis (BLISS)". In *47th AIAA/ASME/ASCE/AHS/ASC Structures, Structural Dynamics, and Materials Conference, Newport, RI*, 1-4 May 2006.

[20] S. Kodiyalam and J. Sobieszczanski-Sobieski. "Bi-Level Integrated System Synthesis with Response Surface". *AIAA Journal*, 38(8):1479–1485, August 2000.

[21] J.M. Lee. *"MSC/NASTRAN Linear Static Analysis", User's Guide.* The MacNeal-Schwendler Corporation, 1997.

[22] K. Blakely. *"MSC/NASTRAN Basic Dynamic Analysis", User's Guide.* The MacNeal-Schwendler Corporation, 1993.

[23] L. Morino and G. Bernardini. "On Modeling for Innovative Configuration MDO with Recent Aerodynamics Developments". *In A. Frediani and A. Miele (Eds.), Advanced Design Problems in Aerospace Engineering,Plenum Press, New York, NY*, 2003.

[24] L. Morino. "Boundary Integral Equations in Aerodynamics". *Appl. Mech. Rev.*, 46:445–466, 1993.

[25] L. Morino and G. Bernardini. "Singularities in BIE's for the Laplace Equation; Joukowski Trailing–Edge Conjecture Revisited". *Journal of Engineering Analysis with Boundary Elements*, 25:805–818, 2001.

[26] L. Morino. "A General Theory of Unsteady Compressible Potential Aerodynamics". Technical report, NASA CR-2464, 1974.

[27] L. Morino, G. Bernardini, W. Da Riz, and V. Del Rio. "Aerodynamic Issues in MDO for Preliminary Design of an Innovative Configuration". In *Proceedings of IABEM 2002 (International Association for Boundary Element Methods), UT Austin, TX, USA*, May 28-30, 2002.

[28] L. Morino and L.T. Chen. "Indicial Compressible Potential Aerodynamics Around Complex Aircraft Configurations". In *Aerodynamic Analisys Requiring Advanced Computers, NASA SP-347, P.*

[29] L. Morino, F. Mastroddi, R. De Troia, G.L. Ghiringhelli, and P. Mantegazza. "Matrix Fraction Approach for Finite–State Aerodynamic Modeling". *AIAA Journal*, 33(4):703–711, April 1995.

[30] L. Morino, L.T. Chen, and E.O. Suciu. "Steady and Oscillatory Subsonic and Supersonic Aerodynamic around Complex Configuratio". *AIAA Journal*, 13:368–374, 1975.

[31] K.F. Hulme and C.L. Bloebaum. "A simulation-based comparison of multidisicplinary design optimization solution strategies using CASCADE". *Structural Multidisicplinary OPtimization*, 19:17–35, 2000.

[32] G. Carrier. "Multi-disicplinary Optimisation of a Supersonic transport Aircraft Wing Platform". In *Proceedings of European Congress on Computational Methods in Applied Sciences and EngineeringECCOMAS'04*, 2004.

[33] I.R. Chittick and J.R.R.A. Martins. "A New Subspace Optimization Method for Aero-Structural Design". In *48th AIAA/ASME/ASCE/AHS/ASC Structures, Structural Dynamics, and Materials Conference, Honolulu, HI*, April 2007.

[34] P. Conti Puorger, F. Mastroddi, F. Pinna, and G. Bernardini. "Multidisciplinary Design Optimization for Aircraft Configurations". In *Proceedings of 2nd AIAA Multidisciplinary Design Optimization Specialist Conference, Newport, RI, USA*, 1-4 May 2006.

[35] A.G. Striz and V.B. Venkayya. "Influence of Structural and Aerodynamic Modeling on Flutter Analysis". *AIAA Journal*, 31(5):1205–1211, Sept-Oct 1994.

[36] M. Gennaretti, F. Salvatore, and L. Morino. "Forces and Moments in Incompressible Quasi–Potential Flows". *Journal of Fluids and Structures*, 10(7):281–303, 1996.

[37] E. Trefftz. "Prandtlsche Tragflächen und Propeller-Theorie". *Zeitschrift für Angewandte Mathematik und Mechanik*, 1:206–218, 1921.

[38] G. Bernardini, A. Frediani, and L. Morino. "Aerodynamics for MDO of an Innovative Configuration". In *Symposium on Aerodynamic Design and Optimization of Flight Vehicles in a Concurrent Multi–Disciplinary Environment, RTO–MP–35, Ottawa, Canada*, 1999.

[39] P.D. Gall and H.C. Smith. "Aerodynamic Characteristics of Biplanes with Winglets". *Journal of Aircraft*, 24(8):518–522, 1987.

[40] L. Morino, G. Bernardini, D.D. Gregorio, K.E. Willcox, and W.L. Harris. "Life-Cycle Cost Multidisciplinary Optimization for Prandtl–Plane". In *Proceedings of ICCES'04, Madeira, Portugal*, 2004.

[41] G. Corning. *"Airplane Design, Supersonic and Subsonic CTOL and VTOL"*. Helen Corning, Box no 415, Kensington, Maryland, 4th edition.

[42] J.V. Wehausen S.Flugge and E.V. Laitone. *"Handbuch der Physik Surface Waves"*. Springer-Verlag, Berlin, 1960.

[43] A. Plotkin. "A note on the Thin-Hydrofoil Theory of Keldysh and Lavrentiev". *Journal of Ship Research*, 20(2):95–97, 1976.

[44] A. Plotkin. "The Thin-Hydrofoil Thickness Problem Including Leading-Edge Corrections". *Journal of Ship Research*, 19(2):122–129, 1975.

[45] A. Plotkin and S.S. Dodbele. "Slender Wing in Ground Effect". *AIAA Journal*, 26(4), April 1988.

[46] A. Plotkin and C.G. Kennell. "Thickness-Induced Lift on a Thin Airfoil in Ground Effect". *AIAA Journal*, 19(11), November 1981.

[47] P. Conti Puorger. *"Caratteristiche aero-idroelastiche di superfici portanti in presenza di effetti di parete"*. Tesi di Laurea in Ingegneria Aerospaziale, Università degli Studi di Roma 'La Sapienza', a.a. 2002 – 2003.

[48] M.D. Van Dyke. "Second-Order Subsonic Airfoil Theory Including Edge Effects". Technical report, NACA Report, 1974.

[49] R.L. Bisplinghoffand, H. Ashley, and R.L. Halfman. *"Aeroelasticity"*. Dover Publications Inc., Mineola, New York.

[50] F. Mastroddi. *"Dispense del corso di Aeroelasticità Applicata"*. Università degli Studi di Roma 'La Sapienza', a.a. 1998 – 1999.

[51] M. Strani. *"Lezioni di Aeroelasticità "*. Dispense in distribuzione presso l'Università degli Studi di Roma 'La Sapienza', Facoltà di Ingegneria.

[52] G. Bernardini and F. Mastroddi. "Multidisciplinary Design Optimization for the Preliminary Design of Aeronautical Configuration". In *45th AIAA/ASME/ASCE/AHS/ASC Structures, Structural Dynamics, and Materials Conference, Palm Springs, CA*, April 2004.

[53] P. Conti Puorger and D. Dessi. "Analisi dei profili di Karman-Trefftz in effetto di superficie". Technical report, INSEAN Thecnical Report, RT2005-073, 2005.

[54] A. Plotkin and C.H. Tan. "Lifting-Line Solution for a Symmetrical Thin Wing in Ground Effect". *AIAA Journal*, 24(7), July 1986.

[55]

[56] P. Bartholomew. "The Role of MDO within Aerospace Design and Progress towards an MDO Capability". *AIAA Journal*, (4705), 1998.

[57] C.R. Gumbert, G.J.W. Hou, and P.A. Newman. "High-Fidelity Computational Optimization for 3-D Flexible Wings: Part I- Simultaneous Aero-Structural Design Optimization (SASDO)". *Optimization and Engineering*, 6:117–138, 2005.

[58] J.A. Young, R.D. Anderson, and R.N. Yurkovich. "A Description of the F/A-18/F Design and Design Process". *AIAA Journal*, (4701), 1998.

[59] N. Radovcich and D. Layton. "The F-22 Structural/Aeroelastic Design Process with MDO Examples". *AIAA Journal*, 1998.

[60] G.R. Shubin. "Application of Alternative Multidisciplinary Optimization Formulations to a Model Problem for Static Aeroelasticity". *Journal of Computational Physics*, 118:73–85, 1995.

[61] T.W. Simpson. "Multidisciplinary Design Optimization". *Aerospace America*, (12):34, 2004.

[62] S. Hosder, L.T. Watson, B. Grossman, W.H. Mason, H. Kim, R.T. Haftka, and S.E. Cox. "Polynomial Response Surface Approximations for the Multidisciplinary Design Optimization of a High Speed Civil Transport". *Optimization and Engineering*, (2):431–452, 2001.

[63] G. Bernardini and F. Mastroddi. "Multidisciplinary Design Optimization for the Preliminary Design of Aeronautical Configurations". *AIAA Journal*, (1544), 2004.

[64] X. Huang, J. Dudley, R.T. Hafka, B. Grossman, and W.H. Mason. "Structural Weight Estimation for Multidisciplinary Optimization of a High-Speed Civil Transport". *Journal of Aircraft*, 33(3):608–616, 1996.

[65] G.L. Giles. "Equivalent Plate Analysis of Aircraft Wing Box Structures with General Planform Geometry". *Journal of Aircraft*, 23(11):859–864, 1986.

[66] A.A. Groenwold, J.A. Snyman, and N. Stander. "Modified Trajectory Method for Practical Global Optimization Problems". *AIAA Journal*, 34(10):2126–2131, 1996.

[67] M. Karpel and L. Brainin. "Stress Considerations in Reduced-Size Aeroelastic Optimization". *AIAA Journal*, 33(4):716–722, 1995.

[68] F.H. Gern, A.H. Naghshineh-Pour, E. Sulaeman, R.K. Kapania, and R. T. Haftka. "Structural Wing Sizing for Multidisciplinary Design Optimization of a Strut-Braced Wing". *Journal of Aircraft*, 38(1):154–163, 2001.

[69] F. van Dalen, C. Bil, A. Rothwell, and P. Arendsen. "Finite-Element Based Preliminary Design Procedures for Wing Structures". *AIAA Journal*, pages 2233–2246, 1994.

[70] A. Plotkin and C. Kennell. "A Second-Order Theory for the Potential Flow About Thin Hydrofoils". *Journal of Ship Research*, 28(1):55–64, March 1984.

[71] C. Coulliette and A. Plotkin. "Aerofoil Ground Effect Revisited". *Aeronautical Journal*, pages 65–74, February 1996.

[72] D. Dessi, A. Giorgi, L. Morino, and P. Conti Puorger. "Steady and Unsteady Loads on Airfoils in Ground Effect and Marine Applications". In *Proceedings of International Conference on Fast Sea Transportation, St. Petersburg, Russia*, June 2005.

[73] P. Conti Puorger, D. Dessi, and F. Mastroddi. "Preliminary Design of an Amphibious Aircraft by the Multidisciplinary Design Optimization Approach". In *Proceedings of 3rd AIAA Multidisciplinary Design Optimization Specialist Conference, Honolulu, HI, USA*, April 2007.